

Polarons in atomic gases and two-dimensional semiconductors

Pietro Massignan

*Departament de Física,
Universitat Politècnica de Catalunya,
Campus Nord B4-B5,
E-08034 Barcelona,
Spain*

Richard Schmidt

*Institute for Theoretical Physics,
Heidelberg University,
Philosophenweg 16,
69120 Heidelberg,
Germany*

Grigori E. Astrakharchik

*Departament de Física,
Universitat Politècnica de Catalunya,
Campus Nord B4-B5,
E-08034 Barcelona,
Spain*

Ataç İmamoglu

*Institute for Quantum Electronics,
ETH Zürich, Zürich,
Switzerland*

Martin Zwierlein

*MIT-Harvard Center for Ultracold Atoms,
Research Laboratory of Electronics,
and Department of Physics,
Massachusetts Institute of Technology,
Cambridge, Massachusetts 02139,
USA*

Jan J. Arlt

*Center for Complex Quantum Systems,
Department of Physics and Astronomy,
Aarhus University, Ny Munkegade,
DK-8000 Aarhus C,
Denmark*

Georg M. Bruun

*Center for Complex Quantum Systems,
Department of Physics and Astronomy,
Aarhus University, Ny Munkegade,
DK-8000 Aarhus C,
Denmark*

(Dated: January 17, 2025)

In this work we provide a comprehensive review of theoretical and experimental studies of the properties of polarons formed by mobile impurities strongly interacting with quantum many-body systems. We present a unified perspective on the universal concepts and theoretical techniques used to characterize polarons in two distinct platforms, ultracold atomic gases and atomically-thin transition metal dichalcogenides, which are linked by many deep parallels. We review polarons in both fermionic and bosonic environments, highlighting their similarities and differences including the intricate interplay between few- and many-body physics. Various kinds of polarons with long-range interactions or in magnetic backgrounds are discussed, and the theoretical and experimental progress towards understanding interactions between polarons is described. We outline how polaron

physics, regarded as the low density limit of quantum mixtures, provides fundamental insights regarding the phase diagram of complex condensed matter systems. Furthermore, we describe how polarons may serve as quantum sensors of many-body physics in complex environments. Our work highlights the open problems, identifies new research directions and provides a comprehensive framework for this rapidly evolving research field.

CONTENTS

I. Introduction	2	X. Perspectives	59
A. Experimental platforms	3	Acknowledgments	60
1. Atomic gases	3	References	60
2. Two-dimensional semiconductors	3		
B. Bose and Fermi polarons	4		
C. General properties of polarons	4		
II. The Fermi polaron in atomic gases	7		
A. Temperature effects	9		
B. Non-equilibrium dynamics	9		
III. The Bose polaron	10		
A. Ladder approximation	12		
B. Experiments	14		
C. Static impurity and the orthogonality catastrophe	15		
D. Weak interactions	17		
E. Expansion in bath excitations	17		
F. Gross-Pitaevskii approach	19		
G. Gaussian state approach	21		
H. Quantum Monte-Carlo calculations	23		
I. Other methods	24		
J. Bose polaron at unitarity	25		
K. Temperature dependence	27		
L. Non-equilibrium dynamics	28		
IV. Polarons with long-range interactions	30		
A. Ions in a BEC/Fermi gas	30		
B. Dipolar polarons	33		
C. Rydberg polarons	34		
D. Rotating molecules in a quantum bath: angulons	35		
V. Polarons in 2D materials	35		
A. Excitons in TMDs	36		
B. Exciton-polarons	37		
C. Polaron-polaritons	39		
D. Bose polarons in TMDs	41		
E. Feshbach resonances	42		
F. Excitons as robust impurities	42		
G. Exciton-polarons as quantum probes	43		
VI. Polaron-polaron interactions	45		
A. Mobile impurities	45		
B. Static impurities	47		
C. Experimental detection	48		
D. Bi-polarons	49		
VII. Polarons as a limit of many-body phases	50		
A. Fermi mixtures	50		
1. Chandrasekhar-Clogston limit	50		
2. Phase separation	52		
3. Equation of state at unitarity	52		
B. Bose-Fermi mixtures	53		
VIII. Complex environments and sensing	54		
A. Polarons in optical lattices	54		
B. Polarons in spinor quantum gases	55		
C. Polarons in baths with non-trivial topology	56		
IX. Magnetic polarons	57		

I. INTRODUCTION

Polarons, quasiparticles formed by dilute mobile impurities interacting with their environment, represent one of the most fascinating, powerful, and versatile concepts in quantum many-body physics. The concept of polarons originated in solid-state physics, in the seminal works of Landau and Pekar (Landau, 1957a,b; Landau and Pekar, 1948), and it was first applied to describe electrons interacting with lattice vibrations in crystals. Since then, polarons became a key ingredient for analyzing quantum systems consisting of many interacting particles. A main reason is that polarons are canonical realizations of quasiparticles, which (barring any phase transitions) smoothly emerge from bare impurities when their interaction with the environment is adiabatically switched on. Put forward by Landau, this argument was considered a highlight in *gedanken* experiments for more than half a century and leads to the powerful theory of quasiparticles, which dramatically simplifies the description of quantum many-body systems, as strong interaction effects can be included via the “dressing” of the bare impurities by excitations of the environment (Baym and Pethick, 2008; Landau, 1957a,b). The quasiparticle framework is therefore used across a vast range of energy scales in physics from ultracold atomic gases, liquid Helium, over condensed matter systems, to atomic nuclei and high energy quark gluon plasmas.

In recent years we have witnessed a surge of interest in polarons, driven largely by experimental breakthroughs in ultracold atomic gases and two-dimensional (2D) semiconductors. While polarons in these experimental platforms at first glance seem quite unrelated, with e.g. densities and masses differing by many orders of magnitude, they in fact share many properties and can be described using similar theoretical tools as will become apparent in this review. These striking similarities speak to the universality and general importance of polarons, and while we now have a fairly good understanding of some of their universal properties in these two systems, this convergence of fields opens up new research directions with far-reaching applications in quantum many-body physics, quantum simulation, and quantum sensing.

	Atomic gases	TMD monolayer
Dimension	quasi 1D, quasi 2D, 3D	2D
Impurity	Atom (boson/fermion)	Exciton or polariton (\sim boson)
Fermionic environment	Atoms (neutral)	Electrons/holes (negative/positive)
Bosonic environment	Atoms (neutral)	Excitons/polaritons (neutral)
Bound states	Dimer, trimer, ...	Bi-exciton, trion, ...
Density	$10^{12} \sim 10^{14} \text{cm}^{-3}$ [3D], tunable	$\sim 10^{12} \text{cm}^{-2}$, tunable
Bose-Bose interaction	Short range $1/r^6$, tunable	Short range $1/r^6$, tunable
Bose-Fermi interaction	Short range $1/r^6$, tunable	$1/r^4$, tunable
Fermi-Fermi interaction	Short range $1/r^6$, tunable	Screened Coulomb
Temperature range	Quantum degenerate to classical	Quantum degenerate to classical

TABLE I Properties of polarons in atomic gases and atomically thin transition metal dichalcogenides (TMDs).

Given these exciting developments, it is timely to provide a comprehensive review that brings together the diverse threads of polaron physics. This review provides a broad perspective on the common concepts used to understand polarons, bridging the gap between different subfields, and presents a unified treatment applicable to ultracold atomic gases, semiconductors, and beyond. It furthermore discusses impurities in both fermionic and bosonic environments, highlighting their similarities and differences. The review is aimed at both the expert researchers as well as PhD students entering this vast and rapidly evolving topic, and it aims to foster new collaborations and research directions.

A. Experimental platforms

We focus in this review on the realization of polarons in two experimental platforms, which in recent years have experienced substantial breakthroughs: ultracold atomic gases and atomically thin transition metal dichalcogenides. As we shall see, there are many deep parallels between polarons in these two experimental systems, which are compared in Table I. Note that here we will not discuss polarons in one-dimension, as this problem has quite unique aspects (for example, in 1D quasiparticles have a vanishing residue) and has been covered in a recently published and comprehensive review (Mistakidis *et al.*, 2023).

1. Atomic gases

Atomic gases are pristine quantum systems offering precise control over parameters such as the interaction strength, particle statistics, and system geometry (Baroni *et al.*, 2024b; Bloch *et al.*, 2008; Dalfovo *et al.*, 1999; Giorgini *et al.*, 2008). They are one of the most powerful quantum simulators available today, solving problems of practical importance for physics and materials science beyond the reach of classical computers (Daley *et al.*, 2022).

Relevant to this review, they provide an ideal platform for exploring polarons since one can create mixtures of a few impurity atoms immersed in a gas of either fermionic or bosonic majority atoms. By smoothly increasing the impurity-majority atom interaction with a Feshbach resonance (Chin *et al.*, 2010), one can then experimentally realize Landau’s gedanken experiment and test the emergence of quasiparticles. This flexibility, combined with high precision measurements opened up opportunities to study polarons systematically and in new regimes. Recent experimental progress furthermore enabled the immersion of Rydberg and ionic impurities in a bath of ultracold atoms. This introduces yet another paradigm in polaron physics, due to the long-range nature of the bath-impurity interactions.

2. Two-dimensional semiconductors

In parallel, atomically thin transition metal dichalcogenides (TMDs) such as MoSe₂, MoS₂, WSe₂ and WS₂ emerged as a powerful new platform for exploring truly two-dimensional (2D) physics (Schaibley *et al.*, 2016; Wang *et al.*, 2018a). TMDs are direct band-gap semiconductors with a rich set of degrees of freedom, experimental tuning knobs, and measurement techniques, opening up a vast playground for designing novel materials with exciting perspectives both for fundamental science and technology, and with capabilities complementing and often rivalling those of atomic gases. This includes a striking realization of polarons resulting from interactions between excitons playing the role of the impurity particles and itinerant electrons. Polarons have also been created using excitons in different spin states, and pioneering work with TMDs in optical microcavities pushed the boundaries of polaron research by creating novel hybrid light-matter quasiparticles.

	Fermi polaron	Bose polaron
Compressibility of bath	small	large
Number of particles in dressing cloud ΔN	$\mathcal{O}(1)$	can be macroscopic
Residue Z	$\mathcal{O}(1)$ (unless large mass)	can be very small
Minimal interaction parameters	scattering length a	scatt. lengths a, a_b + short range params.
$(n > 2)$ -body correlations important	only for light impurities	always for strong interactions
Orthogonality catastrophe	only for static impurities	possible for static and mobile impurities
Temperature effects	limited	strong due to BEC transition in the bath
Transition between polaron and dressed dimer	present	absent (smooth cross-over)

TABLE II General characteristics of Fermi and Bose polarons, which will be discussed in detail throughout this review.

B. Bose and Fermi polarons

The polarons explored in this review generally fall into two broad classes: Bose polarons formed when the majority particles are bosons, and Fermi polarons formed when the majority particles are fermions. As we shall see, whereas many properties of Fermi polarons are by now quite well understood even for strong interactions, many fundamental questions remain open for Bose polarons. The basic reason for this is that a Bose gas is much more compressible than a Fermi gas so that its density can be strongly modified in the vicinity of an impurity, leading to a dressing cloud that involves many particles. Microscopically, this means that correlations between the impurity and an arbitrary number of bosons may be important, complicating the description significantly, whereas correlations with many fermions are suppressed by the Pauli exclusion principle for short range interactions. Despite these challenges, recent experiments made significant progress in probing Bose polarons, and theoretical approaches provided new insights into their behavior. Table II compares the most important properties of Bose and Fermi polarons. For a detailed recent review of the Bose polaron, see Ref. (Grusdt *et al.*, 2024).

C. General properties of polarons

Before going into details, this section describes the generic properties of polarons that are robust and independent of the details of the specific system at hand. The concept of quasiparticles is based on expanding the energy E of a given system in increasing powers of their populations as (Baym and Pethick, 2008)

$$E = E_0 + \sum_{\mathbf{p}} \varepsilon_{\mathbf{p}} n_{\mathbf{p}} + \frac{1}{2} \sum_{\mathbf{p}, \mathbf{p}'} f_{\mathbf{p}, \mathbf{p}'} n_{\mathbf{p}} n_{\mathbf{p}'}. \quad (1)$$

Here, E_0 is the energy of the system when no quasiparticles are present, $\varepsilon_{\mathbf{p}}$ is the energy of a single quasiparticle with momentum \mathbf{p} , $n_{\mathbf{p}}$ its occupation number, and $f_{\mathbf{p}, \mathbf{p}'}$ is the interaction between quasiparticles. The system volume is taken to be unity throughout this review.

Equation (1) can be regarded as a Taylor expansion in the number of quasiparticles, and higher order terms neglected here correspond to three- and more-body interactions. One can straightforwardly extend Eq. (1) to the case when several kinds of quasiparticle are present by introducing a spin index.

For most systems, the zero momentum polaron has the smallest energy, and assuming rotational symmetry a Taylor expansion in momentum gives

$$\varepsilon_{\mathbf{p}} = \varepsilon + \frac{p^2}{2m^*}, \quad (2)$$

where ε is the polaron energy for zero momentum and m^* defines its effective mass, which generally differs from the bare impurity mass m due to the interactions with the environment. Another important property is the residue, which gives the overlap between the polaron wave function $|\Psi_{\mathbf{p}}\rangle$ and the eigenstate $c_{\mathbf{p}}^{\dagger}|\Psi_0\rangle$ for no interactions between the impurity and the majority particles, i.e.

$$Z_{\mathbf{p}} = |\langle \Psi_{\mathbf{p}} | \hat{c}_{\mathbf{p}}^{\dagger} | \Psi_0 \rangle|^2. \quad (3)$$

Here, $|\Psi_0\rangle$ is the many-body ground-state of the majority particles, and $\hat{c}_{\mathbf{p}}^{\dagger}$ creates an impurity particle with momentum \mathbf{p} . Physically, the residue measures how much the polaron wave function resembles that of a non-interacting (bare) impurity particle. The polaron is a well-defined quasi-particle when $Z_{\mathbf{p}} > 0$, and the residue moreover affects many observables.

A key quantity in the problem is the impurity spectral function

$$A(\mathbf{p}, \omega) = \int_{-\infty}^{\infty} dt e^{i\omega t} \langle \Psi_0 | \hat{c}_{\mathbf{p}}(t) \hat{c}_{\mathbf{p}}^{\dagger}(0) | \Psi_0 \rangle, \quad (4)$$

where $\hat{O}(t) = \exp(i\hat{H}t)\hat{O}\exp(-i\hat{H}t)$ is the operator \hat{O} in the Heisenberg picture, evolving under the action of the system Hamiltonian \hat{H} . Throughout this review, we use units in which the (reduced) Planck and Boltzmann constants \hbar and k_B are unity. In Eq. (4), we have assumed that there is only a single impurity particle present to simplify the usual expression for the spectral function of a particle in a many-body system (Mahan,

2000). The spectral function $A(\mathbf{p}, \omega)$ gives the overlap between the eigenstate $\hat{c}_{\mathbf{p}}^{\dagger}|\Psi_0\rangle$ of a non-interacting impurity and the eigenstates of the interacting system with energy ω relative to E_0 . It follows that an undamped polaron with energy $\varepsilon_{\mathbf{p}}$ and residue $Z_{\mathbf{p}}$ yields a contribution $2\pi Z_{\mathbf{p}}\delta(\omega - \varepsilon_{\mathbf{p}})$ to the spectral function. If the polaron is damped, the corresponding peak in the spectral function has a non-zero width proportional to its decay rate. In addition, the spectral function in general exhibits a continuum corresponding to excited many-body states.

The spectral function can be measured by radio-frequency (RF) spectroscopy in cold atomic gases and by optical spectroscopy in TMDs and therefore serves as a workhorse providing a wealth of information regarding polarons. One uses RF pulses that are spatially homogeneous over the sample size, to either inject impurity particles from a state that does not (or only weakly) interact with the majority particles to one that does, or vice versa to eject the impurities from the interacting state to a non-interacting auxiliary state. Ejection RF spectroscopy (Schlotzke *et al.*, 2009) probes the interacting ground-state, while injection spectroscopy also gives direct information regarding excited states. The transfer rates $I(\omega)$ obtained by ejection and injection are not independent, but actually linked via the relation $I_{\text{ej}}(\omega) = \exp[\beta(\Delta F + \omega)]I_{\text{inj}}(-\omega)$, where ω is the RF frequency measured with respect to the transition frequency of an isolated impurity, $\beta = 1/k_B T$ (with k_B the Boltzmann constant and T the temperature) and $\Delta F = F - F_0$ is the difference in free energy between the states with an interacting and a non-interacting impurity (Liu *et al.*, 2020b).

The real-time dynamics and polaron formation can be probed using Ramsey interferometry, which measures the Fourier transform of the spectral function

$$S(\mathbf{p}, t) = \langle \Psi_0 | c_{\mathbf{p}}(t) c_{\mathbf{p}}^{\dagger}(0) | \Psi_0 \rangle = iG^{>}(\mathbf{p}, t), \quad (5)$$

where $G^{>}$ is the so-called greater Green's function. Experimentally, $S(t)$ which is sometimes called the Loschmidt amplitude, is measured for $t \geq 0$ and one can then use $S(-t) = S(t)^*$ to obtain this function for negative times as well. For a well-defined polaron with energy $\varepsilon_{\mathbf{p}}$ and residue $Z_{\mathbf{p}}$, one has $S(\mathbf{p}, t) \rightarrow Z_{\mathbf{p}} \exp(-i\varepsilon_{\mathbf{p}}t)$ for $t \rightarrow \infty$ when the many-body continuum decoheres. This provides a useful interferometric way to measure the polaron energy complementing RF spectroscopy. Spin-echo interferometry is a more complex and powerful technique to explore many-body dynamics with strongly reduced noise. It measures $\langle \Psi_0 | \hat{c}_{\mathbf{p}} e^{i\hat{H}_0 t} e^{i\hat{H}t} e^{-i\hat{H}_0 t} e^{-i\hat{H}t} \hat{c}_{\mathbf{p}}^{\dagger} | \Psi_0 \rangle$ where \hat{H}_0 is the non-interacting part of the Hamiltonian. Equations (3)-(5) are straightforwardly generalized to non-zero temperature using a thermal average instead of $\langle \Psi_0 | \dots | \Psi_0 \rangle$. Further details regarding RF, Ramsey and spin-echo techniques can be found in earlier reviews (Massignan *et al.*, 2014; Schmidt *et al.*, 2018a).

One can of course calculate these observables directly from the (time-dependent) many-body wave function. They can also (except the spin echo signal) be obtained from the retarded impurity Green's function $G(\mathbf{p}, t) = -i\theta(t)\langle [\hat{c}_{\mathbf{p}}(t), \hat{c}_{\mathbf{p}}^{\dagger}(0)]_{\pm} \rangle$ where $[\hat{A}, \hat{B}]_{\pm} = \hat{A}\hat{B} \pm \hat{B}\hat{A}$ is for fermionic/bosonic impurities (Fetter and Walecka, 1971). Indeed, the energy $\varepsilon_{\mathbf{p}}$ of a polaron with momentum \mathbf{p} can be found by solving

$$\varepsilon_{\mathbf{p}} = \epsilon_{\mathbf{p}} + \text{Re} \Sigma(\mathbf{p}, \varepsilon_{\mathbf{p}}), \quad (6)$$

where $\Sigma(\mathbf{p}, \omega)$ is the self-energy and $G(\mathbf{p}, \omega) = 1/[\omega - \epsilon_{\mathbf{p}} - \Sigma(\mathbf{p}, \omega)]$ is the Green's function in momentum/frequency space with $\epsilon_{\mathbf{p}}$ is the dispersion of free impurities. In this review, we adopt the notation ε to denote quasiparticle energies and ϵ for bare energies. We suppress here and in the following an infinitesimal positive imaginary part of the frequency ω in the retarded Green's function. The polaron decay rate is $\Gamma_{\mathbf{p}} \propto -Z_{\mathbf{p}} \text{Im} \Sigma(\mathbf{p}, \varepsilon_{\mathbf{p}})$, its residue is

$$Z_{\mathbf{p}} = \frac{1}{1 - \partial_{\omega} \text{Re}[\Sigma(\mathbf{p}, \omega)]|_{\varepsilon_{\mathbf{p}}}}, \quad (7)$$

and its effective mass (at zero momentum) is

$$m^* = \frac{m}{Z[1 + \partial_{\varepsilon_{\mathbf{p}}} \text{Re}[\Sigma(\mathbf{p}, \varepsilon_{\mathbf{p}})]|_{p=0}}}. \quad (8)$$

The impurity spectral function can be found from the Green's function as $A(\mathbf{p}, \omega) = -2\text{Im} G(\mathbf{p}, \omega)$. For a single impurity, we moreover have $G(\mathbf{p}, t) = \theta(t)G^{>}(\mathbf{p}, t)$, which means that its real-time dynamics as probed via Ramsey interferometry can be calculated from the retarded Green's functions with no need to resort to more elaborate non-equilibrium Keldysh Green's functions.

Interactions with the impurity change the density of majority particles in its neighborhood. The total number ΔN of extra majority particles attracted to the impurity ($\Delta N < 0$ if they are repelled), often referred to as the number of particles in its "dressing cloud". It can be calculated from thermodynamic arguments by requiring that the density of the majority particles far away from the impurity remains constant. This corresponds to keeping constant the chemical potential μ_b of the majority particles and gives (Massignan *et al.*, 2005)

$$\Delta N \equiv \left(\frac{\partial n}{\partial n_i} \right)_{\mu_b} = - \left(\frac{\partial \varepsilon}{\partial \mu_b} \right)_{n_i} \quad (9)$$

where n/n_i is the density of the majority/impurity particles. In this review, the subscript b refers to majority ("bath") particles. When the impurity-majority particle interaction is short ranged and can be characterised by the associated scattering length a , it is useful to consider

the contact given by (Tan, 2008a,b)

$$C = 8\pi m_r \frac{\partial \varepsilon}{\partial(-1/a)}. \quad (10)$$

with $m_r = m_b m / (m_b + m)$ the reduced mass. The contact is proportional to the impurity-majority pair correlation function and describes the likelihood that a particle from the bath is close to the impurity. It also determines the coefficient of the $1/k^4$ tail of the impurity momentum distribution (Werner and Castin, 2012).

Simple scaling arguments show that many of these quantities are tightly linked (Scazza *et al.*, 2022). For Fermi polarons at a broad Feshbach resonance and at $T = 0$, one indeed finds

$$\varepsilon + \Delta N \epsilon_F + \frac{C}{16\pi m_r a} = 0, \quad (11)$$

with ϵ_F the Fermi energy of the bath, which leads to $\Delta N = -\varepsilon/\epsilon_F$ at resonance where $1/a = 0$. The properties of Bose polarons also depend on the scattering length a_b between the majority bosons, and one obtains

$$\varepsilon + \frac{3}{2}\Delta N \mu_b + \frac{C}{16\pi m_r a} + \frac{a_b}{2} \frac{\partial \varepsilon}{\partial a_b} = 0, \quad (12)$$

with $\mu_b = 4\pi a_b n / m_b$ for a dilute BEC.

Finally, the interaction between quasiparticles $f_{\mathbf{p},\mathbf{p}'}$ in Eq. (1) is key for understanding the thermodynamic and dynamical properties of a collection of polarons. In addition to any direct interaction between the impurities, an inherent source for $f_{\mathbf{p},\mathbf{p}'}$ is the exchange of modulations in the medium between two quasiparticles. As shown in Eq. (9), one impurity changes the density of majority particles in its surroundings, which is felt by another impurity. While this mediated interaction in general is attractive for two static and therefore distinguishable impurities, the interaction $f_{\mathbf{p},\mathbf{p}'}$ between quasiparticles can be either attractive or repulsive as discussed in Sec. VI.

The microscopic Hamiltonian describing impurity particles of mass m immersed in a bath of majority particles with mass m_b reads

$$H = \sum_j \frac{\mathbf{P}_j^2}{2m} + \sum_j \frac{\mathbf{p}_j^2}{2m_b} + \frac{1}{2} \sum_{j \neq k} V_i(\mathbf{R}_j - \mathbf{R}_k) + \frac{1}{2} \sum_{j \neq k} V_b(\mathbf{r}_j - \mathbf{r}_k) + \sum_{j,k} V(\mathbf{r}_j - \mathbf{R}_k), \quad (13)$$

where \mathbf{R}_j and \mathbf{P}_j (\mathbf{r}_j and \mathbf{p}_j) are the positions and momenta of the impurities (of the majority particles). The potentials V_i , V_b and V describe, respectively, the interactions between impurity particles, between majority particles and between impurity and majority particles.

The interaction between neutral atoms has a α_{vdW}/r^6 van der Waals form for large separations. Comparing the

latter with the kinetic term one obtains a length scale $(\alpha_{\text{vdW}} m)^{1/4} \sim 10^2 a_0$ (with a_0 the Bohr radius) which is typically much shorter than the interparticle distance $\gtrsim 5 \cdot 10^3 a_0$ in atomic gas experiments (Pethick and Smith, 2002), suggesting that it should be possible to describe the polaron in terms of a few parameters characterizing the low energy impurity-majority particle scattering. The interaction between excitons and electrons in TMDs has a classical charge-dipole $1/r^4$ tail, which for many purposes also can be regarded as short range.

The low energy scattering matrix for a pair of particles with center-of-mass momentum \mathbf{K} , energy ω and total mass $M = m + m_b$ with vanishing interaction range is

$$\mathcal{T}_v(\mathbf{K}, \omega) = \begin{cases} \left[\frac{m_r}{2\pi} \ln \left(\frac{\epsilon_B}{\omega - K^2/2M} \right) \right]^{-1} & \text{2D,} \\ \left(\frac{m_r}{2\pi a} + i \frac{m_r^{3/2}}{\sqrt{2\pi}} \sqrt{\omega - K^2/2M} \right)^{-1} & \text{3D} \end{cases} \quad (14)$$

with $\ln(-1) = i\pi$. A two-particle bound state with energy $\epsilon_B < 0$ is always present in 2D, while in 3D the $\mathbf{K} = 0$ scattering matrix has a pole at energy $\epsilon_B = -1/2m_r a^2$ only when the 3D scattering length a is positive.

A remarkable feature of atomic gases is that this bound state energy can be controlled by an external magnetic field, yielding so-called Feshbach resonances, which can be used to tune the scattering length a to essentially any value (Chin *et al.*, 2010). In a many-body setting, the corresponding interaction strength can be characterised by $k_n a$ with $1/k_n$ a typical interparticle spacing (Bloch *et al.*, 2008; Giorgini *et al.*, 2008). In 3D, strongly-interacting physics takes place near the so-called unitary point where a vacuum dimer appears, and correspondingly a diverges. In 2D, instead, there is always a bound state and therefore no analog of the unitary point: one can define a scattering length from $\epsilon_B = -1/2m_r a^2$, and the strongly interacting regime is found for $\ln(k_n a) \sim 0$. While the atomically-thin TMDs are truly 2D, ‘‘quasi-2D’’ configurations in atomic gases are created by squeezing one spatial (z) direction by means of a tight harmonic trap with frequency ω_z , and this leads to significant corrections to the 2D scattering matrix. A detailed treatment of scattering in quasi-2D may be found in (Levinson and Parish, 2013, 2015; Liu *et al.*, 2024; Petrov and Shlyapnikov, 2001).

A widely used approach to develop a low energy polaron theory is to systematically replace the microscopic interactions in Eq. (13) by the scattering matrices in Eq. (14), possibly generalized to take into account finite range and trapping effects. This method includes two-body correlations and gives accurate predictions for Fermi polarons in atomic gases and TMDs, as we will see in Secs. II and V, while it less faithfully describes polarons in Bose or multicomponent Fermi environments where correlations between three- and more particles can be important, as we will discuss in Secs. III and VIII.

Finally, we note that the scattering between ultracold atoms is in principle a multichannel problem, since the interaction mixes different hyperfine states. In particular, Feshbach molecules typically have a component in a closed channel. This gives rise to effective range corrections to the scattering matrices given Eq. (14), which can be important for narrow Feshbach resonances (Chin *et al.*, 2010; Massignan *et al.*, 2014). While the effects of the multichannel nature of the scattering in general are well understood for the Fermi polaron, there are several questions related to this for the Bose polaron as we shall see. In the rest of this review we will mostly use a single channel model where the impurity-bath interaction can be described through the potential $V(\mathbf{r})$, and explicitly state when a multichannel approach is used.

II. THE FERMI POLARON IN ATOMIC GASES

In a pioneering experiment, the Fermi polaron was created by admixing a small number of ^6Li atoms in one hyperfine state in a large quantum degenerate gas of ^6Li atoms in another hyperfine state (Schirotzek *et al.*, 2009). Using a Feshbach resonance to tune the interaction between the two hyperfine components, the Fermi polaron was systematically explored both in the weak and strong coupling regimes, see Fig. 1. This inspired several other experimental groups to explore the Fermi polaron in atomic gases (Adlong *et al.*, 2020; Cetina *et al.*, 2016, 2015; Darkwah Oppong *et al.*, 2019; Fritsche *et al.*, 2021; Kohstall *et al.*, 2012; Koschorreck *et al.*, 2012; Nascimbène *et al.*, 2009; Ness *et al.*, 2020; Ong *et al.*, 2015; Scazza *et al.*, 2017; Vivanco *et al.*, 2023; Wenz *et al.*, 2013; Yan *et al.*, 2019; Zhang *et al.*, 2012), and sparked a large amount of theoretical research. As a result, we have now a good understanding of many aspects of Fermi polarons in their simplest version where the bath is an ideal Fermi gas, even for strong impurity-fermion interactions. The atomic Fermi polaron has been thoroughly discussed in earlier reviews (Baroni *et al.*, 2024b; Chevy and Mora, 2010; Massignan *et al.*, 2014; Scazza *et al.*, 2022; Schmidt *et al.*, 2018a), and in this Section we therefore focus on its basic properties and theoretical methods it shares with its solid-state counterpart discussed in Sec. V. We will also discuss recent results not covered in earlier reviews.

As discussed in Sec. I.C, the range of the van der Waals $1/r^6$ interaction is typically small compared to the interparticle distance in atomic gases. It follows that a bath of single component fermions is essentially non-interacting at low temperatures due to the Pauli principle. In this case, one can ignore $V_i(\mathbf{R})$ and $V_b(\mathbf{r})$ in Eq. (13), and the Hamiltonian can be written as

$$\hat{H}_F = \sum_{\mathbf{k}} (\epsilon_{b\mathbf{k}} \hat{f}_{\mathbf{k}}^\dagger \hat{f}_{\mathbf{k}} + \epsilon_{\mathbf{k}} \hat{c}_{\mathbf{k}}^\dagger \hat{c}_{\mathbf{k}}) + \sum_{\mathbf{k}, \mathbf{k}', \mathbf{q}} V(\mathbf{q}) \hat{c}_{\mathbf{k}+\mathbf{q}}^\dagger \hat{f}_{\mathbf{k}'-\mathbf{q}} \hat{f}_{\mathbf{k}'} \hat{c}_{\mathbf{k}}, \quad (15)$$

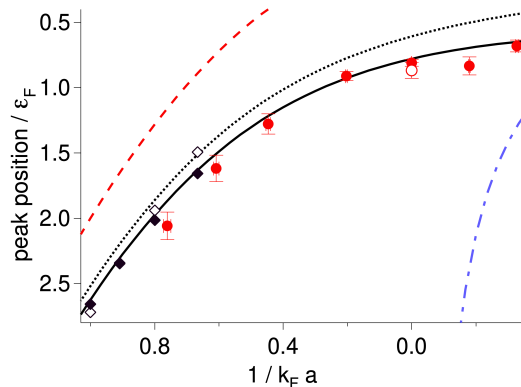


FIG. 1 **Attractive Fermi polarons.** Solid circles show the energy ϵ of the attractive Fermi polaron as a function of the impurity-fermion scattering length a . The open circle shows a measurement with reversed roles of impurity and environment. The dotted/solid line is the variational energy of the Ansatz (16) excluding/including final state interactions. The dashed line is the dimer energy in vacuum, and the blue dash-dotted line is the mean field energy. Solid/open diamonds are diagrammatic MC polaron/dressed dimer energies (Prokofev and Svistunov, 2008a). From (Schirotzek *et al.*, 2009).

where the operators $\hat{f}_{\mathbf{k}}^\dagger$ and $\hat{c}_{\mathbf{k}}^\dagger$ create a majority fermion and an impurity with momentum \mathbf{k} respectively. Here, $\epsilon_{b\mathbf{k}} = k^2/2m_b$ is the dispersion of the majority particles, and $V(\mathbf{q})$ is the Fourier transform of the interaction between the fermions and the impurity. Of the many different theoretical techniques that have been successfully applied to describe Fermi polarons (in both ultracold gases and TMDs), this section focuses on two: variational wave functions and Green's functions.

The incompressibility of the Fermi gas at low temperatures suggests a variational ansatz based on an expansion in the number of particle-hole excitations created by the impurity in the Fermi sea |FS>. For a single polaron with momentum \mathbf{p} in a zero-temperature Fermi sea, this expansion reads (Chevy, 2006)

$$|\psi_{\mathbf{p}}\rangle = \left(\sqrt{Z_{\mathbf{p}}} \hat{c}_{\mathbf{p}}^\dagger + \sum_{|\mathbf{q}| < k_F < |\mathbf{k}|} \alpha_{\mathbf{p}, \mathbf{q}, \mathbf{k}} \hat{c}_{\mathbf{p}+\mathbf{q}-\mathbf{k}}^\dagger \hat{f}_{\mathbf{k}} \hat{f}_{\mathbf{q}} + \dots \right) |\text{FS}\rangle \quad (16)$$

where k_F is the Fermi momentum. Minimizing the energy of this ansatz with respect to the parameters $Z_{\mathbf{p}}, \alpha_{\mathbf{p}, \mathbf{q}, \mathbf{k}} \dots$ leads to closed equations determining the various quasiparticles properties. For most purposes it is sufficient to truncate Eq. (16) at one particle-hole excitation, commonly called the Chevy ansatz, to obtain accurate results even for strong interactions. This is due to the Pauli principle suppressing $n > 2$ body correlations (Combescot *et al.*, 2007). Notable exceptions appear at large mass imbalance (Bazak and Petrov, 2017, 2018; Blume, 2012; Castin *et al.*, 2010; Efimov, 1973; Kartavtsev and Malykh, 2007; Levinsen and Parish, 2015;

Levinsen *et al.*, 2009; Li *et al.*, 2023; Liu *et al.*, 2022; Mathy *et al.*, 2011; Naidon, 2018; Petrov, 2003; Pricoupenko and Pedri, 2010; Sun and Cui, 2019).

For a contact interaction in a continuum system, the Chevy ansatz truncated at one particle-hole excitation is equivalent to the so-called ladder approximation for the self-energy, which reads

$$\Sigma(\mathbf{p}, \omega) = \sum_{\mathbf{q}} \mathcal{T}(\mathbf{p} + \mathbf{q}, \omega + \epsilon_{b\mathbf{q}}) n_F(\epsilon_{b\mathbf{q}} - \mu), \quad (17)$$

where we have generalised to the case of a non-zero temperature. Here, $n_F(\epsilon) = 1/[\exp(\epsilon/T) + 1]$ is the Fermi function and

$$\mathcal{T}(\mathbf{k}, \omega) = \frac{\mathcal{T}_0}{1 - \mathcal{T}_0[\Pi(\mathbf{k}, \omega) - \Pi_v(0, 0)]} \quad (18)$$

is the scattering matrix in the ladder approximation with $\mathcal{T}_0 = 2\pi a/m_r$. The pair propagator of an impurity and a fermion with total center-of-mass (COM) momentum/energy (\mathbf{k}, ω) in the presence of a Fermi sea reads

$$\Pi(\mathbf{k}, \omega) = \sum_{\mathbf{p}} \frac{1 - n_F(\epsilon_{b\mathbf{q}} - \mu)}{\omega - \epsilon_{\mathbf{k}-\mathbf{p}} - \epsilon_{b\mathbf{p}}}, \quad (19)$$

with its vacuum form $\Pi_v(\mathbf{k}, \omega)$ obtained by setting $n_F = 0$ in Eq. (19). The difference between Eq. (18) and the 3D vacuum scattering matrix \mathcal{T}_v in Eq. (14) is that Eq. (19) takes into account the Pauli blocking of available scattering states. Indeed, Eq. (14) is recovered when replacing $\Pi(\mathbf{k}, \omega) \rightarrow \Pi_v(\mathbf{k}, \omega)$ in Eq. (18). We have assumed a momentum-independent impurity-fermion interaction $V(\mathbf{q}) = g$, which is replaced by the 3D scattering matrix in Eq. (14) via the Lippmann-Schwinger equation

$$\mathcal{T}_0 = \mathcal{T}_v(0, 0) = g + g\Pi_v(0, 0)\mathcal{T}_v(0, 0). \quad (20)$$

Physically, the self-energy $\Sigma(\mathbf{k}, \omega)$ in Eq. (17) describes the energy shift coming from the impurity scattering fermions from inside to outside the Fermi sea. The Chevy ansatz Eq. (16) in fact also includes terms describing the scattering of the impurity on holes in the Fermi sea not included in the ladder approximation. While these terms are not important for continuum systems, they can be important when the hole states have significant spectral weight as in lattice systems (Amelio *et al.*, 2024).

A typical experimental RF injection spectrum is shown in Fig. 2, where the impurity spectral function for zero momentum is plotted as a function of the impurity-fermion interaction strength $X = -1/k_F a$. Two quasiparticle branches are clearly visible: one at negative energies denoted the attractive polaron (which is the ground state for $X \gtrsim 0.2$), and one at positive energies denoted the repulsive polaron. The repulsive polaron can roughly be thought of as the lowest scattering state and it is continuously connected to the non-interacting impurity par-

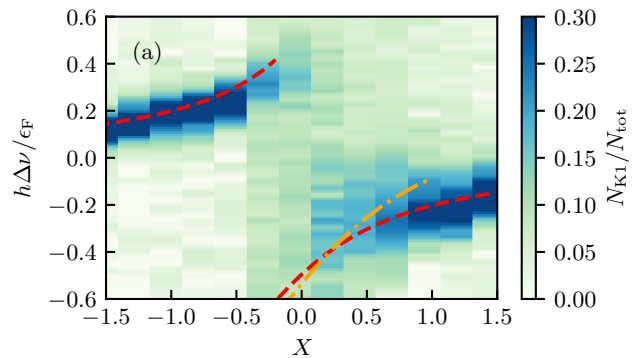


FIG. 2 **Complete Fermi polaron spectrum.** Spectral response of few bosonic ^{41}K impurities in a ^6Li Fermi sea, as a function of the interaction parameter $X = -1/(k_F a)$ and the RF detuning $\Delta\nu$. The upper/lower red lines (dashed) show the variational predictions for the repulsive/attractive polarons, and the orange line (dash-dotted) is the prediction for the dressed molecule. From Ref. (Fritsche *et al.*, 2021).

ticle for $a \rightarrow 0_+$ (Cui and Zhai, 2010; Massignan and Bruun, 2011). The red dashed lines are the energies of these two quasiparticles as obtained from the Chevy ansatz Eq. (16) truncated to one particle-hole excitation (ladder approx.), which agree very well with the experimental results. A multichannel model was used to obtain this agreement, since the Feshbach resonance used in this experiment is relatively narrow, giving rise to significant effective range effects [for details, see the earlier review (Massignan *et al.*, 2014)]. The orange dash-dotted line shows the energy of another fundamental quasiparticle, i.e., the dimer (formed by the impurity and a bath particle) dressed by particle-hole excitations in the bath, which becomes the ground state for $X \lesssim 0.2$ for the specific case in Fig. 2. This dressed molecule has however a low spectral weight in injection spectra, since its Franck-Condon overlap with a non-interacting impurity is small. The first order transition can alternatively be interpreted as the polaron abruptly changing its momentum from zero to the Fermi momentum (Cui, 2020). Figure 2 also shows a continuum of many-body states for strong interactions, which consists of states such as a molecule and a hole with total momentum zero.

In general, the ladder approximation provides a description of the energy of individual attractive and repulsive Fermi polarons which agrees remarkably well with most experiments. Still, many questions regarding the damping rate of polarons remain open, since they require a careful analysis of the different decay channels. For instance, even for weak coupling a non-self consistent ladder approximation predicts that the energy of a zero momentum ($p = 0$) repulsive polaron is increased by the mean-field term up into a continuum of $p > 0$ bare impurity states leading to damping, which is unphysical since these states experience the same mean-field shift

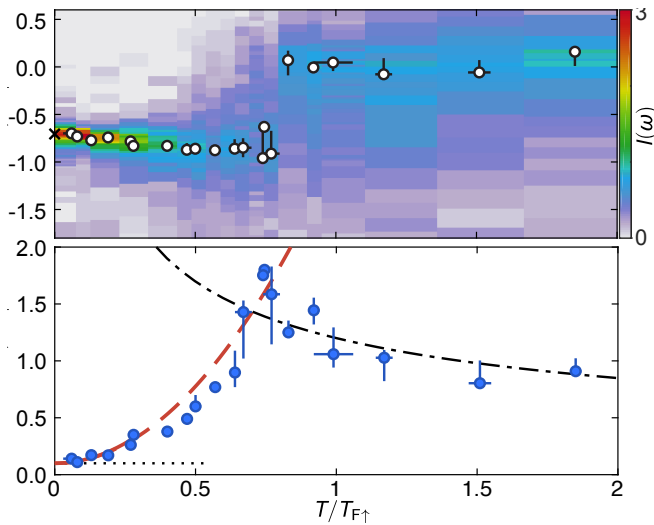


FIG. 3 **Temperature dependence of Fermi polarons.** Energy $\varepsilon/\varepsilon_F$ (top) and decay rate Γ/ε_F (bottom) of unitary Fermi polarons as a function of the bath temperature. The red dashed line shows the Fermi liquid prediction $\Gamma \propto T^2$ (Bruun *et al.*, 2008), and the black dash-dotted line indicates the high-temperature behavior $\Gamma \propto 1/\sqrt{T}$ (Enss *et al.*, 2011; Sun and Leyronas, 2015). From Ref. (Yan *et al.*, 2019).

and therefore have a higher energy so that there is no damping from such processes. Bruun *et al.* (2008) explored the collisional damping of polarons for non-zero momenta and temperatures using the Boltzmann equation, and Adlong *et al.* (2020) used a time-dependent variational approach to show that the lifetime of repulsive polarons is dominated by many-body dephasing in both 2D and 3D. The damping of polarons and dressed dimers was further investigated theoretically and experimentally in Refs. (Bruun and Massignan, 2010; Cetina *et al.*, 2015; Kohstall *et al.*, 2012; Schmidt and Enss, 2011).

Further details on Fermi polaron experiments together with the many theoretical techniques that have been used to analyze them have been described in detail in earlier reviews (Massignan *et al.*, 2014; Scazza *et al.*, 2022; Schmidt *et al.*, 2018a). In the next two subsections, we will briefly discuss new developments regarding the Fermi polaron in atomic gases not covered in these earlier reviews. Section VI concerns the interaction $f_{\mathbf{p},\mathbf{p}'}$ between two Fermi polarons, which in some sense is “the second half” of Landau’s quasiparticle theory crucial for many dynamical and thermodynamic properties, and for which experimental results have been obtained only recently.

A. Temperature effects

Most experiments have explored the Fermi polaron at a low temperature $T \ll T_F$ with $T_F = \varepsilon_F$ the Fermi temperature. As the temperature of a Fermi gas containing dilute impurities is raised, one expects that the Fermi-

liquid picture of weakly-interacting quasiparticles will eventually stop working. At temperatures well above T_F , an accurate description in terms of a classical Boltzmann approach should eventually be obtainable. The transition between these two regimes was studied in detail in Ref. (Yan *et al.*, 2019) for unitarity-limited impurity-bath interactions with $1/a = 0$. For low temperatures $T \lesssim 0.75T_F$ the spectra showed a sharp peak corresponding to the attractive polaron, whose energy starts from the $T = 0$ prediction $\varepsilon = -0.6\varepsilon_F$ and lowers gently with increasing temperature. One reason for this is that the Pauli repulsion between bath fermions gradually decreased in agreement with theoretical calculations (Muklerin *et al.*, 2019; Tajima and Uchino, 2018). Likewise, the width of the polaron peak increases as T^2 due to the collisional broadening as expected in Fermi liquids (Bruun *et al.*, 2008). It reaches a width $\gtrsim \varepsilon_F$ corresponding to a lifetime smaller than the Fermi time $1/\varepsilon_F$ at $T \sim 0.75T_F$, see Fig. 3. Above this temperature the maximum of the RF spectra suddenly shifts and remains locked at the energy $\omega \sim 0$, and the peak width decreases slowly as $\Gamma \sim 1/\sqrt{T}$, precisely as expected in a classical Boltzmann gas with unitarity limited interactions. In this regime, indeed, one has a cross section $\sigma_{\text{th}} \sim 1/k_{\text{th}}^2 \sim 1/T$ and a typical velocity $v_{\text{th}} \sim \sqrt{T}$, giving a scattering rate $\Gamma_{\text{th}} = nv_{\text{th}}\sigma_{\text{th}} \sim 1/\sqrt{T}$, and an energy given to lowest order by the real part of the scattering amplitude, i.e., $\varepsilon \sim 0$. As we shall see in Sec. III.K, similar effects are observed for the Bose polaron in the classical regime.

This experiment further permitted precise measurements of the temperature dependence of Tan’s contact. In the non-degenerate regime, the latter decreased rapidly as predicted by the third-order virial calculation of Ref. (Liu and Hu, 2010), and an excellent agreement at all temperatures was obtained using a finite-temperature variational method (Liu *et al.*, 2020a). The experiment also confirmed the $T = 0$ polaron effective mass $m^* \sim 1.2m$ at unitarity $1/a$ predicted from the ladder approximation, as well as the excess majority fermions around an impurity atom $\Delta N \sim 0.6$ in perfect agreement with the value $-\varepsilon/\varepsilon_F$ given by Eq. (11). Interestingly, ΔN displayed no detectable dependency on the impurity density up to concentrations as large as 30%, indicating an inherent robustness of a Fermi liquid description in terms of polarons at low temperatures.

B. Non-equilibrium dynamics

A characteristic time-scale for the onset of many-body dynamics is $\tau_F = 1/\varepsilon_F$. For solid state systems this is typically very short ($\tau_F \simeq 10^{-16}\text{s}$), whereas $\tau_F \simeq 10^{-6}\text{s}$ in atomic gases due to their diluteness and large atomic mass. This makes them well suited for studying quantum many-body dynamics (Schmidt *et al.*, 2018a). Following theoretical proposals in Refs. (Goold *et al.*, 2011; Knap

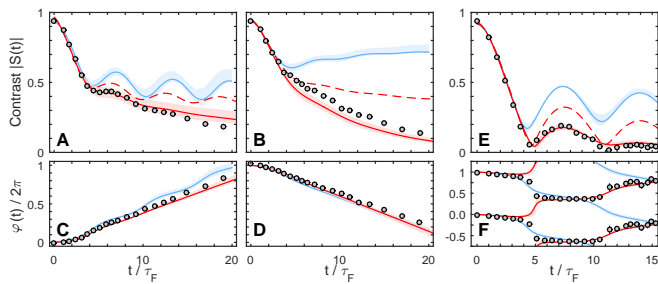


FIG. 4 **Dynamical formation of Fermi polarons.** The top and bottom rows show the contrast $|S(t)|$ and the phase $\varphi(t)$ measured by Ramsey spectroscopy as a function of the interaction time t . From left to right, the three columns illustrate the results obtained in the repulsive polaron regime ($X = -0.2$, with $X \equiv -1/k_F a$), in the attractive polaron regime ($X = 0.9$), and for resonant interactions ($X = 0.1$). The corresponding Chevy ansatz calculations are shown by solid blue lines, and the red lines indicate the results of the FDA calculations (solid: at the measured temperature; dashed: at $T = 0$). From Ref. (Cetina *et al.*, 2016).

et al., 2012), the dynamical formation of the Fermi polaron was explored in Ref. (Cetina *et al.*, 2016) using a Ramsey scheme, as illustrated in the top panel of Fig. 4: ^{40}K impurity atoms were driven by a $\pi/2$ pulse into an equal superposition of two hyperfine states with one of them interacting with a surrounding bath of fermionic ^6Li atoms; the system was then allowed to evolve for a time t after which a second $\pi/2$ probe pulse was applied.

The response function probed by this experimental procedure is given by Eq. (5), and the bottom panel of Fig. 4 shows its experimentally-measured amplitude and phase as a function of time for different impurity-majority interaction strengths. For short times, the dynamics is governed by high energy ($\epsilon \gg \epsilon_F$) two-body impurity-fermion scattering, which is independent of the quantum statistics of the bath (Parish and Levinsen, 2016). The dynamics can be solved analytically in this regime as discussed in detail for the Bose polaron in Sec. III.L. For weak interactions, one observes a linear evolution of the phase consistent with $S(t) = Z \exp(-i\epsilon t)$ coming from the existence of well-defined attractive or repulsive polarons with energy ϵ and residue Z as discussed below Eq. (5) (the experiment had no momentum resolution). Figure 4 however shows that the amplitude decays exponentially for long times instead of approaching Z , which can be explained quantitatively by decoherence due to polaron-polaron scattering as described with the Boltzmann equation (Cetina *et al.*, 2015).

For strong interactions close to resonance, the amplitude $|S(t)|$ in Fig. 4 oscillates strongly while the phase exhibits plateaus as a function of time. This behavior is for early to intermediate times well described by the zero-temperature Chevy ansatz Eq. (16) generalized to time-dependent phenomena (Parish and Levinsen, 2016), but the latter overestimates the amplitude for longer times

where thermal effects play a role. This was later improved by extending the underlying variational method to finite temperature dynamics (Liu *et al.*, 2019). The red lines in Fig. 4 show an exact solution for a static impurity in a Fermi gas taking into account a non-zero temperature obtained using a functional determinant approach (FDA) (Knap *et al.*, 2012; Schmidt *et al.*, 2018a). This approach agrees excellently with the experimental data indicating that recoil effects are small or masked by thermal effects. The oscillations at strong interactions can be attributed to the simultaneous presence of attractive and repulsive polaron peaks in the spectral function, giving rise to a quantum beat between the two polaron states and a revival of the contrast after a time corresponding to their energy difference. Similar effects for the Bose polaron are discussed in Sec. III.L.

As discussed above, the equilibrium spectral function can be measured by a weak RF pulse coupling two internal states of the impurity so that linear response applies. For stronger pulses, on the other hand, the impurity performs Rabi oscillations between the two internal states well beyond what can be described by linear response. When the Rabi frequency Ω is small compared to the Fermi energy ϵ_F , the polaron has time to form and the frequency is reduced by a factor $\Omega \rightarrow \sqrt{Z}\Omega$ due to the smaller overlap between the polaron wave function and the non-interacting plane wave, see Eq. (16). Rabi oscillations have been used to measure the residue and lifetime of Fermi polarons in Refs. (Adlong *et al.*, 2020; Darkwah Oppong *et al.*, 2019; Kohstall *et al.*, 2012; Scazza *et al.*, 2017). When the Rabi frequency is large, intriguing experimental results show large deviations from linear response (Vivanco *et al.*, 2023). To analyse such experiments requires solving the challenging non-equilibrium many-body problem of an impurity strongly driven by a Rabi pulse (Knap *et al.*, 2013), which has been approached using variational, diagrammatic, and quantum kinetic theories (Adlong *et al.*, 2020; Hu and Liu, 2023; Wasak *et al.*, 2024). Thermodynamic relations generalizing Eqs. (11)-(12) to presence of Rabi driving and non-zero temperatures have been derived in Ref. (Mulkerin *et al.*, 2024).

III. THE BOSE POLARON

We now turn to the properties of Bose polarons, which in their simplest incarnation emerge when a mobile quantum impurity is immersed into a weakly interacting Bose gas that may have undergone condensation. At first sight, the Bose polaron problem seems very similar to that of the Fermi polaron discussed in the previous section, but as we shall see there are surprisingly many open questions and conflicting theoretical predictions concerning its properties in the strongly interacting regime.

The setting of a mobile impurity interacting with the

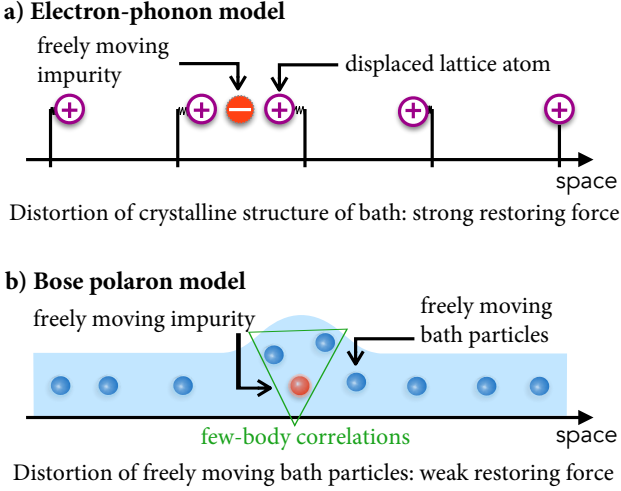


FIG. 5 **The Bose polaron problem.** (a) An electron moving through a crystal generates small displacements of the atoms from their equilibrium positions, which are well described by a linear approximation. (b) In a Bose gas, on the other hand, the impurity can strongly distort the surrounding Bose gas, and correlations between the impurity and $n = 1, 2, \dots$ bosons (here exemplified by 3-body Efimov correlations) may be important.

low energy phonon modes of the bath is reminiscent of electrons interacting with a bath of crystal phonons (Landau and Pekar, 1948). In the latter case, the theoretical model is derived from considering how the negative electron charge displaces the positively charged ions in the crystal of the solid away from their equilibrium positions, see Fig. 5(a). Assuming this displacement to be small, quantization gives rise to bosonic phonons, which couple *linearly* to the electrons. The Bose polaron problem at hand is however distinct from such a linear model. The main reason is that the bosonic particles, which are atoms or molecules in the context of quantum degenerate gases and excitons in the context of TMDs, are *not fixed* in space and thus can move freely, see Fig. 5(b). As a result, the "stiffness" of the environment is much reduced and a linear approximation is bound to fail. This makes the description of Bose polarons a particularly challenging problem. For a detailed review of the Bose polaron including the Fröhlich case, see Ref. (Grusdt *et al.*, 2024).

The basic Hamiltonian for the Bose polaron problem is given by Eq. (13), which in second quantized form reads

$$\begin{aligned} \hat{H}_B = & \sum_{\mathbf{k}} (\epsilon_{\mathbf{k}} \hat{c}_{\mathbf{k}}^\dagger \hat{c}_{\mathbf{k}} + \epsilon_{b\mathbf{k}} \hat{b}_{\mathbf{k}}^\dagger \hat{b}_{\mathbf{k}}) + \sum_{\mathbf{k}, \mathbf{k}', \mathbf{q}} \frac{V_b(\mathbf{q})}{2} \hat{b}_{\mathbf{k}+\mathbf{q}}^\dagger \hat{b}_{\mathbf{k}'-\mathbf{q}}^\dagger \hat{b}_{\mathbf{k}'} \hat{b}_{\mathbf{k}} \\ & + \sum_{\mathbf{k}, \mathbf{k}', \mathbf{q}} V(\mathbf{q}) \hat{c}_{\mathbf{k}+\mathbf{q}}^\dagger \hat{b}_{\mathbf{k}'-\mathbf{q}}^\dagger \hat{b}_{\mathbf{k}'} \hat{c}_{\mathbf{k}}, \end{aligned}$$

where $\hat{b}_{\mathbf{k}}^\dagger$ creates a bosonic majority particle. The second term in Eq. (21) describes the interaction between the majority bosons, which is assumed to be repulsive

in order to stabilise the system. In contrast to fermions, the interaction V_b between the majority bosons, which is assumed to be repulsive, is important even when short range as it stabilises the system. The last term in Eq. (21) may be written as $\sum_{\mathbf{k}, \mathbf{q}} V(\mathbf{q}) \exp\langle -i\mathbf{R}\mathbf{q} \rangle \hat{b}_{\mathbf{k}+\mathbf{q}}^\dagger \hat{b}_{\mathbf{k}}$.

The repulsion between the bosons is typically rather weak, resulting in an environment that, compared to an ideal Fermi gas, has a high compressibility. As a consequence, the density around the impurity can be greatly increased with a large number of bosons in the polaron dressing cloud, see Fig. 5. Equivalently, while the Pauli principle typically suppresses correlations of the impurity with more than one fermion, a priori no such prohibition of $n > 2$ body correlations is present in the case of Bose polarons. Indeed, bosonic gases generally support Efimov bound states at strong interactions (Braaten and Hammer, 2006; Efimov, 1970; Greene *et al.*, 2017; Naidon and Endo, 2017). These three-body bound states have been observed for the first time in cold atoms (Kraemer *et al.*, 2006; Zaccanti *et al.*, 2009), with experimental signs of bound states involving four bosons (tetramers) also reported (Ferlaino *et al.*, 2009) in agreement with theory (Hammer and Platter, 2007; Schmidt and Moroz, 2010; von Stecher *et al.*, 2009). Bound states involving even more particles are also predicted (Blume and Yan, 2014; von Stecher, 2011). While the physics of weakly bound dimers is universally captured by the scattering lengths, the description of Efimov states requires the specification of another three-body parameter, which intrinsically carries information about the short-distance physics. As a result, the properties of Efimov states, such as their energy and size, depend on short-range physics (the van-der Waals range for cold atoms (Chapurin *et al.*, 2019; Mestrom *et al.*, 2017; Schmidt *et al.*, 2012b; Wang *et al.*, 2012)). As it turns out, these Efimov states can hybridize with the Bose polaron state further complicating the theoretical description. Contrary to the Fermi polaron, one therefore in general needs length scales in addition to the scattering length a in order to describe Bose polarons like for example the boson-boson scattering length a_b , a three body-parameter, or the ranges of the interaction potentials. Related to this, while effective range effects are important only in the vicinity of narrow Feshbach resonances for the Fermi polaron, they are more important for the Bose polaron. They naturally emerge in two-channel models for Feshbach resonances (Levinsen *et al.*, 2015; Massignan *et al.*, 2014; Yoshida *et al.*, 2018a), but also in single channel models where one is often forced to consider potentials with non-vanishing ranges, see for example Refs. (Christianen *et al.*, 2024; Drescher *et al.*, 2020; Guenther *et al.*, 2021; Massignan *et al.*, 2005).

Due its complexity, the Bose polaron problem has been theoretically studied using many different techniques, as summarized in Fig. 6. One challenge when comparing these predictions arises from the fact that the corresponding works apply different approximations to the Hamil-

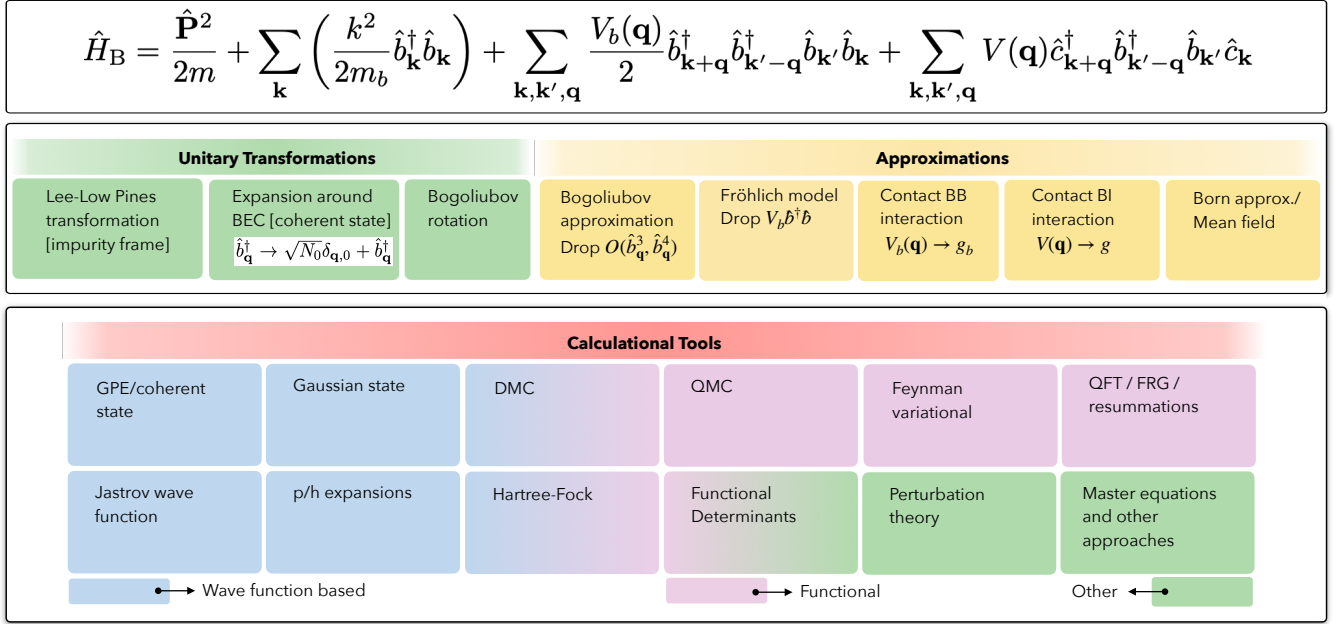


FIG. 6 **Theoretical approaches for the Bose polaron.** Illustration of approximation schemes and transformations for the Bose polaron problem, and overview of common theoretical techniques.

tonian (21). In particular, it is difficult to compare variational energies arising from different Hamiltonians, and hence there is no notion of “better” wave function by comparison of results. As an example, we have already assumed a single channel model for the boson-impurity interaction in Eq. (21), even though the compressibility of the BEC may make its underlying two-channel Feshbach nature important as we shall see. We now turn to a more detailed discussion of the theoretical and experimental results on Bose polarons.

A. Ladder approximation

Inspired by its accuracy for the Fermi polaron, the ladder approximation was in a pioneering paper adapted to explore the Bose polaron (Rath and Schmidt, 2013). While it is not as accurate for the Bose polaron, it describes correctly the essential features of the problem and sets the stage for the ensuing discussion. In this work, the Bogoliubov approximation was used to describe the bosonic bath assuming a weakly interacting homogeneous BEC. Keeping all terms up to second order in the bosonic creation and annihilation operators, the Hamiltonian in Eq. (21) can be written as

$$H_{\text{Bog}} = \sum_{\mathbf{k}} E_{\mathbf{k}} \hat{\gamma}_{\mathbf{k}}^\dagger \hat{\gamma}_{\mathbf{k}} + \sum_{\mathbf{p}} (\epsilon_{\mathbf{p}} + g n_0) \hat{c}_{\mathbf{p}}^\dagger \hat{c}_{\mathbf{p}} \quad (21)$$

$$+ g \underbrace{\sum_{\mathbf{p}, \mathbf{q}} M(\mathbf{q}) \hat{c}_{\mathbf{p}+\mathbf{q}}^\dagger \hat{c}_{\mathbf{p}} (\hat{\gamma}_{-\mathbf{q}}^\dagger + \hat{\gamma}_{\mathbf{q}})}_{\text{Fröhlich interaction}} + g \sum_{\mathbf{p}, \mathbf{q}, \mathbf{k}} \hat{c}_{\mathbf{p}+\mathbf{q}}^\dagger \hat{c}_{\mathbf{p}} \hat{b}_{\mathbf{k}-\mathbf{q}}^\dagger \hat{b}_{\mathbf{k}}$$

Here $\hat{\gamma}_{\mathbf{p}}^\dagger = u_{\mathbf{p}} \hat{b}_{\mathbf{p}}^\dagger + v_{\mathbf{p}} \hat{b}_{-\mathbf{p}}$ creates a Bogoliubov excitation in the BEC with energy $E_{\mathbf{p}} = \sqrt{\epsilon_{\mathbf{p}b}(\epsilon_{\mathbf{p}b} + 2\mu)}$, $\mu = g_b n_0$ is the chemical potential, $u_{\mathbf{p}}^2 = 1 + v_{\mathbf{p}}^2 = [(\epsilon_{\mathbf{p}b} + \mu)/E_{\mathbf{p}} + 1]/2$, and n_0 is the condensate density (Pethick and Smith, 2002; Pitaevskii and Stringari, 2016). We have assumed weak short-range boson-boson and boson-impurity interactions with strengths $g_b = 4\pi a_b/m_b$ and $g = 2\pi a/m_r$. A constant term giving the energy of the BEC ground state is omitted in Eq. (21), $M(\mathbf{q}) = \sqrt{n_0 \epsilon_{\mathbf{q}b}/E_{\mathbf{q}}}$, and all momenta \mathbf{k} and \mathbf{q} for the boson and Bogoliubov operators are different from zero. In the last term we kept the expression in terms of the untransformed boson operators for notational brevity.

The second term in Eq. (21) is the kinetic energy of the impurity shifted by a mean-field interaction term with the condensate, and the third term describes how it emits or absorbs Bogoliubov modes as it moves through the BEC. The first three terms correspond to the Fröhlich model describing how an electron emits or absorbs phonons in a crystal, see Fig. 5, and it was the basis of early investigations of the Bose polaron (Cucchietti and Timmermans, 2006; Tempere *et al.*, 2009). As discussed in the previous section and first noted in (Rath and Schmidt, 2013), and later rigorously shown in a perturbative calculation (Christensen *et al.*, 2015), the Fröhlich Hamiltonian alone is however insufficient to describe impurities that interact strongly with atomic BECs such as realized by Feshbach resonances. In the following, we will therefore not discuss in detail the many papers analyzing the Bose polaron within the Fröhlich model and refer instead the reader to earlier reviews (Alexandrov and Mott,

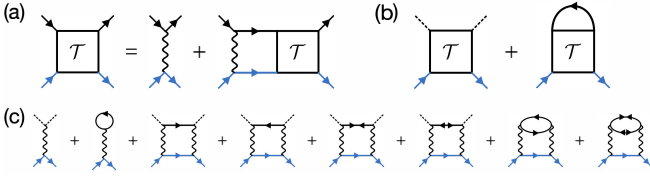


FIG. 7 **Feynman diagrams for Bose polarons.** (a) Ladder approximation of the \mathcal{T} -matrix. (b) Self-energy in the ladder approximation. (c) Second order self-energy. Solid blue and dashed/solid black lines indicate, respectively, impurities and condensate/non-condensate bath bosons.

1996; Devreese, 1996; Grusdt and Demler, 2016).

Note that even when the last term in Eq. (21) is included, the Bogoliubov approximation omits terms involving three and four boson operators. These terms describe the interaction between Bogoliubov modes and can typically be neglected when the gas parameter $n a_b^3$ is small (Pethick and Smith, 2002; Pitaevskii and Stringari, 2016). They may however be important in the presence of an impurity, which can increase the surrounding density so much that the gas parameter becomes large thereby invalidating the Bogoliubov approximation as we shall discuss later (Christianen *et al.*, 2024).

In Ref. (Rath and Schmidt, 2013) a quantum field theoretical resummation approach was applied to analyze the spectrum of Eq. (21). In analogy with the ladder approximation for the Fermi polaron one includes the diagrams shown in Fig. 7, which gives for the impurity self-energy

$$\begin{aligned} \Sigma(\mathbf{k}, \omega) = & n_0 \mathcal{T}(\mathbf{k}, \omega) + \sum_{\mathbf{q}} u_{\mathbf{q}}^2 n_B(E_{\mathbf{q}}) \mathcal{T}(\mathbf{k} + \mathbf{q}, \omega + E_{\mathbf{q}}) \\ & + \sum_{\mathbf{q}} v_{\mathbf{q}}^2 [1 + n_B(E_{\mathbf{q}})] \mathcal{T}(\mathbf{k} + \mathbf{q}, \omega - E_{\mathbf{q}}) \end{aligned} \quad (22)$$

where $n_B(E) = 1/[\exp(E/T) - 1]$ is the Bose distribution function. The in-medium scattering matrix is again given by Eq. (18) but now with the boson-impurity pair propagator in the presence of the BEC given by

$$\Pi(\mathbf{k}, \omega) = \sum_{\mathbf{p}} \left\{ \frac{u_{\mathbf{p}}^2 [1 + n_B(E_{\mathbf{p}})]}{\omega - \epsilon_{\mathbf{k}+\mathbf{p}} - E_{\mathbf{p}}} + \frac{v_{\mathbf{p}}^2 n_B(E_{\mathbf{p}})}{\omega - \epsilon_{\mathbf{k}+\mathbf{p}} + E_{\mathbf{p}}} \right\}. \quad (23)$$

The first term in Eq. (22) describes the scattering of the impurity on bosons in the condensate with density n_0 as illustrated by the first diagram in Fig. 7(b), whereas the second and third terms describe the scattering on bosons excited out of the condensate either due to temperature or boson-boson interactions as illustrated by the second diagram in Fig. 7(b). The ladder approximation includes two-body correlations between the impurity and the bosons exactly at the vacuum level but ignores $n \geq 3$ -body correlations. Note that the last term in Eq. (21) describing the scattering of the impurity on bosons outside the condensate is crucial for obtaining this, which tech-

nically is why the Fröhlich Hamiltonian is insufficient to describe strong interactions¹.

The first term for the self-energy in Eq. (22) gives the following self-consistent equation or the energy ε of a zero momentum Bose polaron at zero temperature,

$$\frac{\varepsilon}{\epsilon_n} = \frac{2m_b}{3\pi m_r} \frac{1}{(k_n a)^{-1} - \Xi(\varepsilon/\epsilon_n, k_n \xi, m/m_b)}. \quad (24)$$

We define $k_n = (6\pi^2 n_0)^{1/3}$ and $\epsilon_n = k_n^2/2m_b$ as a characteristic momentum and energy. For $m = m_b$, the quantity Ξ takes a remarkably simple analytic form,

$$\Xi(e, x, 1) = \frac{1 - e x^2 \operatorname{arctanh}(\sqrt{1 + e x^2})}{\sqrt{2} \pi x \sqrt{1 + e x^2}}. \quad (25)$$

The ladder approximation therefore predicts that the energy of the Bose polaron measured in units of ϵ_n depends only on the impurity-boson scattering length a , the BEC healing length ξ , and the mass ratio m/m_b .

The spectral function $A(\mathbf{k}, \omega) = -2\operatorname{Im}G(\mathbf{k}, \omega)$ of an impurity in a BEC obtained from the ladder approximation is plotted in Fig. 8 for zero momentum ($\mathbf{k} = 0$), mass ratio $m/m_b = 1$, and different boson-boson scattering lengths. We see that it is very similar to that of the Fermi polaron also plotted in Fig. 8, and from this we identify the sharp quasiparticle peak at negative energies with an attractive Bose polaron whose energy approaches the bound state energy $-1/2m_r a^2$ for $a \rightarrow 0_+$, and the broader peak at positive energy with a damped repulsive polaron. Contrary to the Fermi polaron however, there is no crossing of the attractive polaron and molecule energies since they have the same quantum statistics and therefore can hybridize. The broadening of the upper branch comes from decay of the polaron into a continuum, which to be described correctly however requires the inclusion of $n > 2$ body correlations ignored in the ladder approximation. This remains an open and challenging problem, like for the Fermi polaron.

Figure 8 shows that the ladder approximation predicts the Bose polaron energy to depend rather weakly on the boson-boson scattering length a_b via the BEC healing length. Taking an ideal BEC with $a_b = 0$ gives the energy $\varepsilon = -(2\pi^2 n_0^2)^{1/3}/m_r = -0.7115\bar{\epsilon}_n$ at unitarity $1/a = 0$ with $\bar{\epsilon}_n = k_n^2/(4m_r)$.² For equal masses, this energy is slightly lower than the energy $\varepsilon = -0.61\epsilon_F$ of the Fermi polaron at unitarity as obtained from the ladder

¹ A renormalization group analysis of the relevance of coupling constants was performed in (von Milczewski *et al.*, 2024).

² We introduce here $\bar{\epsilon}_n = k_n^2/(4m_r)$, defined in terms of the reduced two-body mass m_r . For $m = m_b$, $\bar{\epsilon}_n$ coincides with the previously-introduced $\epsilon_n = k_n^2/(2m_b)$.

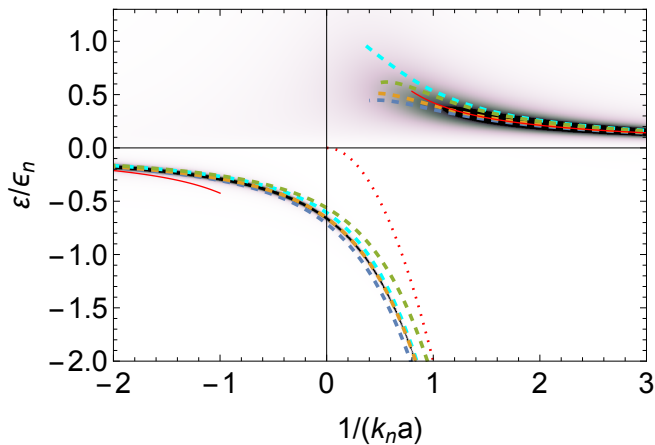


FIG. 8 **Impurity spectral function in a BEC** obtained from the ladder approximation for equal masses $m = m_b$, $k_n \xi = 2$, and zero momentum. The dashed lines show the energies computed from Eq. (24) for $k_n \xi = 1$ (green), 2 (yellow) and ∞ (blue). The latter corresponds to an ideal BEC. For comparison, the cyan dashed lines are the attractive and repulsive Fermi polaron. The red solid and dotted lines are the mean-field energy and the energy of the vacuum dimer.

approximation. The ladder approximation also gives

$$Z = \frac{2}{3 - \varepsilon/gn_0} \quad \text{and} \quad C = \frac{3\pi^2 k_n}{2} Z \left(\frac{\varepsilon}{\bar{\varepsilon}_n} \right)^2 \quad (26)$$

for the residue (Yan *et al.*, 2020) and Tan’s contact. The effective mass is $m^* = m + z m_b$, where z is a function which monotonously grows from 0 in the BCS limit $1/k_n a \rightarrow 0_-$ to 1 in the BEC limit $1/k_n a \rightarrow 0_+$. At unitarity one finds $Z = 2/3$, $z = 1/(3 + 2m_b/m)$ and $C = 4.997 k_n$. These results for an ideal BEC are however an artifact of the ladder approximation. In fact, the polaron energy in an ideal BEC approaches the mean-field value (i.e., it diverges to $-\infty$ approaching unitarity) while its residue vanishes due to a macroscopic number of bosons in its dressing cloud as will be discussed in Sec. III.C. This is well beyond the reach of the ladder approximation, which describes correlations between the impurity and at most one boson at a time. The ladder approximation was also used to identify attractive and repulsive Bose polarons in 2D (Cardenas-Castillo and Camacho-Guardian, 2023).

All in all, the ladder approximation suggests that the behavior of Bose polarons should be rather similar to that of Fermi polarons where two well-defined quasiparticles exist, and where, as the only major difference, the polaron-to-molecule transition in the ground state is replaced by a smooth crossover. However, while these features are qualitatively correct, it turns out that experimental observations pointed quickly to a much more involved problem which still presents many open questions, as we will describe in the following Sections.

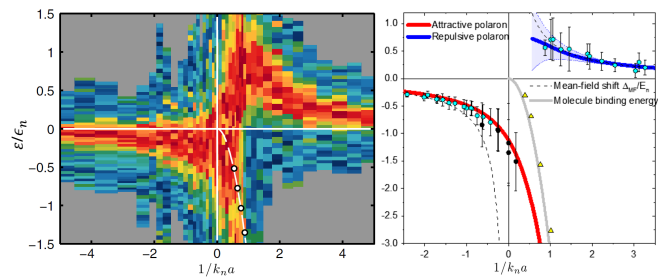


FIG. 9 **First observations of Bose polarons.** RF injection spectra as a function of interaction strength $1/k_n a$ showing two branches corresponding to the repulsive and attractive Bose polaron. Left panel: A mass balanced $m = m_b$ impurity in a ^{39}K BEC. From (Jørgensen *et al.*, 2016). Right panel: ^{40}K impurities in a ^{87}Rb BEC. Predictions from the ladder approximation Eq. (34) are shown as blue and red lines. From (Hu *et al.*, 2016). In both panels, the molecular state was obtained from independent measurements (white dots and yellow triangles) and the corresponding lines show the two-body predictions for the energy of Feshbach molecules.

B. Experiments

First signatures of large shifts in the RF spectrum of impurities immersed in a Bose gas were found in Ref. (Wu *et al.*, 2012). While the large loss rate in BECs close to the unitary point $1/k_n a = 0$ seemed to hinder further studies, a groundbreaking experiment showed that the momentum distribution was accessible even in this regime (Makotyn *et al.*, 2014). The question arose whether there is a region of interaction strengths where a significant energy shift of the polaron state can be observed while losses remain moderate. This question was evaluated in detail for a single neutral impurity in a BEC (Hohmann *et al.*, 2015).

The first experiments observing the Bose polaron as well-defined peaks in the impurity spectral function measured using RF injection spectroscopy are shown in Fig. 9 (Hu *et al.*, 2016; Jørgensen *et al.*, 2016). These works, and subsequent more refined ones (Etrych *et al.*, 2024; Morgen *et al.*, 2023; Peña Ardila *et al.*, 2019; Skou *et al.*, 2022, 2021a; Yan *et al.*, 2020), reported the presence of both an attractive and a repulsive polaron for weak to moderate interaction strengths, in agreement with the predictions of the ladder approximation and closely mimicking the picture known from the fermionic case. In Ref. (Hu *et al.*, 2016) fermionic ^{40}K atoms were immersed in a BEC of ^{87}Rb atoms, which has the advantage that impurity atoms are transferred between independent states, and that losses are reduced due to their fermionic character. In Ref. (Jørgensen *et al.*, 2016) on the other hand the impurity atoms were derived directly from the BEC facilitating a single-mode approximation for the evaluation, whereas the detection relies on loss measurements of the BEC so that depletion had to be considered. In both cases the number of transferred

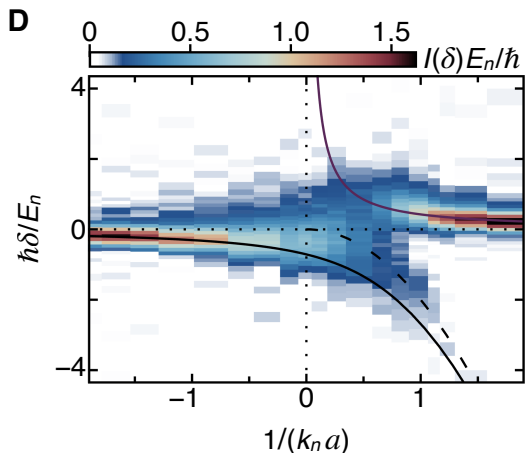


FIG. 10 **Bose polaron spectrum in a homogeneous BEC** for equal masses ($m = m_b$) with ^{39}K atoms at $k_n a_b = 0.008$ (i.e., $k_n \xi \approx 20$). The solid black line is the energy of the attractive polaron given by the 1-mode Bogolubov ansatz for an ideal BEC, the dashed black line is the energy of the dimer in vacuum, and the purple line is the mean-field energy of the repulsive polaron. From Ref. (Etrych *et al.*, 2024).

atoms as a function of RF frequency was evaluated for interaction strengths $-3 \lesssim 1/k_n a \lesssim 3$ and energy was extracted from fits to the data.

Figure 9 shows that the observed spectra are significantly broader in the strongly interacting region as compared to that of the Fermi polaron shown in Fig. 2. Besides losses, a common source for spectral broadening is the presence of a harmonic trap causing an inhomogeneous bath density. This was addressed in a recent experiment using a box potential where the BEC is spatially homogeneous except at the trap edges (Etrych *et al.*, 2024). In Fig. 10, the corresponding impurity spectral function is shown as measured with injection RF spectroscopy. One again observes sharp spectral peaks at negative and positive energies for weak to moderate interaction strength corresponding to well-defined attractive and repulsive Bose polarons. Importantly, the spectrum remains however quite broad for strong interactions $k_n |a| > 1$ with both spectral peaks acquiring a width larger than their energy in contrast to the Fermi polaron case. In fact, the spectrum has a similar width to that in the presence of a trap (compare with left panel of Fig. 9), indicating that the broadening is mainly due to impurity-boson correlations and not simply the trap. The fact that all Bose polaron experiments so far have observed such broad spectra even in absence of trapping shows the challenging nature of the problem, and it even raises the basic question regarding whether well-defined Bose polarons exist for strong interactions.

The ladder approximation for the attractive polaron is compared to experimental results in Fig. 9 (right panel) and Fig. 10. There is a fairly good agreement regarding the spectral function peaks not only for weak but

also for strong impurity-boson interactions across different experiments especially for the attractive polaron, indicating that two-body correlations included by the ladder approximation are dominant in determining the observable impurity spectrum peaks. This holds even for a very weakly interacting and therefore highly compressible Bose gas with $a_b = 9a_0$ (Peña Ardila *et al.*, 2019). Here, the discrepancies between experiment and the ladder approximation are however significantly larger than for the Fermi polaron, which points to an increased role of $n > 2$ -body correlations as expected due to the absence of the Pauli principle.

To summarize, these observations hint at physics that requires theoretical approaches beyond the ones that have typically been applied for Fermi polarons. Some fundamental open questions include which length scales are important for determining the properties of the Bose polaron and which aspects are universal allowing for a unified description, whether the Bose polaron even exists as a well-defined quasiparticle for strong interactions, if there are observable states involving large numbers of bosons correlated with the impurity with lower energy, and what is the role of temperature and phase transition of the surrounding Bose gas. Progress towards answering some of these questions has been made in the past decade as we will review in the following sections.

C. Static impurity and the orthogonality catastrophe

We now consider the case of an infinitely massive impurity, which can be solved exactly in the case of an ideal BEC. The solution corresponds to a state involving a macroscopic number of bosons around the impurity which has zero overlap with the case of no impurity leading to an *orthogonality catastrophe* (OC) in the thermodynamic limit.³ Contrary to the case of fermions, in a Bose gas the OC arises also for mobile impurities.

Treating the infinitely massive impurity as a static scattering potential, the ground state energy of an ideal BEC is simply determined by that of the lowest single-particle scattering state which yields the usual mean-field result (Collin *et al.*, 2007; Huang and Meng, 1992)

$$\varepsilon = \frac{2\pi a}{m_r} n_0, \quad (27)$$

for $a \leq 0$, where one should set $m_r = m_b$ for an infinitely massive impurity and n_0 is the BEC density in the ab-

³ The other exactly solvable case of a mobile impurity in a gas of infinitely heavy bosons was shown to connect Bose polarons and Anderson localization in the context of disorder physics (Rose and Schmidt, 2022), see also (Breu *et al.*, 2024).

sence of the impurity. The same calculation also yields

$$Z = e^{-\kappa N^{1/3}(k_n a)^2}, \quad (28)$$

for the residue for large N with $\kappa = (1/3 + 1/4\pi^2)/3^{2/3}$. At unitarity, one obtains $Z = (8/3\pi)^{2N}$. Hence, the residue vanishes as a stretched-exponential with the number N of bosons in the BEC (Guenther *et al.*, 2021). This gives rise to a bosonic OC (Sun *et al.*, 2004) in the sense that the non-interacting and interacting ground states have zero overlap in the thermodynamic limit. A similar OC was predicted by P. W. Anderson for a static impurity in an ideal Fermi gas, for which however the residue decays as a much slower power law (Anderson, 1967; Combescot and Nozières, 1971). The faster decay in the bosonic case arises because all bosons cluster around the impurity giving rise to a macroscopic number of particles in its dressing cloud, while only particles close to the Fermi surface participate in the fermionic case.

Contrary to the Fermi polaron, the Bose polaron exhibits the OC when immersed in an ideal BEC also for a finite impurity mass (Guenther *et al.*, 2021; Shchadilova *et al.*, 2016). This is apparent already at the mean-field level. Indeed, the energy of an impurity in an interacting BEC with chemical potential $\mu_b = 4\pi a_b n/m_b$ is for weak bath-impurity interactions given by Eq. (27). Taken together with Eq. (9) this yields (Massignan *et al.*, 2005)

$$\Delta N = -\frac{m_b}{2m_r} \frac{a}{a_b} \quad (29)$$

for the number of bosons in the dressing cloud around the impurity. It follows that $\Delta N \rightarrow \infty$ when $a_b \rightarrow 0$, so that a macroscopic number of bosons are in the dressing cloud due to the infinite compressibility of an ideal BEC. Indications of this OC also emerge in perturbation theory, see Sec. III.D, and from a variational approach based on an expansion in Bogoliubov modes, see Sec. III.E, but these schemes cannot fully describe this effect involving a diverging number of bosons in the dressing cloud. The variational approach based on the Gross-Pitaevskii equation described in Sec. III.F instead recovers this mobile impurity OC, with $Z \rightarrow 0$, $\Delta N \rightarrow \infty$, and the energy approaching Eq. (27) for $a_b \rightarrow 0$.

When $a > 0$, there appears a two-body impurity-bath bound state with energy $\epsilon_B = -1/2m_r a^2$. For an infinite mass impurity in an ideal BEC, the ground state is then formed by all bosons in this state giving the energy $-N/2m_b a^2$. This result is based on single channel model treating the impurity as a static potential. In atomic gases, a resonant interaction between the impurity and the bosons is however mediated by a Feshbach molecule in a different channel (Chin *et al.*, 2010). The fact that an impurity can only form a Feshbach molecule with one boson at a time was argued to lead to correlations between the bosons equivalent to a repulsive 3-body force (Shi *et al.*, 2018; Yoshida *et al.*,

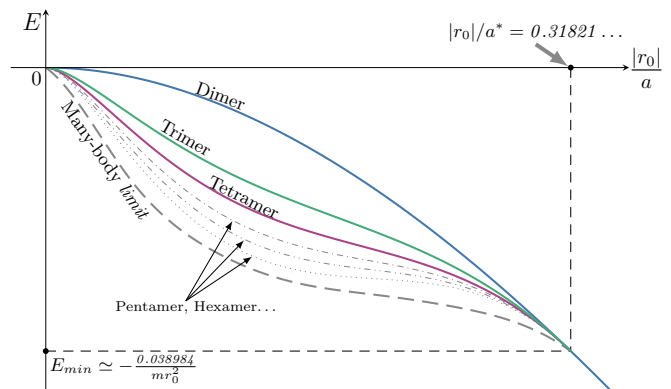


FIG. 11 **Multi-body bound states.** Spectrum of states consisting of N non-interacting bosons bound to an infinitely heavy impurity via a multichannel boson-impurity interaction with effective range r_0 and scattering length a . Solid lines are microscopic calculations whereas dashed and dotted lines are conjectures. From Ref. (Shi *et al.*, 2018).

2018b). Using a multichannel model reminiscent of the Anderson impurity model (Anderson, 1961) for infinite impurity mass, it was shown that this repulsion significantly increases the binding energy of states involving two (trimer) and three (tetramer) bosons compared to a single channel model. As illustrated in Fig. 11, close to unitarity there are states with an arbitrary number N of bosons bound to the static impurity with an energy given by $\epsilon_{N+1}/\epsilon_B \simeq -N + N(N-1)\pi/\ln a$ for $a \rightarrow +\infty$ where the first term is the result of a contact single channel interaction. Within this framework, in the thermodynamic limit all bath bosons collapse within the same multi-body bound state with a finite energy independent of N .

Chen *et al.* (2018) obtained similar results for a static impurity in a gas of *interacting* bosons. Using the Gross-Pitaevskii equation (GPE) as well as path integral Monte-Carlo calculations, they found that under quite general conditions when there is a weakly bound two-body state the impurity can bind any number of bosons even when the boson-boson repulsion is non-zero.

The time evolution of the condensate wave function for $T = 0$ and the density matrix for $T > 0$ ensuing the sudden insertion of a static impurity in an ideal BEC was calculated exactly by Drescher *et al.* (2021). The spectral function obtained by Fourier transforming $S(t)$ defined in Eq. (5) proved to be very broad for strong attractive interactions $-1 \lesssim 1/k_n a < 0$ with the main peak given by Eq. (27). For repulsive interactions $k_n a > 0$, several peaks were found with an energy separation given by the 2-body binding energy.

In conclusion, the OC for an ideal BEC as well as the existence of multi-body bound states illustrate the challenging nature of the Bose polaron problem, which involves correlations between the impurity and a large number of bosons in a many-body environment. The multi-body states have zero density far away from the

impurity, whereas the bath density in the Bose polaron problem remains finite everywhere with $n(r) \rightarrow n_0$ away from the impurity. Since the size of the multi-body states rapidly increases with the number of bound bosons, one expects them to survive only provided that their size is smaller than the typical inter-particle distance $n_0^{-1/3}$.

D. Weak interactions

We now turn to the case when the impurity-boson interactions are weak. In this case one can apply diagrammatic perturbation theory to derive reliable results. As we shall see, signs of the importance of three-body correlations already show up at this level.

To apply perturbation theory, we will assume that the bosonic bath is a weakly interacting BEC which can be described by the Bogoliubov approximation leading to Eq. (21), and we will calculate the impurity properties as an expansion in the impurity-boson interaction strength. The first- and second-order diagrams for the impurity self-energy are shown in Fig. 7. Note that the ladder approximation described in Sec. III.A includes only the first second-order diagram in Fig. 7, which however is the lowest order in the BEC gas parameter and therefore dominates in a weakly interacting Bose gas. Including all diagrams up third order for the impurity self-energy $\Sigma(\mathbf{k}, \omega)$ yields (Christensen *et al.*, 2015)

$$\varepsilon = \frac{2\pi n_0 a}{m_r} \left\{ 1 + A(\alpha) \frac{a}{\xi} + \left[B(\alpha) \frac{a^2}{\xi^2} + \tilde{B}(\alpha) \frac{aa_b}{\xi^2} \right] \ln(a^*/\xi) + \mathcal{O}(n_0 a^{*3}) \right\} \quad (30)$$

for the energy of a zero-momentum Bose polaron. Here $\xi = 1/\sqrt{8\pi n_0 a_b}$ is the healing length of the BEC, $a^* = \max(a, a_b)$ and $\alpha = m/m_b$ is the mass ratio. The function $A(\alpha)$ is given in Refs. (Casteels and Wouters, 2014; Christensen *et al.*, 2015; Novikov and Ovchinnikov, 2009), whereas $B(\alpha)$ is given in Ref. (Christensen *et al.*, 2015) and $\tilde{B}(1)$ in Ref. (Levinsen *et al.*, 2017). For later reference, we give the values $A(1) = 8\sqrt{2}/(3\pi)$ and $A(\infty) = \sqrt{2}$. The energy is non-analytic in both the boson-boson scattering length a_b and the impurity-boson scattering length a , and setting $a = a_b$ and $m = m_b$ in Eq. (30) one recovers the same two leading terms as in the chemical potential of a weakly interacting Bose gas including the Lee-Huang-Yang term (Fetter and Walecka, 1971).

The logarithmic, third-order term in Eq. (30) arises from three-body correlations, and can be understood as a perturbative precursor of Efimov physics. Interestingly, it has the same form as that derived by Wu for the chemical potential (Wu, 1959). Note that the Fröhlich Hamiltonian recovers only the first and second order terms for the energy whereas the full Hamiltonian Eq. (21) is

needed to calculate third order terms and beyond. Likewise, perturbation theory yields

$$Z = 1 - C(\alpha) \frac{a^2}{a_b \xi} + \mathcal{O}(n_0 a^{*3}) \quad (31)$$

$$\frac{m^*}{m} = 1 + F(\alpha) \frac{a^2}{a_b \xi} + \mathcal{O}(n_0 a^{*3}) \quad (32)$$

for the polaron residue and effective mass. The functions $C(\alpha)$ and $F(\alpha)$ are given in Ref. (Christensen *et al.*, 2015). In particular, for a heavy impurity one finds $C(\infty) = 1/(\sqrt{2}\pi)$ and $F(\alpha \rightarrow \infty) = 1/(3\sqrt{2}\alpha)$.

While the expansion for the energy given by Eq. (30) indicates that perturbation theory is accurate for $|a|/\xi \ll 1$, Eq. (31) gives the additional condition $a^2/(a_b \xi) \ll 1$ in order for the residue to be close to unity. Since $\xi \propto 1/\sqrt{n_0 a_b}$, this may be written as $\sqrt{n_0 a^4/a_b} \ll 1$, showing that perturbation theory becomes unreliable when $a_b \rightarrow 0$. Physically, this reflects that a weakly-interacting Bose gas is strongly affected around the impurity. Equation (31) is indeed a perturbative hint at the OC with $Z \rightarrow 0$ arising for an ideal BEC irrespectively of the impurity mass, as discussed in Sec. III.C. Although this prediction is, of course, well beyond the range of validity of perturbation theory, we shall see in Sec. III.F that a variational theory taking into account large deformations of the BEC predicts that Eqs. (30)-(31) hold in a surprisingly large range of interaction strengths.

Perturbation theory for the Bose polaron has also been performed in 2D (Pastukhov, 2018; Peña Ardila *et al.*, 2020). Care has to be taken since the 2D scattering matrix in Eq. (14) depends logarithmically on the scattering energy. This results in a logarithmic dependence on the scattering length of the polaron energy, which at zero momentum and for $m = m_b$ reads

$$\varepsilon = \frac{4\epsilon_n}{\ln(4\pi) - 2\ln(k_n a)}, \quad (33)$$

where $k_n = \sqrt{4\pi n_0}$ in 2D. A similar logarithmic behavior emerges also for the effective mass and residue. As will see further in Sec. V, logarithmic dependencies are typical in 2D systems.

E. Expansion in bath excitations

As we have seen, there is no reason to expect $n \geq 3$ correlations to be negligible for the Bose polaron. A systematic way to analyse such correlations is to use a variational polaron wave function based on expanding in the number of Bogoliubov excitations that the impurity creates in the BEC, in close analogy with the Chevy ansatz Eq. (16) for the Fermi polaron. Starting again

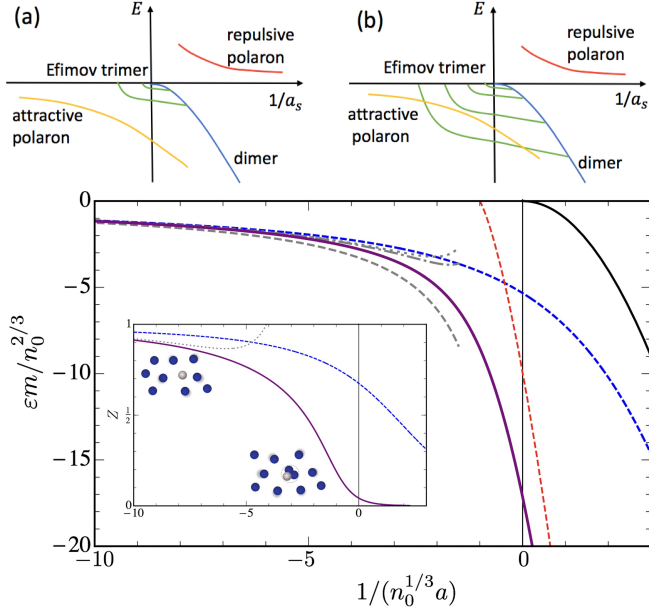


FIG. 12 **Efimov trimers and the Bose polaron.** Top: When $n|a_-|^3 \gg 1$ (left panel), all Efimov trimers lie close to the free-particle continuum and have negligible effects on the attractive polaron, whereas for $na_-^3 \simeq -1$ (right panel) the lowest Efimov trimer hybridizes with the attractive polaron, lowering notably its energy. From Ref. (Sun *et al.*, 2017). Bottom: The energy of the attractive Bose polaron with $m = m_b$ for $na_-^3 = -1$ and $a_- = -50a_b$ from Eq. (34) including one (blue dashed) and two (solid purple) Bogoliubov modes. The gray dashed, dot-dashed, and dotted lines are the perturbative results Eq. (30) to first, second, and third order. The red-dashed and black-solid lines are the energies of the ground trimer and dimer in vacuum. The inset shows the quasiparticle residue Z . From Ref. (Levinsen *et al.*, 2015).

from Eq. (21), this expansion reads

$$|\Psi_{\mathbf{p}}\rangle = \left(\sqrt{Z_{\mathbf{p}}} \hat{c}_{\mathbf{p}}^\dagger + \sum_{\mathbf{k} \neq 0} \alpha_{\mathbf{p},\mathbf{k}} \hat{c}_{\mathbf{p}-\mathbf{k}}^\dagger \hat{\gamma}_{\mathbf{k}}^\dagger + \sum_{\mathbf{k},\mathbf{k}' \neq 0} \alpha_{\mathbf{p},\mathbf{k},\mathbf{k}'} \hat{c}_{\mathbf{p}-\mathbf{k}-\mathbf{k}'}^\dagger \hat{\gamma}_{\mathbf{k}}^\dagger \hat{\gamma}_{\mathbf{k}'}^\dagger + \dots \right) |\text{BEC}\rangle \quad (34)$$

where $|\text{BEC}\rangle$ is the ground state of a weakly interacting BEC in absence of the impurity defined by $\hat{\gamma}_{\mathbf{k}}|\text{BEC}\rangle = 0$ and \mathbf{p} is the total momentum. Correlations between the impurity and n bosons can now be described by including terms with up to n Bogoliubov modes in Eq. (34). The variational parameters $\sqrt{Z_{\mathbf{p}}}, \alpha_{\mathbf{p},\mathbf{k}}, \dots$ are then determined by minimizing the energy $\langle \Psi_{\mathbf{p}} | H | \Psi_{\mathbf{p}} \rangle$. Equation (34) was first used in Ref. (Li and Das Sarma, 2014), truncating it after the first two terms (including a single Bogoliubov mode), which is equivalent to the ladder approximation discussed above.

To explore the effects of three-body correlations and Efimov trimers on the Bose polaron, the variational

ansatz Eq. (34) was employed including up to two Bogoliubov modes (Levinsen *et al.*, 2015; Sun and Cui, 2017; Sun *et al.*, 2017). The ground Efimov trimer emerges from the continuum at the scattering length $a_- < 0$, which introduces a three-body length scale depending on short range physics. Since the Efimov state has a size $\sim a_-$ and a binding energy $\sim 1/m_r a_-^2$, one would intuitively expect that it is destroyed by many-body effects when $n|a_-|^3 \gg 1$ so that it has little influence on the Bose polaron, whereas its presence becomes relevant when $na_-^3 \simeq -1$ (Sun *et al.*, 2017), see top panel of Fig. 12. Likewise, deeply-bound Efimov states for $n|a_-|^3 \ll 1$ would likely have little effect on the visible spectrum. The bottom panel of Fig. 12 shows the attractive polaron energy calculated from the ansatz Eq. (34) including one and two Bogoliubov modes as well as the perturbative results up to third order given by Eq. (30) for $na_-^3 = -1$ (Levinsen *et al.*, 2015). One clearly sees an avoided crossing between the polaron and the Efimov trimer due to hybridization, which lowers its energy. Correspondingly, the inset shows that the residue becomes very small when the polaron hybridizes with the trimer.

So far, clear signatures of Efimov states on the Bose polaron spectrum remain unobserved, which may be changed by using light impurities (Sun and Cui, 2017; Sun *et al.*, 2017). The inclusion of two Bogoliubov modes however turns out to improve the agreement with experimental data, especially in the spectral region between the two branches for strong interactions, as visible in Fig. 13. The expansion of Eq. (34) was extended further to include up to three Bogoliubov modes assuming a resonant impurity-boson interaction with $1/a = 0$ (Yoshida *et al.*, 2018a). Taking the limit $a_b \rightarrow 0$ of an ideal BEC, it was found that the polaron energy is strongly affected by the Efimov trimers even when $n|a_-|^3 \gg 1$, at odds with the intuition above. We will discuss this point in more detail in Sec. III.J. In Ref. (Nakano *et al.*, 2024b), the variational wave function Eq. (34) was used to explore the Bose polaron in 2D and significant differences in the spectral function were found between including one and two Bogoliubov modes in the wave function indicating the importance of $n \geq 3$ body correlations.

In general, the variational ansatz in Eq. (34) yields valuable insights into the properties of the Bose polaron and the role of $n \geq 3$ body correlations. A disadvantage of this approach is that the truncation at a small number of Bogoliubov modes excludes the description of states involving a large number of bosons correlated with the impurity and in particular the OC. A related disadvantage is that the expansion assumes a uniform condensate and thus cannot include the back-action of the impurity on the condensate wave function. Also, the Bogoliubov approximation treats the boson-boson repulsion at the quadratic level neglecting phonon-phonon repulsion. This can lead to unphysical behavior for states where the gas density is large in the vicinity of the impu-

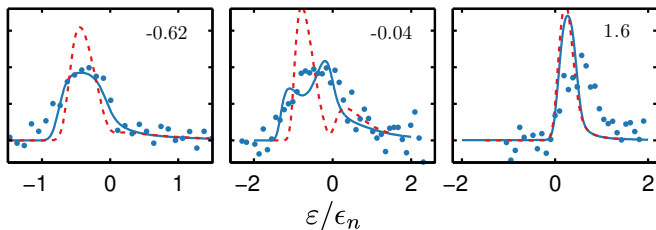


FIG. 13 **Expansion in Bogoliubov modes.** The impurity spectral function in the equal masses case as measured in the Aarhus experiment for three values of the interaction strength $1/k_n a$. Lines show variational results obtained from the ansatz Eq. (34) including up to one (red dashed) and two (solid blue) Bogoliubov modes. The theory curves are trap-averaged and take into account the Fourier broadening of the RF pulse. From (Jørgensen *et al.*, 2016).

urity. On the other hand, such states typically have a very small spectral weight and are therefore hard to observe. Indeed, the variational ansatz describes quite well most observable spectral features.

F. Gross-Pitaevskii approach

We now discuss a different variational wave function closely related to the Gross-Pitaevskii (GP) mean-field theory (Gross, 1962; Pitaevskii, 1961). With respect to the expansion in excitations of the bath, Eq. (34), this wave function has the advantage that it naturally describes the back-action of the impurity on the BEC. It also takes into account the boson-boson repulsion energy to quartic order at the mean-field level. It should thus be well suited to describe the large deformations of the BEC around the impurity involving many bosons in weakly interacting BECs leading to the OC for $a_b \rightarrow 0$ analyzed in Sec. III.C. On the other hand, this wave function assumes that the BEC instantly adjusts to the motion of the impurity in a manner akin to the Born-Oppenheimer approximation, and it must therefore be expected to be most accurate for heavy impurities. As we shall see, this variational approach indeed agrees very well with DMC calculations for an infinite mass impurity. Finally, this mean-field approach neglects higher order correlations such as Efimov states.

As a warm-up, consider first a very heavy impurity with $m_r \approx m_b$ moving with constant velocity \mathbf{v} through a weakly interacting BEC. The mean-field GP energy functional is given by (Astrakharchik and Pitaevskii, 2004)

$$E = \int \left[\frac{|\nabla\psi|^2}{2m} + V(\mathbf{r} - \mathbf{v}t)|\psi|^2 + \frac{g_b}{2}|\psi|^4 \right] d^3x. \quad (35)$$

By treating the impurity as a weak perturbation, the condensate wave function can be split into a sum of the unperturbed solution $\phi_0 = \sqrt{n_0}$ and a small correction (dressing cloud): $\psi(\mathbf{r}, t) = \phi_0 + \delta\psi(\mathbf{r}, t)$. For a static

impurity ($\mathbf{v} = 0$), we have $\delta\psi_{\mathbf{k}} = -V(\mathbf{k})\phi_0/[\frac{\hbar^2 k^2}{2m} + 2\mu]$ in the momentum space. It follows that for a contact pseudopotential $V(\mathbf{r}) = g\delta(\mathbf{r}) \Leftrightarrow V(\mathbf{k}) = g$ relevant for neutral atoms, the dressing cloud has the Yukawa form

$$\delta\psi(r) = -a \frac{e^{-\sqrt{2}r/\xi}}{r} \phi_0 \quad (36)$$

with a size set by the healing length ξ of the BEC. Likewise, the energy can be calculated from Eq. (35) in a perturbative manner giving

$$E = E_0 + \frac{2\pi n_0 a}{m_b} \left(1 + \sqrt{2} \frac{a}{\xi} \right) + \frac{1}{2} m_{\text{ind}} v^2, \quad (37)$$

where E_0 is the energy of the BEC in the absence of the impurity and $m_{\text{ind}} = m_b a^2 / (3\sqrt{2} a_b \xi)$ is the “induced” mass of fluid moving with the impurity. The second term in Eq. (37) agrees with Eq. (30) for the energy of an infinitely heavy impurity up to second order in the impurity-boson interaction. Likewise, by writing $m^* = m + m_{\text{ind}}$ one recovers Eq. (32) taking the mass ratio to infinity. This illustrates how these perturbative results can be obtained using two different approaches. Interestingly, the induced mass is directly related to the suppression of the superfluid density n_s of the BEC caused by the presence of impurities with concentration n_i as $n - n_s = n_i m_{\text{ind}} / m_b$ (Astrakharchik *et al.*, 2002; Huang and Meng, 1992).

The GP treatment presented until now applies to a heavy impurity in the perturbative regime. We now consider the general situation of a mobile impurity and arbitrary interaction strengths. To do so, we switch to the reference frame where the impurity is at rest by applying the Lee-Low-Pines (LLP) transformation $\hat{H}_{\text{LLP}} = \hat{U}_{\text{LLP}}^\dagger \hat{H}_B \hat{U}_{\text{LLP}}$ with $\hat{U}_{\text{LLP}} = e^{-i\hat{W}}$ and $\hat{W} = \hat{\mathbf{R}} \cdot \sum_j \hat{\mathbf{p}}_j$, where $\hat{\mathbf{R}}$ is the position of the impurity (Girardeau, 1961; Lee *et al.*, 1953; Shchadilova *et al.*, 2016). Applying this to the Hamiltonian, Eq. (21), one finds

$$\hat{H}_{\text{LLP}} = \sum_j \left[\frac{\hat{\mathbf{p}}_j^2}{2m_b} + V(\hat{\mathbf{r}}_j) \right] + \sum_{i < j} V_b(\hat{\mathbf{r}}_i - \hat{\mathbf{r}}_j) + \frac{(\hat{\mathbf{p}}_0 - \sum_j \hat{\mathbf{p}}_j)^2}{2m} \quad (38)$$

where \mathbf{p}_0 is the total momentum. In this way, the motional degrees of freedom of the impurity have been eliminated, giving rise to an entanglement of the boson momenta in the last term of Eq. (38). Assuming a weak and short-ranged boson-boson repulsion parametrized by $g_b = 4\pi a_b / m_b > 0$, one can now apply GP theory. For zero total momentum $\mathbf{p}_0 = 0$ and a spherically symmetric ground state the last term in Eq. (38) reduces to $\sum_j \hat{\mathbf{p}}_j^2 / 2m$, and minimizing the energy functional yields

(Guenther *et al.*, 2021; Schmidt and Enss, 2022)

$$\left[-\frac{\hbar^2 \nabla^2}{2m_r} + V(r) + g_b |\phi(r)|^2 \right] \phi(r) = \mu \phi(r). \quad (39)$$

This is similar to the standard GPE with the presence of the impurity entering through the static scattering potential $V(r)$ and the impurity-boson reduced mass $m_r = 1/(m_b^{-1} + m^{-1})$. Equation (39) can also be derived directly from Eq. (21) using the variational ansatz

$$|\Psi\rangle = \int d^3r \hat{c}_r^\dagger e^{\int ds [\phi(\mathbf{r}-\mathbf{s}) \hat{b}_s^\dagger - \text{h.c.}]} |0\rangle, \quad (40)$$

where $\hat{c}_r^\dagger/\hat{b}_r^\dagger$ creates an impurity/boson at position \mathbf{r} . Equation (40) describes a BEC in a coherent state $\hat{b}_s^\dagger |\phi(\mathbf{r})\rangle = \phi(\mathbf{r}-\mathbf{s}) |\phi(\mathbf{r})\rangle$ following instantaneously the impurity located at \mathbf{r} in the spirit of the Born-Oppenheimer approximation. This shows explicitly that this approach should be most accurate for heavy impurities whose motion is much slower than that of the bosons.

Balancing the kinetic and mean-field terms in Eq. (39) yields the “modified healing length” $\bar{\xi} = 1/\sqrt{8\pi n_0 a_b m_r/m_b}$ as a characteristic length in the problem. In the limit of infinite impurity mass, $\bar{\xi}$ reduces to the usual healing length ξ of a weakly-interacting BEC. Introducing $\mathbf{x} = \mathbf{r}/\bar{\xi}$ and $\tilde{\phi}(\mathbf{x}) = \phi(x\bar{\xi})/\sqrt{n_0}$, Eq. (39) can be written in the dimensionless form $[-\nabla_x^2 + 2m_r \bar{\xi}^2 V(x) + |\tilde{\phi}(x)|^2 - 1] \tilde{\phi}(x) = 0$. For the polaron energy ε , i.e. the ground state energy measured with respect to the homogeneous solution $|\tilde{\phi}(\mathbf{x})|^2 = 1$ in the absence of the impurity, we obtain (Guenther *et al.*, 2021; Massignan *et al.*, 2005; Schmidt and Enss, 2022)

$$\varepsilon = -\frac{1}{2} E_{\bar{\xi}} \int d^3x (|\tilde{\phi}(x)|^4 - 1) \quad (41)$$

with the characteristic energy scale $E_{\bar{\xi}} = n_0 \bar{\xi}^3 / (2m_r)$. Likewise, the residue and number of particles in the dressing cloud around the BEC can be expressed as integrals over the condensate function,

$$Z = e^{-N_{\bar{\xi}} \int d^3r |\tilde{\phi}(\mathbf{r}) - 1|^2} \quad \text{and} \quad \frac{\Delta N}{N_{\bar{\xi}}} = \int d^3r (|\tilde{\phi}(\mathbf{r})|^2 - 1) \quad (42)$$

where $N_{\bar{\xi}} = n_0 \bar{\xi}^3$. Equations (41)-(42) show that within this variational approach, the effects of the boson-boson interaction enter through the (modified) healing length in agreement with the ladder approximation.

The mean-field GP equation is reliable only when the gas parameter $n(r)a_b^3$ remains small everywhere, even in the vicinity of the impurity where the bath density $n(r)$ may grow rapidly. A detailed perturbative analysis showed that this condition is satisfied when $(n_0 a_b^3)^{1/4} a_b \ll R$. Here n_0 is the bulk bath density and $R = 4\pi / \int d^3r |\psi_0|^4$ is a typical range of the potential, with ψ_0 the zero energy solution of the single particle

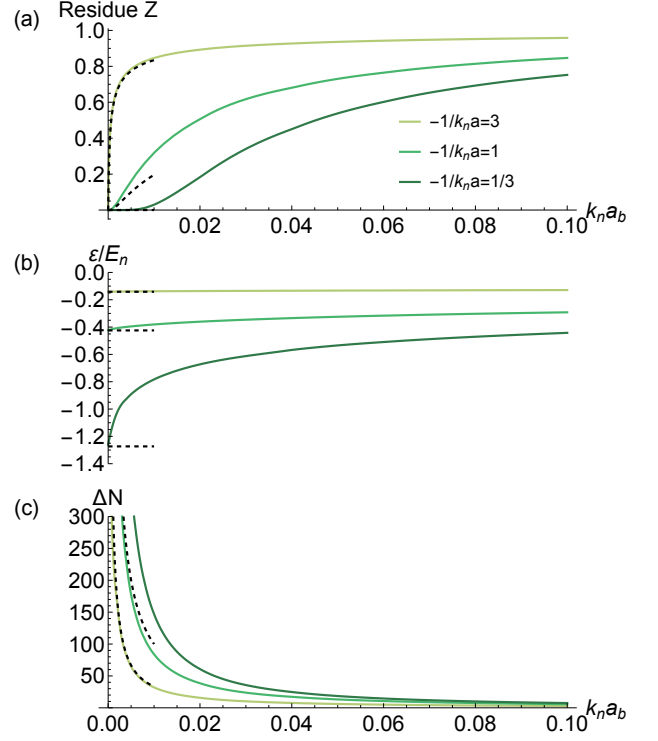


FIG. 14 **Properties of the Bose polaron.** The residue (a), energy (b), and number of particles in the dressing cloud (c) of the Bose polaron as a function of $k_n a_b$ for $-1/k_n a = (3, 1, 1/3)$ (darker lines correspond to stronger boson-impurity attraction). In all panels, we consider mobile impurities with $m = m_b$ and $k_n r_e = 0.05$, where r_e is the effective range of $V(r)$. The dashed lines are the perturbative expressions Eqs. (27), (29), and (43) valid in the region $|a|^3 \ll \xi^2 R$ where the OC takes place. From Ref. (Guenther *et al.*, 2021).

Schrödinger equation with the impurity-boson interaction potential $V(\mathbf{r})$ normalized as $\psi_0 \rightarrow 1/r$ for large r (Massignan *et al.*, 2021; Yegovtsev *et al.*, 2022). When $|a|^3 \ll \xi^2 R$ and for infinite impurity mass, Eq. (41) recovers the perturbative expression Eqs. (30) for the polaron energy to second order, and ΔN in Eq. (42) recovers Eq. (29). Likewise, the residue and Tan’s contact become (Guenther *et al.*, 2021)

$$Z = e^{-\sqrt{2\pi n_0} \bar{\xi} a^2} \quad \text{and} \quad C = 16\pi^2 n_0 a^2. \quad (43)$$

When expanded, the residue has the same functional dependence as Eq. (31) although with a slightly different prefactor. Remarkably, the condition $|a|^3 \ll \xi^2 R$, which may be rewritten as $n_0 |a|^3 \ll R/a_b$, suggests that when $a_b \rightarrow 0$ these expression hold even for large $|a|$, which is well beyond the expected range of perturbation theory. In particular, this variational ansatz recovers the OC where the residue vanishes and the number of particles in the dressing cloud diverges as $a_b \rightarrow 0$ also for a finite mass impurity mass as discussed in Sec. III.C.

Figure 14 plots the polaron residue, energy, and num-

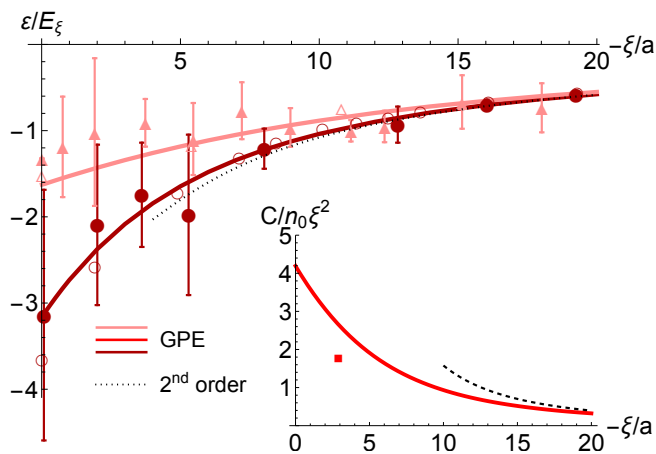


FIG. 15 **Polaron energy and contact.** The main panel shows the polaron energy: filled triangles/circles experimental data from Aarhus (Jørgensen *et al.*, 2016) / JILA (Hu *et al.*, 2016), whereas empty symbols are QMC data (Peña Ardila and Giorgini, 2016; Peña Ardila *et al.*, 2019). The solid lines are obtained from Eq. (39) for effective ranges $r_e/\xi = 0.002$ (pink) and 0.02 (dark red), corresponding to the conditions at Aarhus and JILA. The dotted line is the perturbative result Eq. (30) up to second order. The inset shows Tan’s contact C with $r_e/\xi = 0.01$. The red square is experimental data from MIT (Yan *et al.*, 2020), and the dashed line is the weak-coupling result Eq. (43). From Ref. (Guenther *et al.*, 2021).

ber of particles in the dressing cloud obtained from Eq. (39) as a function of $k_n a_b$ for different boson-impurity scattering lengths. It clearly shows how the polaron becomes increasingly dressed with a smaller residue and lower energy as the BEC gets softer. In particular, when $a_b \rightarrow 0$ one finds $Z \rightarrow 0$, $\varepsilon \rightarrow 2\pi a n_0/m_r$ and $\Delta N \rightarrow \infty$, as expected for the bosonic OC. We have assumed a zero-range boson-boson interaction $V_b(\mathbf{r}) = g_b \delta(\mathbf{r})$ when deriving Eq. (39). This leads to a divergence in the mean-field energy if the impurity-boson interaction is also taken to be zero range, and therefore a non-zero ranged $V(r)$ impurity-boson interaction potential must be used. Nonetheless, it was found that a wide range of experimentally relevant interaction potentials $V(r)$ with the same values of $a \leq 0$ and effective range r_e yielded the same results when $k_n r_e \ll 1$ (Guenther *et al.*, 2021; Schmidt and Enns, 2022). Hence, within the experimentally-relevant potentials examined, there emerged an effective two-parameter universality, in the sense that it was enough to describe the interaction with a and r_e .

The polaron energy obtained from Eq. (39) is plotted in Fig. 15 as a function of $1/k_n a$ using mass ratios and effective ranges corresponding to the Aarhus and JILA experiments (where m/m_b was equal to 1 and 40/87, respectively). There is excellent agreement between theory and these two experiments as well as with QMC calculations, even though the impurity is not heavy. The inset shows the contact (with $m/m_b = 40/23$), again obtaining

good agreement with the MIT experiment. Differently from the ladder and variational approaches, which also recovers the experimental data as previously discussed, the GP ansatz however predicts large dressing clouds involving many bosons and small residues. This illustrates the general situation where different theories reproduce experimental data, in particular for the attractive polaron, and where possible discrepancies are difficult to quantify since the observed spectra are broad for strong interactions. Figure 15 also shows that the GP approach predicts the range of the impurity-boson interaction potential to be a new relevant length scale for the polaron energy, as will be discussed further in Sec. III.J.

A complementary approach to the one discussed above is to consider a zero-range impurity-boson interaction V and a non-zero range boson-boson interaction V_b . This leads to an integro-differential (i.e., non-local) GP equation (Drescher *et al.*, 2020). A later analysis which kept non-zero ranges for both interaction potentials (Yegovtsev *et al.*, 2024) showed that the polaron energy depends most strongly on the range of the impurity-boson interaction, see Fig. 20. A coherent state Ansatz (with a Fröhlich Hamiltonian) was used to explore the momentum relaxation of impurities, showing that impurities injected in a bosonic bath with momentum larger than $p_c = mc$ (with c the speed of sound) emit phonon shock waves akin to Cherenkov radiation, and slow down until they reach p_c (Seetharam *et al.*, 2021).

G. Gaussian state approach

As described in the previous sections, the major challenge in describing the Bose polarons arises from the interplay between its formation as a well-defined quasiparticle, the tendency towards decoherence and loss due to the scattering on an infinite number of low-energy excitations of the BEC, the existence of few-body bound states, and the ultimate self-stabilization of the dressing cloud by Bose repulsion, with the latter beyond the reach of schemes based on the Bogoliubov approximation. In three consequent works (Christianen *et al.*, 2022a,b, 2024), a theory capturing all these aspects including the self-stabilization of the dressing cloud was developed using a combination of the Lee-Low-Pines transformation with a Gaussian state variational ansatz.

The main idea of the Gaussian state approach is derived from the Efimov effect, where three particles collectively suppress kinetic energy and bind even when two of them cannot bind (Naidon and Endo, 2017). In Ref. (Christianen *et al.*, 2022b), it was investigated how this cooperative mechanism translates to the many-body regime. To this end, the authors included the possibility of infinitely many boson excitations, as well as the Efimov effect, by combining several canonical transformations in

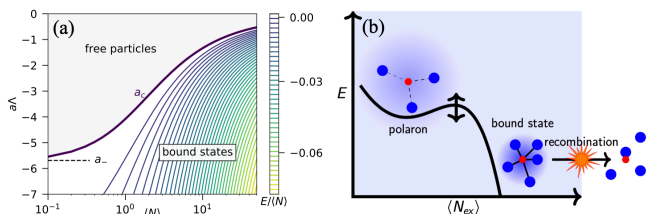


FIG. 16 **Gaussian state approach.** (a) A single light impurity having strong attractive interactions with an environment of average $\langle N \rangle$ bosons (in absence of a background condensate density) can form $n \geq 3$ -body bound states (here the mass ratio is $m/m_b = 6/133$, and Λ is a three-body parameter). (b) Variational energy landscape given by the Gaussian state approach as a function of the average excitations $\langle \hat{N}_{\text{ex}} \rangle$ over a background BEC with non-zero density. A local minimum supports the existence of a metastable Bose polaron, and an energy barrier separates it from decay to deeply bound Efimov-like clusters, which are rapidly destroyed by three-body recombination. From Ref. (Christianen *et al.*, 2022b).

one variational ansatz

$$|\psi\rangle = \hat{U}_{n_0} \hat{U}_{LLP} \hat{A}[\mathbf{x}]|0\rangle. \quad (44)$$

Here, \hat{U}_{n_0} is a coherent state shift describing the presence of a background BEC, whereas \hat{U}_{LLP} is the LLP transformation given in Sec. III.F. Finally,

$$\hat{A}(\mathcal{N}, \phi, \xi) = \mathcal{N} e^{\int_{\mathbf{k}} [\phi(\mathbf{k}) \hat{b}_{\mathbf{k}}^\dagger - \text{h.c.}]} e^{\frac{1}{2} \int_{\mathbf{k}} \int_{\mathbf{k}'} \hat{b}_{\mathbf{k}}^\dagger \xi(\mathbf{k}, \mathbf{k}') \hat{b}_{\mathbf{k}'}} \quad (45)$$

with \mathcal{N} a normalization constant, starts from a variational coherent state (that recovers the GPE solution discussed before) and extends it by a Gaussian state transformation. The ground state is obtained minimizing the Hamiltonian Eq. (21) over the variational parameters $\phi(\mathbf{k})$ and $\xi(\mathbf{k}, \mathbf{k}')$. In particular, the correlation matrix $\xi(\mathbf{k}, \mathbf{k}')$ allows to fully include three-body impurity-boson-boson correlations. Indeed, expanding the Gaussian state in the vacuum limit of $n_0 \rightarrow 0$, the exact solution of the three-body problem, and thus the Efimov effect, is recovered. The ansatz describes exactly the case of an infinitely heavy impurity in a non-interacting BEC. Nonetheless, as discussed below, it works well also for very light impurities for typical values of Bose repulsion (see, e.g., Fig. 18 below).

Applying the Bogoliubov approximation (i.e., keeping only terms up to quadratic order in the boson $\hat{b}_{\mathbf{k}}$ operators in the Hamiltonian) and considering a cloud of finite extension containing on average $\langle N \rangle$ bosons (i.e., in absence of a background condensate), Christianen *et al.* (2022b) found that every boson will become bound to the impurity, even if the impurity is mobile. As shown in Fig. 16(a), when plotting the total energy per particle obtained using the wave function Eq. (44) as a function of $\langle N \rangle$ and a , one finds that the binding energy per particle $|E|/\langle N \rangle$ monotonously increases with particle number.

This indicates a cooperative mechanisms where binding becomes stronger when more and more particles participate in the formation of a deeply bound many-body cluster state. In other words, within the Bogoliubov approximation one finds that a single mobile impurity can trigger the complete collapse of the Bose gas driven by the build-up of three-body correlations. It was also found that the thus enhanced effect of attractive impurity-bath interactions leads to a shift of the scattering length a_- at which Efimov states appear in the three-body limit. As a result Efimov three-body recombination is modified by many-body effects.

Having shown that within this approximation the ground state corresponds to a deeply bound many-body cluster raises questions on the existence of the Bose polaron as a quasiparticle. Studying the variational energy in presence of a background condensate, Christianen *et al.* (2022a,b) showed that, despite the existence of deeply bound clusters, the Bose polaron indeed survives as an excited, metastable state on top of that, protected by an energy barrier in the variational landscape [see Fig. 16(b)]. This barrier gradually reduces as attraction increases, and it disappears at a critical scattering length a^* . Remarkably, up to that point, the Bose polaron is well described by the result of a coherent variational state. As the density of the background BEC n_0 is reduced, the scattering length a^* converges to the value a_- of the three-body problem, highlighting the intimate link of this Bose-polaron instability to the Efimov effect. Hence, the value of a^* is effectively determined by the three-body recombination of two Bogoliubov modes and a Bose polaron (Christianen *et al.*, 2022b). Performing a similar analysis (using Gaussian variational states) for the repulsive polaron, Mostaan *et al.* (2023) found multiple many-body states with energies in between those of the attractive and repulsive polaron.

The above results are based on the Bogoliubov approximation, which neglects quartic terms in the boson-boson repulsion. As discussed above, however, accounting for those shall stabilize the dressing cloud of the cluster states. To investigate this, Christianen *et al.* (2024) applied the variational state (45) to the full Hamiltonian (21). Finite range attractive impurity-boson and repulsive boson-boson interaction potentials were employed with potential ranges L_g and L_U fitted to the corresponding van der Waals lengths l_{vdw} of the atomic species under consideration. Importantly, the ansatz (45) treats the boson-boson repulsion beyond the Born approximation employed in the GPE discussed in Sec. III.F. This analysis gives the “phase diagram” for strong coupling Bose polarons shown in Fig. 17. The Bose polaron is a stable quasiparticle up to a critical scattering length a , which depends on the density and the boson-boson scattering length a_B . At the critical value, the system undergoes a first-order “phase transition” to a Efimov-like cluster ground state, with a region of metastability

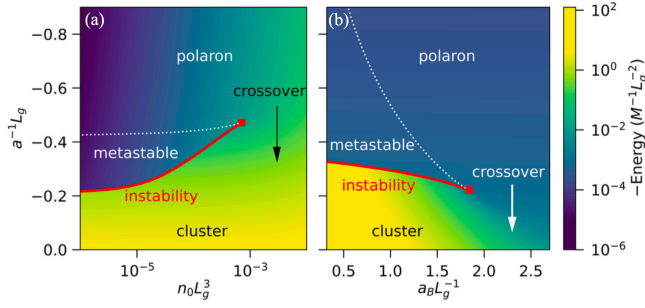


FIG. 17 **Phase diagram for Bose polarons.** The Gaussian state ansatz predicts an effective phase diagram of Bose polarons reminiscent of a liquid-gas transition. Here L_g denotes the range of the impurity-boson interaction. Depending on (a) boson density (for $a_B = 1.2L_g$) or (b) boson-boson scattering length a_B (at $n_b L_g^3 \approx 3 \cdot 10^{-5}$, appropriate for typical experimental settings), a first-order phase transition occurs from a phase where the polaron is a stable quasiparticle to a phase where the ground state is a deep Efimov-like cluster. These phases are separated by a region where the polaron is a metastable state. The first-order transition terminates in a critical point where the transition turns second order, and beyond it a crossover occurs. The mass ratio for both plots is $m/m_b = 6/133$. From Ref. (Christianen *et al.*, 2024).

(as usual in first-order transitions) of the Bose polaron in between. At a critical endpoint, this first-order transition turns second order, beyond which a continuous crossover from the Bose polaron into the Efimov-like cluster appears. A Landau energy functional was derived, which precisely recovers this phase diagram without the need of the full computationally-expensive numerical solution.

The Gaussian state ansatz was also directly compared to a ‘‘Chevy’’ double-excitation ansatz as given by Eq. (34) keeping terms up to second order in Bogoliubov excitations, which is then applied to the full Hamiltonian including the quartic terms in the boson-boson repulsion. As can be seen in Fig. 18, the Gaussian state ansatz yields an energy lower than the double-excitation ansatz for light impurities and weak Bose repulsion, but the trend is reversed for moderate mass ratios and stronger Bose repulsion, in particular close to unitarity. This behavior can be attributed to the ability of the DE ‘‘Chevy’’ ansatz to describe the detailed structure of correlations close to the impurity, while the Gaussian state ansatz is better suited to describe large dressing clouds at the expense of requiring many bosons to follow the same correlation structure. The comparison of both approaches highlights that there is presently no unique best variational wave function for all cases. Instead, depending on the system parameters and questions addressed (e.g. static versus dynamic properties) different approaches have to be employed. This is much similar to the case one encounters in the theoretical description of electronic structure and dynamics in solid-state physics.

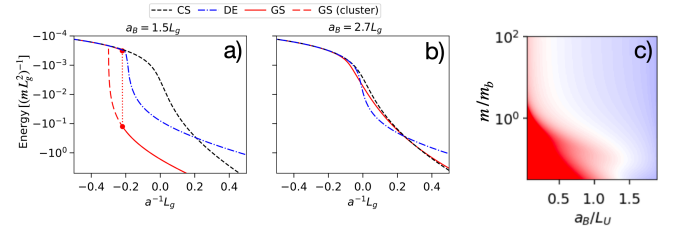


FIG. 18 **Comparison of variational functions.** (a,b) Ground state energies obtained from a coherent state ansatz (CS) which corresponds to the GPE solution discussed in the previous sections, a double excitation Chevy ansatz (DE), a Gaussian state ansatz (GS), and the energy of the Efimov-like cluster states (dashed red). In all calculations the Bose repulsion is accounted for beyond the Born approximation. In (a,b) the mass ratio is $m/m_b = 6/133$ and the ratio of intraboson to impurity-boson interaction range is $L_U/L_g = 2.3$. (a) For moderate Bose repulsion, the GS outperforms the DE ansatz and a region of metastability is found. (b) For larger Bose repulsion, the DE ansatz yields the lower energy close to unitarity. (c) Ratio of the variational energies E_{GS}/E_{DE} at unitarity ($a \rightarrow \infty$) as function of mass ratio and boson-boson scattering length (here $L_g = L_U$). Red (blue) color indicates a lower energy of the GS (DE) ansatz. From Ref. (Christianen *et al.*, 2024).

H. Quantum Monte-Carlo calculations

Given the complexity of the Bose polaron problem, it is very useful to have access to exact numerical results. The polaron energy ε can be calculated as $\varepsilon = E_{\text{tot}}(N; 1) - E_{\text{tot}}(N; 0)$ where $E_{\text{tot}}(N; M)$ is the energy of N majority particles and M impurities. These energies can be obtained using exact diagonalisation as has been done for $N \lesssim \mathcal{O}(10)$ fermions in 2D (Amelio, 2023; Amelio and Goldman, 2024). While this provides useful information both on the ground and excited states of mesoscopic systems, the computational cost of exact diagonalization typically increases exponentially with N making the thermodynamic limit out of reach.

Quantum Monte Carlo methods offer a reliable solution to this problem by evaluating multidimensional integrals with stochastic techniques. They are generally more effective for the Bose polaron than for the Fermi polaron, since the latter suffers from the infamous ‘‘sign problem’’. The Fermi polaron can be analysed using a Fixed-Node Diffusion Monte Carlo (FN-DMC) method based on a suitable guess for the nodal surface of the many-body wave function (Bombin *et al.*, 2021, 2019a; Pessoa *et al.*, 2021; Pilati *et al.*, 2021). It has also been explored with Bold Diagrammatic Monte Carlo (BDMC) methods based on evaluating Feynman diagrams by stochastic sampling (Goulko *et al.*, 2016; Mishchenko *et al.*, 2014; Prokofev and Svistunov, 2008a,b; Van Houcke *et al.*, 2020; Vlietinck *et al.*, 2013, 2014). Monte Carlo methods have also been applied to the Bose polaron problem both at zero and at finite temperatures, which we now discuss

for the 3D and 2D cases. The case of polarons with long range interactions is discussed in Sec. IV.

In three dimensions, the zero-temperature properties of the attractive and repulsive Bose polaron for $m = m_b$ have been analysed using Diffusion Monte Carlo (DMC), which solves the many-body Schrödinger equation in imaginary time. The repulsive boson-boson interaction was modeled by hard spheres of diameter equal to the scattering length a_b , and the impurity-boson interaction was modeled as either a square-well potential or as a hard sphere for $a > 0$ (Peña Ardila and Giorgini, 2015). For weak impurity-boson interactions, the numerical results recovered the second-order perturbation theory results for the energy and effective mass given by Eq. (30) and Eq. (32). This agreement remained for the repulsive polaron up to surprisingly strong interactions, whereas significant deviations from perturbation theory were found for the attractive polaron close to unitarity $1/a = 0$. The effective mass was found never to exceed twice the impurity mass ruling out self-localization, which would be signaled by a diverging effective mass. In subsequent studies, the impurity-boson interaction was modeled by a zero-range pseudopotential and good agreement was found with the JILA experiment (Hu *et al.*, 2016) as shown in Fig. 19 (Peña Ardila and Giorgini, 2016). Good agreement with the Aarhus experiment was also obtained (Peña Ardila *et al.*, 2019). The dependence of the polaron energy on the mass ratio m/m_b and the boson-boson scattering length a_b at unitarity $1/a = 0$ was explored, with the latter fitted to a polynomial function. This fit was later replaced by a logarithmic ansatz (Shi *et al.*, 2018) as discussed in Sec. III.J.

The Bose polaron at non-zero temperature was explored using both the Path Integral Monte Carlo (PIMC) and Path Integral Ground State (PIGS) methods (Pascual and Boronat, 2021). It was found that in the bulk, the energy of the attractive/repulsive branch increases/decreases with temperature and that the polaron ceases to exist above the critical temperature T_c of the BEC. This technique was furthermore used for impurities in a harmonic trap in the case where the impurity-boson interaction V is more repulsive than the intra-boson interaction V_b (Pascual *et al.*, 2024b). This technique was further applied to impurities in a harmonic trap, exploring different scenarios where the impurity-boson interaction, V , could be either weaker or stronger than the intra-boson interaction, V_b (Pascual *et al.*, 2024b). At low temperatures, strong impurity-boson interactions caused the impurities to be expelled to the surface of the gas. In contrast, at higher temperatures, though still below the critical temperature T_c , the impurities remained mixed with the gas.

In two dimensions, the repulsive Bose polaron was examined with DMC method using repulsive hard disk boson-boson and boson-impurity interactions (Akaturk and Tanatar, 2019). Good agreement was found with

the perturbative result Eq. (33) (Pastukhov, 2018) for weak interactions and low values of the gas parameter, $na_b^2 = 10^{-5}$. The effective mass was found to increase more than in the 3D case, reaching values as large as $m^*/m \simeq 2.5$ for the largest considered values of a . The 2D Bose polaron was also studied using variational Monte Carlo (VMC) method, where a variational wave function is optimized to obtain an upper bound of the ground-state energy, as well as DMC technique with soft-disk interactions between bosons and square-well boson-impurity interactions (Peña Ardila *et al.*, 2020). Good agreement with perturbation theory Eq. (33) was obtained for weak interactions and values of the gas parameter as small as $na_b^2 = 10^{-40}$, see lower panel of Fig. 19. Interactions were found to have a larger effect on the effective mass and residue of the polaron leading to significant disagreement with perturbation theory as shown in the inset in the lower panel of Fig. 19. Indeed, large values of the effective mass and a vanishing quasi-particle residue Z were predicted for strong interactions, signaling a transition to a cluster state with no broken translational symmetry, i.e., no localization.

I. Other methods

A complementary view on polaron physics is provided by the Functional Renormalization Group (FRG) approach, a non-perturbative method which allows to account systematically for many-body correlations (Dupuis *et al.*, 2021). Applications to the case of Fermi polarons were among the first to demonstrate the use of advanced approximation schemes that included full frequency- and momentum resolved correlation functions (Duda *et al.*, 2023; von Milczewski and Schmidt, 2024; Schmidt and Enss, 2011), complementing approaches that relied on simpler approximations (Kamikado *et al.*, 2017; von Milczewski *et al.*, 2022; Pawłowski *et al.*, 2017). FRG methods were applied to Bose polarons in later works. Ref. (von Milczewski *et al.*, 2024) provided a general RG analysis that compared the Fröhlich model and the full Hamiltonian given by Eq. (21) assuming an ideal BEC. In particular, Ref. (Isaule *et al.*, 2021) studied the problem of Bose polarons at zero temperature across all interaction strengths, in both 2D and 3D, while Ref. (Isaule and Morera, 2022) studied also the case of balanced Bose-Bose mixtures. These works reported polaron energies that compare favorably with the perturbative expansion in Eq. (30), with the variational approaches presented in Sec. III.E, and with Monte-Carlo simulations, especially when three-body correlations were explicitly included. The calculations were extended to consider finite temperature Bose polarons in both 2D and 3D (Isaule, 2024), finding the energy of the attractive polaron at unitarity to decrease with temperature for $T < T_c$, in agreement with the theoretical findings of Ref. (Guenther *et al.*, 2018)

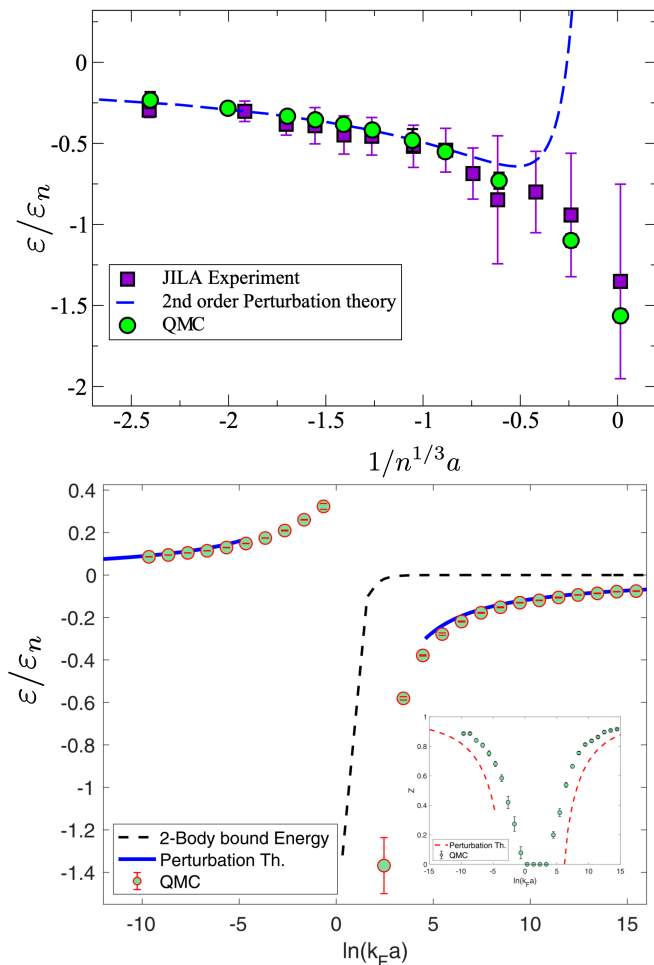


FIG. 19 **Bose polarons in 3D and 2D.** Top panel: DMC calculation (green points) of the 3D attractive Bose polaron energy as a function of the impurity-boson scattering length for mass ratio $m/m_b = 1/2$ and gas parameter $na_b^3 = 2.66 \times 10^{-5}$ close to the parameters in the JILA experiment (pink squares) (Hu *et al.*, 2016). The dashed line is second order perturbation theory given by Eq. (30). From (Peña Ardila and Giorgini, 2016). Bottom panel: DMC calculation of the 2D attractive and repulsive Bose polaron energy as a function of the interaction strength $\ln(k_F a)$ with $na_b^2 = 10^{-40}$. The dashed line shows the dimer binding energy and the solid line the perturbative result Eq. (33). The inset shows the residue. From Ref. (Peña Ardila *et al.*, 2020).

and the MIT experiment (Yan *et al.*, 2020).

The Jensen-Feynman variational path integral method was introduced in an early paper as a new powerful approach for analysing the Bose polaron within the Fröhlich model (Tempere *et al.*, 2009). This was later applied to discuss Bragg spectroscopy (Casteels *et al.*, 2011a,b) and reduced dimensional systems (Casteels *et al.*, 2012). Importantly, the variational path integral method was extended beyond the Fröhlich model to the full Hamiltonian (Ichmoukhamedov and Tempere, 2019). More recently, further progress was made by including higher-

order corrections (Ichmoukhamedov and Tempere, 2022), which led to an improved agreement with Bold Diagrammatic Monte Carlo calculations.

Starting from a quantum Brownian motion model and solving the emerging quantum Langevin equation which describe the dynamics of impurities in a BEC by including memory effects, it was shown that the polaron can exhibit superdiffusive motion and position-squeezing (Lampo *et al.*, 2018, 2017). When the bath is a coherently-coupled two-component BEC, this model even predicted a subdiffusive regime (Charalambous *et al.*, 2020).

J. Bose polaron at unitarity

In the previous sections we have seen that different theories for the Bose polaron generally agree for weak interactions but tend to give diverging predictions for strong interactions. In particular, there is no consensus yet regarding the number of parameters that are important in the strongly interacting region. To illustrate this, we now focus on the properties of the Bose polaron at unitarity where the impurity-boson scattering length a diverges and therefore disappears from the problem. Unlike for the Fermi polarons described in Sec. II, where the only remaining relevant parameters for a broad resonance are the interparticle spacing $\sim k_F^{-1}$ and the mass ratio m/m_b , here the importance of further length scales such as the boson-boson scattering length a_b , the ranges of V and V_b and other scales related to $n > 2$ -body correlations remains largely an open question.

As discussed in Sec. III.A, see Eq. (24) and Fig. 8, the ladder approximation predicts that the energy of the attractive Bose polaron at unitarity depends only on the mean distance between the bosons $\sim k_n^{-1}$, the BEC healing length ξ , and the mass ratio m/m_b . Since the ladder approximation only includes 2-body correlations, it cannot capture effects arising from processes involving one impurity and $n \geq 2$ bosons such as three-body physics. As a consequence, it predicts rather well the maximum of the spectral density but it cannot describe the large dressing clouds of the ground state which arise for strong interactions and in a soft BEC.

The variational wave function discussed in Sec. III.E provides a systematic way to explore the effects of few-body correlations on the Bose polaron. In Ref. (Yoshida *et al.*, 2018a), the Bose polaron at unitarity was analyzed using Eq. (34) including up to three Bogoliubov modes. Focusing on an ideal BEC with $a_b \rightarrow 0$, the energies of the three- and four-body bound states were calculated using both a multi-channel model with non-zero effective range and a single channel model with a cut-off in the 3-body sector. Tuning the two models such that they yielded the same 3-body parameter a_- , excellent agreement was found between the two models regarding the

Bose polaron energy. In particular, the energy ε of the polaron obtained from the two models were found to coincide when $nr_0^3 \ll 1 \ll n|a_-|^3$, where r_0 is a short range scale of the interaction. This agreement lead the authors to conjecture that ε is a universal function of na_-^3 . Nonetheless, the energy ε and the residue Z were found to steadily decrease with the number of Bogoliubov modes included, which is consistent with the OC and the disappearance of the polaron for $a_b = 0$. This instability might be cured by the multichannel nature of the interaction leading to an effective 3-body repulsive force as discussed in Sec. III.C, although close to a broad resonance this will likely happen only at a very low energy.

A different prediction was obtained from the modified GP Eq. (39), which can be solved analytically for short range impurity-boson interactions satisfying $(n_0a_b^3)^{1/4}a_b \ll R \ll \xi$. The first of these inequalities ensures that the local gas parameter $n(r)a_b^3$ remains small also in the vicinity of the impurity making a mean-field GP description reliable. The range R defined in Sec. III.F naturally emerges within this treatment and is (like the effective range r_e) typically of the order of the physical range r_c of V .⁴ At the unitary point where $|a| \rightarrow \infty$ one obtains (Massignan *et al.*, 2021; Yegovtsev *et al.*, 2022)

$$\varepsilon = -2\pi E_\xi \left(3\delta^{1/3} - 2^{3/2}\delta^{2/3} + 4\delta \ln \delta + \dots \right) \quad (46)$$

$$\Delta N = 4\pi N_\xi \left(\delta^{1/3} - 5\delta^{2/3}/(3\sqrt{2}) + 2\delta \ln \delta + \dots \right) \quad (47)$$

$$\ln Z = -\sqrt{2}\pi n_0 \xi^3 \delta^{2/3}, \quad (48)$$

for the energy, number of particles in the dressing cloud, and residue of the attractive polaron. This predicts that the properties of the attractive Bose polaron at unitarity depend on the range of the impurity-boson interaction and the boson-boson interaction via the ratio $\delta = R/\xi$ with no more interaction parameters needed. Equations (46)-(48) were later generalized to the neighborhood of the unitary point, finding that the first corrections to both ε/E_ξ and $\Delta N/N_\xi$ scale as $\delta^{2/3}\xi/a$ (Yegovtsev *et al.*, 2022). The same formalism was also used to compute the induced mass m_{ind} of a heavy polaron, and the interaction energy between two distant ones (Yegovtsev and Gurarie, 2023). It is at present unclear how to relate the predictions of Ref. (Yoshida *et al.*, 2018a) obtained from a variational wave function including Efimov correlations but unable to describe large dressing clouds

(and in particular the OC), with Eqs. (46)-(48) based on a wave function capable of describing large dressing clouds including the OC but excluding $n \geq 3$ correlations and finite impurity mass corrections. The [variational wave functions discussed in Section III.G that include Efimov correlations (Christianen *et al.*, 2022a,b, 2024) apply the theory on a model that features direct boson repulsion. In contrast, Ref. (Yoshida *et al.*, 2018a) studies a two-channel model that introduces an effective repulsion between bosons. Due to the differences in the model studied, a direct comparison of the predictions of these works is not straightforward, despite their predictions being similar. Note that there are no Efimov states for an infinitely heavy impurity.

A different prediction for the energy of an infinitely heavy impurity resonantly interacting ($1/a = 0$) with a Bose gas was obtained comparing DMC calculations with the variational ansatz Eq. (34) (Levinsen *et al.*, 2021). A fit of the DMC results, obtained using contact impurity-boson and hard-sphere boson-boson interactions, indicated that in the dilute limit the polaron energy depends logarithmically on the gas parameter: $\varepsilon \propto -(n^{2/3}/m) \ln(n_0a_b^3)$, consistent with the ‘‘Anderson’’ model discussed in Sec. III.C, where boson-boson correlations however arise from to the multichannel nature of the interaction rather than from a direct repulsion with $a_b > 0$. From this it was argued that the a_b -dependence is due to a quantum blockade effect beyond the reach of mean-field GP theory, since only one boson at a time can interact with the impurity when $a_b \gtrsim r_0$, with r_0 a typical range of the impurity-boson interaction.

The energy of the attractive Bose polaron at unitarity for an infinitely heavy impurity was later studied further with DMC (Yegovtsev *et al.*, 2024) method. Figure 20 shows the obtained energy Eq. (40) as a function of the gas factor $n_0a_b^3$ using Pöschl-Teller impurity-boson and Gaussian boson-boson interactions with ranges r_c and r_b respectively. Since the size of the polaron cloud is determined by the BEC healing length $\xi \propto 1/\sqrt{n_0a_b}$ and contains $\Delta N \propto 1/a_b$ bosons, it increases with decreasing gas factor, rendering the DMC calculations more challenging with larger system sizes. The vertical arrows in Fig. 20 indicate the gas parameter below which finite size effects become important for the DMC calculations involving $N \sim 100$ particles, which is indeed the region where the DMC results of (Levinsen *et al.*, 2021) predicted the logarithmic dependence of ε discussed above (gray squares and gray dashed line). In experiments one typically has $r_b \sim r_c \sim a_b$ and $n_0a_b^3 \gtrsim 10^{-6}$, for which the two DMC calculations reassuringly agree. The energy obtained from the GP variational wave function Eq. (40) (dashed lines) agrees very well with the DMC results in the region where finite-size effects are small, explicitly demonstrating the accuracy of this approach for heavy impurities. For low BEC densities where $(n_0a_b^3)^{1/4}a_b \ll R \ll \xi$, the GP energy converges to the analytical result Eq. (46)

⁴ For a unitary square well interaction $V = -\pi^2\Theta(r_c-r)/[8m_r r_c^2]$, one finds $R = 0.56r_c$ and $r_e = r_c$, while for a unitary Pöschl-Teller $V = -1/[m_r r_c^2 \cosh^2(r/r_c)]$ interaction one finds $R = 1.05r_c$ and $r_e = 2r_c$. However, there exist ‘‘shape-resonant’’ potentials having $|r_e| \ll r_c$ even though $R \sim r_c$ and $|a| \gg r_c$. For these peculiar fine-tuned cases, the effective two-parameter universality of the GPE discussed in Sec. III.F does not hold (Massignan *et al.*, 2021; Yegovtsev *et al.*, 2024, 2022).

(thick solid lines). For high densities ($R \gtrsim \xi$), instead, both the DMC and GP energies are well captured by the local density approximation (LDA) discussed in Sec. IV. Finally, the +’s give the energy from a non-local GP equation including a non-zero boson-boson interaction range r_b , which deviates negligibly from the that obtained from Eq. (40). This shows that the boson-boson interaction range has small effects on the polaron energy under experimentally relevant conditions where $r_b \sim r_c$.

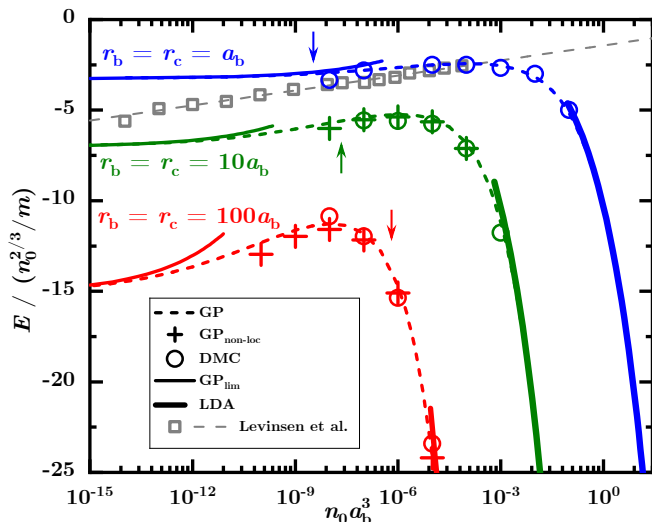


FIG. 20 **Heavy attractive polaron at unitarity.** Energy of a static impurity interacting resonantly ($1/a = 0$) with a BEC as a function of the gas parameter for three values of the ratio between the boson-boson scattering length a_b and the boson-impurity interaction range r_c . The circles show DMC results (statistical error bars smaller than symbol size) with arrows indicating when the polaron size becomes comparable to the box size and finite size effects set in. The dashed lines represent the numerical solution of the GP Eq. (39) (where $r_b = 0$), whereas +’s is the energy obtained from a non-local GP equation with $r_b > 0$. Thin solid lines at low density show the analytic result Eq. (46), while the solid thick lines on the right side indicate the LDA prediction, see Sec. IV. The grey squares and grey dashed line show DMC data and their logarithmic fit from Ref. (Levisen *et al.*, 2021) where $a_b = r_b$ and $r_c = 0$. From Ref. (Yegovtsev *et al.*, 2024).

This Section illustrated the challenges connected to understanding the properties of the Bose polaron at strong interactions. Open questions include the role of $n > 2$ correlations (Efimov trimers, tetramers, ...) and their associated length scales, which are likely most important for light impurities, and the differences between a single channel and a multichannel interaction. On the repulsive side $a > 0$ where there is a bound impurity-boson dimer state, the role of short range physics and $n > 2$ correlations and bound states is likely even greater as we saw in Sec. III.C for a static impurity, and it is presently unclear whether universal results for the Bose polaron exists in this region. Since the experimental spectra at

strong interactions are all broad, they have unfortunately not been able to resolve these questions so far, and it is in fact not even clear when/if the Bose polaron is a well-defined quasiparticle for strong interactions.

K. Temperature dependence

The Bose polaron has a qualitatively new feature compared to the Fermi polaron in the sense that its environment undergoes a phase transition at the critical temperature T_c of the BEC. Since the low energy spectrum of the Bose gas changes from linear for $T < T_c$ to quadratic for $T \geq T_c$, this phase transition should affect the Bose polaron significantly. Exploring the Bose polaron for non-zero temperature is an even more challenging problem than at zero temperature and there are several different theoretical predictions, as we will now discuss.

For high temperatures $T \gg T_c$, one can perform reliable calculations for all interaction strengths using a virial expansion (Mulkerin *et al.*, 2019; Sun and Cui, 2017; Sun *et al.*, 2017). When truncated to second order in the fugacity, this is equivalent to the ladder approximation, and it yields a polaron damping rate $\Gamma \propto a^2 \sqrt{T}$ for weak interactions and $\Gamma \propto 1/\sqrt{T}$ at unitarity. This can easily be understood from the classical expression $\Gamma = n\sigma v$ with a thermal relative velocity $v \propto \sqrt{T}$, as discussed for the Fermi polaron in Sec. II.A. For low temperatures $T \ll T_c$, a calculation to second order in a gives for a zero momentum polaron (Levisen *et al.*, 2017)

$$\varepsilon(T) \simeq \varepsilon(0) + \frac{\pi^2 a^2 T^4}{60 a_b^2 n c^3} \quad (49)$$

when $m = m_b$. Interestingly, the T^4 increase in the energy is identical to the change in the chemical potential of a weakly interacting Bose gas due to a thermal population of the phonon branch when $a = a_b$ (Khalatnikov, 1989). Perturbation theory furthermore predicts a non-monotonic behavior of the energy and a large increase in the damping close to T_c . Early calculations considered thermal effects on the Bose polaron using mean-field theory (Boudjemâa, 2014).

A diagrammatic calculation based on a ladder approximation extended to take into account a thermally populated Bogoliubov mode predicts that in the strong coupling regime, the energy of the attractive polaron decreases with increasing temperature reaching a minimum at T_c (Guenther *et al.*, 2018). The same calculation shows that the polaron damping increases with temperature making it ill-defined above T_c , and that a second quasiparticle branch appears for strong interactions for $0 < T < T_c$ in analogy with what has been found for quasiparticles in quark-gluon plasmas (Weldon, 1989). The decrease in the polaron energy with temperature and the appearance of another quasiparticle branch was

also found using a functional RG approach (Isaule, 2024). The properties of the Bose polaron for non-zero temperature were later further explored using an operator form of the ansatz Eq. (34) generalized to take into account a thermal BEC (Field *et al.*, 2020). Assuming an ideal BEC, the attractive polaron was found to split into two and three branches for $T > 0$ when two and three Bogoliubov modes were included respectively. From this it was argued that the predicted splitting of the attractive polaron is an artifact of the expansion in Bogoliubov modes, and that it should instead remain a single peak with a width $\propto T^{3/4}$. Using a dynamical variational approach based on the coherent state applicable to a thermal BEC combined with a Lee-Low-Pines transformation (Dzsotjan *et al.*, 2020), an improved agreement with the data of the Aarhus experiment (Jørgensen *et al.*, 2016; Peña Ardila *et al.*, 2019) was obtained when a non-zero temperature was taken into account. No splitting of the attractive polaron branch was found.

Path integral MC calculations (Pascual and Boronat, 2021) found that the energy of the attractive/repulsive polaron increases/decreases with temperature in contrast to the theoretical work discussed above. A direct comparison is however not straightforward since in QMC calculations the impurity is in thermal equilibrium with the bath and therefore it has a non-zero kinetic energy. By developing a functional determinant approach to calculate the spectral properties of a static impurity (infinite mass) in an ideal Bose gas, the spectral width of the ground state was predicted to decrease as a function of temperature near unitarity, which somewhat surprisingly would correspond to an increasing life-time (Drescher *et al.*, 2024).

Experimentally, the properties of the attractive Bose polaron as a function of temperature were explored using RF ejection spectroscopy (Yan *et al.*, 2020). As shown in Fig. 21, the energy was observed to decrease with temperature for strong interaction and the damping to increase in agreement with the theoretical predictions above (Dzsotjan *et al.*, 2020; Field *et al.*, 2020; Guenther *et al.*, 2018). The energy was seen to converge to that given by the ladder approximation as $T \rightarrow 0$ for different interaction strengths (open diamonds in Fig. 21), whereas it jumped to zero at T/T_c , where the polaron becomes ill-defined due to large damping. The damping was found to increase linearly with T at unitarity, subsequently also found theoretically (Dzsotjan *et al.*, 2020), and its scale given by the ‘‘Planckian’’ rate $\sim k_B T/\hbar$, a signature of quantum critical behavior (Ludwig *et al.*, 2011; Sachdev, 2011).

This section illustrates the challenges of understanding the Bose polaron at non-zero temperature. Moreover, an accurate theoretical description of the Bose polaron in the critical region $|T - T_c|/T_c \lesssim n_0^{1/3} a_b$ of the BEC is lacking and challenging, since it requires a formalism that includes fluctuations at all length scales such as the renormalisation group (Andersen, 2004).

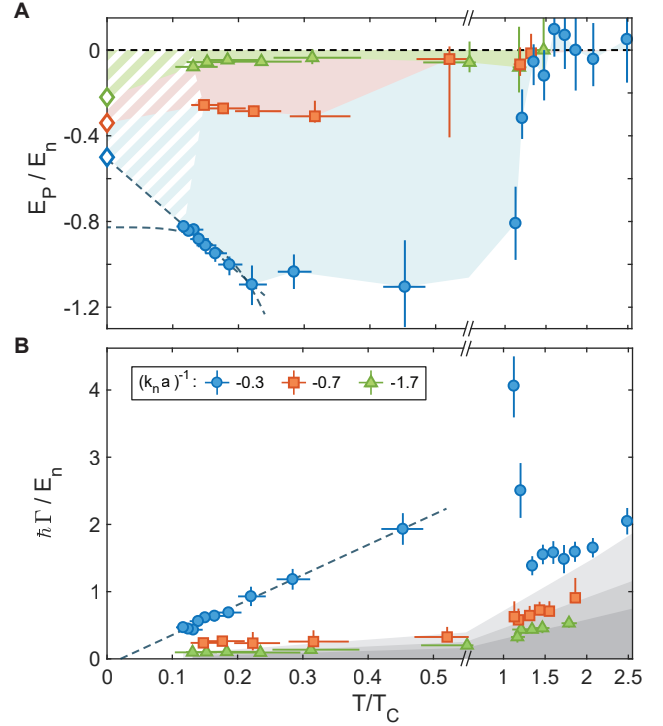


FIG. 21 **Bose polarons at non-zero temperatures.** The attractive polaron energy (a) and decay rate (b) (half-width at half-maximum of the spectral function) as a function of temperature measured by ejection RF spectroscopy using ^{40}K impurity atoms in a ^{23}Na BEC for various values interaction strengths. The dashed line in (b) is a linear fit to the data below T_c . From (Yan *et al.*, 2020).

L. Non-equilibrium dynamics

As for the Fermi polaron discussed in Sec. II.B, the relatively low density of atomic BECs and correspondingly long time-scales make them well suited to explore non-equilibrium many-body physics using interferometry with short pulses. This furthermore offers a useful alternative for measuring equilibrium properties, as the short lifetime of the Bose polaron sets an inherent limitation for the duration and hence resolution that can be achieved with RF spectroscopy (Spethmann *et al.*, 2012a,b).

The observed signal in Ramsey type experiments is proportional to $S(t)$ given by Eq. (5) precisely as for the Fermi polaron described in Sec. II.B. Theoretically, $S(t)$ can be obtained by a Fourier transform of the exact expression for the impurity spectral function at high energies (Braaten *et al.*, 2010) as discussed in Sec. I.C. This yields (Skou *et al.*, 2021a)

$$S(t) \simeq \begin{cases} 1 - (1-i) \frac{16}{9\pi^{3/2}} \left(\frac{t}{t_n}\right)^{3/2} & t \ll t_a \\ 1 + \frac{2}{3\pi} (k_n |a|)^3 - (1+i) \sqrt{t/t_w} - iE_{\text{mf}} t & t \gg t_a \end{cases} \quad (50)$$

where $t_a = ma^2$, $t_w = m/32\pi n^2 a^4$, $t_n = 2m/k_n^2$, and

$E_{\text{mf}} = 4\pi a n/m$ is the mean-field polaron energy. This result was later extended to second-order for $t \ll t_a$ by taking the presence of the attractive polaron branch into account (Skou *et al.*, 2022).

The dynamical regimes in Eq. (50), shown as colored regions in Fig. 22, can be understood from simple two-body scattering. The rate of decoherence is determined by the scattering rate as $\dot{S}(t) = -n\sigma v$ with the collisional cross-section σ and the typical relative velocity v . The typical energy of the scattering processes contributing to the decoherence at time t after inserting the impurity is $E \sim 1/t$, which gives the relative velocity $v \sim \sqrt{2E/m_r}$. Since the cross-section for high energies is given by its vacuum expression $\sigma(k) = 4\pi a^2/[1+(ka)^2]$ with $k = m_r v$, one obtains $\sigma(k) \sim 1/k^2$ for $t \ll t_a$ giving $\dot{S}(t) \sim -n\sqrt{t}/m_r^{3/2}$, and $\sigma(k) \sim 4\pi a^2$ for $t \gg t_a$ giving $\dot{S}(t) \sim -na^2/\sqrt{m_r t}$. Integrating these expressions then yields Eq. (50). Note that the $t^{3/2}$ dynamics for short times is universal in the sense that it is independent of the scattering length.

Since the short-time dynamics is determined by high energy two-body scattering, it is independent of the quantum statistics of the bath. The initial $t^{3/2}$ dynamics in Eq. (50) has indeed also been derived in the context of the Fermi polaron discussed in Sec. II.B, where it was shown that a non-zero range of the impurity-bath interaction gives rise to a $1 - t^2$ dependence (Parish and Levinsen, 2016). Using the Master equation, the time evolution of $S(t)$ has been analyzed rigorously for weak interactions demonstrating a critical slow down of the formation of the Bose polaron when its velocity approaches the critical velocity of the BEC (Nielsen *et al.*, 2019). The cooling dynamics via the emission of Cherenkov radiation was studied with the Boltzmann equation (Lausch *et al.*, 2018). These works complemented earlier studies of $S(t)$ employing a LLP transformation combined with time-dependent coherent states (Shchadilova *et al.*, 2016). Here it was found that the Bose polaron peak undergoes significant broadening as the Feshbach resonance is approached so that the Bose polaron indeed loses its meaning as a well-defined quasiparticle. A similar approach was at the basis of the analysis of the spatially resolved formation dynamics of the Bose polaron (Drescher *et al.*, 2019, 2021), and the formation of magnetic polarons was examined in Ref. (Ashida *et al.*, 2018).

The experimental points in Fig. 22 were measured in a ^{39}K BEC using a Ramsey scheme similar to that described in Sec. II.B: an initial pulse created a small admixture of the BEC in the impurity state, and after time t a second pulse with variable phase then compared the evolved state with the initial BEC (Skou *et al.*, 2021a). The observed signal was shown to be proportional to $S(t)$. The two upper panels of Fig. 22 show the experimentally measured evolution of the amplitude $|S(t)|$ for two values of the impurity-boson interaction, together with the predictions of Eq. (50). Based on these measure-

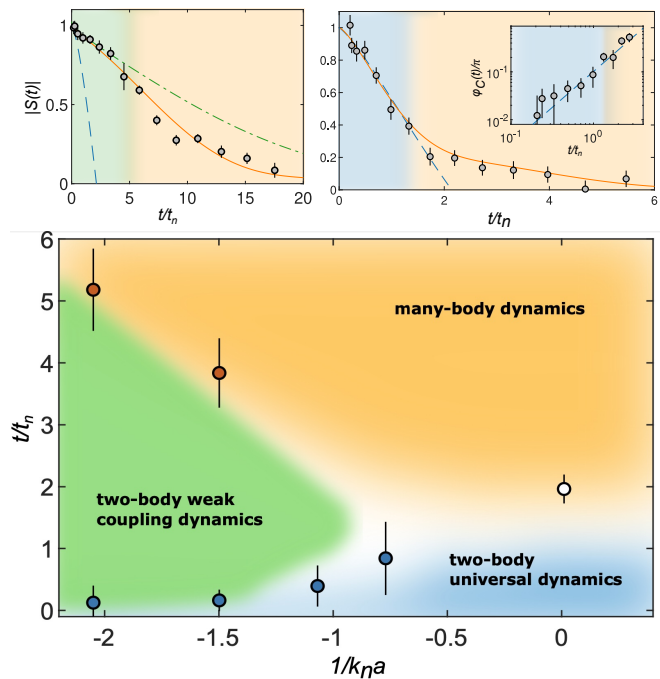


FIG. 22 **Formation of Bose polarons.** Top: Amplitude of the Ramsey signal measured for $1/k_n a = -2$ (left) and $1/k_n a = 0$ with the inset showing its phase (right). The blue dashed and green dashed-dotted lines show the short- and long-time behaviors of Eq. (50), and the solid orange line is the result of the ladder approximation. From Ref. (Skou *et al.*, 2021a). Bottom: Regimes of impurity dynamics as described by Eq. (50) and obtained from interferometric measurements. At short times the evolution is determined by universal high-energy two-body scattering (blue). For weak interactions low energy collisions dominate and the dynamics is governed by the mean field phase evolution (green). At longer times many-body correlations set in (orange).

ments, the transition times between the two dynamical regimes of Eq. (50) can be obtained, which is shown as blue points in the upper panel. At unitarity, t_a diverges and the system transitions directly from two-body universal $t^{3/2}$ dynamics to the many-body regime. The solid lines in Fig. 22 are obtained by Fourier transforming the impurity spectral function obtained from the ladder approximation, which includes the short time two-body dynamics exactly. This result agrees remarkably well with the experimental data even at unitarity, when an independently measured exponential decay due to three-body decay processes is included. The smooth crossover between the regimes of Eq. (50) was further analysed in Ref. (Skou *et al.*, 2021b). The impurity dynamics measured in Ref. (Skou *et al.*, 2021a) was later analysed using a time-dependent variational coherent ansatz obtaining good agreement (Peña Ardila, 2021). The real-time dynamics of an impurity in an ideal Bose gas was also explored using the ladder approximation (Volosniev *et al.*, 2015).

Based on these interferometric experiments, a detailed analysis of the time scales of polaron formation and loss was performed (Skou *et al.*, 2022). This indicated that significant decay at strong interaction indeed limits the RF spectroscopy resolution, and showed that the phase evolution at long times offers a useful alternative to measure the polaron energy in agreement with $S(t) \rightarrow Z \exp(-i\epsilon t)$. Recently, interferometric investigations of the Bose polaron were extended to repulsive interactions $1/k_n a > 0$ (Etrych *et al.*, 2024; Morgen *et al.*, 2023; Skou *et al.*, 2022). In this case, one observed oscillations in $S(t)$ due to quantum beats between the attractive and repulsive Bose polaron like for the Fermi polaron discussed in Sec. II.B, which was used to extract their energy difference.

In another experiment probing non-equilibrium dynamics, a BEC of Helium-4 containing impurities expanded rapidly upon releasing it from a trap (Cayla *et al.*, 2023). The measured momentum distribution of the impurities at long times exhibited a remarkably clean $1/k^4$ tail, which disappeared in absence of bath atoms, or when the bath was thermal. While these features resemble those expected from two-body interactions at equilibrium and Tan's contact, their origin must be clearly different, because the equilibrium $1/k^4$ tail is known to vanish over a very short time during an expansion in presence of interactions (Qu *et al.*, 2016). Furthermore, the $1/k^4$ tails observed in this experiment have amplitudes which are orders of magnitude larger than the ones predicted at equilibrium.

IV. POLARONS WITH LONG-RANGE INTERACTIONS

The formation of polarons when the impurity-bath interaction is not short range involves an interesting and highly non-trivial interplay between few- and many-body physics, cold chemistry, and cluster physics. Experimentally, such systems can be created for example by immersing ions or Rydberg atoms in neutral atomic gases or by trapping atoms with magnetic/electric dipole moments.

Before turning to these concrete cases, we first analyze the GPE in the presence of a static potential with a range larger than the BEC healing length. We note that by using the Born-Oppenheimer approximation described in Sec. III.F, see Eq. (40), the following analysis also applies to heavy but mobile impurities. When the range of the interaction potential is large, one may resort to the LDA to obtain analytical expressions. This gives (Massignan *et al.*, 2005)

$$\psi(r) \approx \sqrt{n_0} \left[1 - \frac{V(r)}{2gn_0} \left(1 + \frac{6\xi^2}{r^2} \right) + C \frac{e^{-\sqrt{2}r/\xi}}{r} \right], \quad (51)$$

for the wave function far away from the impurity, with C a suitable constant. The LDA term proportional to

$V(r)$ dominates the long range behavior when the typical range of $V(r)$ is larger than ξ , while the Yukawa term proportional to $e^{-\sqrt{2}r/\xi}$ gives the leading contribution when the potential has a smaller range, but also whenever the BEC is sufficiently dilute. For smooth interaction potentials with a range r_c much larger than the healing length ξ , one finds from Eq. (51) the polaron energy

$$\epsilon = \frac{n_0 r_c}{2m_r} \int d\mathbf{y} \left(\mathcal{V}(y) - \frac{\mathcal{V}(y)^2}{2(r_c/\xi)^2} + \frac{(\nabla \mathcal{V}(y))^2}{4(r_c/\xi)^4} + \dots \right), \quad (52)$$

with $\mathcal{V} = V/(2m_r r_c^2)$, $\mathbf{y} = \mathbf{r}/r_c$, and a number of particles in the polaron cloud $\Delta N = -\frac{r_c}{8\pi a_b} \int d\mathbf{y} \mathcal{V}(y) + \dots$. Remarkably, these expressions hold also for strongly attractive potentials, and for shape-resonant ones, which are fine-tuned to have a vanishing effective range r_e . They accurately match DMC calculations in the regime $r_c \gg \xi$, see the Fig. 20. An explicit evaluation of these integrals for various unitary model potentials (Pöschl-Teller, Gaussian, exponential, and the simplest shape-resonant one) was given in Ref. (Yegovtsev *et al.*, 2024). These expressions were shown to match accurately numerically-exact Diffusion Monte-Carlo calculations in the regime $r_c \gg \xi$ (see the right hand-side of Fig. 20).

A. Ions in a BEC/Fermi gas

We now turn to the specific case of ions in neutral atomic gases. Experiments have explored atom-ion collisions and buffer gas cooling (Ewald *et al.*, 2019; Feldker *et al.*, 2020), three-body recombination and molecule formation (Dieterle *et al.*, 2020; Mohammadi *et al.*, 2021), charge transport (Dieterle *et al.*, 2021), ions in a BEC (Kleinbach *et al.*, 2018; Zipkes *et al.*, 2010), Feshbach resonances (Weckesser *et al.*, 2021), and high resolution microscopy (Veit *et al.*, 2021). They have however not yet reached the quantum degenerate regime of polarons, which is the focus of this review. The following discussion will therefore focus on theoretical results regarding charged polarons, and we refer the reader to earlier excellent reviews giving a broader discussion of experimental and theoretical results regarding hybrid ion-atom systems (Lous and Gerritsma, 2022; Tomza *et al.*, 2019).

At large distances, the interaction is attractive and arises from the electric field of the ion polarizing the atoms so that $V(r) \rightarrow -C_4/r^4$, where C_4 is proportional to the polarizability of the atoms. The $1/r^4$ tail is longer range than the $1/r^6$ tail of the van der Waals interaction between neutral atoms. It sets the characteristic length $r_{ion} = \sqrt{2m_r C_4}$ and energy $\epsilon_{ion} = 1/(2m_r r_{ion}^2)$. For a $^{87}\text{Rb}^+$ ion in a ^{87}Rb BEC this gives $\epsilon_{ion} \approx 80\text{nK}$ and $r_{ion} \approx 260\text{ nm}$, which is the same order as a typical mean interparticle distance in atomic gases. This means that there is no separation of length scales so that the atom-ion interaction cannot in general be described by

a contact pseudopotential. Its strength furthermore implies that the atomic bath is much more affected by an ion as compared to a neutral impurity.

At short distances, the electron clouds of the ion and the atom start to overlap giving rise to a strong repulsion. A model potential commonly used in the literature (Krych and Idziaszek, 2015)

$$V(r) = -C_4 \frac{r^2 - c^2}{r^2 + c^2} \frac{1}{(b^2 + r^2)^2}. \quad (53)$$

features a $1/r^4$ attractive tail at large distances and strong repulsion at shorter ones, with a single minimum as a function of r . The parameter c determines the onset of repulsion and typically $c \ll r_{ion}$. Different values of b and c give different short-range physics, but one typically assumes that the many-body physics is essentially the same as long as they give the same scattering length and energy of the highest bound state. In Fig. 23 the scattering length of the interaction potential Eq. (53) is plotted as a function of b for mass balance $m = m_b$ and $c = 0.0023r_{ion}$. One clearly sees the presence of several Feshbach resonances due to the emergence of bound atom-ion dimers. Given the large strength of the atom-ion interaction, this may lead to a “snow-ball” state with many atoms bound to the ion as the dimer state energy decreases. As we shall see shortly, theoretical calculations indeed predict this to occur for a bosonic bath in analogy with what has been experimentally observed for ions in liquid Helium (Atkins, 1959; Chikina *et al.*, 2007).

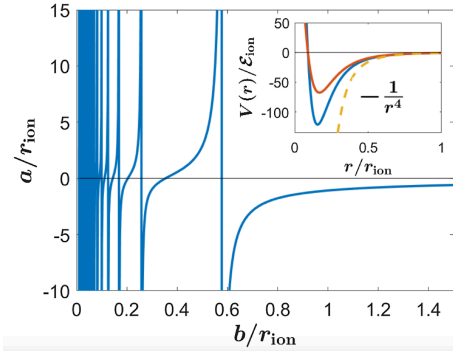


FIG. 23 **Atom-ion interaction.** The atom-ion scattering length of Eq. (53) as a function of b (at fixed $c = 0.0023r_{ion}$) with the interaction potential plotted for $b/r_{ion} = 0.3$ and 0.35 in the inset. From (Christensen *et al.*, 2021).

Figure 24 shows the total ground state energy, E , of an ion in a bath of N bosons of equal mass ($m = m_b$) with the interaction potential given by Eq. (53). The results are obtained with DMC calculations, using a number of atoms N in the range of a few hundreds (Astrakharchik *et al.*, 2021). For small negative scattering lengths, such as $a = -0.1r_{ion}$ (red) and $a = -r_{ion}$ (green), the system energy is close to the sum of the GP bulk energy and the polaron energy ε , i.e. $E(N) = \varepsilon + Ng_b n/2$ with

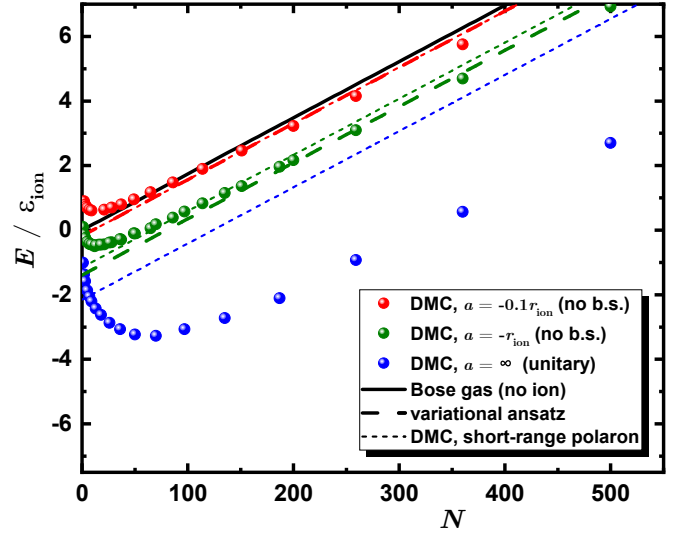


FIG. 24 **Ionic Bose polarons.** The ground state energy of a single ion and N bosons with equal masses in the regime where no two-body bound state is present. Symbols show DMC results, the long-dashed lines is Eq. (54), and short-dashed lines show the DMC results for a short-ranged impurity-boson interaction (Peña Ardila and Giorgini, 2015). The gas parameter is $n_0 a_b^3 = 10^{-6}$, which for the interaction potential used here corresponds to $nr_{ion}^3 = 0.1288$. From Ref. (Astrakharchik *et al.*, 2021).

$g_b = 4\pi a_b/m_b$ where a_b is the boson-boson scattering length. Here, the polaron energy agrees well with the variational approximation (Shchadilova *et al.*, 2016),

$$\varepsilon = 4\pi n a_b^3 \left(\frac{r_{ion}}{a_b} \right)^2 \left(\frac{a_b}{a} - \frac{a_b}{a_0} \right)^{-1} \varepsilon_{ion}, \quad (54)$$

where $a_0 = \frac{32}{3\sqrt{\pi}} \sqrt{n a_b^3}$ is the shift of the atom-ion scattering resonance position due to bath. In this weakly-interacting regime, the energy closely matches that of a short-range interaction with the same scattering length, as indicated by the dashed lines from the DMC calculations (Peña Ardila and Giorgini, 2015). In contrast, at unitarity ($1/a = 0$), Eq. (54) is no longer applicable and the energy becomes of the same order as ε_{ion} significantly different from that of a neutral impurity.

The effects of the strong atom-ion interaction become even more dramatic in the regime of positive scattering lengths $a > 0$, where the atom-ion scattering problem supports a bound state. The left panel of Fig. 25 shows the energy as a function of the number of bosons in the bath for the same system as in Fig. 24, but now in the region of stronger attraction, where the atom-ion potential supports a two-body bound-state. One clearly sees that the energy initially decreases linearly as $E(N) \approx NE_b$ with E_b the energy of the bound state, indicating that the ion binds the bosons in the bath, creating a many-body bound state similar to the so-called “snowballs” formed by ions in liquid Helium (Atkins, 1959; Chikina

et al., 2007). This reflects that the characteristic ion energy ϵ_{ion} is much larger than the chemical potential of the bath $g_b n$. Eventually, as the number of atoms is increased further, the energy flattens out reaching a minimum at a certain number of atoms $N_c \approx 140$, and then increases for larger N as the ion cannot bind more atoms. Figure 25(b) shows DMC calculations for the mass imbalanced case of a mobile $^{174}\text{Yb}^+$ ion in a gas of bosonic ^7Li atoms for different atom-ion potentials either given by Eq. (53) or by $V(r) = C_8/r^8 - C_4/r^4$ (Chowdhury and Perez-Ríos, 2024). These calculations predicted that the ion can bind around 8 bosons. Also, the short range details of the potential were found to be important for determining the energy. This leaves an uncertainty regarding how many parameters are needed for a precise description of a mobile ion in a Bose gas.

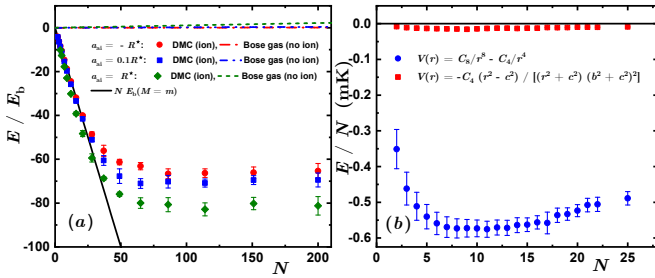


FIG. 25 **Snowball states of ion-bosonic atom systems.** (a) Ground state energy of a single ion and N bosons for atom-ion attraction strong enough to support a two-body bound state of energy E_b . Symbols show DMC results and the solid line is $E(N) = NE_b$ where E_b is the binding energy of an atom-ion dimer (specifically, $E_b/\epsilon_{ion} = -1.6, -9.0, -35$ for $a/r_{ion} = 1, 0.1, -1$). From Ref. (Astrakharchik *et al.*, 2021). Right panel: The ground state energy of a $^{174}\text{Yb}^+$ ion in the presence of bosonic ^7Li atoms as a function of the number of atoms obtained in DMC calculations for two characteristic models for atom-ion interaction potential. Adapted from (Chowdhury and Perez-Ríos, 2024).

The spectral function of an ion in a BEC obtained from a coherent state ansatz (able to account for large dressing clouds) is shown in Fig. 26: it features well-defined polarons, which are also captured by the ladder approximation (red lines). The white dashed lines are states containing an increasing number of bosons bound to the ion in agreement with the snowball states found in the DMC calculations described above. The red stars indicate when the coherent state ansatz becomes unreliable due to a large local gas parameter close to the ion. Recently, a mobile ion in a BEC was explored using the LLP transformation combined with mean-field GP theory leading to Eq. (39) with the atom-ion interaction potential given by Eq. (53) (Cavazos Olivás *et al.*, 2024). The polaron energy obtained from this approach agrees with that from the ladder approximation shown in Fig. 26 for weak to moderate interaction strengths, whereas deviations were found close to resonance. An alternative

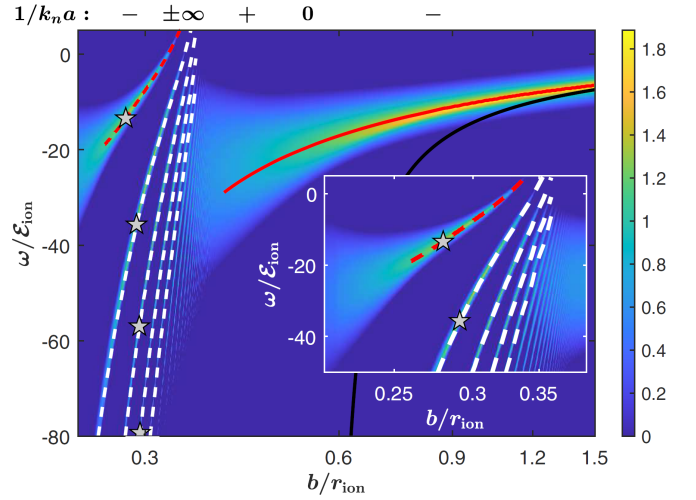


FIG. 26 **Spectrum of a $p = 0$ ion in a BEC** as a function of b (the corresponding a is shown above the graph) with $n_0 r_{ion}^3 = 1$, $c = 0.0023r_{ion}$ and $m = m_b$. The red solid and dashed lines are polaron energies from the ladder approximation, the black line is the mean-field energy, and the white lines are ionic molecules containing an increasing number of bosons. The stars indicate where the BEC density at the ion reaches $n(0) = 0.01a_b^{-3}$. From (Christensen *et al.*, 2021).

approach to describing a moving ion was proposed in Ref. (Oghittu *et al.*, 2024), where a master equation was derived to capture the system's dynamics.

We now turn to the properties of an ion in an ideal Fermi gas, which should be more robust towards the formation of snowball states due to the Pauli principle. The top panel of Fig. 27 shows the spectral function of an ion in a Fermi gas obtained from the ladder approximation. Another polaron branch emerges every time the interaction supports a new bound state so that there are $N + 1$ branches when the interaction supports N bound states in agreement with the results of Ref. (Massignan *et al.*, 2005) and Fig. 23. For this low density, the polaron is well described by a short range interaction with the same scattering length. The ionic Fermi polaron was also explored using fixed node MC calculations and the results are shown in the bottom panel of Fig. 27 using the interaction Eq. (53) again with $c = 0.0023r_{ion}$ (Pessoa *et al.*, 2024), $m = m_b$ and the densities $nr_{ion}^3 = 1$ and $nr_{ion}^3 = 0.1$. Large deviations between the predictions of the fixed node MC and the ladder approximation were found for strong interactions. Using a Landau-Pekar energy functional and the Thomas-Fermi approximation, an ion interacting with a neutral ideal Fermi gas via a $-C_4/r^4$ potential was predicted to develop a diverging effective mass and therefore localize (self-trap) (Myśliwi and Jachymski, 2024).

The picture emerging from these works is that the number of bosonic atoms bound to an ion can be much larger than for neutral impurities leading to the formation of snowball states in agreement with what is found

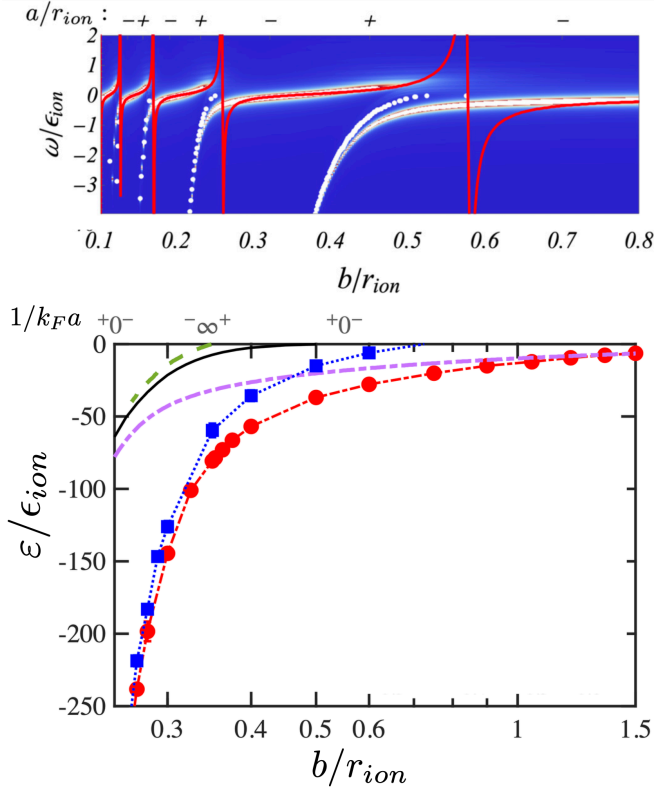


FIG. 27 **Spectrum of a $p = 0$ ion in a Fermi gas.** Top: Spectrum in a dilute bath ($n_0 r_{ion}^3 = 0.01$) obtained from the ladder approximation, with $c = 0.0023 r_{ion}$ and $m = m_b$ (Christensen *et al.*, 2022). The red line is the mean-field result. From (Christensen *et al.*, 2022). Bottom: Spectrum in a dense bath ($n r_{ion}^3 = 1$). Red circles and blue squares are the polaron and dimer energies obtained by DMC method, purple dash-dotted and green dashed lines are the corresponding results from the ladder approximation, and the black line is the dimer energy in vacuum. From (Pessoa *et al.*, 2024). The scattering length is shown above each graph.

using different methods (Côté *et al.*, 2002; Massignan *et al.*, 2005; Schurer *et al.*, 2017). Also, contrary to the case of a neutral Fermi polaron, the accuracy of the ladder approximation in the ionic case remains uncertain, since the suppression of $n \geq 2$ correlations is less efficient for the long-range atom-ion interaction.

B. Dipolar polarons

Significant progress has been made on the trapping and cooling of atoms with a permanent magnetic or electric dipole moment (Bigagli *et al.*, 2024; Chomaz *et al.*, 2022; Schindewolf *et al.*, 2022; Valtolina *et al.*, 2020). These advances provide promising experimental platforms to explore the rich physics of dipolar interactions including novel quantum many-body physics (Baranov *et al.*, 2012; Trefzger *et al.*, 2011). So far there are however no experimental results regarding polarons in dipolar sys-

tems, so in the rest of this Section we will focus on the theoretical predictions for the cases illustrated in Fig. 28.

The interaction between two parallel dipoles is

$$V(\mathbf{r}) = \frac{D^2}{4\pi r^3} (1 - 3 \cos^2 \theta), \quad (55)$$

where θ is the angle between their dipole moments \mathbf{d} and their relative separation \mathbf{r} . For magnetic dipoles one has $D^2 = d^2 \mu_0$ whereas $D^2 = d^2 / \epsilon_0$ for electric dipoles. Crucially, the dipolar interaction has attractive and repulsive regions: when two dipole moments are oriented head to tail they attract each other, whereas they repel when they are oriented side by side. This anisotropy leads to polarons with unique properties.

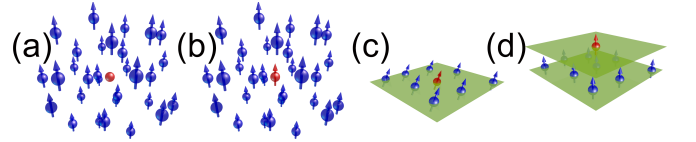


FIG. 28 **Dipolar polarons.** A variety of configurations may be obtained with fully-aligned dipoles: (a) non-dipolar impurity (red) in a dipolar gas (blue); (b) dipolar impurity in a dipolar gas; (c) dipolar impurity in a dipolar gas, all trapped in the same 2D layer. (d) dipolar impurity in one layer interacting with a dipolar gas in another parallel layer.

The cases of a non-dipolar and dipolar impurity immersed in a dipolar Bose gas, see Fig. 28(a)-(b), were considered using a coherent-state variational ansatz. The anisotropic dressing and relaxation dynamics of the impurity after a sudden switching on of the dipolar interaction were computed, finding an effective mass that depends on the direction of motion relative to the polarization axis (Volosniev *et al.*, 2023). The case of a static impurity in a dipolar gas was explored in Ref. (Shukla *et al.*, 2024). The spectral function of a non-dipolar impurity in a dipolar Bose gas, Fig. 28(a), was calculated using second order perturbation theory revealing an anisotropic dispersion (Kain and Ling, 2014). It was furthermore analysed how the anisotropy of the phonon spectrum affects the Cherenkov radiation when the impurity moves faster than the speed of sound (Čerenkov, 1937). Using a time-dependent GPE, the density profile and breathing dynamics of a dipolar condensate in a harmonic trap interacting with a non-dipolar impurity was calculated (Guebli and Boudjemâa, 2019). The breathing modes were also analysed using a variational approach (Hu and Xue, 2014). A Fermi polaron formed by a non-dipolar impurity in a dipolar Fermi gas was shown using the Chevy ansatz Eq. (16) to have anisotropic properties stemming from the Fermi surface being deformed by the dipolar interaction (Nishimura *et al.*, 2021).

The energy, effective mass, and quasiparticle residue of a Bose polaron formed by a dipolar impurity in a quasi-2D dipolar Bose gas [as shown in Fig. 28(c)], were

calculated using second order perturbation theory (Peña Ardila and Pohl, 2018). Analysing dipolar mixtures using a Lee-Huang-Yang energy functional, it was shown that quantum fluctuations of a dipolar Bose gas can strongly modify the miscibility of dipolar impurities (Bisset *et al.*, 2021). The same 2D problem was examined using DMC for an arbitrary angle of the dipoles with respect to the plane (Sánchez-Baena *et al.*, 2024) [see Fig. 28(c)], finding that the polaron energy and the quasiparticle residue follow a universal behavior with respect to the angle when scaled in terms of the s -wave scattering length. The properties of a Fermi polaron formed by a dipolar impurity interacting with a gas of dipolar fermions were calculated using DMC method in 2D (Bombín *et al.*, 2019b). By comparing with the case of short range interactions, it was found that polaron properties are universal depending only on the scattering length a for low densities, while for larger densities the specific shape of the interaction becomes important.

Dipoles in one or more layers give rise to new and interesting effects. Even the problem of one dipole in one layer interacting with a dipole in another parallel layer with both dipole moments perpendicular to the layers is quite delicate, since the integral of their mutual interaction is exactly zero. It follows that one cannot use the usual criterion for a bound state in 2D - namely that the integral of the interaction is negative (Landau and Lifshitz, 1977). Eventually, it was shown that a two-body bound state in fact always exists although its energy can be exponentially small (Baranov *et al.*, 2011). Trimers and tetramers were later predicted for interlayer distances beyond a certain threshold (Guijarro *et al.*, 2021, 2020).

The Fermi polaron formed by a dipole in one layer interacting with a dipolar Fermi gas in another parallel layer with all dipole moments perpendicular to the planes was analysed using fixed-node DMC (Matveeva and Giorgini, 2013). The top panels of Fig. 29 show the polaron energy and effective mass as a function of the interlayer separation λ , for different values of the dipole strength r_0 . In the regime where the dipolar Fermi gas forms a Wigner crystal, the properties of the polaron can be understood as an impurity coupled to lattice phonons much like the Fröhlich model for electrons interacting with crystal phonons, see Sec. III. The effective mass of this polaron was found to become very large for small layer distances indicating self-trapping. For large layer distances, the results agree with perturbation theory. Tiene *et al.* (2024) studied the same bilayer geometry using the Chevy variational wave function Eq. (16) neglecting interactions between the fermions. The impurity spectral function is shown in the bottom panel of Fig. 29. Multiple polaron branches are found, which arise from two-body interlayer bound states with different angular momenta. The branch with the strongest spectral weight and lowest energy is the one associated with the s -wave scattering, and its energy is consistent with the DMC

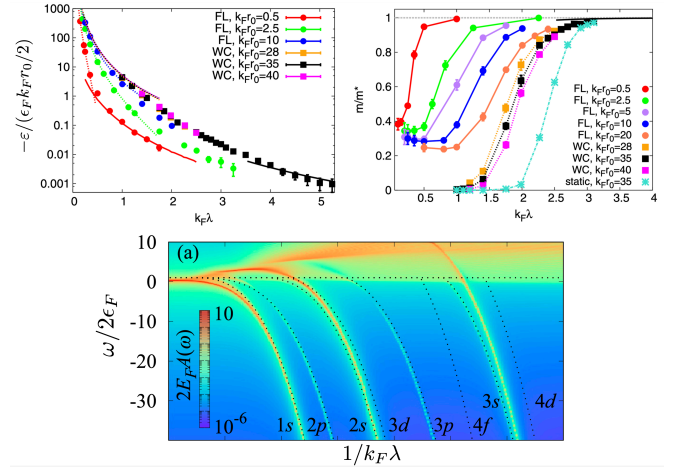


FIG. 29 **Dipolar Fermi polaron in a bi-layer.** Top left: The energy of a Fermi polaron in a bilayer geometry as a function of the distance between layers λ for different values of in-plane interaction strength $r_0 = mD^2/4\pi$. The dipolar impurity, confined to the first layer, interacts with a gas of dipolar fermions, confined to the second layer [see Fig. 28(d)]. Dashed lines represent the two-body binding energies and solid lines correspond to perturbation theory. Circles/squares refer to the fermions forming a Fermi liquid/Wigner crystal. Top right: The polaron effective mass with stars corresponding to a static Wigner crystal (no phonons). From Ref. (Matveeva and Giorgini, 2013). Bottom: Zero momentum spectral function of a dipolar impurity in the same setup as the panel above using the Chevy ansatz. The (black) dotted lines are 1s to 4d dimer energies with unbinding occurring at $\omega = 2\epsilon_F$ (horizontal dotted line). From Ref. (Tiene *et al.*, 2024).

calculations of Ref. (Matveeva and Giorgini, 2013).

In conclusion, dipolar interactions give rise to interesting effects for Bose and Fermi polarons not present for short range interactions. This includes anisotropic properties, multiple bound states and polaron branches. Many open questions remain such as a complete understanding of the possible self-localisation for dipolar polarons (Myśliwy and Jachymski, 2024), and the effects of a non-zero temperature.

C. Rydberg polarons

The excitation of atoms to Rydberg states results in the formation of atoms of greatly enhanced size and increased polarizability, generating strong and long-range interactions, which have been explored in a wide range of studies, from polariton physics to spin models. Shifts and broadening of the atomic Rydberg lines have been observed in BECs and dense atomic gases, arising from the scattering of ground-state atoms with the outer electron of the excited Rydberg atom. The underlying electron-atom interaction has the typical attractive $1/r^4$ form, which for many alkali species gives rise to a negative scattering length $a_e < 0$. As a result, the neutral atoms

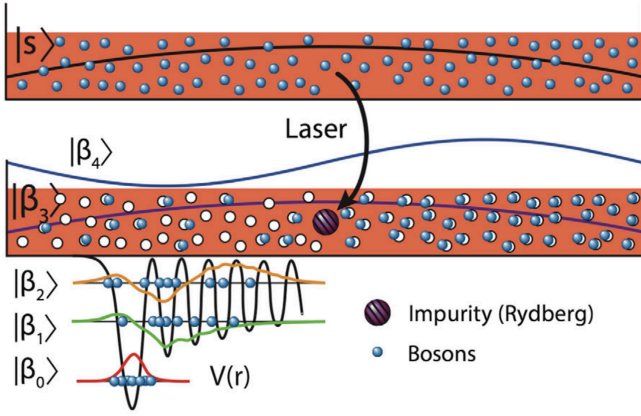


FIG. 30 **Rydberg polarons.** Exciting an impurity to a Rydberg state inside a Bose gas leads to the formation of a very large quasiparticle. From Ref. (Camargo *et al.*, 2018).

experience an effective attractive potential generated by the Rydberg atom that is an image of the Rydberg wave function $\psi_n(\mathbf{r})$ and given by

$$V_{\text{Ryd}}(\mathbf{r}) = \frac{2\pi\hbar^2 a_e}{m_e} |\psi_n(\mathbf{r})|^2. \quad (56)$$

This interaction can be extremely long-ranged and supports a multitude of bound states (so-called Rydberg molecules) between the Rydberg atom and atoms from its environment, see Fig. 30. In Ref. (Schmidt *et al.*, 2016), the physical mechanism responsible for the shifts and the specific shape of the Rydberg lines, which so far had escaped explanation, was attributed to the formation of a “superpolaron” state, in which the impurity atom is dressed by a large number of bound states of the Rydberg potential. This state was later observed, confirming the underlying bound-state physics as the driving mechanism behind the formation of Rydberg polarons (Camargo *et al.*, 2018). In order to describe the formation of Rydberg polarons in a BEC, a hybrid approach using a time-dependent coherent state and functional determinants following a Lee-Low-Pines transformation was employed (Schmidt *et al.*, 2016, 2018b), which was later adapted to describe the excitation of heavy impurities in a Bose gas (Drescher *et al.*, 2024).

The description of Rydberg polarons in a Fermi gas requires accounting for a competition between formation of bound states with high-angular momentum and Pauli blocking (Sous *et al.*, 2020). It was recently proposed that Rydberg excitations allow for an in-situ, spatially resolved, real-time probe of the formation of the dressing cloud Fermi polarons (Gievers *et al.*, 2024) on suboptical length scales reaching down to the 50nm regime, see Fig. 31.

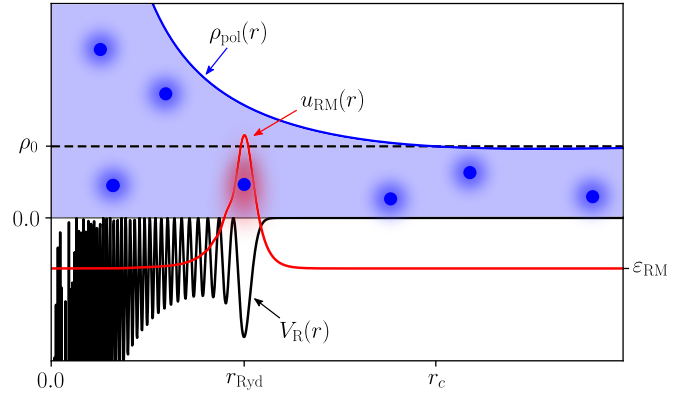


FIG. 31 **Rydberg sensing of polaron clouds.** Rydberg impurities can be used to observe the real-time formation of polaron clouds on suboptical length scales. From (Gievers *et al.*, 2024).

D. Rotating molecules in a quantum bath: angulons

In most parts of this review we discuss how the translational motion of an impurity is changed by its interaction with a quantum many-body environment. One can, however, also raise the question how *rotation* may be modified by similar polaronic effects. This question is indeed of central importance for the spectroscopy of molecules in solvents, in particular superfluid He^4 nanodroplets, and it was observed in quantum chemistry experiments that the rotational constant of molecules is changed by interaction with a many-body environment. In Ref. (Schmidt and Lemeshko, 2015), it was proposed that this effect can be understood in terms of the formation of a dressed quantum rotor similar to a Bose polaron, where a rotating polaron cloud inhibits the bare molecular rotation (Schmidt and Lemeshko, 2016). It was later shown how the dynamics of such an “angulon” formation can be used for rotational cooling (Will *et al.*, 2019). Using variational ansätze (Zeng *et al.*, 2023), the concept of angulons was adapted to molecular ions (Midya *et al.*, 2016) as well as inter-angulon interactions (Li *et al.*, 2020). Moreover, it was shown how bound state formation requires accounting for the full Bose polaron model extended to rotation (Dome *et al.*, 2024). Angulons were also studied in real space using the GPE (Suchorowski *et al.*, 2024). For an in-depth review of the progress on angulons we refer to the review (Lemeshko and Schmidt, 2017).

V. POLARONS IN 2D MATERIALS

With advances in fabrication of atomically thin TMDs such as MoSe_2 , MoS_2 , MoTe_2 , WSe_2 , and WS_2 and their van der Waals heterostructures, a whole new class of 2D quantum materials can be designed and fabricated with applications in fundamental science and technology (Schaibley *et al.*, 2016; Wang *et al.*, 2018a). As dis-

cussed in this section, this includes recent realisations of both the Fermi polaron formed by excitons interacting with electrons, and Bose the polaron formed by excitons in two spin states. At first glance, TMDs appear very different from ultra-cold atoms due to their non-equilibrium nature involving a short-lifetime quantum impurity (exciton) coupled to interacting fermions (electrons), as well as their much higher densities and smaller particle masses. In a way, the success of the polaron model in describing the optical excitation spectrum of these 2D materials is a manifestation of the power and universal applicability of this framework.

Before proceeding with a detailed discussion of polarons in TMDs, we highlight some of the unique features of these materials: 1) they are truly 2D since the layers are atomically thin with even the size of the quantum impurity (exciton) larger than the layer thickness d ; 2) they are very cold, reaching $T/T_F \lesssim 0.01$ in dilution refrigerators (Smoleński *et al.*, 2021); 3) the hybridisation of excitons with photons in an optical cavity gives rise to polaritons acting as impurities with an extremely light mass; 4) the strongly interacting nature of the electrons and holes imply that a plethora of many-body phenomena affect the polaron spectra, and therefore the latter may be used as optical probes of interesting strongly-correlated electronic states (such as Wigner crystals, kinetic magnetism, or integer and fractional Chern insulators); 5) at high exciton densities, it is possible to reach a degenerate Bose-Fermi regime, and the ability to tune the exciton decay rate using hybrid excitons ensures that one could study both driven-dissipative as well as equilibrium regimes.

A. Excitons in TMDs

TMDs are direct band gap semiconductors with extrema of their dispersion located at the so-called K and K' points in the hexagonal Brillouin zone, which are connected by time-reversal symmetry. There is a large spin-valley splitting as well as valley selective light-matter coupling using circularly polarized light (Mak *et al.*, 2012; Zeng *et al.*, 2012), see Fig. 32. The optical excitation spectrum is dominated by a strongly bound exciton state of a conduction band (CB) electron and a valence band (VB) hole due to the relatively heavy carrier mass and reduced dielectric screening in 2D (Chernikov *et al.*, 2014). As a consequence, the exciton has a small radius, which we refer to as the Bohr radius even though the attractive potential yielding the bound state deviates from Coulomb at short distances and is better described as Rytova-Keldysh potential (Keldysh, 1979). It follows that, to a good approximation, the excitons in the present context can be regarded as bosonic impurity particles, which is a crucial feature for realising polarons in these systems.

The relevant length and energy scales include (Goryca

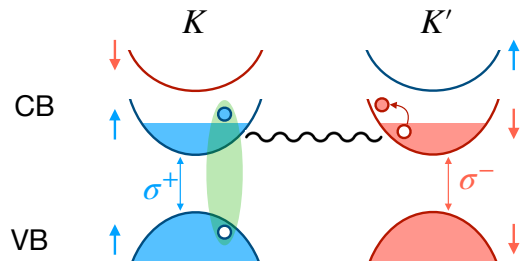


FIG. 32 **Exciton-polarons.** TMD layers have a bipartite honeycomb lattice structure and the minima (maxima) of the conduction (valence) band are located at the K and K' points of the Brillouin zone. Absence of inversion symmetry ensures that the electronic spectrum is gapped at these points. Electrons in the K (K') valley can be optically excited using right (left) hand circularly polarized light. Large spin-orbit splitting in turn ensures that, by choosing appropriate light polarization and energy, it is possible to generate electrons with a well defined spin-valley quantum number. An exciton (green ellipse) excited in the K valley by light with σ^+ circular polarization interacts strongly with electrons of opposite spin in the K' valley, leading to the formation of an *exciton-polaron*.

et al., 2019; Wang *et al.*, 2018b):

1. The lattice constant and layer thickness are $a_L \simeq 0.3$ nm and $d \simeq 0.7$ nm. These are the smallest length-scales in the problem, which justifies a continuum 2D treatment.
2. The exciton radius ranges from $a_x = 1.2$ nm in MoSe₂ to $a_x = 1.7$ nm in WSe₂. Even though a_x is only approximately four times larger than the lattice constant a_L , the excitons can be described as Wannier excitons.
3. The measured binding energy is $|\epsilon_X| \simeq 200$ meV for the ground state $1s$ exciton when the monolayers are encapsulated by hexagonal boron nitride (hBN). For a suspended monolayer, the binding energy is predicted to be $\epsilon_x \simeq 500$ meV.
4. The binding energy of an exciton-electron or exciton-hole state, i.e. a trion, is $|\epsilon_T| \sim 20 - 30$ meV.
5. The rms size of the trion is $a_T \simeq 2.0 - 2.5$ nm.
6. The Fermi momentum is in the range $1/k_F \simeq 1.5 - 20$ nm corresponding to a Fermi energy 0.1 meV $\lesssim \epsilon_F \lesssim 20$ meV, which is readily tunable using applied gate voltages. The lower limit for k_F arises either from disorder or many-body correlations that compete with the formation of a Fermi liquid. The upper limit is determined by the breakdown of the description of an exciton as a point particle.

We note that the fundamental parameters of TMD excitons, such as ϵ_x and a_x cannot be measured directly. Instead, the diamagnetic shift of the $1s$ exciton

is $\Delta\epsilon = e^2 a_x^2 B_z^2 / 8m_r$ at high magnetic fields (B_z) can be used to determine a_x ; this method relies on an estimate of the reduced mass m_r from a combination of ARPES and transport measurements or from DFT calculations. In turn, ϵ_x can be determined through measurement of Rydberg exciton resonances (principal quantum numbers $2 \leq n \leq 5$) together with calculations based on the Rytova-Keldysh potential. In contrast, the trion binding energy ϵ_T is directly accessible in optical spectroscopy (Xu *et al.*, 2014); an estimate of a_T from $\epsilon_T = \hbar^2 / 2m_r a_T^2$ is in good agreement with calculations based on exact diagonalization (Fey *et al.*, 2020).

B. Exciton-polarons

The chemical potential μ and hence the itinerant electron or hole density in TMD layers can be tuned by gate voltages. When μ is set in between the valence band maximum and conduction band minimum, the material is charge neutral. In this case, the optical excitation spectrum is dominated by the 1s-exciton, with a linewidth determined by the radiative decay rate in high quality samples. Upon increasing (decreasing) μ above (below) the conduction (valence) band minimum (maximum), one injects itinerant electrons (holes) into the monolayer. Experimentally, this leads to the observation of a red-detuned resonance that appears in the spectrum upon injection of charged carriers, which initially was attributed to formation of trions (Cadiz *et al.*, 2016; Chernikov *et al.*, 2015; Courtade *et al.*, 2017; Mak *et al.*, 2013; Ross *et al.*, 2013; Zhang *et al.*, 2014; Zhu *et al.*, 2015). The large oscillator strength and narrow linewidth of this red-shifted resonance is however inconsistent with a trion-based description, since the trion has only a small oscillator strength. This in close analogy with the small spectral weight of the dimer state in the atomic impurity spectral function as discussed in Sec. II. Pioneering theoretical and experimental work then demonstrated that for $\epsilon_F \lesssim \epsilon_T \ll \epsilon_X$, the Fermi-polaron framework instead provides a more appropriate description of the elementary optical excitations (Efimkin and MacDonald, 2017; Fey *et al.*, 2020; Rana *et al.*, 2020; Sidler *et al.*, 2016). A similar framework was previously developed to describe the interacting exciton-electron problem (Suris, 2003).

Even though the validity of Fermi-polaron description was initially demonstrated experimentally for a MoSe₂ monolayer embedded inside an optical cavity (Sidler *et al.*, 2016), the majority of the experiments are carried out where excitons couple to free-space radiation field modes. In this case, the coupling between the photons and the excitons can be treated as a weak perturbative probe and one is left with the problem of analysing an exciton interacting with itinerant electrons, which will be discussed in this section. The case of a strong photon-exciton coupling achieved by immersing the semiconduc-

tor in an optical cavity is discussed in the next section.

When neglecting the interaction between the electrons and treating the excitons as point bosons, the Hamiltonian describing an exciton interacting with itinerant electrons is given once more by Eq. (15), where the operators $\hat{c}_{\mathbf{k}}^\dagger$ and $\hat{f}_{\mathbf{k}}^\dagger$ now create an exciton and an electron with momentum \mathbf{k} . The exciton-electron interaction has a range $\sim a_x$ following the classical charge-dipole interaction $-\alpha_0 e^2 / (4\pi\epsilon r^4)$ for distances $r \gg a_x$, where α_0 is the polarizability. Thus, one should expect it for most present purposes to be well described by a contact interaction when a_x and $r_0 = \sqrt{\alpha_0 m_e e^2 / (2\pi\epsilon\hbar^2)}$ are much smaller than the interparticle distance. Microscopic calculations indeed show that for most purposes a phenomenological contact potential gives accurate results (Efimkin *et al.*, 2021; Fey *et al.*, 2020; Kumar *et al.*, 2024).

Within these approximations, the problem becomes identical (apart from being 2D) to that discussed in Sec. (II): A mobile impurity (exciton) interacting via a short range potential with a Fermi sea (electrons). This means that these quasiparticles can be studied by means of the approaches developed for Fermi polarons. Like in 3D, a momentum independent interaction g_{ex} gives rise to an ultraviolet divergence, which can be cured by relating the energy ϵ_T of a bound exciton-electron or exciton-hole state, i.e. a trion, to g_{ex} . Indeed, a bound state corresponds to a pole in the scattering matrix, $1 - g_{ex}\Pi_v(0, \epsilon_T) = 0$, which gives (Carusotto *et al.*, 2010; Levinsen and Parish, 2013; Randeria *et al.*, 1990; Schmidt *et al.*, 2012a; Wouters, 2007; Zöllner *et al.*, 2011)

$$\frac{1}{g_{ex}} = \sum_{|\mathbf{k}| < \Lambda} \frac{1}{\epsilon_T - \epsilon_{x\mathbf{k}} - \epsilon_{e\mathbf{k}}}, \quad (57)$$

where Λ is an UV cut-off related to $1/a_x$. This relation can be used to eliminate the coupling constant g_{ex} and the cut-off in favor of the trion energy. Since a_x is smaller than all other relevant length-scales, one may take the limit $\Lambda \rightarrow \infty$ at the end of the calculation. Using this approach, the 2D scattering matrix can be written as

$$\mathcal{T}(\mathbf{k}, \omega) = \frac{1}{\Pi_v(0, \epsilon_T) - \Pi(\mathbf{k}, \omega)} = \frac{g_2}{1 - g_2 \Delta\Pi(\mathbf{k}, \omega)} \quad (58)$$

where the pair propagators are given by Eq. (19) for 2D, $\Delta\Pi(\mathbf{k}, \omega) = \Pi(\mathbf{k}, \omega) - \text{Re}\Pi_v(0, \epsilon_F)$, and

$$g_2 = -\frac{\pi}{m_r} \frac{1}{\ln(k_F a m_r / m)}. \quad (59)$$

The second equality in Eq. (58) is obtained by adding and subtracting the vacuum pair propagator evaluated at a typical many-body energy $\text{Re}\Pi_v(0, \epsilon_F)$ in the denominator. In this way, we can extract the typical interaction strength given by Eq. (59), which should be

compared with the corresponding 3D parameter $k_F a$. This shows that the strongly interacting regime is for $k_F a \sim 1$ (Bloom, 1975; Engelbrecht and Randeria, 1992), and that there is no unitarity regime $1/a = 0$ since a bound state always exists in 2D.

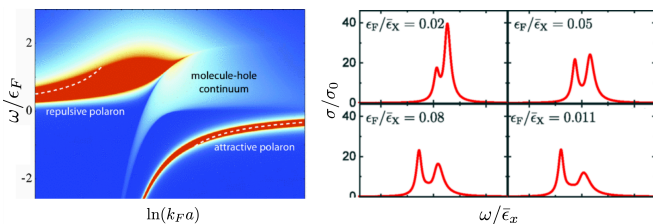


FIG. 33 **Exciton spectra.** Left: Zero momentum exciton spectral function for $m_x = m_e$ at fixed electron density. From (Schmidt *et al.*, 2012a). Right: Optical conductivity of a 2D semiconductor (proportional to the $p = 0$ exciton spectral function) for different electron densities. Here $\bar{\epsilon}_x$ is the exciton binding energy in the absence of the Fermi sea, and the trion binding energy is fixed at $|\epsilon_T| = 0.07\bar{\epsilon}_x$. From (Efimkin and MacDonald, 2017). Recall that $\epsilon_T \propto 1/a^2$.

The left panel of Fig. 33 shows the exciton spectral function obtained from the ladder approximation Eqs. (16)-(17) (Schmidt *et al.*, 2012a). We clearly see two branches corresponding to an attractive and repulsive polaron. The energy unit is ϵ_F since this is typically constant in atomic gases while a is tuned. The right panel shows the optical conductivity of 2D semiconductors, which is proportional to the zero momentum exciton spectral function calculated using a similar approach (Efimkin and MacDonald, 2017). This shows a characteristic prediction of the polaron theory: the spectral weight of the attractive polaron and its energy splitting to the repulsive polaron increases with the electron density, where the energy unit is ϵ_x since in semiconductors one typically tunes the Fermi density at fixed trion binding energy ϵ_T (recall that $\epsilon_T \propto 1/a^2$). The ladder approximation should be accurate when $\epsilon_F \lesssim |\epsilon_T| \ll |\epsilon_X|$, whereas three-body correlations not included in the theory may become important for $\epsilon_F \ll |\epsilon_T|$. It has however been shown that the polaron picture yields oscillator strengths almost indistinguishable from a description based on independent trion excitations in the regime of a Fermi energy smaller than the line broadening (Glazov, 2020). We also remark that Fermi polarons within the ladder approximation can be mapped to the formation of bright polaritons within the Tavis-Cummings model, which allows new insight into the nature of Fermi polarons (Imamoglu *et al.*, 2021).

We emphasize that the Hamiltonian Eq. (15) assumes that the excitons are robust mobile bosonic impurities in the $1s$ -state of the quantized relative electron-hole motion. An experimental validation of this assumption is discussed in Sec. V.F. Equation (15) also suppresses any valley and spin degrees of freedom since we assume that

excitons generated in the K (K') valley interact predominantly with electrons in the lowest energy spin state of the K' (K) valley as illustrated in Fig. 32. This is a consequence of (i) the large spin-orbit interaction ensuring that only the lowest energy spin state of either valley is occupied for $\epsilon_F \lesssim 20$ meV, and (ii) Pauli exclusion ensuring that a bound trion state exists only if the exciton and the electron occupy opposite valleys so that they have different spins, see Fig. 32. On the other hand, the interaction between an exciton and an electron (or hole) in the same valley does not generally support a bound state, since the Pauli exclusion principle prohibits the electron bound in the exciton from coming close to those in the Fermi sea (Tiene *et al.*, 2022). Since attractive and repulsive polaron physics mainly arise from interactions between excitons and electron (or holes) occupying opposite valleys, we will mostly ignore intra-valley interaction in the following. These assumptions hold for all hole-doped TMD monolayers, as well as for electron-doped MoSe₂ and MoTe₂ layers. The opposite sign of spin-orbit interaction in W-based TMD monolayers leads to a richer polaron spectrum (Wang *et al.*, 2018b).

The intrinsic radiative decay of the excitons is also neglected in a description based on the Hamiltonian in Eq. (15), which is justified when the decay rates are small compared to the relevant energies of the problem. In practice, the radiative decay rate can be reduced to $\Gamma_{\text{rad}} \simeq 0.5$ meV by properly choosing the thickness of the hBN layers, which is comparable to a thermal energy $T \approx 4$ K. Finally, we have ignored Coulomb interactions between electrons so far, which completes the mapping to the Fermi polaron problem in atomic gases. At a first glance this looks problematic since this interaction is not a-priori small. We will return to the role of electron-electron interactions when discussing exciton-polarons as probes for correlated electron states in Sec. V.G. Interestingly, the charge of the electrons in the dressing cloud also makes it possible to manipulate the polarons via a Coulomb drag effect (Cotlet *et al.*, 2019; Efimkin and MacDonald, 2018), which has been experimentally realised using the polaron-polaritons (Chervy *et al.*, 2020). In a similar context it has recently been shown that the dressing of excitons by electrons can lead to a striking change in the diffusion of excitons (Upadhyay *et al.*, 2024), see also (Zerba *et al.*, 2024b).

The top panel of Fig. 34 shows the measured optical spectrum of monolayer MoSe₂ as a function of electron Fermi energy controlled by gating (Sidler *et al.*, 2016), compared to a theoretical calculation based on the Chevy ansatz given by the first two terms of Eq. (16). The excellent agreement between theory and experiment is obtained with only one fitting parameter: A density dependent blue shift $\beta\epsilon_F$ has been added to the calculated spectrum with β a free parameter. The origin of this blue shift that is not captured by Eq. (15) is a combination of (i) the repulsive interactions between excitons and

electrons occupying the same valley (intra-valley interaction) as the gating injects electrons both in the K and K' valleys, (ii) phase-space-filling effects that render low momentum states unavailable for exciton formation in the same valley as degenerate electrons, and (iii) band-gap renormalization due to finite electron density.

Figure 34 illustrates how the polaron model recovers the energies of the two peaks as well as several other key features, which confirms its validity. First, the high energy peak is continuously blue-shifted from the bare exciton peak with increasing electron concentration while it gradually loses spectral weight. Second, a new well defined low energy peak emerges with an oscillator strength that increases linearly with electron density n_e for $n_e \leq 1 \times 10^{12} \text{ cm}^{-2}$. These features are captured by the Chevy ansatz and allow the identification of the low (high) energy resonance as the attractive (repulsive) polaron. The bottom panel of Fig. 34 shows the energy splitting between the upper and lower polaron as a function of the Fermi energy ϵ_F as measured in a doped MoSe₂ monolayer (Huang *et al.*, 2023a). The dashed line is a calculation based on the Chevy ansatz predicting a linear increase in the splitting as a function of ϵ_F .

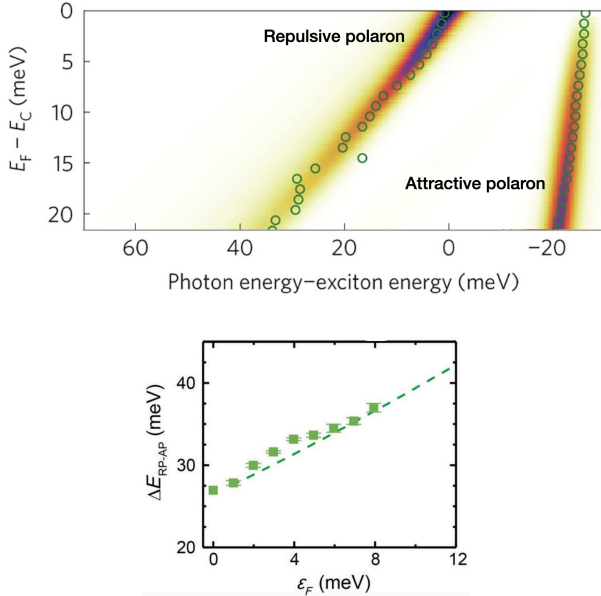


FIG. 34 **Observation of Fermi polarons in TMDs.** Top: Exciton spectral function as a function of the Fermi energy of the electrons from the Chevy ansatz. Green dots are experimental data for the attractive and repulsive polarons obtained from differential reflection spectra for a MoSe₂ monolayer. From Ref. (Sidler *et al.*, 2016). Bottom: energy splitting between the attractive and repulsive polaron measured in a MoSe₂ monolayer. The dashed line is the prediction of the Chevy ansatz. From (Huang *et al.*, 2023a).

Finally, Tiene *et al.* (2023) analyzed the temperature dependence of the 2D Fermi polaron in TMDs, finding

that the attractive polaron is replaced by a trion-hole continuum at high temperatures.

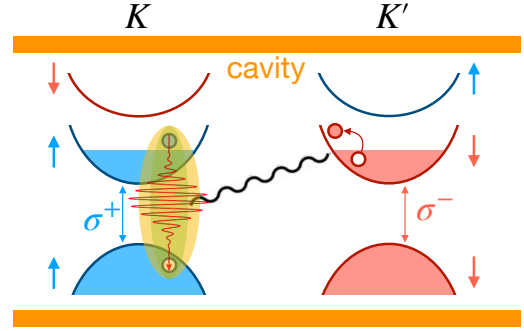


FIG. 35 **Polaron-polaritons.** When a TMD material is embedded in an optical cavity, the excitons hybridize with the cavity photons, leading to the formation of polaritons (orange ellipse). Polaritons interact with electrons of opposite spin in the opposite valley to form *polaron-polaritons*.

C. Polaron-polaritons

A useful feature of 2D materials such as TMDs is that one can embed them inside an optical cavity. This realises a coupling Ω between the cavity photons and the excitons, which can be tuned to be very strong by changing the cavity length as illustrated in Fig. 35. When Ω is comparable to or larger than the photon-exciton detuning (i.e. the difference in their energies) as well as the cavity photon and exciton decay rates, the excitons hybridise with the photons to form polaritons (Carusotto and Ciuti, 2013). In the presence of an electron gas, this gives rise to an interesting interplay between polaron and polariton physics. In addition, since the polariton energy is tunable by changing the cavity length this opens up the possibility to realise Feshbach resonances to increase the interaction strength using a bi-exciton state as we shall discuss in Sec. V.E.

The minimal Hamiltonian describing the interacting exciton-electron system in a TMD monolayer coupled to a cavity mode can be written as

$$H_{xe} = \sum_{\mathbf{k}} \begin{bmatrix} \hat{x}_{\mathbf{k}}^\dagger & \hat{a}_{\mathbf{k}}^\dagger \end{bmatrix} \begin{bmatrix} \epsilon_{x\mathbf{k}} & \Omega \\ \Omega & \epsilon_{c\mathbf{k}} \end{bmatrix} \begin{bmatrix} \hat{x}_{\mathbf{k}} \\ \hat{a}_{\mathbf{k}} \end{bmatrix} + \sum_{\mathbf{k}} \epsilon_{e\mathbf{k}} e_{\mathbf{k}}^\dagger e_{\mathbf{k}} + g_{ex} \sum_{\mathbf{k}, \mathbf{k}', \mathbf{q}} \hat{x}_{\mathbf{k}+\mathbf{q}}^\dagger \hat{x}_{\mathbf{k}} \hat{e}_{\mathbf{k}'-\mathbf{q}}^\dagger \hat{e}_{\mathbf{k}'}. \quad (60)$$

Here, $x_{\mathbf{k}}^\dagger$, $a_{\mathbf{k}}^\dagger$, and $e_{\mathbf{k}}^\dagger$ are the creation operators of excitons of mass m_x , cavity photons of mass m_c , and electrons of mass m_e , all with in-plane momentum \mathbf{k} . The corresponding dispersions are $\epsilon_{x\mathbf{k}} = \mathbf{k}^2/2m_x$, $\epsilon_{c\mathbf{k}} = \mathbf{k}^2/2m_c + \delta$, and $\epsilon_{e\mathbf{k}} = \mathbf{k}^2/2m_e$, where δ is the cavity detuning. Compared to Eq. (15), we have added the coupling Ω (assumed real) to the cavity photons. Diag-

analysing the non-interacting part of Eq. (60) using the transformation $\hat{x}_{\mathbf{k}} = \mathcal{C}_{\mathbf{k}}\hat{L}_{\mathbf{k}} - \mathcal{S}_{\mathbf{k}}\hat{U}_{\mathbf{k}}$ and $\hat{a}_{\mathbf{k}} = \mathcal{S}_{\mathbf{k}}\hat{L}_{\mathbf{k}} + \mathcal{C}_{\mathbf{k}}\hat{U}_{\mathbf{k}}$ yields the eigenoperators $\hat{L}_{\mathbf{k}}^{\dagger}$ and $\hat{U}_{\mathbf{k}}^{\dagger}$ creating lower and upper polaritons, which are hybrid light-matter particles (Al-Ani *et al.*, 2022; Carusotto and Ciuti, 2013). Their energies are $\epsilon_{\mathbf{k}}^{\pm} = (\epsilon_{x\mathbf{k}} + \epsilon_{c\mathbf{k}} \pm \sqrt{\delta_{\mathbf{k}}^2 + 4\Omega^2})/2$, where $\delta_{\mathbf{k}} = \epsilon_{c\mathbf{k}} - \epsilon_{x\mathbf{k}}$ is the photon-exciton detuning and $\mathcal{C}_{\mathbf{k}}^2 = 1 - \mathcal{S}_{\mathbf{k}}^2 = (1 + \delta_{\mathbf{k}}/\sqrt{\delta_{\mathbf{k}}^2 + 4\Omega^2})/2$ are the corresponding Hopfield coefficients (Hopfield, 1958).

When electrons are present, interactions lead to the formation of polaron-polaritons, which like polarons can be analysed with many methods. Here, we shall use field theory providing a convenient way to include a non-zero exciton concentration and temperature. Defining a 2×2 retarded Green's function $G(\mathbf{p}, t) = -i\theta(t)\langle[\hat{\Psi}_{\mathbf{k}}(\tau)\hat{\Psi}_{\mathbf{k}}^{\dagger}(0)]_{-}\rangle$ for excitons coupled to cavity photons with $\Psi_{\mathbf{k}} = [\hat{x}_{\mathbf{k}} \ \hat{c}_{\mathbf{k}}]^T$, the Dyson equation is

$$G^{-1}(k) = \begin{bmatrix} \omega - \epsilon_{x\mathbf{k}} & 0 \\ 0 & \omega - \epsilon_{c\mathbf{k}} \end{bmatrix} - \begin{bmatrix} \Sigma_x(k) & \Omega \\ \Omega & 0 \end{bmatrix} \quad (61)$$

in momentum/frequency space $k = (\mathbf{k}, \omega)$ with $\Sigma_x(k)$ the exciton self-energy coming from interactions with the electrons (Bastarrachea-Magnani *et al.*, 2021b; Levinsen *et al.*, 2019; Tan *et al.*, 2020; Wasak *et al.*, 2021). Equation (61) is a matrix generalisation of the impurity retarded Green's function introduced in Sec. I.C, and its poles give the energies $\epsilon_{\mathbf{k}}$ of the quasi-particles. From Eq. (61) we obtain the self-consistent equations

$$\epsilon_{\mathbf{k}}^{\pm} = \frac{1}{2} \left[\epsilon_{x\mathbf{k}} + \Sigma_x(\mathbf{k}, \epsilon_{\mathbf{k}}^{\pm}) + \epsilon_{c\mathbf{k}} \pm \sqrt{\tilde{\delta}_{\mathbf{k}}^2 + 4\Omega^2} \right] \quad (62)$$

where $\tilde{\delta}_{\mathbf{k}} = \epsilon_{c\mathbf{k}} - \epsilon_{x\mathbf{k}} - \Sigma_x(\mathbf{k}, \epsilon_{\mathbf{k}}^{\pm})$. Importantly, since the energy $\epsilon_{c\mathbf{k}}$ of the cavity photons depend on the cavity length, it is possible to tune the quasiparticle energy.

Equations (61)-(62) illustrate the interplay between polaron physics (entering via the self-energy Σ_x) and polariton physics (entering via the coupling Ω to cavity photons). Indeed, the dispersion of the quasiparticles given by Eq. (62) is identical to that of polaritons except for the replacement $\epsilon_{x\mathbf{k}} \rightarrow \epsilon_{x\mathbf{k}} + \Sigma_{x\mathbf{k}}(\mathbf{k}, \epsilon_{\mathbf{k}})$. Likewise, the Hopfield coefficients are given by the vacuum expressions above with the replacement $\delta_{\mathbf{k}} \rightarrow \tilde{\delta}_{\mathbf{k}}$. The small photon mass $m_c \sim 10^{-5}m_x$ moreover means that the light coupling has only small effects on the self-energy $\Sigma_x(\mathbf{k}, \omega)$ even for a small detuning δ and large Ω , since the electrons scatter the excitons predominantly to states where the photon is off-resonant (large $\delta_{\mathbf{k}}$). This can be seen explicitly by using the ladder approximation to calculate the self-energy Σ_x entering Eq. (62), which again gives Eq. (17) with the scattering matrix given in Eq. (58). The coupling to the cavity photons enters only through the pair propagators, which are however essentially the same as in the absence of light, due to the small photon mass (Bastarrachea-Magnani *et al.*, 2021a,b; Tan *et al.*,

2020; Wasak *et al.*, 2021).

It follows that the quasiparticle emerging from the exciton being strongly coupled to light while simultaneously interacting with electrons can be understood as a *polaron-polariton*, i.e. a coherent superposition of a cavity photon and a polaron with essentially the same properties as in the absence of light. Since the Rabi coupling between the cavity photon and the polaron is $\sqrt{Z_{\mathbf{k}}}\Omega$ with $Z_{\mathbf{k}}$ the polaron residue, the minimal splitting between the upper and lower polaron-polariton branch is reduced by a factor $\sqrt{Z_{\mathbf{k}}}$ as can explicitly be shown from Eq. (62). As we shall see in Sec. V.F, this intuitive picture of polaron-polaritons is corroborated by experimental findings.

Figure 36 shows the zero momentum cavity photon spectral function as a function of detuning δ obtained from Eq. (61) using the ladder approximation. The avoided crossings of the attractive and repulsive polarons with the cavity photon lead to the formation of three polaron-polariton branches. Note that a Feshbach resonance is realized when the lower polariton (L) is tuned into resonance with the trion (horizontal green line) leading to strong interactions. Such a resonance was analyzed in detail taking into account the composite electron-hole nature of the exciton (Kumar *et al.*, 2023).

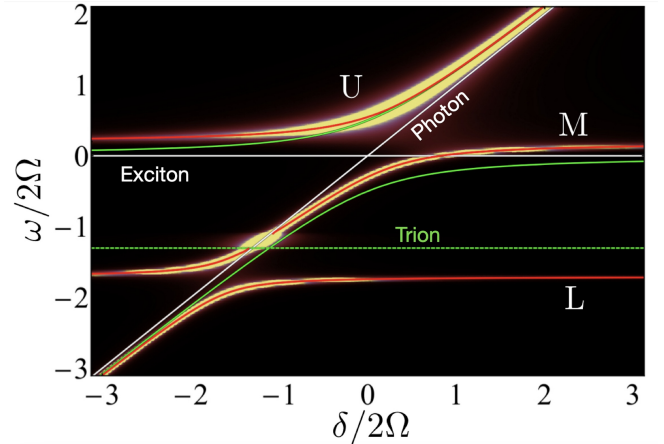


FIG. 36 **Polaron-polaritons.** The zero momentum cavity spectral function as a function of energy ω and detuning δ . The white lines are the uncoupled photon and exciton energies, green lines are the upper and lower polariton in the absence of electrons, the horizontal dashed green line is the trion energy, and the red lines are solutions to Eq. (62). Here $m_x = 2m_e$, $m_c = 10^{-5}m_e$, $\epsilon_F/2\Omega = 0.23$, and $|\epsilon_T|/2\Omega = 1.56$. From Ref. (Bastarrachea-Magnani *et al.*, 2021a).

Polaron-polaritons were first observed in the pioneering experiment by Sidler *et al.* (2016). In Fig. 37 we show results from a later experiment measuring the light transmission spectrum of a MoSe₂ monolayer in a zero-dimensional optical cavity as a function of cavity length (Tan *et al.*, 2020). The energy of the cavity photon and thereby the detuning δ depends on the cavity length. In the left panel, the gate voltage is such that

there are no itinerant electrons and one clearly observes the typical polariton spectrum with an avoided crossing between the cavity photon and the exciton as described by Eq. (62) with $\Sigma_x = 0$, i.e. $\epsilon_{\mathbf{k}=0}^{\pm}$. In the right panel, the gate voltage is increased so that the conduction band is partially filled with electrons that interact with the excitons. This gives rise to two avoided crossings and three polaron-polariton branches as in Fig. 36. The first is continuously blue shifted with increasing electron density from the crossing in the left panel, and it arises from the crossing of the repulsive polaron with the cavity mode. The second crossing on the other hand has no analogue for zero electron density, and it emerges at low energy with increasing electron density from the crossing of the attractive polaron with the cavity mode. Consistent with this picture, the mode splittings at the avoided crossings are reduced compared to the bare splitting when there are no electrons. These experimental results thus clearly demonstrate the formation of polaron-polaritons.

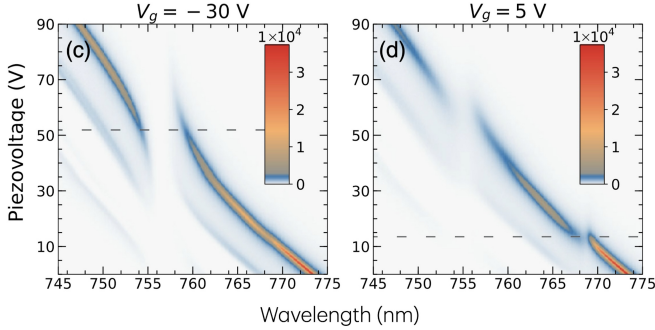


FIG. 37 **Observation of polaron-polaritons.** Light transmission spectrum of a MoSe₂ monolayer in an optical cavity as a function of the cavity mode energy. In the left panel, there are no itinerant electrons and we see a characteristic polariton spectrum with an avoided crossing between the cavity and exciton modes. In the right panel, there are itinerant electrons leading to two avoided crossings of the photon with the repulsive and attractive polarons and the formation of three polaron-polaritons branches. From Ref. (Tan *et al.*, 2020).

Interactions with electrons give rise to a range of non-linear effects concerning coherent states of polaron-polaritons (Julku *et al.*, 2021). One can furthermore use light to probe polaron-polariton physics in a non-demolition manner (Camacho-Guardian, 2023). Polaron-polaritons also emerge for light propagation in atomic gases under the condition of electromagnetically induced transparency (EIT) leading to a number of interesting effects such as self-trapping (Grusdt and Fleischhauer, 2016), a cross-over from a bare polariton to a polaron-polariton (Camacho-Guardian *et al.*, 2020), and superfluid flow above Landau’s critical velocity (Camacho-Guardian *et al.*, 2020; Grusdt and Fleischhauer, 2016; Nielsen *et al.*, 2020).

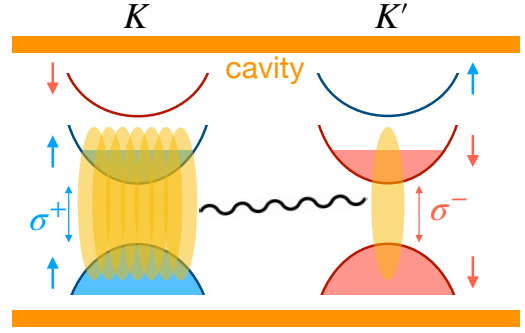


FIG. 38 **Bose polarons in TMD.** A pump beam creates a sizable number of polaritons in the K valley and a probe beam creates few “impurity” polaritons in the K' valley, leading to the formation of Bose polarons.

D. Bose polarons in TMDs

While the Fermi polaron naturally emerges from the interactions between excitons and electrons as discussed above, a solid state realisation of the Bose polaron requires a different mechanism. Early experiments used a pump beam to create a bath of spin \uparrow polaritons in a GaAs microcavity, and a probe beam to create spin \downarrow polaritons as sketched in Fig. 38 (Navadeh-Toupchi *et al.*, 2019; Takemura *et al.*, 2017, 2014). The interaction potential between the two kinds of excitons supported a bound state, i.e. a biexciton, which could be brought into resonance by tuning the energy of the polaritons via the cavity length. A Feshbach resonance between the polaritons was in this way realised giving rise to significant shifts in the transmission spectrum of the probe pulse (Navadeh-Toupchi *et al.*, 2019; Takemura *et al.*, 2017, 2014). Subsequent theoretical works based on a Chevy type variational function including three-body correlations (Levinsen *et al.*, 2019) and a diagrammatic ladder approach (Bastarrachea-Magnani *et al.*, 2019) argued that the experiment could be interpreted in terms of the spin \downarrow polaritons forming a Bose polaron by interacting with the bath of \uparrow polaritons. Fitting the theory to the experimental data however indicated a large damping rate of the bi-exciton, which strongly suppresses the Feshbach resonance.

Recently, clear signatures of the Bose polaron were reported in an experiment, where polaritons consisting of cavity photons and excitons on the K' -valley of a monolayer MoSe₂ were created by a probe beam, while polaritons in the K valley were created by a pump beam (Tan *et al.*, 2023). The polaritons in the K' valley served as impurities whereas the polaritons in the K valley formed the bosonic bath, and the interaction between the two kinds of polaritons supported a bound state (a biexciton). By changing the cavity length, the energy of a pair of polaritons in the two valleys was tuned to that of the bi-exciton thereby realising a Feshbach resonance. This

was observed to lead to two quasiparticle branches in the transmission spectrum of the probe beam, see Fig. 39. Good agreement was obtained comparing to a theory for the Bose polaron based on the Chevy ansatz Eq. (34) generalised to include light coupling and with the bosonic bath of polaritons described as a Fock state, using the bath density and biexciton decay rate as fit parameters. This allowed to identify the two branches in the transmission spectrum as the attractive and repulsive Bose polaron. The observed spectra depended strongly on the delay time between the pump and probe pulses reflecting the inherently non-equilibrium nature of the experiment due to the rapid decay of the polaritons and biexcitons.

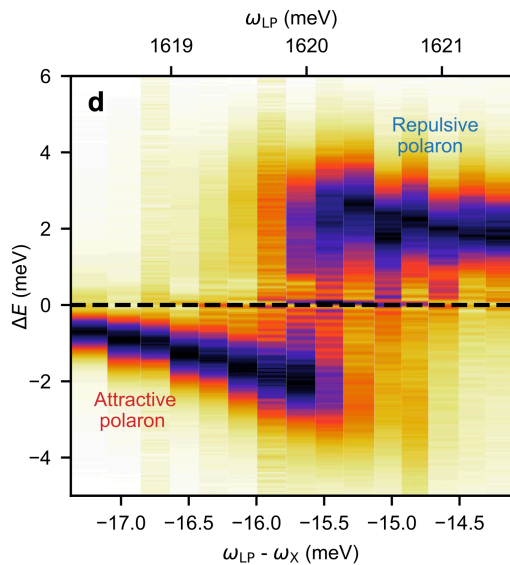


FIG. 39 **Bose polaron in TMDs.** Transmission spectrum of a probe pulse creating polaritons in the K' valley of mono-layer MoSe_2 , when a pump probe has created a bath of polaritons in the K valley. The two branches are identified as attractive and repulsive Bose polarons. The energy ΔE is relative to an undressed polariton with energy ω_{LP} and ω_X is the energy of an exciton. From Ref. (Tan *et al.*, 2023).

Attractive and repulsive Bose polarons formed by intralayer excitons in a degenerate bath of interlayer excitons were recently observed in the photoluminescence spectrum of a 2D semiconductor heterostructure, with an energy splitting increasing with the density of the interlayer excitons in agreement with theory (Szwed *et al.*, 2024). The Bose polaron formed by an impurity interacting with a BEC of polaritons in a microcavity was investigated in Ref. (Vashisht *et al.*, 2022). Several dynamical regimes were identified by calculating the effective mass and the drag force acting on the impurity.

E. Feshbach resonances

Given their tremendous utility in cold atomic gases, it is highly desirable to have Feshbach resonances available

for tuning the interaction also in TMDs. In Sec. V.C, we saw how this can be achieved for the electron-polariton interaction by tuning a polariton into resonance with a trion (Bastarrachea-Magnani *et al.*, 2021a; Kumar *et al.*, 2023). The very steep polariton dispersion however means that the resonance condition is only valid for a small momentum range ~ 0.2 times the photon momentum. In Sec. V.D we discussed a Feshbach resonance between two excitons using bi-excitons, whose typically short lifetime however broadens and suppresses the resonance significantly. One way to avoid this is to use a bi-layer setup where the direct (intralayer) excitons are hybridized with long-lived interlayer excitons, which can then form bound states (Camacho-Guardian *et al.*, 2022).

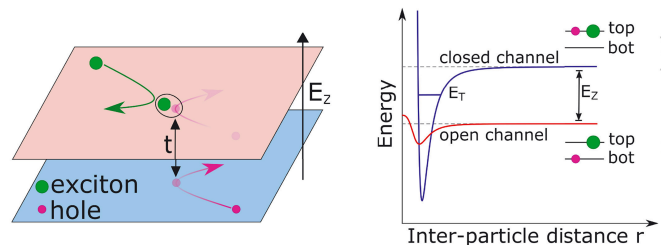


FIG. 40 **Feshbach resonances in TMDs.** A Feshbach resonance between a hole in the bottom layer and an exciton in the top layer is realised when the hole can tunnel to the top layer and bind with the exciton forming a trion, whose energy E_T matches that of the free exciton and hole in the top and bottom layers respectively. From Ref. (Schwartz *et al.*, 2021).

In order to realize a Feshbach resonance between excitons and electrons/holes, a different approach based on a bi-layer setup has been implemented. Investigating an exciton in one MoSe_2 layer (top) interacting with holes in the other MoSe_2 layer (bottom), avoided crossings were observed for the polaron branches as a function of an electric field (Schwartz *et al.*, 2021). This experiment provides a direct observation of a Feshbach resonance arising from holes tunneling to the top layer where they can bind to the exciton forming a trion. As was later analysed in detail theoretically (Kuhlenkamp *et al.*, 2022), when the trion energy equals that of the exciton in the top layer and a hole in the bottom layer, scattering between a bottom layer hole and a top layer exciton is resonant leading to strong interaction effects and avoided crossings, see Fig. 40. Wagner *et al.* (2023) explored this further by solving the full three-body problem of two holes and one electron/hole (or two electrons + one hole).

F. Excitons as robust impurities

In most optically active semiconductors that form the backbone of the optoelectronics devices, the exciton binding diminishes in the presence of itinerant carriers, due to screening of the electron-hole attraction. On the other

hand, the polaron framework requires that the quantum impurity is robust in the presence of a degenerate Fermi or Bose gas, implying that the exciton wave function remains unchanged. Therefore, it is important to determine the range of electron densities where this holds.

To assess the modification of the electron-hole exciton wavefunction, one can use the fact that the optical oscillator strength of an exciton resonance is proportional to $1/a_x^2$. If we assume that the optical excitation spectrum can be described using the Fermi-polaron model, then the total oscillator strength of the attractive and repulsive polaron plus the trion-hole continuum should be the same as that of the bare exciton in the absence of free electrons. Two independent experiments have been used to check the limits of validity of this assumption.

In the first set of experiments, a monolayer MoSe₂ was embedded inside a zero-dimensional cavity, leading to the formation of polaritons when the monolayer is devoid of carriers, and attractive/repulsive polaron-polaritons when free electrons are introduced (Tan, 2022). The minimal polariton (normal mode) splitting is given by

$$\Omega \simeq \frac{ev_D}{a_x} \frac{\hbar}{\sqrt{\epsilon_x \epsilon_r L_{\text{cav}}}} \quad (63)$$

where v_D is the Dirac velocity assuming that MoSe₂ can be described using a massive Dirac model, ϵ_r is the dielectric constant and L_{cav} is the cavity length. Consequently, measuring Ω allows to determine the product $a_x \sqrt{L_{\text{cav}}}$.

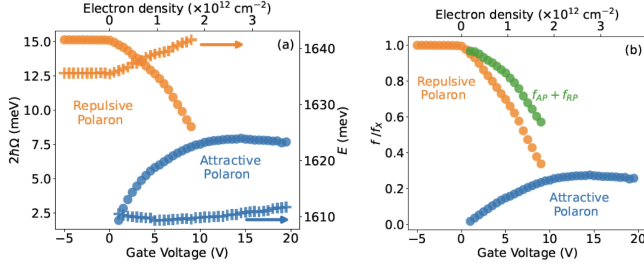


FIG. 41 **Polaron energies and oscillator strengths.** Left: Energy and normal-mode splitting of the attractive (AP) and repulsive (RP) polaron as a function of electron density and extracted polariton splittings. Normal mode-splitting is plotted in circles with respect to the left axis and energies are plotted in crosses with respect to the right axis. Right: Normalized oscillator strength of the AP, RP and their sum as a function of doping density. The oscillator strength is extracted from the normal-mode splitting of the polarons. From Ref. (Tan, 2022).

In the presence of free electrons, both repulsive and attractive polarons were observed. As described in Sec. V.C, if the exciton remains a well-defined impurity particle and the polaron model applies, then the respective normal-mode couplings are $\Omega_{RP} = \sqrt{1 - Z}\Omega$ and $\Omega_{AP} = \sqrt{Z}\Omega$ with Ω_0 the splitting in the absence of the electrons and Z is the residue of the attractive polaron. It follows that $\Omega_{AP}^2 + \Omega_{RP}^2 = \Omega_0^2$ provided we can

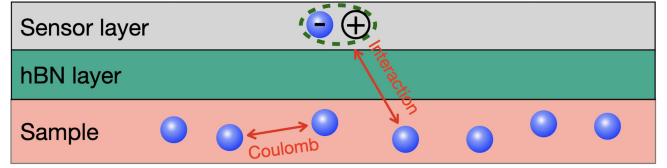


FIG. 42 **Quantum sensing with excitons.** An exciton in a probe TMD layer acts as a quantum sensor by interacting with electrons in an adjacent material of interest. The exciton can also be in the same layer as the material to be probed.

ignore the weight of the trion-hole continuum. By experimentally measuring the normal mode splittings, one can test this prediction. The left panel of Fig. 41 shows the measured energy and normal splitting of the attractive and repulsive polaron as a function of electron density n_e . The splitting of the attractive/repulsive polaron increases/decreases with n_e , which is consistent with an increasing/decreasing residue as predicted by the polaron model. The right panel shows the normalized oscillator strengths $f = \Omega^2/\Omega_0^2$ of the attractive and repulsive polaron, together with their sum $\Omega_{RP}^2 + \Omega_{AP}^2$. The decrease in this sum corresponds to a reduction of a_x via Eq. (63) of the order of 20% for $n_e = 1 \times 10^{12} \text{ cm}^{-2}$ (Fermi energy $\epsilon_F = 3 \text{ meV}$). This is an upper bound since the trion-hole continuum has been ignored, and the relatively small reduction confirms that the exciton wave function to a good approximation is unaffected by the electrons.

In a second set of experiments, the oscillator strengths of the attractive and repulsive polarons were determined using a transfer-matrix fit to the observed reflection lineshapes. The results of these measurements are in full agreement with the experiments based on polaritons (Tan, 2022).

G. Exciton-polarons as quantum probes

As mentioned above, a major difference between the Fermi polaron in atomic gases and in TMDs is that the electrons in the Fermi bath of the exciton-polaron interact. This affects the electronic many-body state, which in turn influences the dressing of the exciton and thereby the spectrum of the exciton-polarons thanks to strong exciton-electron interactions. While at first sight these multiple interactions sound like a major complication, they can be turned around to be a feature since they provide an invaluable tool for optically probing strongly correlated electron states via the exciton spectrum, as illustrated in Fig. 42.

Such probing is important as mono- and multi-layer semiconductors can realise strongly correlated 2D phases, since the large electron and hole band masses together with reduced dielectric screening of Coulomb interactions lead to very large interaction-to-kinetic energy ratios. Of particular interest are semiconductor moiré materials

composed of TMD bilayers (Bistritzer and MacDonald, 2011; Mak and Shan, 2022). A moiré superlattice potential for the electrons emerges when the two TMD layers have a lattice mismatch, or when they are stacked with a non-zero twist angle. Typical superlattice constants are ~ 10 nm and moiré potentials have strengths in the 50 – 100 meV range, generically resulting in almost-flat electronic bands in the reduced Brillouin zone. Semiconductor moiré systems provide a very high degree of tunability of the lattice parameters relevant for electron correlations, such as the carrier density and the ratio of interaction energy to the hopping strength (Pan *et al.*, 2020; Wu *et al.*, 2018). They therefore realise a powerful quantum simulation platform for many-body physics. However, even though strongly-correlated electrons have been traditionally explored using transport spectroscopy, the difficulty in making good electrical contacts to TMDs renders such measurements challenging. Likewise, X-rays and neutrons couple weakly to the layers, rendering spectroscopy difficult. All this leaves an urgent need for new sensors, which exciton-polarons address.

As a first example, exciton-polarons have been used to detect broken symmetry states of electrons in the charge sector. In a charge-tunable MoSe₂ monolayer, one can make the ratio of Coulomb interaction energy to kinetic energy very large so that it is favorable for the electrons to break translational symmetry and form a Wigner crystal (Smoleński *et al.*, 2021). The excitons in turn feel a periodic mean-field potential from this Wigner crystal, which leads to a folding of the exciton spectrum into the Brillouin zone of the Wigner lattice. The result is a new optically active Umklapp-Bragg resonance at the Γ point as shown in the left panel of Fig. 43. The energy of this new branch was observed to depend linearly on the electron density n_e , which can be understood simply from the fact that the kinetic energy of the exciton folded into the Γ point ($\mathbf{k} = 0$) is given by $k_w^2/2m_x$, where $k_w \propto \sqrt{n_e}$ is the Wigner crystal reciprocal vector, see right panel of Fig. 43. The appearance of umklapp terms in the exciton-polaron spectrum has also been used to detect incompressible Mott-like correlated states in a MoSe₂/MoSe₂ bilayer (Shimazaki *et al.*, 2021, 2020).

Exciton-polarons have also been used to detect broken time-reversal symmetry and spin ordering in a triangular moiré lattice formed by a MoSe₂/WS₂ bi-layer (Ciorciaro *et al.*, 2023), see left panel in Fig. 44. This observation is based on the fact that excitons in the K/K' valley, which have spin \uparrow/\downarrow due to spin-valley locking respectively, form trions only with electrons with the opposite spin in the K'/K valley as we discussed in Sec. V.B. It follows that the spectral weight (peak area) of the attractive exciton-polaron in the K/K' valley, which arises from these trion states, is roughly proportional to the density of \downarrow/\uparrow electrons. The experimental results shown in the right panel of Fig. 44 demonstrate that the spectral weight of the attractive polaron formed by a spin \downarrow

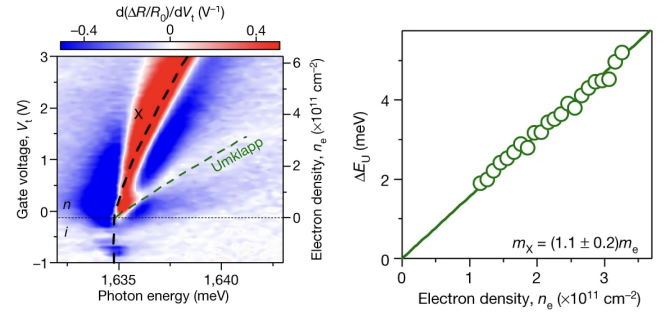


FIG. 43 **Observation of a Wigner crystal.** Left: Derivative of the reflectance contrast spectrum of a MoSe₂ monolayer as a function of gate voltage (or equivalently electron density) and photon energy. In addition to the main exciton branch "X", which is blue shifted corresponding to a repulsive polaron with increasing electron density, an extra high energy umklapp branch appears. Right: The energy difference between the umklapp and polaron branch increases linearly with the electron density. From (Smoleński *et al.*, 2021).

exciton interacting with a spin \uparrow electrons is larger than that of the attractive polaron formed by a spin \uparrow exciton interacting with spin \downarrow electrons. From this it was concluded that the density of \uparrow electrons is larger than that of spin \downarrow electrons corresponding to a ferromagnetic state in the moiré lattice. This experiment demonstrates the more general fact that the degree of circular polarization of the attractive polaron resonance provides a way to determine the spin-susceptibility and magnetic properties of strongly correlated electrons.

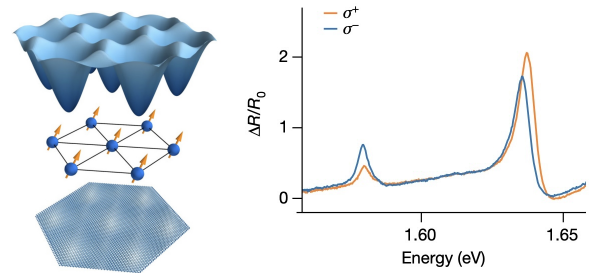


FIG. 44 **Observation of spin ordering.** Left: Electrons in a triangular moiré lattice formed by a MoSe₂/WS₂ bi-layer. Right: Polarization-resolved reflection spectrum at unit filling. The low energy peak of the blue (orange) line corresponds to the attractive polaron formed by a \downarrow (\uparrow) exciton interacting with \uparrow (\downarrow) electrons. From (Ciorciaro *et al.*, 2023).

When electrons undergo a phase transition from a compressible to an incompressible state, their ability to dynamically screen excitons is partially suppressed. If the energy gap of the electronic state is small compared to the trion binding energy, both polaron energies are to first order unmodified. Even in this regime however, the phase transition results in a cusp-like blue shift in the attractive polaron resonance, whereas the repulsive polaron resonance is narrowed due to lack of low energy

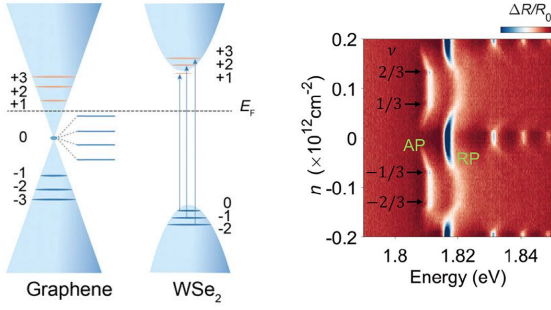


FIG. 45 **Observation of incompressible states.** Left: Excitons formed in a WSe_2 layer interact with electrons in Landau levels in an adjacent graphene layer. Right: Corresponding attractive and repulsive polaron branches observed in reflection contrast spectra as a function the electron density. The attractive branch is enhanced at fractional fillings. From (Cui *et al.*, 2024).

electronic excitations. These features have been observed upon application of moderate magnetic fields in a charge tunable MoSe_2 whenever the electrons form an integer quantum Hall state (Smoleński *et al.*, 2019). Recently, the formation of interlayer attractive and repulsive polarons was observed in a bi-layer setup, where excitons in a WSe_2 layer are dressed by electrons in an adjacent graphene layer (Cui *et al.*, 2024). When the graphene layer was doped away from the incompressible states of filled Landau levels, attractive and repulsive polarons were observed, see Fig. 45.

The emergence of exciton-polaron peaks in optical spectroscopy has also been used to argue for the presence of a dipolar exciton insulator in a moiré lattice formed by a WSe_2/WS_2 bilayer (Gu *et al.*, 2022). Changes in the exciton spectrum were taken as signs of various correlated phases such a Wigner crystals in moiré lattices. However, these observations were not interpreted directly in terms of exciton-polaron physics (Jin *et al.*, 2021; Miao *et al.*, 2021; Xu *et al.*, 2020; Zhou *et al.*, 2021).

In addition to these experiments, several theoretical works explored the use of excitons as sensors. For example, (Salvador *et al.*, 2022) studied the umklapp branches emerging from excitons interacting with out-of-plane ferromagnetic and antiferromagnetic order. Furthermore, (Julku *et al.*, 2024) showed that the dressing of an exciton in a probe layer by spin-waves in an adjacent moiré (anti-)ferromagnet leads to the formation of a new kind of "magnetic" polaron in analogy with the dressing of holes in anti-ferromagnet described in Sec. IX, which can be used to detect magnetic order in an arbitrary direction. (Huang *et al.*, 2023b) demonstrated that the coupling of an exciton to spin waves of an anti-ferromagnet in the same layer leads to polaron formation and observable spectral shifts. (Amelio *et al.*, 2023) showed that the properties of an interlayer polaron formed by an exciton interacting with an adjacent excitonic insulator are af-

fected by the hallmarks of the spectrum of the insulating layer. Considering an exciton interacting with electrons in a moiré lattice, (Mazza and Amaricci, 2022) showed that the presence of Wigner metals and Mott insulators can be identified by means of the emergence of double peak structures in the exciton spectrum. (Sorout *et al.*, 2020) explored the dynamics of immobile and mobile impurities interacting with the low energy Dirac fermions as well as the surface states of 2D and 3D solid-state topological insulators, and showed that in specific conditions the impurity spectral function exhibits power law features indicating the breakdown of the polaron picture.

VI. POLARON-POLARON INTERACTIONS

An inherent feature of quasiparticles is that they interact with each other, since the changes made by one quasiparticle on its environment are felt by the other quasiparticles. This interaction mediated by the environment plays a key role for equilibrium as well as non-equilibrium properties of many-body systems, including collective modes (Baym and Pethick, 2008), conventional and high temperature superconductivity (Lee *et al.*, 2006; Scalapino, 1995; Schrieffer, 1983), and giant magnetoresistance (Baibich *et al.*, 1988). At a fundamental level, all interactions between elementary particles are mediated by gauge bosons (Weinberg, 1995). In this section, we discuss interactions between polarons and how they can be explored using the great flexibility of atomic gases and TMDs. Since we focus on mediated interactions, any direct interaction between the impurities is assumed to be weak. Further details can be found in a recent perspective article (Paredes *et al.*, 2024).

A. Mobile impurities

Taking the first derivative of Eq. (1) gives the energy of a quasiparticle with momentum \mathbf{p}

$$\varepsilon_{\mathbf{p}} = \frac{\delta E}{\delta n_{\mathbf{p}}} = \varepsilon_{\mathbf{p}}^0 + \sum_{\mathbf{p}'} f_{\mathbf{p},\mathbf{p}'} n_{\mathbf{p}'} \quad \text{with} \quad f_{\mathbf{p},\mathbf{p}'} = \frac{\delta^2 E}{\delta n_{\mathbf{p}} \delta n_{\mathbf{p}'}} \quad (64)$$

where $\varepsilon_{\mathbf{p}}^0$ is the energy of a *single* quasiparticle and $\varepsilon_{\mathbf{p}}$ its energy for a non-zero quasiparticle concentration. Using Eq. (64) together with second-order perturbation theory, one can rigorously show that the interaction between two Fermi and Bose polarons is (Yu and Pethick, 2012)

$$f_{\mathbf{p},\mathbf{p}'} = \pm g^2 \chi(\mathbf{p} - \mathbf{p}', \varepsilon_{\mathbf{p}a} - \varepsilon_{\mathbf{p}'a}), \quad (65)$$

where the upper/lower sign is for bosonic/fermionic impurities, and the density-density response function is

$$\chi(\mathbf{p}, \omega) = \begin{cases} \sum_{\mathbf{k}} \frac{n_{\mathbf{k}b} - n_{\mathbf{k}+\mathbf{p}b}}{\omega + \epsilon_{\mathbf{k}b} - \epsilon_{\mathbf{k}+\mathbf{p}b}} & \text{Fermi polarons} \\ \frac{2n_0 \epsilon_{\mathbf{p}b}}{\omega^2 - E_{\mathbf{p}}^2} & \text{Bose polarons} \end{cases} \quad (66)$$

for an ideal Fermi gas (Lindhard function) and a weakly interacting BEC respectively. Here $g = (\partial\mu_2/\partial n_1)_{n_2}$ is the Landau interaction between a dressed polaron and the surrounding medium, which is taken to be independent of momentum. For weak impurity-fermion interactions, we have $g = 2\pi a/m_r$. The frequency dependence of $\chi(\mathbf{p}, \omega)$ reflects that density fluctuations propagate with a finite speed through the medium, which leads retardation effects. In the limit of small momentum exchange and zero temperature, the quasiparticle interaction becomes

$$\lim_{|\mathbf{p}| \rightarrow |\mathbf{p}'|} f_{\mathbf{p}, \mathbf{p}'} = \mp g^2 \begin{cases} \mathcal{N}(\epsilon_F) & \text{Fermi polaron} \\ 1/g_b & \text{Bose polaron} \end{cases} \quad (67)$$

where $\mathcal{N}(\epsilon_F) = m_b k_F / 2\pi^2$ is the density of states at the Fermi energy (Giraud and Combescot, 2012; Mora and Chevy, 2010; Yu and Pethick, 2012; Yu *et al.*, 2010). The $1/g_b$ dependence for the Bose polaron shows that the interaction increases with the compressibility of the BEC. For Fermi polarons with arbitrarily strong impurity-bath interactions, Eq. (67) can be written as $\lim_{|\mathbf{p}| \rightarrow |\mathbf{p}'|} f_{\mathbf{p}, \mathbf{p}'} = \mp (\Delta N)^2 / \mathcal{N}(\epsilon_F)$ where ΔN is the number of fermions in the dressing cloud given by Eq. (9).

The \pm sign in Eqs. (65) and (67) explicitly shows the fundamental role of the quantum statistics of the quasiparticles: The quasiparticle interaction is generally repulsive/attractive for fermionic/bosonic quasiparticles. This sign difference arises because the interaction comes from an exchange term (Yu and Pethick, 2012), or equivalently because in a Fermi sea there are less available scattering states for the impurities due to Fermi blocking, which increases their energy (Mora and Chevy, 2010). We note that when taking the derivative in Eq. (64), the majority particle distribution function is assumed to be constant, which corresponds to keeping the majority density constant. Assuming instead a constant chemical potential for the majority particles would yield an additional Hartree term for the interaction between the quasiparticles (Mora and Chevy, 2010). Also, the mediated interaction is zero to second order in the special case where the momenta of the two (bosonic) impurities are strictly identical, since the majority particles would have to change their density to mediate a zero momentum wave. In this case, the interaction mediated by a medium at constant density is given by a higher order process that can be repulsive (Levinson *et al.*, 2024).

For strong impurity-medium interactions, one has to resort to approximations when calculating interactions

between polarons. This is more challenging than the single polaron problem, since the theory now has to take into account the effects of a non-zero polaron concentration as seen from Eq. (64). One way to proceed is to compare Eq. (64) with Eq. (6) giving the energy of the polaron from the impurity self-energy. This yields

$$f(\mathbf{p}, \mathbf{p}') = Z_{\mathbf{p}} \frac{\delta \text{Re} \Sigma_a(\mathbf{p}, \epsilon_{\mathbf{p}})}{\delta n_{\mathbf{p}'}}. \quad (68)$$

Equation (68) completes the link between Landau's quasiparticle theory and microscopic many-body theory, showing that the quasiparticle interaction can be calculated from how the self-energy depends on the impurity concentration (Giuliani and Vignale, 2005).

Given its accuracy for describing single Fermi polarons, a natural approach is to use the ladder approximation for the self-energy in Eq. (68) generalized to a non-zero impurity concentration. This gives rise to the quasiparticle interaction shown diagrammatically in the top panel of Fig. 46 (Baroni *et al.*, 2024a). This approximation recovers the perturbative result Eq. (65) for weak impurity-fermion interactions where $\mathcal{T} \rightarrow g$, and it was recently used to explain experimental model for the interaction between Fermi polarons as discussed in Sec. VI.C. The ladder approximation has also been employed to calculate the interaction between Fermi polaron-polaritons in TMDs using Eq. (68) with the replacement $Z_{\mathbf{p}} \rightarrow Z_{\mathbf{p}} C_{\mathbf{k}}^2$. The Hopfield coefficients $C_{\mathbf{k}}^2$ appear because it is only the exciton part of the polariton that interacts with the surrounding electrons (Bastarrachea-Magnani *et al.*, 2021a,b). It was found that the quasiparticle interaction can be much stronger than the direct interaction between excitons, which is small due to their small radius.

A diagrammatic expression for the interaction between two Bose-polarons in the regime of strong impurity-boson interaction including effects such as retardation and momentum dependence was developed from Eq. (64) (Camacho-Guardian and Bruun, 2018). In order to recover the second order result given by Eq. (65) for weak interactions, it turns out that one has to go beyond the ladder approximation for the impurity self-energy. The result is illustrated in the lower panel of Fig. 46, and it predicts significant energy shifts of the Bose polaron with its concentration via Eq. (64), which however have not been observed so far. A mixed dimensional setup with two Fermi gases separated by a BEC was shown to offer a promising alternative way to unambiguously observe this interaction via the sizeable frequency shift it causes on their out-of-phase dipole mode (Suchet *et al.*, 2017). The interaction between Bose polarons was also considered using a perturbative Hugenholtz-Pines formalism as well as QMC methods (Peña Ardila, 2022). Santiago-Garcia and Camacho-Guardian (2023) studied the interaction between two mobile impurities mediated by collective spin excitations of bosons with a hard core

repulsion in a lattice following a path integral methods. Finally, Charalambous *et al.* (2019) explored the entanglement between two distinguishable impurities due to an interaction mediated by a BEC using a quantum Brownian motion approach.

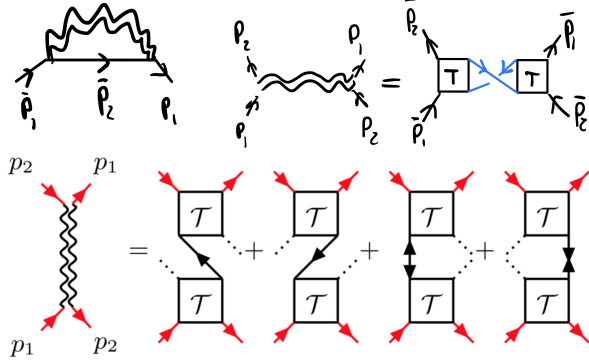


FIG. 46 **Interaction mediated by a Fermi gas and a BEC.** (a) The mediated interaction between polarons enters via an exchange (Fock) term for the impurity self-energy. (b) The interaction between Fermi polarons obtained from the ladder approximation generalised to non-zero impurity concentrations. (c) The interaction between Bose polarons obtained from a diagrammatic theory taking into account strong impurity-boson interactions via the \mathcal{T} -matrix. Solid black/red lines are majority/impurity particle Green's functions and dashed lines are condensate bosons.

B. Static impurities

As for the case of single impurities, the limit of infinitely heavy impurities with $m/m_b \gg 1$ gives major simplifications, since there is no impurity recoil. A popular approach is to regard the impurities as static scattering potentials, although this makes them distinguishable so that the role of their quantum statistics is lost and their quasiparticle residues vanish as discussed in the previous sections. The interaction then arises because the two scattering potentials change the spectrum of the surrounding medium just like the Casimir force (Casimir and Polder, 1948). Using the Born approximation to replace the scattering matrix with the constant g for two short range potentials separated by a distance \mathbf{r} yields the well-known Ruderman–Kittel–Kasuya–Yosida (RKKY) (Kasuya, 1956; Ruderman and Kittel, 1954; Yosida, 1957) and Yukawa interactions

$$V_m(\mathbf{r}) = \begin{cases} g^2 \frac{m_b}{16\pi^3} \frac{2k_{FR} \cos 2k_{FR}r - \sin 2k_{FR}r}{r^4} & \text{Fermi gas} \\ -g^2 \frac{n_0 m_b}{\pi} \frac{e^{-\sqrt{2}r/\xi}}{r} & \text{BEC,} \end{cases} \quad (69)$$

mediated by density modulations in a Fermi gas and a BEC, respectively. Equation (69) can be obtained by Fourier transforming Eq. (65) in the static limit $\omega = 0$.

The interaction between two static impurities mediated by an ideal Fermi gas was explored for a short

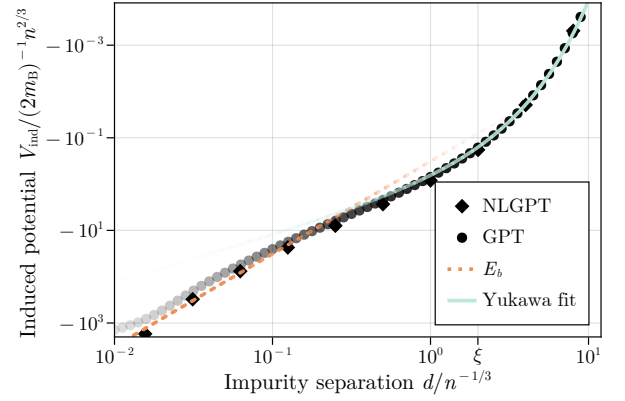


FIG. 47 **Interaction between two static impurities in a BEC.** The impurities interact resonantly ($1/a = 0$) with bosons, and the gas parameter is $na_b^3 = 10^{-6}$. Circles (diamonds) show results with zero (non-zero) range of the boson-boson interaction, and the dashed orange line is the energy of the Efimov trimer. From Ref. (Drescher *et al.*, 2023).

range impurity-medium interaction of arbitrary strength by solving the scattering problem exactly (Enss *et al.*, 2020; Nishida, 2009). It was shown that the interaction can be quite different from the RKKY form in Eq. (69) for strong interactions due to the presence of (Efimov) states where one fermion is bound between the two impurities. These bound states lead to resonances and sign changes in the scattering length (Enss *et al.*, 2020). Likewise, the interaction between two static impurities mediated by a BEC was obtained from the GP equation (Drescher *et al.*, 2023). For distances short compared to the interparticle spacing, the interaction was shown to be dominated by a single boson bound between the two static impurities giving rise to an Efimov scaling $\propto 1/r^2$. For distances larger than the healing length of the BEC, the interaction is of the Yukawa form. This crossover between Efimov and Yukawa scalings for the mediated interaction, shown in Fig. (47), was found for any impurity-boson interaction strength, contrary to results obtained from a variational approach (Naidon, 2018). The same approach was used in Ref. (Jager and Barnett, 2022). Using effective field theory, the interaction between two static impurities mediated by a superfluid with a linear low energy phonon dispersion was explored (Fujii *et al.*, 2022). Assuming weak and short range impurity-superfluid interactions, it was shown that the mediated interaction is dominated by the exchange of two phonons for very large distances $r \gg \xi$ giving rise to a $1/r^7$ interaction instead of the Yukawa interaction mediated by one phonon exchange for shorter distances.

The quasiparticle interaction is affected when the impurity-medium interaction is not short range. One example is the case of ionic impurities discussed in Sec. IV where the atom-ion interaction has the charge-dipole $1/r^4$ form for large separations. Using perturbation

theory as well as a diagrammatic \mathcal{T} -matrix approximation, the interaction between two static ions mediated by a BEC was shown to be proportional to $1/r^4$ for large distances and have a Yukawa form for short distances, whereas it switches from an RKKY to a $1/r^4$ form when mediated by a Fermi gas (Ding *et al.*, 2022). The same $1/r^4$ behavior was found by solving the GPE with two static ion potentials (Cavazos Olivas *et al.*, 2024; Drescher *et al.*, 2023). This interaction gives rise to measurable changes in the phonon spectrum of the two ions in a typical linear RF trap. Quantum Monte-Carlo calculations exploring two static ions in a BEC obtained similar results with corrections for strong atom-ion interaction due to large distortions of the BEC around the ions and the presence of bound states in the atom-ion interaction potential (Astrakharchik *et al.*, 2023).

C. Experimental detection

While pioneering experiments probed the interaction between bosons mediated by a Fermi gas in the perturbative regime (DeSalvo *et al.*, 2017; Edri *et al.*, 2020), the interaction between two Fermi polarons was systematically measured for all coupling strengths only recently (Baroni *et al.*, 2024a). The interaction between Bose polarons remains on the other hand unobserved, which is somewhat surprising since it should be stronger due to the large compressibility of a BEC.

Baroni *et al.* (2024a) measured the energy of Fermi polarons formed by ^{40}K (fermion) or ^{41}K (boson) atoms in a bath of ^6Li atoms as a function of the impurity concentration using RF spectroscopy. The polaron interaction was then extracted by fitting to a momentum average of Eq. (64), $\varepsilon = \varepsilon^0 + \bar{f}n_i$ (the experiment had no momentum resolution). Using a Li-K Feshbach resonance, \bar{f} was measured as a function of impurity-medium scattering length a and by comparing results for ^{40}K or ^{41}K atoms keeping everything else fixed the role of quantum statistics was probed directly. Figure 48 shows the interaction \bar{f} as a function of $X = -1/k_F a$. It shows that the quasiparticle interaction is repulsive/attractive for fermionic/bosonic quasiparticles. For weak to moderate interaction strengths, the results agree well with the second order expression given by Eq. (67) (solid lines), and the experiment therefore confirms two landmark predictions of Landau's Fermi liquid theory: The strength of the effective interaction and its sign dependence on the quantum statistics of the quasiparticles. For stronger interactions across the Li-K Feshbach resonance where a diverges, Eq. (67) does not agree with the experimental results. Here, a non-perturbative diagrammatic theory for the quasiparticle interaction illustrated in Fig. 46(b) explained the experimental results for strong and attractive interactions ($a < 0$), whereas the results for strong and repulsive interactions require further analysis.

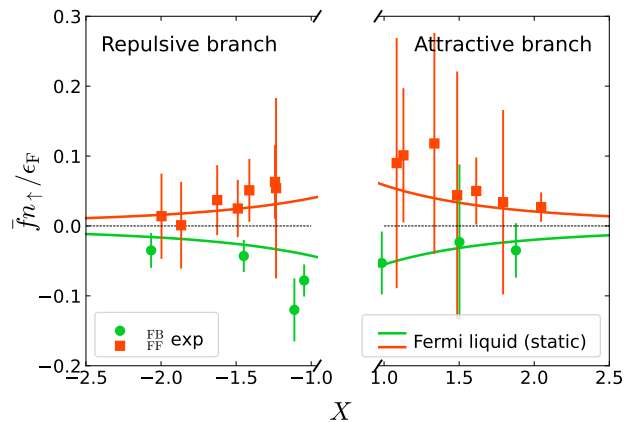


FIG. 48 **Mediated interactions in a Fermi gas.** Measurement of polaron-polaron interaction between K impurities in a Li Fermi gas ($X = -1/k_F a$). Red squares are for fermionic ^{40}K impurity atoms and green circles for bosonic ^{41}K impurity atoms. The solid lines are the perturbative result Eq. (67). From Ref. (Baroni *et al.*, 2024a).

Since the exciton radius in TMDs is small, the direct exciton-exciton interaction is weak, which limits their use for optical devices. This motivates the study of mediated interactions between exciton-polarons (or polariton-polarons) with the aim of increasing non-linear effects. Quasiparticle interactions were explored between the Bose polarons formed by exciton-polaritons in one valley immersed in a bath of exciton-polaritons in the other valley in monolayer MoSe_2 as discussed in Sec. V.D (Tan *et al.*, 2023). Using pump-probe spectroscopy, the energy of the polarons was measured as a function of their density and the interaction extracted from the slope using a momentum averaged Eq. (64). Attractive interactions were found between Bose polarons in the repulsive branch whereas repulsive interactions were found between polarons in the attractive branch. Such repulsive interactions are not expected between bosonic quasiparticles in equilibrium, and they may be due to the inherent non-equilibrium nature of the experiment.

Exploiting the spin-orbit splitting in the K and K' valleys, the interactions between excitons mediated by a surrounding electron gas was explored (Muir *et al.*, 2022). Evidence was found that these interactions mainly occur when they are dressed by electrons in the same valley. The interactions were found to be repulsive, which was attributed to the excitons competing for the same electrons during the time span of the experiment, which was comparable to the time scale $1/\epsilon_F$ for the formation of Fermi polarons. Also, the probe transmission spectrum of the lower polaron-polariton branch of an electron doped MoSe_2 monolayer in an optical cavity was observed to exhibit a blueshift due to the presence of other polaron-polaritons created by a pump beam. This was interpreted as a repulsive interaction arising from

non-equilibrium phase-space filling effect (Tan *et al.*, 2020). An alternative explanation was given in terms of the interaction mediated by the electron gas shown in Fig. 46(b) (Bastarrachea-Magnani *et al.*, 2021a,b). An earlier experiment observed energy shifts of the transmitted light intensity of a doped MoSe₂ monolayer depending on the pump intensity creating the excitons. This was however interpreted in terms of the composite nature of trion-polariton wave functions and not in terms of polaron-polaron interactions (Emmanuele *et al.*, 2020).

D. Bi-polarons

A striking effect of the interaction between quasiparticles is that it can support bound states. Bound states of two polarons, called bi-polarons, are proposed as a mechanism for superconductivity (Alexandrov and Mott, 1994), for charge transport in polymer chains (Bredas and Street, 1985; Mahani *et al.*, 2017), and for magnetoresistance in organic materials (Bobbert *et al.*, 2007). We now discuss various theoretical predictions for the existence of bi-polarons in atomic gases and TMDs. However, bi-polarons remain to be observed.

A general theory of bound states of two quasiparticles in a many-body environment is very challenging. Their energy is given by the poles of the polaron-polaron scattering matrix, which obeys the Bethe-Salpeter equation (Fetter and Walecka, 1971). While this is very complicated to solve in general, one can use its close resemblance to the Lippmann-Schwinger equation in the quasiparticle approximation to derive an effective Schrödinger equation for the bound states of two polarons

$$\varepsilon_{\text{bp}}\psi(\mathbf{k}) = 2\varepsilon_{\mathbf{k}}\psi(\mathbf{k}) + \sum_{\mathbf{k}'} V_{\text{m}}(\mathbf{k}, \mathbf{k}')\psi(\mathbf{k}'), \quad (70)$$

which is much simpler to solve (Camacho-Guardian *et al.*, 2018). Here, $\psi(\mathbf{k})$ is the relative wave function of the bi-polaron in momentum space with energy ε_{bp} , $\varepsilon_{\mathbf{k}}$ is the energy of an isolated polaron, and $V_{\text{m}}(\mathbf{k}, \mathbf{k}')$ is the interaction between two polarons with momenta \mathbf{k} and $-\mathbf{k}$ scattering into \mathbf{k}' and $-\mathbf{k}'$. This interaction in general is non-local [$V_{\text{m}}(\mathbf{k}, \mathbf{k}') \neq V_{\text{m}}(\mathbf{k} - \mathbf{k}')$], which is typical for effective two-body Schrödinger equations in many-body systems such as the Skyrme force in nuclear matter (Ring and Schuck, 2004). The relative wave function $\psi(\mathbf{k})$ has to be symmetric for two bosonic impurities, whereas it is anti-symmetric for fermionic impurities.

Using an effective interaction $V_{\text{m}}(\mathbf{k}, \mathbf{k}')$ between two Bose-polarons derived by ignoring retardation effects in the diagram shown in Fig. 46(c), bound states of Eq. (70) with an energy below that of two isolated polarons $2\varepsilon_0$ were found in a weakly interacting BEC as shown in Fig. 49. The bi-polarons emerge beyond a critical impurity-boson interaction strength with a binding en-

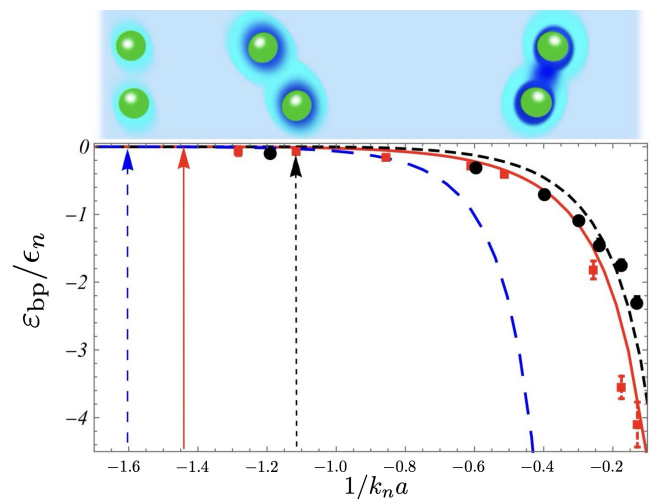


FIG. 49 **Bi-polarons in a BEC.** Top: binding of two polarons due to a mediated interaction. Bottom: binding energy ε_{bp} of the bipolaron (with $m = m_b$). The solid red (black dashed) line show the result obtained from Eq. (70) with the mediated interaction shown in Fig. 46 for a bath density of $n_b a_b^3 = 10^{-6}$ (10^{-5}), and the red squares (black dots) are the corresponding DMC results. Vertical arrows indicate the emergence of the bi-polaron. The blue dashed line gives the energy using the static Yukawa interaction Eq. (69). From (Camacho-Guardian *et al.*, 2018).

ergy that increases with decreasing boson-boson repulsion. This reflects that the BEC becomes more compressible and thus mediates a stronger interaction. For weak impurity-boson interactions $k_n|a| \ll 1$, the interaction is given by Eq. (65) and the bi-polaron energy recovers analytical results for a Yukawa potential (Edwards *et al.*, 2017; Harris, 1962; Rogers *et al.*, 1970). This method was also used to predict the existence of bi-polarons of different symmetries in a 2D lattice containing a BEC (Ding *et al.*, 2023). The effective Schrödinger equation Eq. (70) was also used to predict the presence of bi-polaron in a hard core boson gas in a lattice (Santiago-Garcia and Camacho-Guardian, 2023).

Bi-polarons were also found using diffusion Monte-Carlo calculations (Camacho-Guardian *et al.*, 2018). As can be seen in Fig. 49, these energies agree well with those obtained from Eq. (70) even for strong interactions $k_n|a| \gtrsim 1$, which is remarkable since there is no small parameter in this regime and indicates the accuracy of the effective Schrödinger equation approach.

Equation (70) was generalised to the case of two polaritons in a TMD interacting via the exchange of phonon modes in a condensate of polaritons in the other valley (Camacho-Guardian *et al.*, 2021). It was found that this interaction supports dimer states, which due to the hybrid nature of polaritons corresponds to a bound state of photons. These bound states were predicted to give rise to new transmission lines of the TMD with photon-photon correlations determined by the dimer wave func-

tion. The formation of bi-polarons was also explored by solving a two-body Schrödinger equation using a mediated interaction extracted from the GPE treating the impurities as static potentials (Jager and Barnett, 2022).

Bound states of two Fermi polarons were considered in Ref. (Guo and Tajima, 2024). Using the fermion mediated interaction illustrated in the top panel of Fig. 46 combined with a variational wave function, bi-polarons were found to be stable for a range of interactions strength for different atomic mixtures, and it was pointed out that such atomic experiments may shed light on the properties of α clusters in neutron matter.

Bi-polarons are a many-body effect due to an attractive interaction mediated by a surrounding bath. As such, they are distinct from few-body states such as Efimov trimers, which exist also in a vacuum. As discussed in Sec. VI.B, the presence of Efimov trimers can however affect the mediated interaction at short range, and it was furthermore shown in Sec. III.E that they can have large effects on the Bose polaron when $k_n|a_-| \sim 1$, see Fig. 12. Efimov trimers may therefore also influence bi-polarons in this regime, which was explored using the variational ansatz given by Eq. (34) generalized to the case of two bosonic impurities in a BEC (Naidon, 2018). It was predicted that the bi-polaron, which for weak interactions is bound by a Yukawa potential, smoothly evolves into an Efimov trimer bound by a $1/r^2$ potential for strong interactions $1/k_n|a| \lesssim 1$ as illustrated in the left panel of Fig. 50. The same problem was considered for two heavy ^{133}Cs impurities in a ^6Li Fermi sea, where the mass ratio ensures the existence of Efimov trimers (Sun and Cui, 2019). Bound states with an energy well below that of two uncorrelated Fermi polarons were found for strong interactions. The bound states between two polarons in a dipolar Fermi gas were explored in Ref. (Nakano *et al.*, 2024a). Using an RKKY form of the interaction as in Eq. (65) generalized to the dipolar gas in an effective Schrödinger equation, the regions of stability and binding energy of the bipolarons were analyzed.

VII. POLARONS AS A LIMIT OF MANY-BODY PHASES

The Fermi and Bose polarons discussed in this review define the low-density limit of two-component Fermi-Fermi, Fermi-Bose and Bose-Bose mixtures. Indeed, the Fermi polaron was originally introduced to constrain the equation of state of spin-imbalanced, strongly interacting Fermi mixtures (Chevy, 2006; Combescot *et al.*, 2007; Prokof'ev and Svistunov, 2007, 2008b). The limit of Fermi polarons also constrains the nuclear equation of state, in particular for neutron matter (Forbes *et al.*, 2014). In this Section, we discuss how polaron physics is connected to and can provide important insights into the more general and universal setting of quantum mixtures. This connection has previously been reviewed in

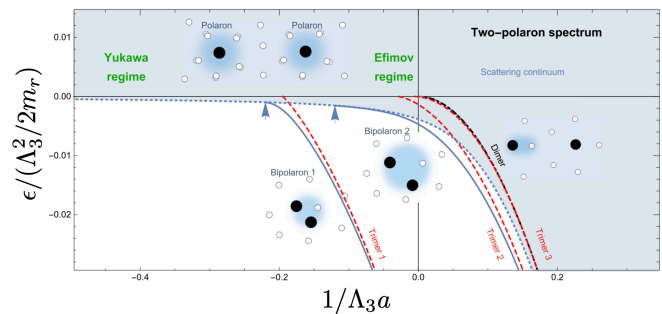


FIG. 50 **Bi-polarons and Efimov states.** Spectrum of two impurities in a BEC as a function of the boson-impurity scattering length (solid blue lines). $\Lambda_3 \simeq 3.2k_n$ is a three-body cut-off parameter related to the range of the impurity-boson interaction. The mass ratio is $m/m_b = 19$ and $k_n|a_-| \simeq 1.6$. The bi-polarons become stable at vertical arrows, red lines show the energies of Efimov trimers, and the black line is the boson-impurity dimer. The shaded area is the scattering continuum of two impurities. From Ref. (Naidon, 2018).

the context of the repulsive Fermi polaron and itinerant ferromagnetism (Massignan *et al.*, 2014), which we will therefore not discuss here. For a recent comprehensive review on atomic quantum mixtures, see Ref. (Baroni *et al.*, 2024b).

A. Fermi mixtures

In an equal population mixture of fermions in two attractively interacting spin states, the ground state is a superfluid of Cooper pairs (Zwinger, 2011; Zwierlein, 2014; Zwierlein *et al.*, 2005). With spin imbalance, some majority spins remain unpaired. The question of the fate of superfluidity in the presence of spin imbalance has a long history. In condensed matter, this relates to the stability of superconductors in strong magnetic field, and one generally has neutron-proton (isospin) asymmetry in nuclear physics. In the core of neutron stars, neutral superfluids of unequal densities of quarks are predicted to exist (Alford *et al.*, 2000). While imbalanced pairing is difficult to study in conventional superconductors since magnetic fields are typically expelled by the Meissner effect, the population in the two (hyperfine) spin states can be freely tuned in atomic gases. This enabled the experimental investigation of the phase diagram of spin-imbalanced Fermi gases (Nascimbène *et al.*, 2009; Nascimbène *et al.*, 2010; Partridge *et al.*, 2006; Schirotzek *et al.*, 2009; Shin *et al.*, 2008, 2006; Shin, 2008; Zwierlein *et al.*, 2006a).

1. Chandrasekhar-Clogston limit

If magnetic fields do enter a superconductor, the superconducting state of electron pairs should be fragile as the field tends to align the spins, and there must be a

critical field beyond which the normal state has lower free energy than the superfluid.

Chandrasekhar (Chandrasekhar, 1962) and independently Clogston (Clogston, 1962) derived an upper (CC) limit for the critical magnetic field of a superconductor. To evaluate this, one compares the free energy $F(h)$ of the normal and the superfluid state in the presence of a “magnetic field” $h = (\mu_\uparrow - \mu_\downarrow)/2$, where μ_\uparrow and μ_\downarrow are the chemical potentials of the majority and minority atoms, respectively. We first work in the BCS regime, and ignore the attractive interaction between opposite spins present already in the normal state. This will lead to an overestimate of the critical field, as it neglects the formation of attractive Fermi polarons. A balanced fermionic superfluid has free energy $F_S = F_N(0) - \frac{1}{2}\mathcal{N}(\epsilon_F)\Delta^2$, lower than the free energy of the balanced normal gas at $h = 0$ by the condensation energy $\frac{1}{2}\mathcal{N}(\epsilon_F)\Delta^2$. Here $\mathcal{N}(\epsilon_F)$ is the density of states at the Fermi energy, and Δ the superfluid gap. The free energy of the normal state as a function of h is $F_N(h) = -\frac{4}{15}\mathcal{N}(\epsilon_F)(\mu_\uparrow^{5/2} + \mu_\downarrow^{5/2}) \simeq F_N(0) - \mathcal{N}(\epsilon_F)h^2$, where $\mu_\uparrow = \epsilon_F + h$, $\mu_\downarrow = \epsilon_F - h$ and $F_N(0) = -\frac{8}{15}\mathcal{N}(\epsilon_F)\epsilon_F^2$. From this, one obtains $h_{CC} = \Delta/\sqrt{2}$ for the critical magnetic field. In conventional superconductors, this corresponds to $h_{CC} \sim 18.5$ Tesla for $T_c \sim 10K$, much larger than the typical critical field H_{c2} where superconductivity breaks down due to vortex generation. Heavy fermion or layered superconductors may however attain this CC regime (Pfleiderer, 2009).

The first-order superfluid-to-normal transition at the critical field was studied by Sarma (Sarma, 1963). Fulde and Ferrell (Fulde and Ferrell, 1964), and independently Larkin and Ovchinnikov (Larkin and Ovchinnikov, 1964) then found that not all the pairs necessarily break at once, but that there exists a novel superfluid state that tolerates a certain amount of majority spins if the remaining Cooper pairs are allowed to have a common non-zero momentum (FFLO or LOFF state). The order parameter is thus not constant, but corresponds to a traveling (FF state) or standing (LO state) wave, and majority spins can reside in its nodes without energy penalty. The number of nodes is given by the number difference between the spin states. The true ground state of spin-imbalanced superfluidity is however still not known. The problem arises in condensed matter for exotic superconductors that are essentially Pauli limited (Bianchi *et al.*, 2003; Casalbuoni and Nardulli, 2004; Radovan *et al.*, 2003), and in the study of superfluid pairing of quarks at unequal Fermi energies (Alford *et al.*, 2000). For strongly interacting atomic Fermi gases, where Δ approaches the Fermi energy, the critical field is a substantial fraction of ϵ_F , and the window of superfluidity as a function of the field h is wide, which presents a new opportunity to study imbalanced superfluidity.

To directly demonstrate the robustness of superfluidity in the strongly interacting regime, the MIT group stud-

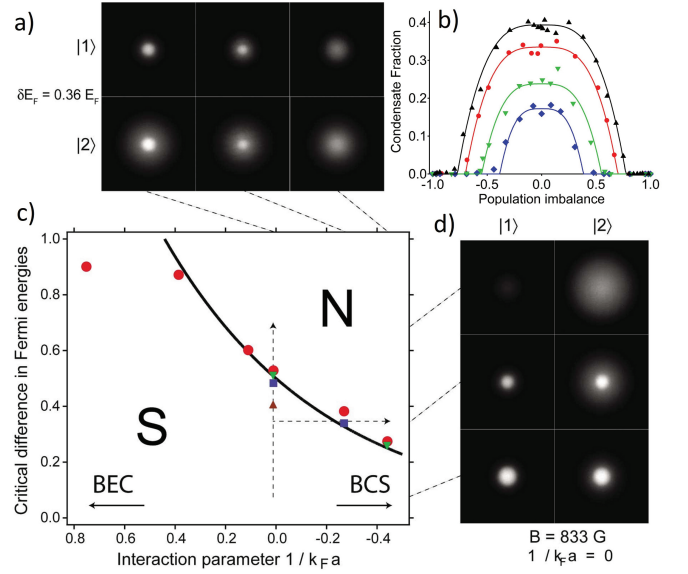


FIG. 51 Clogston-Chandrasekhar limit of superfluidity. The critical Fermi energy mismatch $\delta\epsilon_F$ between the two spin states at the superfluid-to-normal transition shown in c) is observed in the condensate fraction for varying interaction strength at fixed $\delta\epsilon_F$ (a), and at fixed interaction strength and varying $\delta\epsilon_F$ (d). b) Window of superfluidity as obtained from the condensate fraction at $1/k_F a = 0.11$ (triangles pointing up), $1/k_F a = 0$ (resonance, circles), $1/k_F a = -0.27$ (BCS-side, triangles pointing down), $1/k_F a = -0.44$ (diamonds). The normal phase competing with the superfluid is a Fermi liquid of polarons. From (Zwierlein *et al.*, 2006a).

ied spin imbalanced Fermi mixtures in the presence of a stirring beam (Zwierlein *et al.*, 2006a). The part of the mixture that was still superfluid despite the imbalance revealed a lattice of quantized vortices. The normal Fermi mixture above the critical imbalance for superfluidity is well-described as a Fermi liquid of polarons. The window of superfluidity was determined from the number of vortices as a function of imbalance, as well as from condensate fraction measurements (Ketterle and Zwierlein, 2007; Zwierlein, 2016), see Fig. 51. At unitarity, superfluidity was robust up to a critical population imbalance $P = (N_\uparrow - N_\downarrow)/(N_\uparrow + N_\downarrow)$ of about $P_c = 75\%$, which agrees with the phase diagram obtained later by the ENS group (Navon *et al.*, 2010), and with a Monte-Carlo study obtaining $P_c = 77\%$ (Lobo *et al.*, 2006). BCS theory overestimates the critical population difference to $P_c = 92\%$ as it neglects polaron formation in the normal state, which is thus favored at large fields h compared to the superfluid state. Indeed, at high imbalance, the Fermi mixture is normal down to the lowest temperatures realized thus far, and behaves as a Fermi liquid of polarons (Nascimbène *et al.*, 2009; Nascimbène *et al.*, 2011; Nascimbène *et al.*, 2010; Schirotzek *et al.*, 2009).

2. Phase separation

The BCS ground state is fully paired and since excess fermions require an energy of at least Δ to reside within the superfluid, their presence is exponentially suppressed at low temperatures. Beyond the CC limit, the normal state will have imbalanced spin densities and the first order transition from the balanced superfluid to the imbalanced normal state is therefore signaled by a jump in the density difference. First hints of a phase separation between the normal and superfluid phase were seen (Partridge *et al.*, 2006; Zwierlein *et al.*, 2006a), and using tomographic techniques a sharp separation between a superfluid core and a partially polarized normal phase was observed (Shin *et al.*, 2006), see Fig. 52. A jump in the density difference was observed thereby directly demonstrating the first order nature of the phase transition (Shin *et al.*, 2008). At higher temperatures the signature of the first order transition disappears at a tricritical point, in good agreement with theoretical calculations (Gubbels and Stoof, 2008; Lobo *et al.*, 2006).

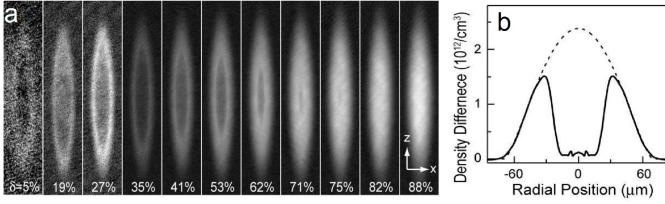


FIG. 52 **Phase separation in an imbalanced Fermi gas.** a) In-situ column density difference between the majority and minority species for various population differences $\delta = (N_\uparrow - N_\downarrow)/(N_\uparrow + N_\downarrow)$. Below an imbalance of $\delta < 75\%$, a central depletion indicates the fully paired superfluid, surrounded by a normal shell. b) Density difference as a function of radial position. The central core has equal spin densities. From (Shin *et al.*, 2006).

3. Equation of state at unitarity

At unitarity and zero temperature, the energy of the gas can only depend on the two Fermi energies $\epsilon_{F\sigma}$. This allows to write for the energy density \mathcal{E}

$$\mathcal{E}(n_\uparrow, n_\downarrow) = \frac{3}{5} n_\uparrow \epsilon_{F\uparrow} g(x)^{5/3} = \frac{3}{5} (n_\uparrow \mu_\uparrow + n_\downarrow \mu_\downarrow) \quad (71)$$

with $g(x)$ a universal function of the density ratio $x = n_\downarrow/n_\uparrow$ (Bulgac and Forbes, 2007). The second equation follows from $\mu_\sigma = \partial\mathcal{E}/\partial n_\sigma$. In terms of $g(x)$, one has $g(x)^{5/3} = \frac{\mu_\uparrow}{\epsilon_{F\uparrow}} (1 + xy)$ with $y = \mu_\downarrow/\mu_\uparrow$. Within the local density approximation, the local chemical potentials vary with the trapping potential $U(\vec{r})$ as $\mu_\sigma(\vec{r}) = \mu_{0,\sigma} - U(\vec{r})$, with the global chemical potentials $\mu_{0,\sigma}$ for each species.

In the outer wings of the atom mixture resides a non-interacting Fermi gas of only majority atoms. One can therefore directly obtain the majority global chemical potential from the radius of the majority cloud R_\uparrow as $\mu_{0,\uparrow} = U(R_\uparrow)$. The minority global chemical potential $\mu_{0,\downarrow}$ can be obtained by noting that the last minority atom at the outermost wing of the minority cloud is a Fermi polaron, and thus $\mu_{0,\downarrow} = A\epsilon_{F\uparrow}(R_\downarrow) = A[U(R_\uparrow) - U(R_\downarrow)]$, where $\epsilon = A\epsilon_{F\uparrow}$ is the energy of a single polaron in a uniform bath. This method was employed in Refs. in (Bulgac and Forbes, 2007; Chevy, 2006) to estimate the polaron energy from the cloud radii measured in (Zwierlein *et al.*, 2006b). Alternatively, if the central part of the mixture is a balanced superfluid, we can write $\mathcal{E} = \frac{3}{5}\xi_B(n_\uparrow + n_\downarrow)$ with ξ_B the Bertsch parameter ξ_B . Since $n_\uparrow = n_\downarrow$ this implies from Eq. (71) $\mu_{0,\uparrow} + \mu_{0,\downarrow} = 2\xi_B\epsilon_F(0)$, where $\epsilon_F(0)$ is the Fermi energy in the center of the trap. This also provides a link between the polaron energy $A = \epsilon/\epsilon_{F\uparrow}$, the Bertsch parameter ξ_B , and the experimental quantities $\epsilon_F(0)$, R_\uparrow and R_\downarrow . One can also obtain ξ_B directly from the normalized compressibilities $\tilde{\kappa} = \kappa/\kappa_0 = d\epsilon_{F\uparrow}/dU$ (κ_0 is the ideal gas compressibility) of the majority species in the fully polarized normal wings where $\tilde{\kappa} = 1$ and in the superfluid region where $\tilde{\kappa} = 1/\xi_B$.

The equation of state of spin-imbalanced Fermi gases in the form of Eq. (71) was measured from the density profiles of the trapped gas (Shin, 2008), see Fig. 53. As in earlier studies at MIT, three distinct phases were found: A superfluid region at equal spin densities in the core at small distances from the trap center, followed by a normal mixed region at unequal densities, and beyond the minority cloud radius R_\downarrow a region of a fully polarized normal gas of majority atoms. In Fig. 53a, the normal-to-superfluid transition is directly visible as the boundary between the spin-balanced region at equal densities and the imbalanced region. The jump in the density difference marks the first-order transition. The form of $g(x)$ is constrained by the limiting cases: In the superfluid region where $(\mu_\uparrow + \mu_\downarrow)/2 = \xi_B\epsilon_{F\uparrow}$, $\mu_\uparrow/\epsilon_{F\uparrow} = 2\xi_B/(1+y)$ and thus $g(1) = (2\xi_B)^{3/5}$; in a fully polarized ($x = 0$) non-interacting Fermi gas one has $\mu_\uparrow = \epsilon_{F\uparrow}$ and $g(0) = 1$. The critical chemical potential ratio y_c above which the superfluid forms was found to be $y_c = 0.03(2)$, at a critical density ratio $x = 0.53(5)$. The polaron energy was estimated to be $y_c = A = -0.58(5)$ from a Thomas-Fermi fit to $g(x)$, and $y_c = A = -0.69(8)$ from the measured cloud radii, assuming $\xi_B = 0.42(1)$, which is however slightly larger than the present value $\xi_B = 0.37(1)$ (Ku *et al.*, 2012). The values for A are in good agreement with later studies via RF spectroscopy (Schirotzek *et al.*, 2009). The experiment found good agreement with a Fermi liquid description of the normal mixed state.

A later experiment by the ENS group (Nascimbène *et al.*, 2010) yielded a low-noise equation of state for imbalanced gases making use of a direct relation between

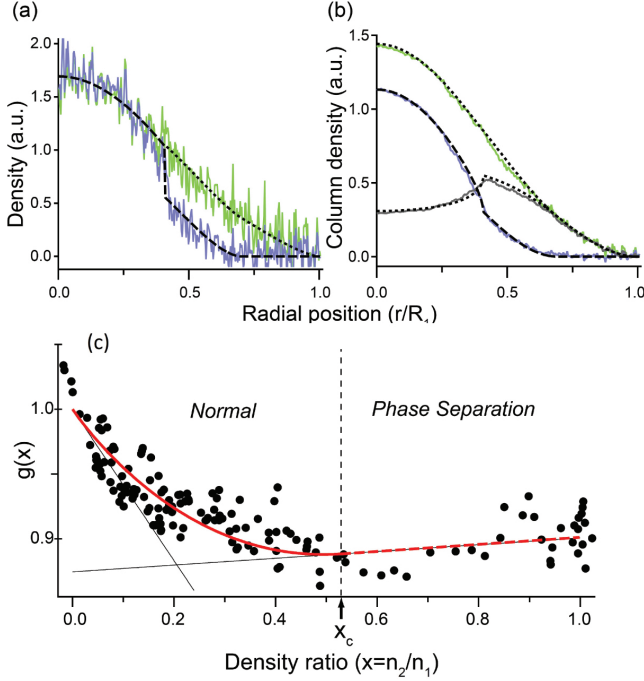


FIG. 53 **Equation of state of a spin-imbalanced Fermi mixture at unitarity.** The 3D density profiles (a) obtained via an inverse Abel transform from the measured column density profiles (b) (at population imbalance of 44%) directly yield the equation of state (c) for spin-imbalanced Fermi gases. The normal-to-superfluid transition takes place at $n_{\uparrow}/n_{\downarrow} \equiv n_2/n_1 = 0.53(5)$. From (Shin, 2008).

the pressure of the gas and the doubly integrated density. In the superfluid region with $\mu_s = (\mu_{\uparrow} + \mu_{\downarrow})/2$ the pressure is $P(\mu_{\uparrow}, \mu_{\downarrow}) = \frac{1}{15\pi^2} \left(\frac{m}{\xi_B \hbar^2} \right)^{3/2} (\mu_{\uparrow} + \mu_{\downarrow})^{5/2}$. In the normal region on the other hand good agreement was found, as in (Shin, 2008), assuming a non-interacting Fermi gas of majority atoms coexisting with a Fermi liquid of polarons with renormalized energy and mass. The corresponding pressure is $P(\mu_{\uparrow}, \mu_{\downarrow}) = \frac{1}{15\pi^2} \left[\left(\frac{m}{\hbar^2} \right)^{3/2} \mu_{\uparrow}^{5/2} + \left(\frac{m^*}{\hbar^2} \right)^{3/2} (\mu_{\downarrow} - \varepsilon_{\downarrow})^{5/2} \right]$ where m^* is the Fermi polaron effective mass. In terms of the energy density, this can be expressed in the canonical form as a Landau-Pomeranchuk functional (Lobo *et al.*, 2006; Mora and Chevy, 2010; Pilati and Giorgini, 2008)

$$\mathcal{E}(n_{\uparrow}, n_{\downarrow}) = \frac{3}{5} n_{\uparrow} \varepsilon_{F\uparrow} \left(1 + \frac{5A}{3} x + \frac{m}{m^*} x^{5/3} + Fx^2 \right) \quad (72)$$

where the first term is the energy of the majority fermions, the second is the polaron energy shift, the third is the energy of a non-interacting gas of polarons, and the fourth is the interaction between polarons discussed in Sec. VI. From Eq. (67) we have $F = \frac{5}{9} \left(\frac{d\varepsilon_{\downarrow}}{d\mu_{\uparrow}} \right)^2$ as confirmed by MC calculations (Pilati and Giorgini, 2008).

The polaron energy given by Eq. (72), $\varepsilon = [\mathcal{E}(n_{\uparrow}, n_{\downarrow}) - \frac{3}{5} n_{\uparrow} \varepsilon_{F\uparrow}] / n_{\downarrow}$ proved to be well reproduced by experiments (Schirotzek *et al.*, 2009) using the MC value $A = -0.615$ (Prokof'ev and Svistunov, 2008a), the analytic result $m^* = 1.2m$ (Combescot and Giraud, 2008), and a weak repulsion between polarons with $F = 0.14$ (Pilati and Giorgini, 2008). Assuming $\xi_B = 0.42(1)$, also the experiment in (Nascimbène *et al.*, 2010) agreed excellently with the theoretical value for the polaron energy $A = -0.615$ and mass $m^*/m = 1.20(2)$. The simple expression Eq. (72) worked well even for a large number of minority atoms, close to the superfluid-to-normal transition. The work was extended to interaction strengths in the BEC and BCS regime in (Navon *et al.*, 2010), and the Fermi liquid picture for the mixed region confirmed in detail in (Nascimbène *et al.*, 2011).

B. Bose-Fermi mixtures

Bose-Fermi mixtures give rise to a rich host of phenomena connected to polarons. Naturally, in the regime of boson densities n_B much smaller than the fermion density n_F , the bosons become dressed into Fermi polarons or, for strong enough attraction, bind to a fermion into a molecule. In the other extreme $n_F \ll n_B$, we obtain Bose polarons, see Fig. 54. Recently, this transition from Fermi to Bose polarons was observed: A small number of thermal ^{41}K atoms formed Fermi polarons by interacting with a ^6Li Fermi sea, whereas for larger concentrations the ^{41}K atoms became a dense BEC in which the ^6Li atoms formed Bose polarons (Fritsche *et al.*, 2021).

For the case of balanced densities, one has at weak interactions a mixture of a BEC and a Fermi gas. As interactions increase, bosons bind with fermions into molecules, which themselves are fermionic, leading, at a quantum critical point, to the complete vanishing of the BEC and the emergence of a Fermi sea of molecules (Ludwig *et al.*, 2011; Powell *et al.*, 2005). Such a vanishing of the condensate and emergence of a molecular Fermi gas was recently observed by sweeping across a Feshbach resonance (Duda *et al.*, 2023). The role of three-body correlations may be important, as such sweeps may potentially also yield trimers or larger clusters instead of only dimers as discussed in Sec. III. Recently, the theory underlying the analysis of this experiment was extended to the description of a mixture of excitons and electrons in TMDs (von Milczewski *et al.*, 2024). It was found that the interplay of Bose and Fermi polaron formation combined with exciton exchange between the electrons can induce an emergent BEC-BCS crossover in such three-component mixtures with critical temperatures up to $T_c/T_F \simeq 0.1$. In general, an attractive interaction between electrons mediated by excitons can give rise to Cooper pairing and superconductivity in TMDs (Bighin *et al.*, 2022; Zerba *et al.*, 2024a), which

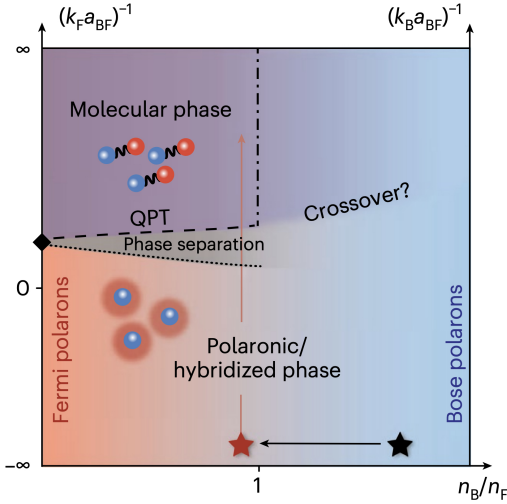


FIG. 54 **Phase diagram for a Bose-Fermi mixture.** In the limit $n_B/n_F \rightarrow 0$ bosons are impurities in the Fermi sea, and can form Fermi polarons. In the opposite limit $n_B/n_F \rightarrow \infty$, the fermions form Bose polaron by interacting with the BEC. For $n_B < n_F$, a quantum phase transition between a polaronic and a molecular phase is expected. The long-dashed line marks the complete depletion of the condensate and, in the case of phase separation, the dotted line marks its onset. The dash-dotted line marks a possible further quantum phase transition of unknown order. From (Duda *et al.*, 2023).

may be of topological nature and with a critical temperature enhanced by strong coupling to light leading to the formation of exciton-polaritons (Julku *et al.*, 2022; Zerba *et al.*, 2024a). Also, Bose-Fermi mixtures consisting of long-lived dipolar inter-layer excitonic insulators interacting with degenerate itinerant electrons can be realised (Mhenni *et al.*, 2024; Nguyen *et al.*, 2023; Qi *et al.*, 2023; Xiong *et al.*, 2023).

The highly imbalanced regime hosts a quantum phase transition from zero to non-zero boson or fermion density (Nikolić and Sachdev, 2007; Sachdev, 2011). Already the non-interacting Fermi and weakly interacting Bose gas can be discussed from this viewpoint (Sachdev, 2011). Neglecting complications from three-body correlations, a Bose-Fermi mixture is described by four parameters: the boson and fermion chemical potentials μ_B and μ_F and the boson-boson and boson-fermion interaction strengths g_{BB} and g_{BF} , with the ratio of fermion to boson mass an additional parameter. This gives rise to several different phases (Ludwig *et al.*, 2011), and Ref. (Yan *et al.*, 2020) explored the case of a quantum phase transition occurring in the presence of a BEC, separating the vacuum of fermions $n_F = 0$ from the Fermi liquid phase with $n_F > 0$. This phase transition is shifted from $\mu_F = 0$ to $\mu_F^* = \varepsilon$ given by the energy of Bose polaron, which is the energy needed to inject a single fermion into the BEC. The critical chemical potential μ_F^* depends on μ_B , g_{BB} and g_{BF} . This quantum critical line at $T = 0$ determines the be-

havior of the polaron gas also at finite temperature. In particular, for unitarity limited Bose-Fermi interactions $a \rightarrow \infty$, the polaron lifetime Γ will take on a "Planckian" limit, just given by temperature, $\Gamma \simeq k_B T / \hbar$.

VIII. COMPLEX ENVIRONMENTS AND SENSING

While the the majority of investigations of polarons so far have considered cases where the environment can be treated as an ideal Fermi gas or a weakly interacting BEC as described in Secs. II and III, there is an increasing focus on situations where the environment has strong quantum/thermal correlations or non-trivial topology. In addition to being conceptually interesting, such studies are also motivated by the idea of using the impurities as probes in the spirit of quantum sensing (Degen *et al.*, 2017). For TMDs, this idea is discussed in Sec. V.G and this section therefore focuses on the atomic case.

The investigation of the impurity regime was in fact recognized as an important tool for probing BECs even before focus was on polarons. Impurities were realized by a blue-detuned laser beam and thus mimicked the movement of a macroscopic object through a superfluid (Onofrio *et al.*, 2000). These results were corroborated in an experiment where atoms in a BEC were accelerated using Raman transitions, which showed a strongly reduced collision rate below the speed of sound (Chikkatur *et al.*, 2000). In Ref. (Catani *et al.*, 2012), K impurities probed a Rb BEC by expanding within it. A superposition of motional states of Li atoms in a Na BEC allowed for an interferometric observation of a phononic Lamb shift (Scelle *et al.*, 2013) in agreement with Fröhlich model of the polaron (Rentrop *et al.*, 2016). An in-situ interferometric technique was used to explore the effective mass and dispersion of the Bose polaron (Marti *et al.*, 2014) (at that time called a magnon) in Rb BECs. These results showed first indications of effects beyond a mean-field description. Finally, impurities have been used to measure the temperature (Bouton *et al.*, 2020; Hohmann *et al.*, 2016; Olf *et al.*, 2015) and density (Adam *et al.*, 2022) of a BEC and the interaction mediated by an ideal Fermi gas (Edri *et al.*, 2020).

A. Polarons in optical lattices

By trapping atomic gases in optical lattices formed by standing laser waves, the famous Hubbard model is realised in a pristine and highly tunable way (Bloch *et al.*, 2008). This provided a wealth of insights into quantum magnetism, topological matter, phase transitions and non-equilibrium physics (Gross and Bloch, 2017).

In a breakthrough result, the superfluid to Mott insulator transition was observed in an atomic Bose gas with large boson-boson repulsion in an optical lattice (Greiner

et al., 2002). This enabled the investigation of the dynamics of impurities and magnon bound states in 1D (Fukuhara *et al.*, 2013a,b). The properties of a mobile impurity in a Bose gas in the quantum critical regime of the Mott insulator to superfluid transition at integer filling were explored using a quantum Gutzwiller approach combined with second-order perturbation theory (Colussi *et al.*, 2023). Extending this to strong interactions with a generalised diagrammatic ladder approximation as well as QMC, the polaron spectrum was shown to exhibit non-analytic features at the Mott transition such as a cusp and the emergence of a new branch, coming from gapless Goldstone and Higgs modes, see Fig. 55.

Effective field theory combined with the Boltzmann equation was used to calculate the spin diffusion of an impurity in a bath of bosons in a 2D lattice near the quantum critical point between the superfluid and insulating phases (Punk and Sachdev, 2013). A mobile impurity in a 2D Fermi Hubbard model were explored using diagrammatic Monte Carlo technique (Pascual *et al.*, 2024a), and the infinite impurity mass case was explored using auxiliary free fermions mimicking properties extracted from dynamical mean-field theory (Amelio *et al.*, 2024). The polaron energy was predicted to exhibit a cusp-like behavior at the Mott insulator to metal transition, see Fig. 55. Polaron formation in Bloch bands and fermionic charge-density waves were also explored. Recently, it was demonstrated that the band geometry of the majority particles affects the exponents describing the Fermi edge singularity of an impurity in a flat lattice band (Pimenov, 2024).

Considering mobile impurities in a lattice containing bosons in the hard core limit of strong repulsion away from half filling, it was shown that the resulting polarons are strongly affected by the properties of the surrounding bath (Santiago-García *et al.*, 2024). In the opposite limit of mobile impurities in a weakly interacting BEC, it was shown that in addition to the attractive and repulsive polaron, a third type of polaron is stable for repulsive impurity-boson interactions with no available decay channels (Ding *et al.*, 2023), since its energy is above the single particle continuum. This is in analogy with the repulsively bound states observed for bosons in an optical lattice (Winkler *et al.*, 2006).

In an early paper using a weak coupling approach, the transport properties of an impurity in an optical lattice interacting with a homogeneous BEC were shown to change from coherent to diffusive with increasing temperature (Bruderer *et al.*, 2007). Its non-equilibrium dynamics including Bloch oscillations and incoherent drift were studied within the Fröhlich model (Grusdt *et al.*, 2014). This was later extended to the case when the impurity occupies two bands in a lattice (Yin *et al.*, 2015), and when also the bosons are in a lattice (Privitera and Hofstetter, 2010).

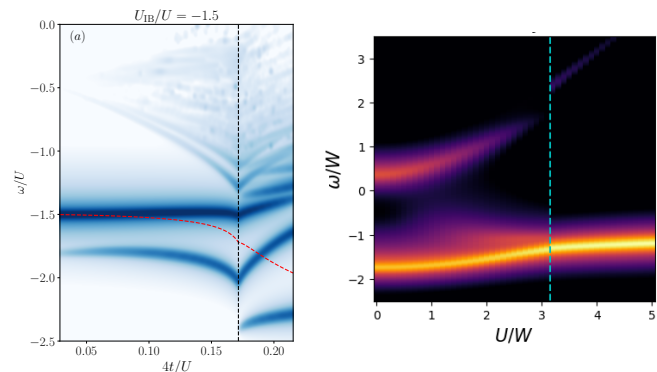


FIG. 55 **Polaron and the Mott transition.** Left: The spectral function of an impurity in a bosonic bath as a function boson-boson interaction strength U with U_{IB} the impurity-boson interaction strength and t the hopping. The bosons undergo a Mott insulator to superfluid transition at the vertical line. From (Alhyder *et al.*, 2024b). Right: The spectral function of an impurity in a two-component fermionic bath with repulsive interaction U and bandwidth W . The fermions are in a metallic/insulating phase left/right of the vertical line. From (Amelio *et al.*, 2024).

B. Polarons in spinor quantum gases

We now turn to the question of what happens when the environment is composed by atoms that feature internal spin degrees of freedom. For a continuum system, this is reminiscent of the Kondo effect (Kondo, 1964), and it has been shown how Rydberg impurities in a BEC allow for the extension of the Kondo model to include atomic bound state formation (Ashida *et al.*, 2019a,b). Experimentally, it was shown how spin-exchange interactions served to engineer impurities that worked as quantum probes of a surrounding spinor BEC (Bouton *et al.*, 2020). In Ref. (Ashida *et al.*, 2018) it was found that spin-flip excitations can dominate the dressing of impurities leading to the formation of magnetic polarons in continuum systems. The corresponding dynamics of impurities in two-component Fermi gases was shown to allow for the study of quantum spin transport at the single atom level (You *et al.*, 2019). Ref. (Wang *et al.*, 2019) considered impurities in a BEC with a synthetic spin-orbit-coupling between two of its hyperfine states, and discussed how the resulting polarons get dressed by roton excitations, and therefore acquire a non-zero momentum and an anisotropic effective mass.

The experimental observation of a smooth cross-over between a weakly interacting BCS superfluid, a strongly correlated superfluid and a BEC of weakly interacting dimers (as the interaction between two hyperfine components of fermionic atoms is tuned across a Feshbach resonance) stands out as a major success of quantum simulation with cold atoms (Giorgini *et al.*, 2008). Adding impurities to such a two-component Fermi superfluid with bosonic atoms, as done experimentally in (Ferrier-Barbut

et al., 2014; Roy *et al.*, 2017; Yao *et al.*, 2016), opens the possibility to explore polarons in the celebrated BCS-BEC crossover, and in particular how they change from Fermi to Bose polarons.

Theoretically, crossovers from polaron to a trimer states were predicted using variational wave functions (Nishida, 2015; Yi and Cui, 2015). Using a generalised Chevy ansatz combined with BCS theory, the spectral function of an impurity across the full BCS-BEC crossover was calculated and avoided crossings due to the coupling to a Higgs mode were predicted (Amelio, 2023). Using the ladder approximation combined with BCS theory, the superfluid gap was predicted to stabilize the attractive polaron and to introduce additional damping for the repulsive polaron (Hu *et al.*, 2022). Second order perturbation theory was used to identify UV divergencies related to 3-body physics in analogy with the case of Bose polarons, see Sec. III.D, which can be regularized using effective field theory (Pierce *et al.*, 2019). Finite values for the polaron energy were obtained in the whole BEC-BCS crossover when the density-density correlation function of the Fermi gas (which enters the second order impurity self-energy) was calculated using the RPA approximation (Alhyder *et al.*, 2024a; Bigué *et al.*, 2022). The problem of a static impurity in a fermionic superfluid was analysed using a functional determinant approach together with BCS theory, and the gap was predicted to protect the polarons against Anderson’s orthogonality catastrophe with in-gap Yu-Shiba-Rusinov bound states present for magnetic impurities (Wang *et al.*, 2022a,b). In these experiments the impurity-fermion interaction was however too weak to see polaron effects beyond mean-field, and an observation of these predictions remains an interesting topic for future investigations.

In 2D, a superfluid undergoes a Kosterlitz-Thouless (KT) phase transition to a normal phase at a critical temperature with a discontinuous jump in the superfluid density (Kosterlitz and Thouless, 1973). For an impurity in a superfluid Fermi gas, (Alhyder and Bruun, 2022) used perturbation theory to predict a rapid increase in the polaron energy at the transition temperature, reflecting that the normal phase is less compressible than the superfluid one (Alhyder and Bruun, 2022). Using stochastic classical-field methods, a low energy polaron branch was predicted to emerge at the KT transition connected to the binding of the impurity to vortex cores (Comaron *et al.*, 2024). The same problem was studied at zero temperature using exact diagonalisation for up to 10 particles on a square lattice at zero temperature, predicting attractive and repulsive polarons with avoided crossings (Amelio and Goldman, 2024). These results may become relevant for experiments exploring mesoscopic atomic gases, where few-body precursors of polaron physics, pairing and Higgs modes have already been observed (Bayha *et al.*, 2020; Wenz *et al.*, 2013).

C. Polarons in baths with non-trivial topology

The realization that phases with non-trivial topological properties are frequent in nature has sparked an intense research effort (Cooper *et al.*, 2019; Hasan and Kane, 2010; Qi and Zhang, 2011). While non-interacting topological phases are well understood by now, many questions remain regarding the interplay between interactions and topological states. Polarons in a bath in a topological phase provide an interesting “bottom up” approach for exploring this scenario, and can be used as new probes for topological order.

(Baldelli *et al.*, 2021; Graß *et al.*, 2020; Grusdt *et al.*, 2016; Muñoz de las Heras *et al.*, 2020) examined theoretically the regime of strong impurity-environment interactions where the impurity binds to the quasiparticle excitations in a surrounding fractional quantum Hall phase, and showed that the resulting molecules can acquire the properties of the quasiparticles in topological phases such as fractional quantum statistics. This may provide new ways to address the challenging problem of probing non-local topological order by e.g. Ramsey spectroscopy or scattering experiments with the impurities.

In the opposite limit of weak impurity-environment interactions, it was shown using diagrammatic perturbation theory that the polaron inherits some of the non-trivial topological properties of the majority particles in its dressing cloud, leading to a discontinuous jump in the transverse conductivity of a Chern insulator at the topological phase transition boundary (Camacho-Guardian *et al.*, 2019; Pimenov *et al.*, 2021). This jump is however not quantized according to the Thouless-Kohmoto-Nightingale-den Nijs relation (Thouless *et al.*, 1982), since the polaron partly consists of a topologically trivial impurity and partly of a topological dressing cloud. (Qin *et al.*, 2019) studied a mobile impurity in a 2D fermionic superfluid and proved that a discontinuity in the second derivative of its energy should appear when its $p_x + ip_y$ pairing undergoes a phase transition from a trivial to a topological symmetry. The polaron properties were shown to closely reflect also the phases of an environment described by a non-Abelian Aubry-André-Harper model, which exhibits an interplay between localisation and topological order (Bai *et al.*, 2018). The dressing of a mobile impurity interacting with the chiral edge modes circulating around both non-interacting Chern insulators and strongly correlated fractional Chern insulators was explored using exact diagonalisation, the Chevy ansatz, as well as tensor network techniques (Vashisht *et al.*, 2024). The resulting chiral polarons were found to exhibit two characteristic features: An asymmetric spectrum and a splitting into two damped states for momenta larger than a critical momentum determined by the velocity of the chiral edge modes times the impurity mass.

IX. MAGNETIC POLARONS

In this section, we discuss a different incarnation of the polaron, which is closely related to those discussed in the rest of this review: the so-called magnetic polarons, also known as spin polarons. Magnetic polarons arise when dopants such as holes or extra particles move in a lattice with spin 1/2 fermions close to half-filling (one fermion per lattice site), which due to a strong repulsive interaction form an anti-ferromagnet (AFM) at zero temperature. The motion of the dopants destroy this AFM order leading to a competition between kinetic and magnetic energy, and to the formation of a polaron consisting of the dopant surrounded by a dressing cloud of magnetic frustration, see Fig. 56(a) (Brinkman and Rice, 1970; Kane *et al.*, 1989; Martinez and Horsch, 1991; Sachdev, 1989; Schmitt-Rink *et al.*, 1988; Shraiman and Siggia, 1988).

Magnetic polarons have been intensely studied in the condensed matter community because many unconventional superconducting phases such as those in cuprates (Schrieffer and Brooks, 2007), pnictides (Wen and Li, 2011), layered organic metals (Wosnitza, 2012), and twisted bilayer graphene (Cao *et al.*, 2018) emerge when doping an AFM away from half-filling. This suggests that the properties of magnetic polarons may cast light on these intriguing phases, and we refer the reader to excellent condensed matter oriented reviews on this vast topic (Dagotto, 1994; Manousakis, 1991). Here, we will give a brief overview of the main features of magnetic polarons highlighting the close connections to the Bose polarons discussed in Sec. III. We will also discuss the new and remarkably detailed spatial information regarding the spatial properties of magnetic polarons obtained with quantum gas microscopes (Ji *et al.*, 2021; Koepsell *et al.*, 2021, 2019).

Consider spin 1/2 fermions in a square lattice close to half-filling. For strong repulsion between the spin \uparrow and \downarrow fermions, they form an AFM ground state, which can be described by the $t - J$ model (Dagotto, 1994)

$$\hat{H} = -t \sum_{\langle i,j \rangle \sigma} (\tilde{f}_{i\sigma}^\dagger \tilde{f}_{j\sigma} + \text{h.c.}) + J \sum_{\langle i,j \rangle} (\hat{\mathbf{S}}_i \cdot \hat{\mathbf{S}}_j - \hat{n}_i \hat{n}_j / 4). \quad (73)$$

Here $\tilde{f}_{i\sigma}^\dagger = \hat{f}_{i\sigma}^\dagger (1 - \hat{n}_{i\bar{\sigma}})$ where the factor $1 - \hat{n}_{i\bar{\sigma}} = 1 - \hat{f}_{i\bar{\sigma}}^\dagger \hat{f}_{i\bar{\sigma}}$ with $\bar{\sigma}$ denoting the opposite spin of σ , ensures that there is maximally one fermion per lattice site. We furthermore have $\hat{n}_i = \sum_{\sigma} \hat{n}_{i\sigma}$ and $\langle i, j \rangle$ denotes nearest neighbors. Also, $\hat{\mathbf{S}}_i = \frac{1}{2} \sum_{\sigma\sigma'} \hat{f}_{i\sigma}^\dagger \boldsymbol{\sigma}_{\sigma\sigma'} \hat{f}_{i\sigma'}$ with $\boldsymbol{\sigma} = (\sigma_x, \sigma_y, \sigma_z)$ a vector of Pauli matrices. When the $t - J$ model is derived from the Hubbard model, $J = 4t^2/U$ is the superexchange interaction where $U \gg t$ is the onsite repulsive interaction between opposite spin fermions.

Using a Holstein-Primakoff transformation generalised

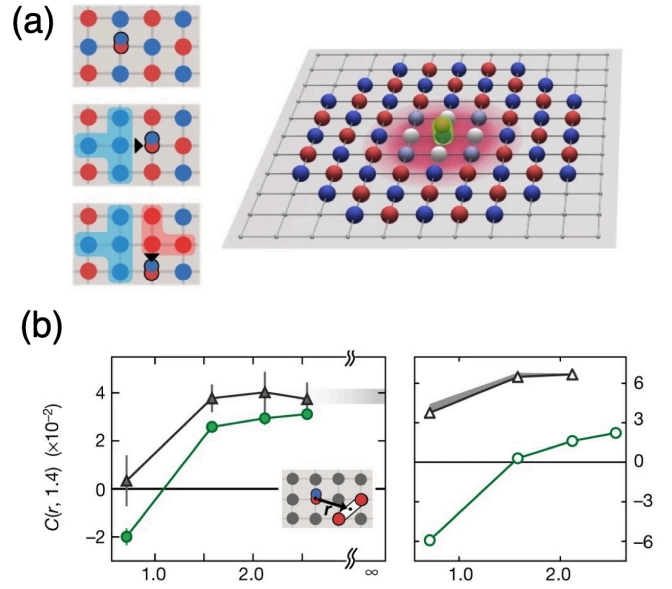


FIG. 56 **Magnetic polarons.** (a) A doublon consisting of a spin \uparrow (blue ball) and a spin \downarrow (red ball) fermions moves through an AFM lattice leaving behind itself a “string” of ferromagnetic correlations (blue and red shading). This leads to the formation of a magnetic polaron consisting of the doublon surrounded by a cloud of magnetic frustration. (b) Correlations between diagonal spins as a function of the distance r to a mobile/static doublon (green/black). The left panel shows experimental results and the right panel theoretical calculations from a string model (mobile doublon) and exact diagonalisation (static doublon). From Ref. (Koepsell *et al.*, 2019).

to include the presence of holes, Eq. (73) becomes

$$\hat{H} = \sum_{\mathbf{k}} \omega_{\mathbf{k}} \hat{\gamma}_{\mathbf{k}}^\dagger \hat{\gamma}_{\mathbf{k}} + \sum_{\mathbf{q}, \mathbf{k}} g(\mathbf{q}, \mathbf{k}) [\hat{h}_{\mathbf{k}+\mathbf{q}}^\dagger \hat{h}_{\mathbf{q}} \hat{\gamma}_{-\mathbf{q}}^\dagger + \text{h.c.}]. \quad (74)$$

Here, \mathbf{k}, \mathbf{q} are crystal momenta inside the first Brillouin zone of the lattice, $\hat{\gamma}_{\mathbf{k}}^\dagger$ is a bosonic operator creating a spin wave with energy $\omega_{\mathbf{k}} = 2J\sqrt{1 - (\cos k_x + \cos k_y)^2/4}$ (unit lattice constant), and $\hat{h}_{\mathbf{k}}^\dagger$ is a fermionic operator creating a holon. We refer to Refs. (Kane *et al.*, 1989; Nielsen *et al.*, 2021; Schmitt-Rink *et al.*, 1988) for an expression of the vertex $g(\mathbf{q}, \mathbf{k})$. One has used linear spin wave theory to derive Eq. (74), which is known to be very accurate for a square lattice (Manousakis, 1991). Note that while this model naturally describes the case of hole doping, it can also describe particle doping (doublons) using a particle-hole transformation (Jiang *et al.*, 2021).

Equation (74) is a so-called slave-fermion representation of the $t - J$ model and describes a fermionic holon emitting or absorbing bosonic spin waves as it moves through the lattice. Comparing with Eq. (21) explicitly demonstrates the close connection between magnetic and Bose polarons. Indeed, the two Hamiltonians have the same structure, apart from two differences: First,

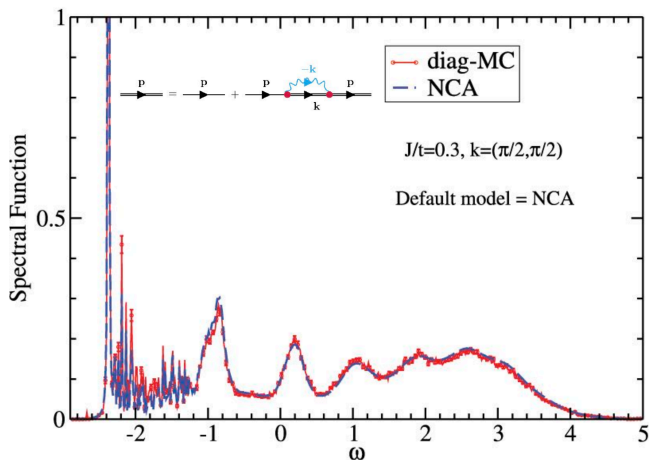


FIG. 57 **Spectral function of a hole in an AFM** computed at momentum $\mathbf{k} = (\pi/2, \pi/2)$, with $J/t = 0.3$ and the frequency in units of t . The inset shows the diagrammatic structure of the SCBA Green's function. From (Diamantis and Manousakis, 2021).

Eq. (74) has no scattering term, i.e. the last term in Eq. (21) and therefore corresponds to the Fröhlich Hamiltonian; second Eq. (74) has no bare kinetic energy of the impurity (holon). The lack of this term reflects that the hole cannot move in a square lattice without destroying magnetic order as illustrated in Fig. 56(a). For other geometries such as the triangular lattice, a bare kinetic term is present (van de Kraats *et al.*, 2022; Trumper *et al.*, 2004). We note that the strongly interacting regime $t \gg J$ physically corresponds to the hole moving rapidly and destroying magnetic order, which in terms of the underlying Hubbard model is equivalent to $U \gg t$.

Figure 57 plots the spectral function of a single hole obtained from Eq. (74) in two ways: Diagrammatic Monte-Carlo and a self-consistent diagrammatic Born approximation (SCBA) [also known as non-crossing approximation (NCA)]. One clearly sees a well-defined quasiparticle peak at low energy, which is the magnetic polaron. The minimum energy of this polaron turns out to be at the crystal momenta $(\pm\pi/2, \pm\pi/2)$ for a square lattice, which is consistent with ARPES experiments in copper-oxides (Damascelli *et al.*, 2003; Kim *et al.*, 1998). There is a remarkable agreement between the diag-MC calculation and the SCBA, which is the widely used approximation for the holon self-energy corresponding to summing a class of non-crossing diagrams shown as an inset in Fig. 57 (Chernyshev and Leung, 1999; Kane *et al.*, 1989; Liu and Manousakis, 1992; Martinez and Horsch, 1991; Schmitt-Rink *et al.*, 1988). A similar accuracy of the SCBA was found in other QMC calculations (Brunner *et al.*, 2000; Mishchenko *et al.*, 2001).

One can intuitively understand the basic physics of magnetic polarons using a so-called geometric string picture, where the hole moves at the fast time-scale t leaving

a string of magnetic frustration in its wake, see Fig. 56(a), which creates a linear potential that is only repaired on the much slower time-scale J . Hence, the hole is effectively bound by a linear string potential whose ground state is the magnetic polaron and excited states are string excitations, which can be seen as broader peaks at higher energies in Fig. 57. This string picture predicts a characteristic energy scaling $(J/t)^{2/3}$ of the polaron and its excited states and is widely used in the literature (Barnes *et al.*, 1989; Bulaevski *et al.*, 1968; Béran *et al.*, 1996; Dagotto *et al.*, 1990; Liu and Manousakis, 1992; Mishchenko *et al.*, 2001; Shraiman and Siggia, 1988). It has recently been revisited and extended in the cold atom context (Bermes *et al.*, 2024; Bohrdt *et al.*, 2021; Grusdt *et al.*, 2019, 2018).

In direct analogy with the Bose polaron, the wave function of the magnetic polaron can be written as an expansion in the number of spin waves that the dopant creates in the AFM background. Formally, one can simply replace the impurity operator $\hat{c}_{\mathbf{k}}$ in Eq. (34) with the holon operator $\hat{h}_{\mathbf{k}}$ and the ground state $|\text{BEC}\rangle$ with $|\text{AFM}\rangle$. Closed expressions for the first three expansion coefficients have been derived using the SCBA (Ramšak and Horsch, 1998; Reiter, 1994), and later extended to infinite order to capture strong interactions $J/t \ll 1$ (Nielsen *et al.*, 2021; Nyhegn *et al.*, 2023).

In a groundbreaking experiment, the spin and density of ${}^6\text{Li}$ atoms in two internal spin states in a 2D square lattice close to half filling was measured with single site resolution (Koepsell *et al.*, 2019). Due to a strong repulsive interaction between the two spin components, the atoms exhibit strong AFM correlations at low temperature. A few sites were occupied with both spin components thereby creating doublons, and a significant reduction and even sign reversal of the AFM correlations was observed in their neighborhood, see Fig. 56(b), in qualitative agreement with a string model for the magnetic polaron (Grusdt *et al.*, 2018). The mobility of the doublon was shown to be key for this, as no sign reversal was measured when it was pinned. This work provided therefore a direct observation of the microscopic spatial structure of a magnetic polaron formed by the doublon and its surrounding dressing cloud of magnetic frustration. The transition between a gas of magnetic polarons and a Fermi liquid was studied in a subsequent experiment (Koepsell *et al.*, 2021) and theoretically analysed using variational functions containing polaronic correlations (Müller *et al.*, 2024; Shackleton and Zhang, 2024).

The non-equilibrium dynamics of a hole released from a given site in a square optical lattice was measured using quantum gas microscopy (Ji *et al.*, 2021). The hole was moving in a background of AFM correlated spins formed by two repulsively interacting spin states of ${}^6\text{Li}$ at half-filling, see Fig. 58. For short times, the hole moved ballistically with a velocity $2t$ in agreement with DMRG simulations on a 18×4 lattice strip (Bohrdt *et al.*,

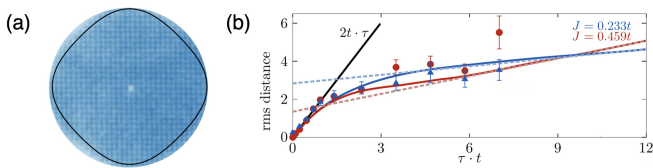


FIG. 58 **Hole dynamics in an AFM.** Left: in-situ image of a hole created in an AFM formed by two repulsively-interacting spin states of ${}^6\text{Li}$ atoms at half-filling. From (Ji *et al.*, 2021). Right: root-mean-square distance of a hole from its initial position as a function of time τ measured by (Ji *et al.*, 2021) compared to a quantum walk of a free particle (black line), and to a non-equilibrium SCBA calculation (red and blue lines). From (Nielsen *et al.*, 2022).

2020b) and short-time analytics (Nielsen *et al.*, 2022). For longer times, the hole slowed down as it became increasingly dressed by magnetic frustration, as shown in Fig. 58, which can be phenomenologically explained by mapping the dynamics onto a free quantum walk in a Bethe lattice (Ji *et al.*, 2021). Using a time-dependent wave function for the hole derived from the SCBA, these experimental observations were quantitatively explained at all time scales in (Nielsen *et al.*, 2022), see Fig. 58. This extends the use and accuracy of the SCBA also to non-equilibrium dynamics, and demonstrate that the slowdown of the hole at long times quantitatively agrees with a theory for polaron formation. The theory furthermore showed that oscillations at intermediate times can be interpreted as quantum beating between string states.

In the seminal paper by (Nagaoka, 1966) it was shown that the motion of a single dopant induces a ferromagnetic ground state in a wide range of different lattices when $t/U \rightarrow 0$ in the Hubbard model ($J/t \rightarrow 0$). This effect emerges in the extreme limit $t/U < N$ with N the number of lattice sites, as a result of the dopant minimizing its kinetic energy, which is only possible in the fully ferromagnetic state. For a very large but finite U/t , it has similarly been proposed that a ferromagnetic bubble forms around the dopant. This so-called Nagaoka polaron has remained elusive in condensed matter systems, but it was recently observed in two experiments exploring doublons with a two-component ${}^6\text{Li}$ gas in a triangular optical lattice. Such a lattice was chosen to enhance the formation of the Nagaoka polaron by suppressing AFM order by geometric frustration (Lebrat *et al.*, 2024; Prichard *et al.*, 2024). Figure 59 shows the experimentally observed increasing size of the ferromagnetic bubble around a doublon with increasing interaction strength, which is consistent with a $(t/J)^{1/4}$ scaling obtained using variational arguments (White and Affleck, 2001).

These results demonstrate that optical lattice experiments can shed light on the spatial properties of magnetic polarons, which complements the spectral information typically obtained in condensed matter experiments. They however provide somewhat indirect evidence of the

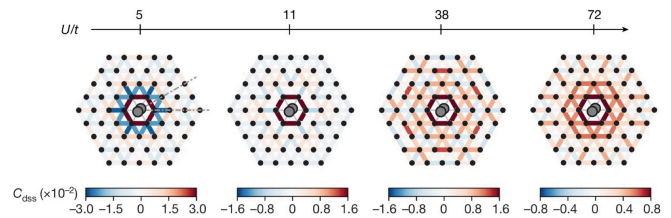


FIG. 59 **Nagaoka polarons.** Ferromagnetic correlations (red) replace AFM correlations (blue) around a doublon with increasing interaction strength U/t corresponding to increasing t/J . From Ref. (Lebrat *et al.*, 2024).

magnetic polaron and it would be very useful in future experimental work to measure the spectral function of dopants in an optical lattice to confirm the presence of a quasiparticle peak (Bohrdt *et al.*, 2020a; Nielsen *et al.*, 2021). This would provide a confirmation of the existence of magnetic polarons without complications from disorder, doping dependent screening, and sample sensitivity typical of condensed matter experiments. Also, the topic of mobile dopants in spin backgrounds is very rich and there are many interesting open questions not discussed here. This includes the effects of non-zero temperature (Shen *et al.*, 2024), polarons in layered systems (Nyhegn *et al.*, 2023, 2022), spin liquids (Jin *et al.*, 2024; Kadow *et al.*, 2024, 2022; Nyhegn *et al.*, 2024), bound states of polarons and pairing (Bohrdt *et al.*, 2023; Grusdt *et al.*, 2023; Hartke *et al.*, 2023), and mixed dimensional systems (Hirthe *et al.*, 2023; Nielsen, 2024), which may improve our understanding of pairing in unconventional superconductors (Lange *et al.*, 2024).

X. PERSPECTIVES

This review provides a comprehensive description of the physics of polarons as realized in cold atomic gases and 2D semiconductors. We highlighted the many common properties characterizing polarons in these two seemingly very different systems, showcasing the power and universal applicability of this concept. With this work, we hope to bridge the gap between different communities and foster collaborations in this rapidly evolving topic. Indeed, while many properties of polarons are by now well understood, there remain still various exciting research directions open for future studies, as we will now briefly outline.

As is clear from Sec. III, there are several questions and different theoretical predictions regarding Bose polarons for strong interactions. This includes the number of relevant parameters and the influence of $n > 2$ -body correlations and few-body states, which may evolve from low energy cluster states that are hard to observe, and the role of the bosonic OC. Indeed, a clear cut experimental confirmation of the existence of well-defined polarons in

the unitarity region is still lacking. Also, the role of the multichannel nature of the impurity-boson interaction is not clear as is the temperature dependence of the Bose polaron and its fate in the critical region of the BEC. Regarding magnetic polarons, the experimental evidences of their existence in optical lattices are rather indirect and related to real space observables, see Sec. IX, and a smoking gun observation of a quasiparticle peak in frequency space is highly desirable.

The non-equilibrium properties of both Bose and Fermi polarons is another interesting topic. This is of particular relevance for the lossy atomic Bose polaron where the competition between scales such as its formation time, decay time, and experimental times complicates its observation. Polarons in TMDs are moreover intrinsically of non-equilibrium nature due to the electron-hole recombination of excitons and photon leakage discussed in Sec. V, and a systematic theory describing this, for instance based on the Keldysh formalism, would be very useful. The fate of atomic polarons under strong RF driving, see Sec. II.B, or polarons in strongly-pumped TMDs is another intriguing open issue.

There are many questions regarding the experimental exploration of mediated interactions between polarons as discussed in Sec. VI. For instance, beyond-mean-field medium-induced interactions between Bose polarons have not yet been observed, despite those are expected to be stronger than the ones between Fermi polarons (due to the higher compressibility of the Bose gas). The puzzling observations of repulsive mediated interactions between polarons in TMDs and the influence of non-equilibrium effects, see Sec. VI, also call for further analysis. The predicted bound states between two polarons, i.e. bipolarons, remains to be seen experimentally. Such an observation would be a major breakthrough as bipolarons are precursors for Cooper pairs and superfluidity, which in the case of magnetic polarons may be closely connected to high T_c superconductivity, as discussed in Sec. IX. This is furthermore important for the exploration of quantum mixtures and their polaronic limit (Sec. VII), where such mediated interactions play a key role in their many-body phase-diagram. Regarding polaron-polaritons in TMDs discussed in Sec. V.C, such interactions may give rise to entirely new hybrid light-matter quantum phases and strong photon-photon interactions with applications in opto-electronics.

A systematic investigation of the role of the composite electron-hole nature of the exciton for polarons in 2D semiconductors, as well as effects of the Coulomb interactions in the electron bath is highly relevant. This would improve our microscopic understanding of polarons in TMDs and likely lead to a better agreement between theory and experiment, which as explained in Sec. V is generally less satisfactory than in atomic gases.

Finally, the use of polarons as quantum sensors for many-body correlations discussed in Secs. V.G and VIII

is still in its infancy with many exciting perspectives for both fundamental science and technology. In particular, there is an urgent need for sensors to probe the properties of the rapidly growing class of TMDs with many possible applications. One can for instance imagine using several pinned polarons in a moiré lattice to create a spatially resolved sensing of multi-point correlation functions. Also, using entangled polarons may lead to entirely new capabilities such as the detection of entanglement by entanglement. This is likely to be a major research topic as many important quantum phases are characterized by subtle many-body correlations, which are hard to detect by conventional means, in particular in TMDs.

ACKNOWLEDGMENTS

We wish to warmly thank I. Amelio, C. Baroni, M. Caldara, A. Camacho-Guardian, O. Cotlet, X. Cui, E. Demler, R. Grimm, F. Grusdt, M. Knap, M. Kroner, C. Kuhlenskamp, J. Levinsen, A. M. Morgen, A. Negretti, M. Parish, F. Scazza, T. Shi, L.B. Tan, and M. Zaccanti for insightful discussions.

P.M. acknowledges support of the *ICREA Academia* program, the Institut Henri Poincaré (UAR 839 CNRS-Sorbonne Université) and the LabEx CARMIN (ANR-10-LABX-59-01). P.M. and G.E.A. further acknowledge support of the Spanish Ministry of Science and Innovation (MCIN/AEI/10.13039/501100011033, grant PID2023-147469NB-C21) and the Generalitat de Catalunya (grant 2021 SGR 01411). R.S. was supported by the Deutsche Forschungsgemeinschaft under Germany's Excellence Strategy EXC 2181/1 - 390900948 (the Heidelberg STRUCTURES Excellence Cluster) and Project-ID 273811115 - SFB 1225 ISOQUANT. A.Í. acknowledges support by the Swiss National Science Foundation (SNSF) under Grant Number 200020_207520. M.Z. acknowledges support by the NSF Center for Ultracold Atoms and NSF PHY-2012110, AFOSR (FA9550-23-1-0402), ARO (W911NF-23-1-0382), and the Vannavar Bush Faculty Fellowship (ONR N00014-19-1-2631). J.A. acknowledges support by the Novo Nordisk Foundation NERD grant (Grant no. NNF22OC0075986). G.B. and J.A. were supported by the Danish National Research Foundation through the Center of Excellence "CCQ" (DNR152).

REFERENCES

- Adam, D., Q. Bouton, J. Nettersheim, S. Burgardt, and A. Widera (2022), "Coherent and dephasing spectroscopy for single-impurity probing of an ultracold bath," *Phys. Rev. Lett.* **129**, 120404.

- Adlong, H. S., W. E. Liu, F. Scazza, M. Zaccanti, N. D. O'pong, S. Fölling, M. M. Parish, and J. Levinsen (2020), "Quasiparticle lifetime of the repulsive fermi polaron," *Phys. Rev. Lett.* **125**, 133401.
- Akaturk, E., and B. Tanatar (2019), "Two-dimensional bose polaron using diffusion monte carlo method," *International Journal of Modern Physics B* **33** (21), 1950238.
- Al-Ani, I. A. M., K. As'ham, O. Klochan, H. T. Hattori, L. Huang, and A. E. Miroshnichenko (2022), "Recent advances on strong light-matter coupling in atomically thin tmdc semiconductor materials," *Journal of Optics* **24** (5), 053001.
- Alexandrov, A. S., and N. F. Mott (1994), "Bipolarons," *Reports on Progress in Physics* **57** (12), 1197.
- Alexandrov, A. S., and N. F. Mott (1996), *Polarons and bipolarons* (World Scientific).
- Alford, M., J. Berges, and K. Rajagopal (2000), "Gapless color superconductivity," *Phys. Rev. Lett.* **84**, 598.
- Allyder, R., and G. M. Bruun (2022), "Mobile impurity probing a two-dimensional superfluid phase transition," *Phys. Rev. A* **105**, 063303.
- Allyder, R., F. Chevy, and X. Leyronas (2024a), "Exploring beyond-mean-field logarithmic divergences in fermi-polaron energy," *Phys. Rev. A* **109**, 033315.
- Allyder, R., V. E. Colussi, M. Čufar, J. Brand, A. Recati, and G. M. Bruun (2024b), "Lattice bose polarons at strong coupling and quantum criticality," [arXiv:2412.07597](https://arxiv.org/abs/2412.07597).
- Amelio, I. (2023), "Two-dimensional polaron spectroscopy of fermi superfluids," *Phys. Rev. B* **107**, 104519.
- Amelio, I., N. D. Drummond, E. Demler, R. Schmidt, and A. Imamoglu (2023), "Polaron spectroscopy of a bilayer excitonic insulator," *Phys. Rev. B* **107**, 155303.
- Amelio, I., and N. Goldman (2024), "Polaron spectroscopy of interacting Fermi systems: Insights from exact diagonalization," *SciPost Phys.* **16**, 056.
- Amelio, I., G. Mazza, and N. Goldman (2024), "Polaron formation in insulators and the key role of hole scattering processes: Band insulators, charge density waves and Mott transition," [arXiv:2408.01377](https://arxiv.org/abs/2408.01377).
- Andersen, J. O. (2004), "Theory of the weakly interacting bose gas," *Rev. Mod. Phys.* **76**, 599.
- Anderson, P. W. (1961), "Localized magnetic states in metals," *Phys. Rev.* **124** (1), 41.
- Anderson, P. W. (1967), "Infrared catastrophe in Fermi gases with local scattering potentials," *Phys. Rev. Lett.* **18** (24), 1049.
- Ashida, Y., R. Schmidt, L. Tarruell, and E. Demler (2018), "Many-body interferometry of magnetic polaron dynamics," *Phys. Rev. B* **97**, 060302.
- Ashida, Y., T. Shi, R. Schmidt, H. R. Sadeghpour, J. I. Cirac, and E. Demler (2019a), "Efficient variational approach to dynamics of a spatially extended bosonic kondo model," *Phys. Rev. A* **100**, 043618.
- Ashida, Y., T. Shi, R. Schmidt, H. R. Sadeghpour, J. I. Cirac, and E. Demler (2019b), "Quantum rydberg central spin model," *Phys. Rev. Lett.* **123**, 183001.
- Astrakharchik, G. E., J. Boronat, J. Casulleras, and S. Giorgini (2002), "Superfluidity versus bose-einstein condensation in a bose gas with disorder," *Phys. Rev. A* **66**, 023603.
- Astrakharchik, G. E., L. A. Peña Ardila, K. Jachymski, and A. Negretti (2023), "Many-body bound states and induced interactions of charged impurities in a bosonic bath," *Nature Communications* **14** (1), 1647.
- Astrakharchik, G. E., L. A. Peña Ardila, R. Schmidt, K. Jachymski, and A. Negretti (2021), "Ionic polaron in a Bose-Einstein condensate," *Communications Physics* **4** (94), 10.1038/s42005-021-00597-1.
- Astrakharchik, G. E., and L. P. Pitaevskii (2004), "Motion of a heavy impurity through a bose-einstein condensate," *Phys. Rev. A* **70**, 013608.
- Atkins, K. R. (1959), "Ions in liquid helium," *Phys. Rev.* **116**, 1339.
- Bai, X.-D., J. Wang, X.-J. Liu, J. Xiong, F.-G. Deng, and H. Hu (2018), "Polaron in a non-abelian aubry-andré-harper model with p -wave superfluidity," *Phys. Rev. A* **98**, 023627.
- Baibich, M. N., J. M. Broto, A. Fert, F. N. Van Dau, F. Petroff, P. Etienne, G. Creuzet, A. Friederich, and J. Chazelas (1988), "Giant magnetoresistance of (001)fe/(001)cr magnetic superlattices," *Phys. Rev. Lett.* **61**, 2472.
- Baldelli, N., B. Juliá-Díaz, U. Bhattacharya, M. Lewenstein, and T. Graß (2021), "Tracing non-abelian anyons via impurity particles," *Phys. Rev. B* **104**, 035133.
- Baranov, M. A., M. Dalmonte, G. Pupillo, and P. Zoller (2012), "Condensed matter theory of dipolar quantum gases," *Chemical Reviews* **112** (9), 5012.
- Baranov, M. A., A. Micheli, S. Ronen, and P. Zoller (2011), "Bilayer superfluidity of fermionic polar molecules: Many-body effects," *Phys. Rev. A* **83**, 043602.
- Barnes, T., E. Dagotto, A. Moreo, and E. S. Swanson (1989), "Spin-hole polaron of the t - J_z model," *Phys. Rev. B* **40**, 10977.
- Baroni, C., B. Huang, I. Fritsche, E. Dobler, G. Anich, E. Kirilov, R. Grimm, M. A. Bastarrachea-Magnani, P. Massignan, and G. M. Bruun (2024a), "Mediated interactions between Fermi polarons and the role of impurity quantum statistics," *Nat. Phys.* **20**, 68.
- Baroni, C., G. Lamporesi, and M. Zaccanti (2024b), "Quantum mixtures of ultracold gases of neutral atoms," *Nat. Rev. Phys.* **6**, 736.
- Bastarrachea-Magnani, M. A., A. Camacho-Guardian, and G. M. Bruun (2021a), "Attractive and repulsive exciton-polariton interactions mediated by an electron gas," *Phys. Rev. Lett.* **126**, 127405.
- Bastarrachea-Magnani, M. A., A. Camacho-Guardian, M. Wouters, and G. M. Bruun (2019), "Strong interactions and biexcitons in a polariton mixture," *Phys. Rev. B* **100**, 195301.
- Bastarrachea-Magnani, M. A., J. Thomsen, A. Camacho-Guardian, and G. M. Bruun (2021b), "Polaritons in an Electron Gas – Quasiparticles and Landau Effective Interactions," *Atoms* **9** (4), 81.
- Bayha, L., M. Holten, R. Klemm, K. Subramanian, J. Bjerlin, S. M. Reimann, G. M. Bruun, P. M. Preiss, and S. Jochim (2020), "Observing the emergence of a quantum phase transition shell by shell," *Nature* **587** (7835), 583.
- Baym, G., and C. Pethick (2008), *Landau Fermi-Liquid Theory: Concepts and Applications* (Wiley, Weinheim, Germany).
- Bazak, B., and D. S. Petrov (2017), "Five-body efimov effect and universal pentamer in fermionic mixtures," *Phys. Rev. Lett.* **118**, 083002.
- Bazak, B., and D. S. Petrov (2018), "Stable p -wave resonant two-dimensional fermi-bose dimers," *Phys. Rev. Lett.* **121**, 263001.
- Bernes, P., A. Bohrdt, and F. Grusdt (2024), "Magnetic po-

- larons beyond linear spin-wave theory: Mesons dressed by magnons,” *Phys. Rev. B* **109**, 205104.
- Bianchi, A., R. Movshovich, C. Capan, P. G. Pagliuso, and J. L. Sarrao (2003), “Possible fulde-ferrell-larkin-ovchinnikov superconducting state in CeCoIn_5 ,” *Phys. Rev. Lett.* **91**, 187004.
- Bigagli, N., W. Yuan, S. Zhang, B. Bulatovic, T. Karman, I. Stevenson, and S. Will (2024), “Observation of bose-einstein condensation of dipolar molecules,” *Nature* **631** (8020), 289.
- Bighin, G., P. A. Murthy, N. Defenu, and T. Enss (2022), “Resonantly enhanced superconductivity mediated by spinor condensates,” [arXiv:2212.07419](https://arxiv.org/abs/2212.07419).
- Bigué, A., F. Chevy, and X. Leyronas (2022), “Mean field versus random-phase approximation calculation of the energy of an impurity immersed in a spin-1/2 superfluid,” *Phys. Rev. A* **105**, 033314.
- Bisset, R. N., L. A. Peña Ardila, and L. Santos (2021), “Quantum droplets of dipolar mixtures,” *Phys. Rev. Lett.* **126**, 025301.
- Bistritzer, R., and A. H. MacDonald (2011), “Moiré bands in twisted double-layer graphene,” *Proc. Natl. Acad. Sci. U.S.A.* **108** (30), 12233.
- Bloch, I., J. Dalibard, and W. Zwerger (2008), “Many-body physics with ultracold gases,” *Rev. Mod. Phys.* **80** (3), 885.
- Bloom, P. (1975), “Two-dimensional fermi gas,” *Phys. Rev. B* **12**, 125.
- Blume, D. (2012), “Universal four-body states in heavy-light mixtures with a positive scattering length,” *Phys. Rev. Lett.* **109**, 230404.
- Blume, D., and Y. Yan (2014), “Generalized efimov scenario for heavy-light mixtures,” *Phys. Rev. Lett.* **113**, 213201.
- Bobbert, P. A., T. D. Nguyen, F. W. A. van Oost, B. Koopmans, and M. Wohlgenannt (2007), “Bipolaron mechanism for organic magnetoresistance,” *Phys. Rev. Lett.* **99**, 216801.
- Bohrdt, A., E. Demler, and F. Grusdt (2021), “Rotational resonances and regge-like trajectories in lightly doped antiferromagnets,” *Phys. Rev. Lett.* **127**, 197004.
- Bohrdt, A., E. Demler, and F. Grusdt (2023), “Dichotomy of heavy and light pairs of holes in the t-j model,” *Nature Communications* **14** (1), 8017.
- Bohrdt, A., E. Demler, F. Pollmann, M. Knap, and F. Grusdt (2020a), “Parton theory of angle-resolved photoemission spectroscopy spectra in antiferromagnetic mott insulators,” *Phys. Rev. B* **102**, 035139.
- Bohrdt, A., F. Grusdt, and M. Knap (2020b), “Dynamical formation of a magnetic polaron in a two-dimensional quantum antiferromagnet,” *New Journal of Physics* **22** (12), 123023.
- Bombín, R., V. Cikojević, J. Sánchez-Baena, and J. Boronat (2021), “Finite-range effects in the two-dimensional repulsive fermi polaron,” *Phys. Rev. A* **103**, L041302.
- Bombín, R., T. Comparin, G. Bertaina, F. Mazzanti, S. Giorgini, and J. Boronat (2019a), “Two-dimensional repulsive fermi polarons with short- and long-range interactions,” *Phys. Rev. A* **100**, 023608.
- Bombín, R., T. Comparin, G. Bertaina, F. Mazzanti, S. Giorgini, and J. Boronat (2019b), “Two-dimensional repulsive fermi polarons with short- and long-range interactions,” *Phys. Rev. A* **100**, 023608.
- Boudjemâa, A. (2014), “Self-consistent theory of a bose-einstein condensate with impurity at finite temperature,” *Journal of Physics A: Mathematical and Theoretical* **48** (4), 045002.
- Bouton, Q., J. Nettersheim, D. Adam, F. Schmidt, D. Mayer, T. Lausch, E. Tiemann, and A. Widera (2020), “Single-atom quantum probes for ultracold gases boosted by nonequilibrium spin dynamics,” *Phys. Rev. X* **10**, 011018.
- Braaten, E., and H.-W. Hammer (2006), “Universality in few-body systems with large scattering length,” *Physics Reports* **428** (56), 259.
- Braaten, E., D. Kang, and L. Platter (2010), “Short-time operator product expansion for rf spectroscopy of a strongly interacting fermi gas,” *Phys. Rev. Lett.* **104**, 223004.
- Bredas, J. L., and G. B. Street (1985), “Polarons, bipolarons, and solitons in conducting polymers,” *Accounts of Chemical Research* **18** (10), 309.
- Breu, D., E. V. Marcos, M. Will, and M. Fleischhauer (2024), “Impurities in a trapped 1d bose gas of arbitrary interaction strength: localization-delocalization transition and absence of self-localization,” [arXiv:2408.11549](https://arxiv.org/abs/2408.11549).
- Brinkman, W. F., and T. M. Rice (1970), “Single-particle excitations in magnetic insulators,” *Phys. Rev. B* **2**, 1324.
- Bruderer, M., A. Klein, S. R. Clark, and D. Jaksch (2007), “Polaron physics in optical lattices,” *Phys. Rev. A* **76**, 011605.
- Brunner, M., F. F. Assaad, and A. Muramatsu (2000), “Single-hole dynamics in the $t-j$ model on a square lattice,” *Phys. Rev. B* **62**, 15480.
- Bruun, G. M., and P. Massignan (2010), “Decay of polarons and molecules in a strongly polarized fermi gas,” *Phys. Rev. Lett.* **105**, 020403.
- Bruun, G. M., A. Recati, C. J. Pethick, H. Smith, and S. Stringari (2008), “Collisional properties of a polarized fermi gas with resonant interactions,” *Phys. Rev. Lett.* **100**, 240406.
- Bulaevski, L. N., É. L. Nagaev, and D. I. Khomskii (1968), “A New Type of Auto-localized State of a Conduction Electron in an Antiferromagnetic Semiconductor,” *Soviet Journal of Experimental and Theoretical Physics* **27**, 836.
- Bulgac, A., and M. M. Forbes (2007), “Zero-temperature thermodynamics of asymmetric fermi gases at unitarity,” *Phys. Rev. A* **75**, 031605.
- Béran, P., D. Poilblanc, and R. Laughlin (1996), “Evidence for composite nature of quasiparticles in the 2d t-j model,” *Nuclear Physics B* **473** (3), 707.
- Cadiz, F., S. Tricard, M. Gay, D. Lagarde, G. Wang, C. Robert, P. Renucci, B. Urbaszek, and X. Marie (2016), “Well separated trion and neutral excitons on superacid treated MoS2 monolayers,” *Appl. Phys. Lett.* **108** (25), 251106.
- Camacho-Guardian, A. (2023), “Polaritons for testing the universality of an impurity in a bose-einstein condensate,” *Phys. Rev. A* **108**, L021303.
- Camacho-Guardian, A., M. Bastarrachea-Magnani, T. Pohl, and G. M. Bruun (2022), “Strong photon interactions from weakly interacting particles,” *Phys. Rev. B* **106**, L081302.
- Camacho-Guardian, A., M. A. Bastarrachea-Magnani, and G. M. Bruun (2021), “Mediated interactions and photon bound states in an exciton-polariton mixture,” *Phys. Rev. Lett.* **126**, 017401.
- Camacho-Guardian, A., and G. M. Bruun (2018), “Landau effective interaction between quasiparticles in a bose-einstein condensate,” *Phys. Rev. X* **8**, 031042.
- Camacho-Guardian, A., N. Goldman, P. Massignan, and G. M. Bruun (2019), “Dropping an impurity into a chern insulator: A polaron view on topological matter,” *Phys.*

- Rev. B* **99**, 081105.
- Camacho-Guardian, A., K. K. Nielsen, T. Pohl, and G. M. Bruun (2020), “Polariton dynamics in strongly interacting quantum many-body systems,” *Phys. Rev. Res.* **2**, 023102.
- Camacho-Guardian, A., L. A. Peña Ardila, T. Pohl, and G. M. Bruun (2018), “Bipolarons in a bose-einstein condensate,” *Phys. Rev. Lett.* **121**, 013401.
- Camargo, F., R. Schmidt, J. D. Whalen, R. Ding, G. Woehl, S. Yoshida, J. Burgdörfer, F. B. Dunning, H. R. Sadeghpour, E. Demler, and T. C. Killian (2018), “Creation of rydberg polarons in a bose gas,” *Phys. Rev. Lett.* **120**, 083401.
- Cao, Y., V. Fatemi, S. Fang, K. Watanabe, T. Taniguchi, E. Kaxiras, and P. Jarillo-Herrero (2018), “Unconventional superconductivity in magic-angle graphene superlattices,” *Nature* **556** (7699), 43.
- Cardenas-Castillo, L. F., and A. Camacho-Guardian (2023), “Strongly interacting bose polarons in two-dimensional atomic gases and quantum fluids of polaritons,” *Atoms* **11** (1), 10.3390/atoms11010003.
- Carusotto, I., and C. Ciuti (2013), “Quantum fluids of light,” *Rev. Mod. Phys.* **85** (1), 299.
- Carusotto, I., T. Volz, and A. Imamoglu (2010), “Feshbach blockade: Single-photon nonlinear optics using resonantly enhanced cavity polariton scattering from biexciton states,” *Europhysics Letters* **90** (3), 37001.
- Casalbuoni, R., and G. Nardulli (2004), “Inhomogeneous superconductivity in condensed matter and QCD,” *Reviews of Modern Physics* **76** (1), 263.
- Casimir, H. B., and D. Polder (1948), “The Influence of Retardation on the London-van der Waals Forces,” *Physical Review* **73** (4), 360.
- Casteels, W., J. Tempere, and J. T. Devreese (2011a), “Many-polaron description of impurities in a Bose-Einstein condensate in the weak-coupling regime,” *Phys. Rev. A* **84**, 063612.
- Casteels, W., J. Tempere, and J. T. Devreese (2011b), “Response of the polaron system consisting of an impurity in a Bose-Einstein condensate to Bragg spectroscopy,” *Phys. Rev. A* **83**, 033631.
- Casteels, W., J. Tempere, and J. T. Devreese (2012), “Polaronic properties of an impurity in a Bose-Einstein condensate in reduced dimensions,” *Phys. Rev. A* **86**, 043614.
- Casteels, W., and M. Wouters (2014), “Polaron formation in the vicinity of a narrow feshbach resonance,” *Phys. Rev. A* **90**, 043602.
- Castin, Y., C. Mora, and L. Pricoupenko (2010), “Four-body efimov effect for three fermions and a lighter particle,” *Phys. Rev. Lett.* **105**, 223201.
- Catani, J., G. Lamporesi, D. Naik, M. Gring, M. Inguscio, F. Minardi, A. Kantian, and T. Giamarchi (2012), “Quantum dynamics of impurities in a one-dimensional Bose gas,” *Phys. Rev. A* **85** (2), 023623.
- Cavazos Olivas, U., L. A. Peña Ardila, and K. Jachymski (2024), “Modified mean-field ansatz for charged polarons in a bose-einstein condensate,” *Phys. Rev. A* **110**, L011301.
- Cayla, H., P. Massignan, T. Giamarchi, A. Aspect, C. I. Westbrook, and D. Clément (2023), “Observation of $1/k^4$ -tails after expansion of bose-einstein condensates with impurities,” *Phys. Rev. Lett.* **130**, 153401.
- Cetina, M., M. Jag, R. S. Lous, I. Fritsche, J. T. M. Walraven, R. Grimm, J. Levinsen, M. M. Parish, R. Schmidt, M. Knap, and E. Demler (2016), “Ultrafast many-body interferometry of impurities coupled to a fermi sea,” *Science* **354** (6308), 96.
- Cetina, M., M. Jag, R. S. Lous, J. T. M. Walraven, R. Grimm, R. S. Christensen, and G. M. Bruun (2015), “Decoherence of impurities in a fermi sea of ultracold atoms,” *Phys. Rev. Lett.* **115**, 135302.
- Chandrasekhar, B. (1962), “A note on the maximum critical field of high-field superconductors,” *Applied Physics Letters* **1**, 7.
- Chapurin, R., X. Xie, M. J. Van de Graaff, J. S. Popowski, J. P. D’Incao, P. S. Julienne, J. Ye, and E. A. Cornell (2019), “Precision test of the limits to universality in few-body physics,” *Phys. Rev. Lett.* **123**, 233402.
- Charalambous, C., M. A. Garcia-March, A. Lampo, M. Mehboud, and M. Lewenstein (2019), “Two distinguishable impurities in BEC: squeezing and entanglement of two Bose polarons,” *SciPost Phys.* **6**, 010.
- Charalambous, C., M. Á. García-March, G. Muñoz-Gil, P. R. Grzybowski, and M. Lewenstein (2020), “Control of anomalous diffusion of a Bose polaron,” *Quantum* **4**, 232.
- Chen, K., N. V. Prokof’ev, and B. V. Svistunov (2018), “Trapping collapse: Infinite number of repulsive bosons trapped by a generic short-range potential,” *Phys. Rev. A* **98**, 041602.
- Chernikov, A., T. C. Berkelbach, H. M. Hill, A. Rigosi, Y. Li, B. Aslan, D. R. Reichman, M. S. Hybertsen, and T. F. Heinz (2014), “Exciton binding energy and nonhydrogenic rydberg series in monolayer ws_2 ,” *Phys. Rev. Lett.* **113**, 076802.
- Chernikov, A., A. M. van der Zande, H. M. Hill, A. F. Rigosi, A. Velauthapillai, J. Hone, and T. F. Heinz (2015), “Electrical tuning of exciton binding energies in monolayer ws_2 ,” *Phys. Rev. Lett.* **115**, 126802.
- Chernyshev, A. L., and P. W. Leung (1999), “Holes in the $t - J_z$ model: A diagrammatic study,” *Phys. Rev. B* **60**, 1592.
- Chervy, T., P. Knüppel, H. Abbaspour, M. Lupatini, S. Fält, W. Wegscheider, M. Kroner, and A. Imamoglu (2020), “Accelerating polaritons with external electric and magnetic fields,” *Phys. Rev. X* **10**, 011040.
- Chevy, F. (2006), “Universal phase diagram of a strongly interacting fermi gas with unbalanced spin populations,” *Phys. Rev. A* **74**, 063628.
- Chevy, F., and C. Mora (2010), “Ultra-cold polarized fermi gases,” *Rep. Prog. Phys.* **73** (11), 112401.
- Chikina, I., V. Shikin, and A. A. Varlamov (2007), “Effective mass of a charged carrier in a nonpolar liquid: Snowball effect in superfluid helium,” *Phys. Rev. B* **75**, 184518.
- Chikkatur, A. P., A. Görlitz, D. M. Stamper-Kurn, S. Inouye, S. Gupta, and W. Ketterle (2000), “Suppression and Enhancement of Impurity Scattering in a Bose-Einstein Condensate,” *Phys. Rev. Lett.* **85** (3), 483.
- Chin, C., R. Grimm, P. Julienne, and E. Tiesinga (2010), “Feshbach resonances in ultracold gases,” *Rev. Mod. Phys.* **82** (2), 1225.
- Chomaz, L., I. Ferrier-Barbut, F. Ferlaino, B. Laburthe-Tolra, B. L. Lev, and T. Pfau (2022), “Dipolar physics: a review of experiments with magnetic quantum gases,” *Reports on Progress in Physics* **86** (2), 026401.
- Chowdhury, S., and J. Perez-Ríos (2024), “Ion solvation in atomic baths: From snowballs to polarons,” *Natural Sciences* **4**, e20240006.
- Christensen, E. R., A. Camacho-Guardian, and G. M. Bruun (2021), “Charged polarons and molecules in a bose-einstein condensate,” *Phys. Rev. Lett.* **126**, 243001.

- Christensen, E. R., A. Camacho-Guardian, and G. M. Bruun (2022), “Mobile ion in a fermi sea,” *Phys. Rev. A* **105**, 023309.
- Christensen, R. S., J. Levinsen, and G. M. Bruun (2015), “Quasiparticle properties of a mobile impurity in a bose-einstein condensate,” *Phys. Rev. Lett.* **115**, 160401.
- Christianen, A., J. I. Cirac, and R. Schmidt (2022a), “Bose polaron and the efimov effect: A gaussian-state approach,” *Phys. Rev. A* **105**, 053302.
- Christianen, A., J. I. Cirac, and R. Schmidt (2022b), “Chemistry of a light impurity in a bose-einstein condensate,” *Phys. Rev. Lett.* **128**, 183401.
- Christianen, A., J. I. Cirac, and R. Schmidt (2024), “Phase diagram for strong-coupling Bose polarons,” *SciPost Phys.* **16**, 067.
- Ciorciaro, L., T. Smoleński, I. Morera, N. Kiper, S. Hiesland, M. Kroner, Y. Zhang, K. Watanabe, T. Taniguchi, E. Demler, and A. Imamoglu (2023), “Kinetic magnetism in triangular moiré materials,” *Nature* **623**, 509.
- Clogston, A. M. (1962), “Upper limit for the critical field in hard superconductors,” *Phys. Rev. Lett.* **9**, 266.
- Collin, A., P. Massignan, and C. J. Pethick (2007), “Energy-dependent effective interactions for dilute many-body systems,” *Phys. Rev. A* **75**, 013615.
- Colussi, V. E., F. Caleffi, C. Menotti, and A. Recati (2023), “Lattice polarons across the superfluid to mott insulator transition,” *Phys. Rev. Lett.* **130**, 173002.
- Comaron, P., N. Goldman, A. Imamoglu, and I. Amelio (2024), “Quantum impurities in finite-temperature bose gases: Detecting vortex proliferation across the bkt and bec transitions,” [arXiv:2412.08546](https://arxiv.org/abs/2412.08546).
- Combescot, M., and P. Nozières (1971), “Infrared catastrophe and excitons in the x-ray spectra of metals,” *J. Phys. France* **32** (11-12), 913.
- Combescot, R., and S. Giraud (2008), “Normal state of highly polarized fermi gases: Full many-body treatment,” *Physical Review Letters* **101** (5), 050404.
- Combescot, R., A. Recati, C. Lobo, and F. Chevy (2007), “Normal state of highly polarized fermi gases: Simple many-body approaches,” *Phys. Rev. Lett.* **98**, 180402.
- Cooper, N. R., J. Dalibard, and I. B. Spielman (2019), “Topological bands for ultracold atoms,” *Rev. Mod. Phys.* **91**, 015005.
- Côté, R., V. Kharchenko, and M. D. Lukin (2002), “Mesoscopic molecular ions in bose-einstein condensates,” *Phys. Rev. Lett.* **89**, 093001.
- Courtade, E., M. Semina, M. Manca, M. M. Glazov, C. Robert, F. Cadiz, G. Wang, T. Taniguchi, K. Watanabe, M. Pierre, W. Escoffier, E. L. Ivchenko, P. Renucci, X. Marie, T. Amand, and B. Urbaszek (2017), “Charged excitons in monolayer wse₂: Experiment and theory,” *Phys. Rev. B* **96**, 085302.
- Cotlet, O., F. Pientka, R. Schmidt, G. Zarand, E. Demler, and A. Imamoglu (2019), “Transport of neutral optical excitations using electric fields,” *Phys. Rev. X* **9**, 041019.
- Cucchiatti, F. M., and E. Timmermans (2006), “Strong-coupling polarons in dilute gas bose-einstein condensates,” *Phys. Rev. Lett.* **96**, 210401.
- Cui, H., Q. Hu, X. Zhao, L. Ma, F. Jin, Q. Zhang, K. Watanabe, T. Taniguchi, J. Shan, K. F. Mak, Y. Li, and Y. Xu (2024), “Interlayer fermi polarons of excited exciton states in quantizing magnetic fields,” *Nano Letters* **24** (23), 7077.
- Cui, X. (2020), “Fermi polaron revisited: Polaron-molecule transition and coexistence,” *Phys. Rev. A* **102**, 061301.
- Cui, X., and H. Zhai (2010), “Stability of a fully magnetized ferromagnetic state in repulsively interacting ultracold fermi gases,” *Phys. Rev. A* **81**, 041602.
- Dagotto, E. (1994), “Correlated electrons in high-temperature superconductors,” *Rev. Mod. Phys.* **66**, 763.
- Dagotto, E., R. Joynt, A. Moreo, S. Bacci, and E. Gagliano (1990), “Strongly correlated electronic systems with one hole: Dynamical properties,” *Phys. Rev. B* **41**, 9049.
- Daley, A. J., I. Bloch, C. Kokail, S. Flannigan, N. Pearson, M. Troyer, and P. Zoller (2022), “Practical quantum advantage in quantum simulation,” *Nature* **607** (7920), 667.
- Dalfovo, F., S. Giorgini, L. P. Pitaevskii, and S. Stringari (1999), “Theory of bose-einstein condensation in trapped gases,” *Rev. Mod. Phys.* **71**, 463.
- Damascelli, A., Z. Hussain, and Z.-X. Shen (2003), “Angle-resolved photoemission studies of the cuprate superconductors,” *Rev. Mod. Phys.* **75**, 473.
- Darkwah Oppong, N., L. Riegger, O. Bettermann, M. Höfer, J. Levinsen, M. M. Parish, I. Bloch, and S. Fölling (2019), “Observation of coherent multiorbital polarons in a two-dimensional fermi gas,” *Phys. Rev. Lett.* **122**, 193604.
- Degen, C. L., F. Reinhard, and P. Cappellaro (2017), “Quantum sensing,” *Rev. Mod. Phys.* **89**, 035002.
- DeSalvo, B. J., K. Patel, J. Johansen, and C. Chin (2017), “Observation of a degenerate fermi gas trapped by a bose-einstein condensate,” *Phys. Rev. Lett.* **119**, 233401.
- Devreese, J. T. (1996), “Polarons,” *Encycl. Appl. Phys.* **14** (cond-mat/0004497), 383.
- Diamantis, N. G., and E. Manousakis (2021), “Dynamics of string-like states of a hole in a quantum antiferromagnet: A diagrammatic monte carlo simulation,” *New Journal of Physics* **23** (12), 123005.
- Dieterle, T., M. Berngruber, C. Hölzl, R. Löw, K. Jachymski, T. Pfau, and F. Meinert (2020), “Inelastic collision dynamics of a single cold ion immersed in a bose-einstein condensate,” *Phys. Rev. A* **102**, 041301.
- Dieterle, T., M. Berngruber, C. Hölzl, R. Löw, K. Jachymski, T. Pfau, and F. Meinert (2021), “Transport of a single cold ion immersed in a bose-einstein condensate,” *Phys. Rev. Lett.* **126**, 033401.
- Ding, S., G. A. Domínguez-Castro, A. Julku, A. Camacho-Guardian, and G. M. Bruun (2023), “Polarons and bipolarons in a two-dimensional square lattice,” *SciPost Phys.* **14**, 143.
- Ding, S., M. Drewsen, J. J. Arlt, and G. M. Bruun (2022), “Mediated interaction between ions in quantum degenerate gases,” *Phys. Rev. Lett.* **129**, 153401.
- Dome, T., A. G. Volosniev, A. Ghazaryan, L. Safari, R. Schmidt, and M. Lemesko (2024), “Linear rotor in an ideal bose gas near the threshold for binding,” *Phys. Rev. B* **109**, 014102.
- Drescher, M., M. Salmhofer, and T. Enss (2019), “Real-space dynamics of attractive and repulsive polarons in bose-einstein condensates,” *Phys. Rev. A* **99**, 023601.
- Drescher, M., M. Salmhofer, and T. Enss (2020), “Theory of a resonantly interacting impurity in a bose-einstein condensate,” *Phys. Rev. Research* **2**, 032011.
- Drescher, M., M. Salmhofer, and T. Enss (2021), “Quench dynamics of the ideal bose polaron at zero and nonzero temperatures,” *Phys. Rev. A* **103**, 033317.
- Drescher, M., M. Salmhofer, and T. Enss (2023), “Medium-induced interaction between impurities in a bose-einstein condensate,” *Phys. Rev. A* **107**, 063301.
- Drescher, M., M. Salmhofer, and T. Enss (2024), “Bosonic

- functional determinant approach and its application to polaron spectra,” *Phys. Rev. A* **110**, 063303.
- Duda, M., X.-Y. Chen, A. Schindewolf, R. Bause, J. von Milczewski, R. Schmidt, I. Bloch, and X.-Y. Luo (2023), “Transition from a polaronic condensate to a degenerate fermi gas of heteronuclear molecules,” *Nature Physics* **19** (5), 720.
- Dupuis, N., L. Canet, A. Eichhorn, W. Metzner, J. Pawłowski, M. Tissier, and N. Wschebor (2021), “The nonperturbative functional renormalization group and its applications,” *Physics Reports* **910**, 1.
- Dzsoţjan, D., R. Schmidt, and M. Fleischhauer (2020), “Dynamical variational approach to bose polarons at finite temperatures,” *Phys. Rev. Lett.* **124**, 223401.
- Edri, H., B. Raz, N. Matzliah, N. Davidson, and R. Ozeri (2020), “Observation of spin-spin fermion-mediated interactions between ultracold bosons,” *Phys. Rev. Lett.* **124**, 163401.
- Edwards, J. P., U. Gerber, C. Schubert, M. A. Trejo, and A. Weber (2017), “The Yukawa potential: ground state energy and critical screening,” *Progress of Theoretical and Experimental Physics* **2017** (8), 083A01.
- Efimkin, D. K., E. K. Laird, J. Levinsen, M. M. Parish, and A. H. MacDonald (2021), “Electron-exciton interactions in the exciton-polaron problem,” *Phys. Rev. B* **103**, 075417.
- Efimkin, D. K., and A. H. MacDonald (2017), “Many-body theory of trion absorption features in two-dimensional semiconductors,” *Phys. Rev. B* **95**, 035417.
- Efimkin, D. K., and A. H. MacDonald (2018), “Exciton-polarons in doped semiconductors in a strong magnetic field,” *Phys. Rev. B* **97**, 235432.
- Efimov, V. (1970), “Energy levels arising from resonant two-body forces in a three-body system,” *Physics Letters B* **33** (8), 563 .
- Efimov, V. (1973), “Energy levels of three resonantly interacting particles,” *Nucl. Phys. A* **210** (1), 157.
- Emmanuele, R. P. A., M. Sich, O. Kyriienko, V. Shahnazaryan, F. Withers, A. Catanzaro, P. M. Walker, F. A. Benimetskiy, M. S. Skolnick, A. I. Tartakovskii, I. A. Shelykh, and D. N. Krizhanovskii (2020), “Highly nonlinear trion-polaritons in a monolayer semiconductor,” *Nature Communications* **11** (1), 3589.
- Engelbrecht, J. R., and M. Randeria (1992), “Low-density repulsive fermi gas in two dimensions: Bound-pair excitations and fermi-liquid behavior,” *Phys. Rev. B* **45**, 12419.
- Enss, T., R. Haussmann, and W. Zwerger (2011), “Viscosity and scale invariance in the unitary fermi gas,” *Annals of Physics* **326** (3), 770.
- Enss, T., B. Tran, M. Rautenberg, M. Gerken, E. Lippi, M. Drescher, B. Zhu, M. Weidemüller, and M. Salmhofer (2020), “Scattering of two heavy fermi polarons: Resonances and quasibound states,” *Phys. Rev. A* **102**, 063321.
- Etrych, J., G. Martirosyan, A. Cao, C. J. Ho, Z. Hadzibabic, and C. Eigen (2024), “Universal quantum dynamics of Bose polarons,” [arXiv:2402.14816](https://arxiv.org/abs/2402.14816) [10.48550/arXiv.2402.14816](https://arxiv.org/abs/2402.14816).
- Ewald, N. V., T. Feldker, H. Hirzler, H. A. Fürst, and R. Gerritsma (2019), “Observation of interactions between trapped ions and ultracold rydberg atoms,” *Phys. Rev. Lett.* **122**, 253401.
- Feldker, T., H. Fürst, H. Hirzler, N. V. Ewald, M. Mazzanti, D. Wiater, M. Tomza, and R. Gerritsma (2020), “Buffer gas cooling of a trapped ion to the quantum regime,” *Nature Physics* **16** (4), 413.
- Ferlaino, F., S. Knoop, M. Berninger, W. Harm, J. P. D’Incao, H.-C. Nägerl, and R. Grimm (2009), “Evidence for universal four-body states tied to an efimov trimer,” *Phys. Rev. Lett.* **102**, 140401.
- Ferrier-Barbut, I., M. Delehaye, S. Laurent, A. T. Grier, M. Pierce, B. S. Rem, F. Chevy, and C. Salomon (2014), “A mixture of bose and fermi superfluids,” *Science* **345** (6200), 1035.
- Fetter, A. L., and J. D. Walecka (1971), *Quantum Theory of Many-Particle Systems* (McGraw-Hill, New York).
- Fey, C., P. Schmelcher, A. Imamoglu, and R. Schmidt (2020), “Theory of exciton-electron scattering in atomically thin semiconductors,” *Phys. Rev. B* **101**, 195417.
- Field, B., J. Levinsen, and M. M. Parish (2020), “Fate of the bose polaron at finite temperature,” *Phys. Rev. A* **101**, 013623.
- Forbes, M. M., A. Gezerlis, K. Hebel, T. Lesinski, and A. Schwenk (2014), “Neutron polaron as a constraint on nuclear density functionals,” *Phys. Rev. C* **89**, 041301.
- Fritsche, I., C. Baroni, E. Dobler, E. Kirilov, B. Huang, R. Grimm, G. M. Bruun, and P. Massignan (2021), “Stability and breakdown of fermi polarons in a strongly interacting fermi-bose mixture,” *Phys. Rev. A* **103**, 053314.
- Fujii, K., M. Hongo, and T. Enss (2022), “Universal van der waals force between heavy polarons in superfluids,” *Phys. Rev. Lett.* **129**, 233401.
- Fukuhara, T., A. Kantian, M. Endres, M. Cheneau, P. Schauß, S. Hild, D. Bellem, U. Schollwöck, T. Giamarchi, C. Gross, I. Bloch, and S. Kuhr (2013a), “Quantum dynamics of a mobile spin impurity,” *Nature Physics* **9** (4), 235.
- Fukuhara, T., P. Schauß, M. Endres, S. Hild, M. Cheneau, I. Bloch, and C. Gross (2013b), “Microscopic observation of magnon bound states and their dynamics,” *Nature* **502** (7469), 76.
- Fulde, P., and R. A. Ferrell (1964), “Superconductivity in a strong spin-exchange field,” *Phys. Rev.* **135**, A550.
- Gievers, M., M. Wagner, and R. Schmidt (2024), “Probing polaron clouds by rydberg atom spectroscopy,” *Phys. Rev. Lett.* **132**, 053401.
- Giorgini, S., L. P. Pitaevskii, and S. Stringari (2008), “Theory of ultracold atomic fermi gases,” *Rev. Mod. Phys.* **80**, 1215.
- Girardeau, M. (1961), “Motion of an impurity particle in a boson superfluid,” *The Physics of Fluids* **4** (3), 279.
- Giraud, S., and R. Combescot (2012), “Interaction between polarons and analogous effects in polarized fermi gases,” *Phys. Rev. A* **85**, 013605.
- Giuliani, G., and G. Vignale (2005), *Quantum theory of the electron liquid* (Cambridge University Press, Cambridge).
- Glazov, M. M. (2020), “Optical properties of charged excitons in two-dimensional semiconductors,” *J. Chem. Phys.* **153** (3), 034703.
- Goold, J., T. Fogarty, N. Lo Gullo, M. Paternostro, and T. Busch (2011), “Orthogonality catastrophe as a consequence of qubit embedding in an ultracold Fermi gas,” *Phys. Rev. A* **84** (6), 063632.
- Goryca, M., J. Li, A. V. Stier, T. Taniguchi, K. Watanabe, E. Courtade, S. Shree, C. Robert, B. Urbaszek, X. Marie, and S. A. Crooker (2019), “Revealing exciton masses and dielectric properties of monolayer semiconductors with high magnetic fields,” *Nature Communications* **10** (1), 4172.
- Goulko, O., A. S. Mishchenko, N. Prokof’ev, and B. Svistunov (2016), “Dark continuum in the spectral function of the resonant fermi polaron,” *Phys. Rev. A* **94**, 051605.
- Graß, T., B. Juliá-Díaz, N. Baldelli, U. Bhattacharya, and M. Lewenstein (2020), “Fractional angular momentum and

- anyon statistics of impurities in Laughlin liquids,” *Phys. Rev. Lett.* **125**, 136801.
- Greene, C. H., P. Giannakeas, and J. Pérez-Ríos (2017), “Universal few-body physics and cluster formation,” *Rev. Mod. Phys.* **89**, 035006.
- Greiner, M., O. Mandel, T. Esslinger, T. W. Hansch, and I. Bloch (2002), “Quantum phase transition from a superfluid to a Mott insulator in a gas of ultracold atoms,” *Nature* **415** (6867), 39.
- Gross, C., and I. Bloch (2017), “Quantum simulations with ultracold atoms in optical lattices,” *Science* **357** (6355), 995.
- Gross, E. (1962), “Motion of foreign bodies in boson systems,” *Annals of Physics* **19** (2), 234.
- Grusdt, F., A. Bohrdt, and E. Demler (2019), “Microscopic spinon-charge theory of magnetic polarons in the t - j model,” *Phys. Rev. B* **99**, 224422.
- Grusdt, F., and E. Demler (2016), “New theoretical approaches to Bose polarons,” in *Quantum Matter at Ultralow Temperatures* (IOS Press) pp. 325–411.
- Grusdt, F., E. Demler, and A. Bohrdt (2023), “Pairing of holes by confining strings in antiferromagnets,” *SciPost Phys.* **14**, 090.
- Grusdt, F., and M. Fleischhauer (2016), “Tunable polarons of slow-light polaritons in a two-dimensional Bose-Einstein condensate,” *Phys. Rev. Lett.* **116**, 053602.
- Grusdt, F., M. Kánasz-Nagy, A. Bohrdt, C. S. Chiu, G. Ji, M. Greiner, D. Greif, and E. Demler (2018), “Parton theory of magnetic polarons: Mesonic resonances and signatures in dynamics,” *Phys. Rev. X* **8**, 011046.
- Grusdt, F., N. Mostaan, E. Demler, and L. A. Peña Ardila (2024), “Impurities and polarons in bosonic quantum gases: a review on recent progress,” [arXiv:2410.09413](https://arxiv.org/abs/2410.09413).
- Grusdt, F., A. Shashi, D. Abanin, and E. Demler (2014), “Bloch oscillations of bosonic lattice polarons,” *Phys. Rev. A* **90**, 063610.
- Grusdt, F., N. Y. Yao, D. Abanin, M. Fleischhauer, and E. Demler (2016), “Interferometric measurements of many-body topological invariants using mobile impurities,” *Nature Communications* **7** (1), 11994.
- Gu, J., L. Ma, S. Liu, K. Watanabe, T. Taniguchi, J. C. Hone, J. Shan, and K. F. Mak (2022), “Dipolar excitonic insulator in a moiré lattice,” *Nature Physics* **18** (4), 395.
- Gubbels, K. B., and H. T. C. Stoof (2008), “Renormalization group theory for the imbalanced Fermi gas,” *Physical Review Letters* **100** (14), 140407.
- Guebli, N., and A. Boudjemâa (2019), “Effects of quantum fluctuations on the dynamics of dipolar Bose polarons,” *J. Phys. B: At. Mol. Opt. Phys.* **52** (18), 185303.
- Guenther, N.-E., P. Massignan, M. Lewenstein, and G. M. Bruun (2018), “Bose polarons at finite temperature and strong coupling,” *Phys. Rev. Lett.* **120**, 050405.
- Guenther, N.-E., R. Schmidt, G. M. Bruun, V. Gurarie, and P. Massignan (2021), “Mobile impurity in a Bose-Einstein condensate and the orthogonality catastrophe,” *Phys. Rev. A* **103**, 013317.
- Guijarro, G., G. E. Astrakharchik, and J. Boronat (2021), “Quantum halo states in two-dimensional dipolar clusters,” *Scientific Reports* **11** (1), 19437.
- Guijarro, G., G. E. Astrakharchik, J. Boronat, B. Bazak, and D. S. Petrov (2020), “Few-body bound states of two-dimensional bosons,” *Phys. Rev. A* **101**, 041602.
- Guo, Y., and H. Tajima (2024), “Medium-induced bosonic clusters in a Bose-Fermi mixture: Toward simulating cluster formations in neutron-rich matter,” *Phys. Rev. A* **109**, 013319.
- Hammer, H. W., and L. Platter (2007), “Universal properties of the four-body system with large scattering length,” *The European Physical Journal A* **32** (1), 113.
- Harris, G. M. (1962), “Attractive two-body interactions in partially ionized plasmas,” *Phys. Rev.* **125**, 1131.
- Hartke, T., B. Oreg, C. Turnbaugh, N. Jia, and M. Zwierlein (2023), “Direct observation of nonlocal fermion pairing in an attractive Fermi-Hubbard gas,” *Science* **381** (6653), 82.
- Hasan, M. Z., and C. L. Kane (2010), “Colloquium: Topological insulators,” *Rev. Mod. Phys.* **82**, 3045.
- Muñoz de las Heras, A., E. Macaluso, and I. Carusotto (2020), “Anyonic molecules in atomic fractional quantum Hall liquids: A quantitative probe of fractional charge and anyonic statistics,” *Phys. Rev. X* **10**, 041058.
- Hirthe, S., T. Chalopin, D. Bourgund, P. Bojović, A. Bohrdt, E. Demler, F. Grusdt, I. Bloch, and T. A. Hilker (2023), “Magnetically mediated hole pairing in fermionic ladders of ultracold atoms,” *Nature* **613** (7944), 463.
- Hohmann, M., F. Kindermann, B. Gänger, T. Lausch, D. Mayer, F. Schmidt, and A. Widera (2015), “Neutral impurities in a Bose-Einstein condensate for simulation of the Fröhlich-polaron,” *EPJ Quantum Technology* **2** (1), 1.
- Hohmann, M., F. Kindermann, T. Lausch, D. Mayer, F. Schmidt, and A. Widera (2016), “Single-atom thermometer for ultracold gases,” *Phys. Rev. A* **93**, 043607.
- Hopfield, J. J. (1958), “Theory of the contribution of excitons to the complex dielectric constant of crystals,” *Phys. Rev.* **112**, 1555.
- Hu, F.-Q., and J.-K. Xue (2014), “Breathing dynamics of a trapped impurity in a dipolar Bose gas,” *Modern Physics Letters B* **28** (22), 1450185.
- Hu, H., and X.-J. Liu (2023), “Fermi spin polaron and dissipative Fermi-polaron Rabi dynamics,” *Phys. Rev. A* **108**, 063312.
- Hu, H., J. Wang, J. Zhou, and X.-J. Liu (2022), “Crossover polarons in a strongly interacting Fermi superfluid,” *Phys. Rev. A* **105**, 023317.
- Hu, M.-G., M. J. Van de Graaff, D. Kedar, J. P. Corson, E. A. Cornell, and D. S. Jin (2016), “Bose polarons in the strongly interacting regime,” *Phys. Rev. Lett.* **117**, 055301.
- Huang, D., K. Sampson, Y. Ni, Z. Liu, D. Liang, K. Watanabe, T. Taniguchi, H. Li, E. Martin, J. Levinsen, M. M. Parish, E. Tutuc, D. K. Efimkin, and X. Li (2023a), “Quantum dynamics of attractive and repulsive polarons in a doped MoSe_2 monolayer,” *Phys. Rev. X* **13**, 011029.
- Huang, K., and H.-F. Meng (1992), “Hard-sphere Bose gas in random external potentials,” *Phys. Rev. Lett.* **69**, 644.
- Huang, T.-S., Y.-Z. Chou, C. L. Baldwin, F. Wu, and M. Hafezi (2023b), “Mott-moiré excitons,” *Phys. Rev. B* **107**, 195151.
- Ichmoukhamedov, T., and J. Tempere (2019), “Feynman path-integral treatment of the Bose polaron beyond the Fröhlich model,” *Phys. Rev. A* **100**, 043605.
- Ichmoukhamedov, T., and J. Tempere (2022), “General memory kernels and further corrections to the variational path integral approach for the Bogoliubov-Fröhlich Hamiltonian,” *Phys. Rev. B* **105**, 104304.
- Imamoglu, A., O. Cotlet, and R. Schmidt (2021), “Exciton-polarons in two-dimensional semiconductors and the Tavis-Cummings model,” *C. R. Phys.* **22** (S4), 89.
- Isaule, F. (2024), “Functional renormalisation group approach to the finite-temperature Bose polaron,” *Europhysics Let-*

- ters .
- Isaule, F., and I. Morera (2022), “Weakly-Interacting Bose-Bose Mixtures from the Functional Renormalisation Group,” *Condens. Matter* **7** (1), 9.
- Isaule, F., I. Morera, P. Massignan, and B. Juliá-Díaz (2021), “Renormalization-group study of bose polarons,” *Phys. Rev. A* **104**, 023317.
- Jager, J., and R. Barnett (2022), “The effect of boson-boson interaction on the bipolaron formation,” *New J. Phys.* **24** (10), 103032.
- Ji, G., M. Xu, L. H. Kendrick, C. S. Chiu, J. C. Brüggengjürgen, D. Greif, A. Bohrdt, F. Grusdt, E. Demler, M. Lebrat, and M. Greiner (2021), “Coupling a mobile hole to an antiferromagnetic spin background: Transient dynamics of a magnetic polaron,” *Phys. Rev. X* **11**, 021022.
- Jiang, S., D. J. Scalapino, and S. R. White (2021), “Ground-state phase diagram of the t-t'-J model,” *Proc. Natl. Acad. Sci. U.S.A.* **118** (44), e2109978118.
- Jin, C., Z. Tao, T. Li, Y. Xu, Y. Tang, J. Zhu, S. Liu, K. Watanabe, T. Taniguchi, J. C. Hone, L. Fu, J. Shan, and K. F. Mak (2021), “Stripe phases in wse2/ws2 moirésuperlattices,” *Nature Materials* **20** (7), 940.
- Jin, H.-K., W. Kadow, M. Knap, and J. Knolle (2024), “Kinetic ferromagnetism and topological magnons of the hole-doped kitaev spin liquid,” *npj Quantum Materials* **9** (1), 65.
- Jørgensen, N. B., L. Wacker, K. T. Skalmstang, M. M. Parish, J. Levinsen, R. S. Christensen, G. M. Bruun, and J. J. Arlt (2016), “Observation of attractive and repulsive polarons in a bose-einstein condensate,” *Phys. Rev. Lett.* **117**, 055302.
- Julku, A., M. A. Bastarrachea-Magnani, A. Camacho-Guardian, and G. M. Bruun (2021), “Nonlinear optical response of resonantly driven polaron-polaritons,” *Phys. Rev. B* **104**, L161301.
- Julku, A., S. Ding, and G. M. Bruun (2024), “Exciton interacting with a moiré lattice: Polarons, strings, and optical probing of spin correlations,” *Phys. Rev. Res.* **6**, 033119.
- Julku, A., J. J. Kinnunen, A. Camacho-Guardian, and G. M. Bruun (2022), “Light-induced topological superconductivity in transition metal dichalcogenide monolayers,” *Phys. Rev. B* **106**, 134510.
- Kadow, W., H.-K. Jin, J. Knolle, and M. Knap (2024), “Single-hole spectra of kitaev spin liquids: from dynamical nagaoka ferromagnetism to spin-hole fractionalization,” *npj Quantum Materials* **9** (1), 32.
- Kadow, W., L. Vanderstraeten, and M. Knap (2022), “Hole spectral function of a chiral spin liquid in the triangular lattice hubbard model,” *Phys. Rev. B* **106**, 094417.
- Kain, B., and H. Y. Ling (2014), “Polarons in a dipolar condensate,” *Phys. Rev. A* **89**, 023612.
- Kamikado, K., T. Kanazawa, and S. Uchino (2017), “Mobile impurity in a fermi sea from the functional renormalization group analytically continued to real time,” *Phys. Rev. A* **95**, 013612.
- Kane, C. L., P. A. Lee, and N. Read (1989), “Motion of a single hole in a quantum antiferromagnet,” *Phys. Rev. B* **39**, 6880.
- Kartavtsev, O. I., and A. V. Malykh (2007), “Low-energy three-body dynamics in binary quantum gases,” *J Phys. B* **40** (7), 1429.
- Kasuya, T. (1956), “A Theory of Metallic Ferro- and Antiferromagnetism on Zener’s Model,” *Progress of Theoretical Physics* **16** (1), 45.
- Keldysh, L. V. (1979), “Coulomb interaction in thin semiconductor and semimetal films,” *Soviet Journal of Experimental and Theoretical Physics Letters* **29**, 658.
- Ketterle, W., and M. Zwierlein (2007), “Making, probing and understanding ultracold fermi gases,” in *Ultra-cold Fermi Gases*, Proceedings of the International School of Physics “Enrico Fermi”, edited by M. Inguscio, W. Ketterle, and C. Salomon (IOS Press) pp. 95–287.
- Khalatnikov, I. (1989), *An Introduction To The Theory Of Superfluidity* (Avalon Publishing).
- Kim, C., P. J. White, Z.-X. Shen, T. Tohyama, Y. Shibata, S. Maekawa, B. O. Wells, Y. J. Kim, R. J. Birgeneau, and M. A. Kastner (1998), “Systematics of the photoemission spectral function of cuprates: Insulators and hole- and electron-doped superconductors,” *Phys. Rev. Lett.* **80**, 4245.
- Kleinbach, K. S., F. Engel, T. Dieterle, R. Löw, T. Pfau, and F. Meinert (2018), “Ionic impurity in a bose-einstein condensate at submicrokelvin temperatures,” *Phys. Rev. Lett.* **120**, 193401.
- Knap, M., D. A. Abanin, and E. Demler (2013), “Dissipative dynamics of a driven quantum spin coupled to a bath of ultracold fermions,” *Phys. Rev. Lett.* **111**, 265302.
- Knap, M., A. Shashi, Y. Nishida, A. Imambekov, D. A. Abanin, and E. Demler (2012), “Time-dependent impurity in ultracold fermions: Orthogonality catastrophe and beyond,” *Phys. Rev. X* **2** (4), 041020.
- Koepsell, J., D. Bourgund, P. Sompet, S. Hirthe, A. Bohrdt, Y. Wang, F. Grusdt, E. Demler, G. Salomon, C. Gross, and I. Bloch (2021), “Microscopic evolution of doped Mott insulators from polaronic metal to Fermi liquid,” *Science* **374** (6563), 82.
- Koepsell, J., J. Vijayan, P. Sompet, F. Grusdt, T. A. Hilker, E. Demler, G. Salomon, I. Bloch, and C. Gross (2019), “Imaging magnetic polarons in the doped fermi-hubbard model,” *Nature* **572** (7769), 358.
- Kohstall, C., M. Zaccanti, M. Jag, A. Trenkwalder, P. Massignan, G. M. Bruun, F. Schreck, and R. Grimm (2012), “Metastability and coherence of repulsive polarons in a strongly interacting Fermi mixture,” *Nature* **485** (7400), 615.
- Kondo, J. (1964), “Resistance minimum in dilute magnetic alloys,” *Progress of theoretical physics* **32** (1), 37.
- Koschorreck, M., D. Pertot, E. Vogt, B. Fröhlich, M. Feld, and M. Köhl (2012), “Attractive and repulsive Fermi polarons in two dimensions,” *Nature* **485** (7400), 619.
- Kosterlitz, J. M., and D. J. Thouless (1973), “Ordering, metastability and phase transitions in two-dimensional systems,” *Journal of Physics C: Solid State Physics* **6** (7), 1181.
- van de Kraats, J., K. K. Nielsen, and G. M. Bruun (2022), “Holes and magnetic polarons in a triangular lattice antiferromagnet,” *Phys. Rev. B* **106**, 235143.
- Kraemer, T., M. Mark, P. Waldburger, J. G. Danzl, C. Chin, B. Engeser, A. D. Lange, K. Pilch, A. Jaakkola, H. C. Nägerl, and R. Grimm (2006), “Evidence for efimov quantum states in an ultracold gas of caesium atoms,” *Nature* **440** (7082), 315.
- Krych, M., and Z. Idziaszek (2015), “Description of ion motion in a paul trap immersed in a cold atomic gas,” *Phys. Rev. A* **91**, 023430.
- Ku, M. J. H., A. T. Sommer, L. W. Cheuk, and M. W. Zwierlein (2012), “Revealing the superfluid lambda transition in the universal thermodynamics of a unitary Fermi gas,” *Science* **335** (6068), 563.
- Kuhlenkamp, C., M. Knap, M. Wagner, R. Schmidt, and

- A. Imamoglu (2022), “Tunable feshbach resonances and their spectral signatures in bilayer semiconductors,” *Phys. Rev. Lett.* **129**, 037401.
- Kumar, S. S., B. C. Mulkerin, M. M. Parish, and J. Levinsen (2023), “Trion resonance in polariton-electron scattering,” *Phys. Rev. B* **108**, 125416.
- Kumar, S. S., B. C. Mulkerin, A. Tiene, F. M. Marchetti, M. M. Parish, and J. Levinsen (2024), “Trions in monolayer transition metal dichalcogenides,” [arXiv:2411.09376](https://arxiv.org/abs/2411.09376).
- Lampo, A., C. Charalambous, M. A. García-March, and M. Lewenstein (2018), “Non-markovian polaron dynamics in a trapped bose-einstein condensate,” *Phys. Rev. A* **98**, 063630.
- Lampo, A., S. H. Lim, M. Á. García-March, and M. Lewenstein (2017), “Bose polaron as an instance of quantum Brownian motion,” *Quantum* **1**, 30.
- Landau, L. (1957a), “Oscillations in a fermi liquid,” *J. Exp. Theor. Phys.* **5** (1), 101.
- Landau, L. (1957b), “The theory of a fermi liquid,” *J. Exp. Theor. Phys.* **3** (6), 920.
- Landau, L., and S. Pekar (1948), “Effective mass of the polaron,” *J. Exp. Theor. Phys.* **423** (5), 71.
- Landau, L. D., and E. M. Lifshitz (1977), *Quantum Mechanics : Non-Relativistic Theory* (Elsevier Science, Burlington).
- Lange, H., L. Homeier, E. Demler, U. Schollwöck, F. Grusdt, and A. Bohrdt (2024), “Feshbach resonance in a strongly repulsive ladder of mixed dimensionality: A possible scenario for bilayer nickelate superconductors,” *Phys. Rev. B* **109**, 045127.
- Larkin, A., and Y. Ovchinnikov (1964), “Inhomogeneous state of superconductors,” *Zh. Eksp. Teor. Fiz.* **47**, 1136.
- Lausch, T., A. Widera, and M. Fleischhauer (2018), “Prethermalization in the cooling dynamics of an impurity in a bose-einstein condensate,” *Phys. Rev. A* **97**, 023621.
- Lebrat, M., M. Xu, L. H. Kendrick, A. Kale, Y. Gang, P. Seetharaman, I. Morera, E. Khatami, E. Demler, and M. Greiner (2024), “Observation of nagaoka polarons in a fermi-hubbard quantum simulator,” *Nature* **629** (8011), 317.
- Lee, P. A., N. Nagaosa, and X.-G. Wen (2006), “Doping a mott insulator: Physics of high-temperature superconductivity,” *Rev. Mod. Phys.* **78**, 17.
- Lee, T. D., F. E. Low, and D. Pines (1953), “The motion of slow electrons in a polar crystal,” *Phys. Rev.* **90**, 297.
- Lemeshko, M., and R. Schmidt (2017), “Molecular impurities interacting with a many-particle environment: From ultracold gases to helium nanodroplets,” in *Cold Chemistry: Molecular Scattering and Reactivity Near Absolute Zero* (The Royal Society of Chemistry).
- Levinsen, J., O. Bleu, and M. M. Parish (2024), “Medium-enhanced polaron repulsion in a dilute bose mixture,” [arXiv:2409.03406](https://arxiv.org/abs/2409.03406).
- Levinsen, J., F. M. Marchetti, J. Keeling, and M. M. Parish (2019), “Spectroscopic signatures of quantum many-body correlations in polariton microcavities,” *Phys. Rev. Lett.* **123**, 266401.
- Levinsen, J., and M. M. Parish (2013), “Bound states in a quasi-two-dimensional fermi gas,” *Phys. Rev. Lett.* **110**, 055304.
- Levinsen, J., and M. M. Parish (2015), “Strongly interacting two-dimensional fermi gases,” in *Annual Review of Cold Atoms and Molecules*, Vol. 3, Chap. 1 (World Scientific, Singapore) pp. 1–75.
- Levinsen, J., M. M. Parish, and G. M. Bruun (2015), “Impurity in a bose-einstein condensate and the efimov effect,” *Phys. Rev. Lett.* **115**, 125302.
- Levinsen, J., M. M. Parish, R. S. Christensen, J. J. Arlt, and G. M. Bruun (2017), “Finite-temperature behavior of the bose polaron,” *Phys. Rev. A* **96**, 063622.
- Levinsen, J., L. A. Peña Ardila, S. M. Yoshida, and M. M. Parish (2021), “Quantum behavior of a heavy impurity strongly coupled to a bose gas,” *Phys. Rev. Lett.* **127**, 033401.
- Levinsen, J., T. G. Tiecke, J. T. M. Walraven, and D. S. Petrov (2009), “Atom-dimer scattering and long-lived trimers in fermionic mixtures,” *Phys. Rev. Lett.* **103**, 153202.
- Li, R., J. von Milczewski, A. Imamoglu, R. Oldziejewski, and R. Schmidt (2023), “Impurity-induced pairing in two-dimensional fermi gases,” *Phys. Rev. B* **107**, 155135.
- Li, W., and S. Das Sarma (2014), “Variational study of polarons in bose-einstein condensates,” *Phys. Rev. A* **90**, 013618.
- Li, X., E. Yakaboylu, G. Bighin, R. Schmidt, M. Lemeshko, and A. Deuchert (2020), “Intermolecular forces and correlations mediated by a phonon bath,” *The Journal of Chemical Physics* **152** (16), 164302.
- Liu, R., C. Peng, and X. Cui (2022), “Emergence of crystalline few-body correlations in mass-imbalanced Fermi polarons,” *Cell Rep. Phys. Sci.* **3** (8), 10.1016/j.xcrp.2022.100993.
- Liu, R., T. Shi, M. Zaccanti, and X. Cui (2024), “Universal clusters in quasi-two-dimensional ultracold fermi mixtures,” *Phys. Rev. Res.* **6**, L042004.
- Liu, W. E., J. Levinsen, and M. M. Parish (2019), “Variational approach for impurity dynamics at finite temperature,” *Phys. Rev. Lett.* **122**, 205301.
- Liu, W. E., Z.-Y. Shi, J. Levinsen, and M. M. Parish (2020a), “Radio-frequency response and contact of impurities in a quantum gas,” *Phys. Rev. Lett.* **125**, 065301.
- Liu, W. E., Z.-Y. Shi, M. M. Parish, and J. Levinsen (2020b), “Theory of radio-frequency spectroscopy of impurities in quantum gases,” *Phys. Rev. A* **102**, 023304.
- Liu, X.-J., and H. Hu (2010), “Virial expansion for a strongly correlated fermi gas with imbalanced spin populations,” *Phys. Rev. A* **82**, 043626.
- Liu, Z., and E. Manousakis (1992), “Dynamical properties of a hole in a heisenberg antiferromagnet,” *Phys. Rev. B* **45**, 2425.
- Lobo, C., A. Recati, S. Giorgini, and S. Stringari (2006), “Normal state of a polarized Fermi gas at unitarity,” *Physical Review Letters* **97** (20), 200403.
- Lous, R. S., and R. Gerritsma (2022), “Chapter two - ultracold ion-atom experiments: cooling, chemistry, and quantum effects,” in *Advances in Atomic, Molecular, and Optical Physics*, Advances In Atomic, Molecular, and Optical Physics, Vol. 71, edited by L. F. DiMauro, H. Perrin, and S. F. Yelin (Academic Press) pp. 65–133.
- Ludwig, D., S. Floerchinger, S. Moroz, and C. Wetterich (2011), “Quantum phase transition in bose-fermi mixtures,” *Phys. Rev. A* **84**, 033629.
- Mahan, G. D. (2000), *Many Particle Physics*, 3rd ed. (Kluwer, New York).
- Mahani, M. R., A. Mirsakiyeva, and A. Delin (2017), “Breakdown of polarons in conducting polymers at device field strengths,” *The Journal of Physical Chemistry C* **121** (19), 10317.
- Mak, K. F., K. He, C. Lee, G. H. Lee, J. Hone, T. F. Heinz, and J. Shan (2013), “Tightly bound trions in monolayer

- mos₂,” *Nature Materials* **12** (3), 207.
- Mak, K. F., K. He, J. Shan, and T. F. Heinz (2012), “Control of valley polarization in monolayer mos₂ by optical helicity,” *Nature Nanotechnology* **7** (8), 494.
- Mak, K. F., and J. Shan (2022), “Semiconductor moiré materials,” *Nature Nanotechnology* **17** (7), 686.
- Makotyn, P., C. E. Klauss, D. L. Goldberger, E. A. Cornell, and D. S. Jin (2014), “Universal dynamics of a degenerate unitary Bose gas,” *Nature Physics* **10** (2), 116.
- Manousakis, E. (1991), “The spin-1/2 Heisenberg antiferromagnet on a square lattice and its application to the cuprous oxides,” *Rev. Mod. Phys.* **63**, 1.
- Marti, G. E., A. MacRae, R. Olf, S. Lourette, F. Fang, and D. M. Stamper-Kurn (2014), “Coherent magnon optics in a ferromagnetic spinor bose-einstein condensate,” *Phys. Rev. Lett.* **113**, 155302.
- Martinez, G., and P. Horsch (1991), “Spin polarons in the t-j model,” *Phys. Rev. B* **44**, 317.
- Massignan, P., and G. M. Bruun (2011), “Repulsive polarons and itinerant ferromagnetism in strongly polarized fermi gases,” *Eur. Phys. J. D* **65** (1-2), 83.
- Massignan, P., C. J. Pethick, and H. Smith (2005), “Static properties of positive ions in atomic bose-einstein condensates,” *Phys. Rev. A* **71**, 023606.
- Massignan, P., N. Yegorov, and V. Gurarie (2021), “Universal aspects of a strongly interacting impurity in a dilute bose condensate,” *Phys. Rev. Lett.* **126**, 123403.
- Massignan, P., M. Zaccanti, and G. M. Bruun (2014), “Polarons, dressed molecules and itinerant ferromagnetism in ultracold fermi gases,” *Reports on Progress in Physics* **77** (3), 034401.
- Mathy, C. J. M., M. M. Parish, and D. A. Huse (2011), “Trimers, molecules, and polarons in mass-imbalanced atomic fermi gases,” *Phys. Rev. Lett.* **106**, 166404.
- Matveeva, N., and S. Giorgini (2013), “Impurity problem in a bilayer system of dipoles,” *Phys. Rev. Lett.* **111**, 220405.
- Mazza, G., and A. Amaricci (2022), “Strongly correlated exciton-polarons in twisted homobilayer heterostructures,” *Phys. Rev. B* **106**, L241104.
- Mestrom, P. M. A., J. Wang, C. H. Greene, and J. P. D’Incao (2017), “Efimov–van der waals universality for ultracold atoms with positive scattering lengths,” *Phys. Rev. A* **95**, 032707.
- Mhenni, A. B., W. Kadow, M. J. Metelski, A. O. Paulus, A. Dijkstra, K. Watanabe, T. Taniguchi, S. A. Tongay, M. Barbone, J. J. Finley, *et al.* (2024), “Gate-tunable bose-fermi mixture in a strongly correlated moiré bilayer electron system,” [arXiv:2410.07308](https://arxiv.org/abs/2410.07308).
- Miao, S., T. Wang, X. Huang, D. Chen, Z. Lian, C. Wang, M. Blei, T. Taniguchi, K. Watanabe, S. Tongay, Z. Wang, D. Xiao, Y.-T. Cui, and S.-F. Shi (2021), “Strong interaction between interlayer excitons and correlated electrons in wse₂/ws₂ moiré superlattice,” *Nature Communications* **12** (1), 3608.
- Midya, B., M. Tomza, R. Schmidt, and M. Lemeshko (2016), “Rotation of cold molecular ions inside a bose-einstein condensate,” *Phys. Rev. A* **94**, 041601.
- von Milczewski, J., X. Chen, A. Imamoglu, and R. Schmidt (2024), “Superconductivity induced by strong electron-exciton coupling in doped atomically thin semiconductor heterostructures,” *Phys. Rev. Lett.* **133**, 226903.
- von Milczewski, J., F. Rose, and R. Schmidt (2022), “Functional-renormalization-group approach to strongly coupled bose-fermi mixtures in two dimensions,” *Phys. Rev. A* **105**, 013317.
- von Milczewski, J., and R. Schmidt (2024), “Momentum-dependent quasiparticle properties of the fermi polaron from the functional renormalization group,” *Phys. Rev. A* **110**, 033309.
- Mishchenko, A. S., N. Nagaosa, and N. Prokof’ev (2014), “Diagrammatic Monte Carlo Method for Many-Polaron Problems,” *Phys. Rev. Lett.* **113**, 166402.
- Mishchenko, A. S., N. V. Prokof’ev, and B. V. Svistunov (2001), “Single-hole spectral function and spin-charge separation in the $t - j$ model,” *Phys. Rev. B* **64**, 033101.
- Mistakidis, S., A. Volosniev, R. Barfknecht, T. Fogarty, T. Busch, A. Foerster, P. Schmelcher, and N. Zinner (2023), “Few-body bose gases in low dimensions—a laboratory for quantum dynamics,” *Physics Reports* **1042**, 1.
- Mohammadi, A., A. Krüchow, A. Mahdian, M. Deiß, J. Pérez-Ríos, H. da Silva, M. Raoult, O. Dulieu, and J. Hecker Denschlag (2021), “Life and death of a cold barb⁺ molecule inside an ultracold cloud of rb atoms,” *Phys. Rev. Res.* **3**, 013196.
- Mora, C., and F. Chevy (2010), “Normal phase of an imbalanced fermi gas,” *Phys. Rev. Lett.* **104**, 230402.
- Morgen, A. M., S. S. Balling, K. K. Nielsen, T. Pohl, G. M. Bruun, and J. J. Arlt (2023), “Quantum beat spectroscopy of repulsive bose polarons,” [arXiv:2310.18183](https://arxiv.org/abs/2310.18183).
- Mostaan, N., N. Goldman, and F. Grusdt (2023), “A unified theory of strong coupling bose polarons: From repulsive polarons to non-gaussian many-body bound states,” [arXiv:2305.00835](https://arxiv.org/abs/2305.00835).
- Muir, J. B., J. Levinsen, S. K. Earl, M. A. Conway, J. H. Cole, M. Wurdack, R. Mishra, D. J. Ing, E. Estrecho, Y. Lu, D. K. Efimkin, J. O. Tollerud, E. A. Ostrovskaya, M. M. Parish, and J. A. Davis (2022), “Interactions between fermi polarons in monolayer ws₂,” *Nature Communications* **13** (1), 6164.
- Mulkerin, B. C., J. Levinsen, and M. M. Parish (2024), “Rabi oscillations and magnetization of a mobile spin-1/2 impurity in a fermi sea,” *Phys. Rev. A* **109**, 023302.
- Mulkerin, B. C., X.-J. Liu, and H. Hu (2019), “Breakdown of the fermi polaron description near fermi degeneracy at unitarity,” *Annals of Physics* **407**, 29.
- Myśliwy, K., and K. Jachymski (2024), “Long-range interacting fermi polaron,” *Phys. Rev. B* **109**, 214208.
- Müller, T., R. Thomale, S. Sachdev, and Y. Iqbal (2024), “Polaronic correlations from optimized ancilla wave functions for the fermi-hubbard model,” [arXiv:2408.01492](https://arxiv.org/abs/2408.01492).
- Nagaoka, Y. (1966), “Ferromagnetism in a narrow, almost half-filled s band,” *Phys. Rev.* **147**, 392.
- Naidon, P. (2018), “Two impurities in a bose–einstein condensate: From yukawa to efimov attracted polarons,” *Journal of the Physical Society of Japan* **87** (4), 043002.
- Naidon, P., and S. Endo (2017), “Efimov physics: a review,” *Reports on Progress in Physics* **80** (5), 056001.
- Nakano, E., T. Miyakawa, and H. Yabu (2024a), “Two-body problem of impurity atoms in dipolar fermi gas,” [arXiv:2404.14866](https://arxiv.org/abs/2404.14866).
- Nakano, Y., M. M. Parish, and J. Levinsen (2024b), “Variational approach to the two-dimensional bose polaron,” *Phys. Rev. A* **109**, 013325.
- Nascimbène, S., N. Navon, K. J. Jiang, L. Tarruell, M. Teichmann, J. McKeever, F. Chevy, and C. Salomon (2009), “Collective oscillations of an imbalanced Fermi gas: Axial compression modes and polaron effective mass,” *Phys. Rev. Lett.* **103** (17), 170402.

- Nascimbène, S., N. Navon, S. Pilati, F. Chevy, S. Giorgini, A. Georges, and C. Salomon (2011), “Fermi-liquid behavior of the normal phase of a strongly interacting gas of cold atoms,” *Phys. Rev. Lett.* **106**, 215303.
- Nascimbène, S., N. Navon, K. J. Jiang, F. Chevy, and C. Salomon (2010), “Exploring the thermodynamics of a universal fermi gas,” *Nature* **463** (7284), 1057.
- Navadeh-Toupchi, M., N. Takemura, M. D. Anderson, D. Y. Oberli, and M. T. Portella-Oberli (2019), “Polaritonic cross feshbach resonance,” *Phys. Rev. Lett.* **122**, 047402.
- Navon, N., S. Nascimbene, F. Chevy, and C. Salomon (2010), “The equation of state of a low-temperature Fermi gas with tunable interactions,” *Science* **328** (5979), 729.
- Ness, G., C. Shkedrov, Y. Florshaim, O. K. Diessel, J. von Milczewski, R. Schmidt, and Y. Sagi (2020), “Observation of a smooth polaron-molecule transition in a degenerate fermi gas,” *Phys. Rev. X* **10**, 041019.
- Smoleński, T., O. Cotlet, A. Popert, P. Back, Y. Shimazaki, P. Knüppel, N. Dietler, T. Taniguchi, K. Watanabe, M. Kroner, and A. Imamoglu (2019), “Interaction-induced shubnikov–de haas oscillations in optical conductivity of monolayer mose_2 ,” *Phys. Rev. Lett.* **123**, 097403.
- Nguyen, P. X., R. Chaturvedi, L. Ma, P. Knuppel, K. Watanabe, T. Taniguchi, K. F. Mak, and J. Shan (2023), “A degenerate trion liquid in atomic double layers,” [arXiv:2312.12571](https://arxiv.org/abs/2312.12571).
- Nielsen, K. K. (2024), “Pairing by disorder of dopants in a magnetic spin ladder,” [arXiv:2407.01252](https://arxiv.org/abs/2407.01252).
- Nielsen, K. K., M. A. Bastarrachea-Magnani, T. Pohl, and G. M. Bruun (2021), “Spatial structure of magnetic polarons in strongly interacting antiferromagnets,” *Phys. Rev. B* **104**, 155136.
- Nielsen, K. K., A. Camacho-Guardian, G. M. Bruun, and T. Pohl (2020), “Superfluid flow of polaron polaritons above landau’s critical velocity,” *Phys. Rev. Lett.* **125**, 035301.
- Nielsen, K. K., L. A. Peña Ardila, G. M. Bruun, and T. Pohl (2019), “Critical slowdown of non-equilibrium polaron dynamics,” *New Journal of Physics* **21** (4), 043014.
- Nielsen, K. K., T. Pohl, and G. M. Bruun (2022), “Nonequilibrium hole dynamics in antiferromagnets: Damped strings and polarons,” *Phys. Rev. Lett.* **129**, 246601.
- Nikolić, P., and S. Sachdev (2007), “Renormalization-group fixed points, universal phase diagram, and $1/n$ expansion for quantum liquids with interactions near the unitarity limit,” *Phys. Rev. A* **75**, 033608.
- Nishida, Y. (2009), “Casimir interaction among heavy fermions in the bcs-bec crossover,” *Phys. Rev. A* **79**, 013629.
- Nishida, Y. (2015), “Polaronic atom-trimer continuity in three-component fermi gases,” *Phys. Rev. Lett.* **114**, 115302.
- Nishimura, K., E. Nakano, K. Iida, H. Tajima, T. Miyakawa, and H. Yabu (2021), “Ground state of the polaron in an ultracold dipolar fermi gas,” *Phys. Rev. A* **103**, 033324.
- Novikov, A., and M. Ovchinnikov (2009), “A diagrammatic calculation of the energy spectrum of quantum impurity in degenerate bose–einstein condensate,” *Journal of Physics A: Mathematical and Theoretical* **42** (13), 135301.
- Nyhegn, J. H., G. M. Bruun, and K. K. Nielsen (2023), “Wave function and spatial structure of polarons in an antiferromagnetic bilayer,” *Phys. Rev. B* **108**, 075141.
- Nyhegn, J. H., K. K. Nielsen, and G. M. Bruun (2022), “Equilibrium and nonequilibrium dynamics of a hole in a bilayer antiferromagnet,” *Phys. Rev. B* **106**, 155160.
- Nyhegn, J. H., K. K. Nielsen, and G. M. Bruun (2024), “Probing a quantum spin liquid with equilibrium and non-equilibrium hole dynamics,” [arXiv:2407.06816](https://arxiv.org/abs/2407.06816).
- Oghittu, L., J. Simonet, P. Wessels-Staarmann, M. Drescher, K. Sengstock, L. Mathey, and A. Negretti (2024), “Cooling dynamics of a free ion in a bose-einstein condensate,” *Phys. Rev. Res.* **6**, 023024.
- Olf, R., F. Fang, G. E. Marti, A. MacRae, and D. M. Stamper-Kurn (2015), “Thermometry and cooling of a bose gas to 0.02 times the condensation temperature,” *Nature Physics* **11** (9), 720.
- Ong, W., C. Cheng, I. Arakelyan, and J. E. Thomas (2015), “Spin-imbalanced quasi-two-dimensional fermi gases,” *Phys. Rev. Lett.* **114**, 110403.
- Onofrio, R., C. Raman, J. M. Vogels, J. R. Abo-Shaer, A. P. Chikkatur, and W. Ketterle (2000), “Observation of superfluid flow in a bose-einstein condensed gas,” *Phys. Rev. Lett.* **85**, 2228.
- Pan, H., F. Wu, and S. Das Sarma (2020), “Band topology, hubbard model, heisenberg model, and dzyaloshinskii-moriya interaction in twisted bilayer wse_2 ,” *Phys. Rev. Res.* **2**, 033087.
- Paredes, R., G. Bruun, and A. Camacho-Guardian (2024), “Interactions mediated by atoms, photons, electrons, and excitons,” *Phys. Rev. A* **110**, 030101.
- Parish, M. M., and J. Levinsen (2016), “Quantum dynamics of impurities coupled to a fermi sea,” *Phys. Rev. B* **94**, 184303.
- Partridge, G. B., W. Li, R. I. Kamar, Y. Liao, and R. G. Hulet (2006), “Pairing and phase separation in a polarized Fermi gas,” *Science* **311**, 503.
- Pascual, G., and J. Boronat (2021), “Quasiparticle nature of the bose polaron at finite temperature,” *Phys. Rev. Lett.* **127**, 205301.
- Pascual, G., J. Boronat, and K. Van Houcke (2024a), “On polarons and dimerons in the two-dimensional attractive Hubbard model,” [arXiv:2411.19725](https://arxiv.org/abs/2411.19725).
- Pascual, G., T. Wasak, A. Negretti, G. E. Astrakharchik, and J. Boronat (2024b), “Temperature-induced miscibility of impurities in trapped bose gases,” *Phys. Rev. Res.* **6**, L022014.
- Pastukhov, V. (2018), “Polaron in dilute 2d bose gas at low temperatures,” *Journal of Physics B: Atomic, Molecular and Optical Physics* **51** (15), 155203.
- Pawlowski, J. M., M. M. Scherer, R. Schmidt, and S. J. Wetzel (2017), “Physics and the choice of regulators in functional renormalisation group flows,” *Ann. Phys.* **384**, 165.
- Peña Ardila, L. A. (2021), “Dynamical formation of polarons in a bose-einstein condensate: A variational approach,” *Phys. Rev. A* **103**, 033323.
- Peña Ardila, L. A. (2022), “Ultra-dilute gas of polarons in a bose–einstein condensate,” *Atoms* **10** (1), 10.3390/atoms10010029.
- Peña Ardila, L. A., G. E. Astrakharchik, and S. Giorgini (2020), “Strong coupling bose polarons in a two-dimensional gas,” *Phys. Rev. Research* **2**, 023405.
- Peña Ardila, L. A., and S. Giorgini (2015), “Impurity in a bose-einstein condensate: Study of the attractive and repulsive branch using quantum monte carlo methods,” *Phys. Rev. A* **92**, 033612.
- Peña Ardila, L. A., and S. Giorgini (2016), “Bose polaron problem: Effect of mass imbalance on binding energy,” *Phys. Rev. A* **94**, 063640.

- Peña Ardila, L. A., N. B. Jørgensen, T. Pohl, S. Giorgini, G. M. Bruun, and J. J. Arlt (2019), “Analyzing a bose polaron across resonant interactions,” *Phys. Rev. A* **99**, 063607.
- Peña Ardila, L. A., and T. Pohl (2018), “Ground-state properties of dipolar bose polarons,” *Journal of Physics B: Atomic, Molecular and Optical Physics* **52** (1), 015004.
- Pessoa, R., S. A. Vitiello, and L. A. Peña Ardila (2021), “Finite-range effects in the unitary fermi polaron,” *Phys. Rev. A* **104**, 043313.
- Pessoa, R., S. A. Vitiello, and L. A. Peña Ardila (2024), “Fermi polaron in atom-ion hybrid systems,” *Phys. Rev. Lett.* **133**, 233002.
- Pethick, C. J., and H. Smith (2002), *Bose-Einstein condensation in dilute gases* (Cambridge university press).
- Petrov, D. S. (2003), “Three-body problem in fermi gases with short-range interparticle interaction,” *Phys. Rev. A* **67**, 010703.
- Petrov, D. S., and G. V. Shlyapnikov (2001), “Interatomic collisions in a tightly confined bose gas,” *Phys. Rev. A* **64**, 012706.
- Pfeiderer, C. (2009), “Superconducting phases of f -electron compounds,” *Rev. Mod. Phys.* **81**, 1551.
- Pierce, M., X. Leyronas, and F. Chevy (2019), “Few versus many-body physics of an impurity immersed in a superfluid of spin 1/2 attractive fermions,” *Phys. Rev. Lett.* **123**, 080403.
- Pilati, S., and S. Giorgini (2008), “Phase separation in a polarized fermi gas at zero temperature,” *Physical Review Letters* **100** (3), 030401.
- Pilati, S., G. Orso, and G. Bertainia (2021), “Quantum monte carlo simulations of two-dimensional repulsive fermi gases with population imbalance,” *Phys. Rev. A* **103**, 063314.
- Pimenov, D. (2024), “Polaron spectra and edge singularities for correlated flat bands,” *Phys. Rev. B* **109**, 195153.
- Pimenov, D., A. Camacho-Guardian, N. Goldman, P. Massignan, G. M. Bruun, and M. Goldstein (2021), “Topological transport of mobile impurities,” *Phys. Rev. B* **103**, 245106.
- Pitaevskii, L., and S. Stringari (2016), *Bose-Einstein Condensation and Superfluidity*, International Series of Monographs on Physics (OUP Oxford).
- Pitaevskii, L. P. (1961), “Vortex lines in an imperfect bose gas,” *Sov. Phys. JETP* **13** (2), 451.
- Powell, S., S. Sachdev, and H. P. Büchler (2005), “Depletion of the bose-einstein condensate in bose-fermi mixtures,” *Phys. Rev. B* **72**, 024534.
- Prichard, M. L., B. M. Spar, I. Morera, E. Demler, Z. Z. Yan, and W. S. Bakr (2024), “Directly imaging spin polarons in a kinetically frustrated hubbard system,” *Nature* **629** (8011), 323.
- Pricoupenko, L., and P. Pedri (2010), “Universal (1+2)-body bound states in planar atomic waveguides,” *Phys. Rev. A* **82**, 033625.
- Privitera, A., and W. Hofstetter (2010), “Polaronic slowing of fermionic impurities in lattice bose-fermi mixtures,” *Phys. Rev. A* **82**, 063614.
- Prokof’ev, N., and B. Svistunov (2007), “Bold diagrammatic monte carlo technique: When the sign problem is welcome,” *Phys. Rev. Lett.* **99**, 250201.
- Prokof’ev, N., and B. Svistunov (2008a), “Fermi-polaron problem: Diagrammatic monte carlo method for divergent sign-alternating series,” *Phys. Rev. B* **77**, 020408.
- Prokof’ev, N. V., and B. V. Svistunov (2008b), “Bold diagrammatic monte carlo: A generic sign-problem tolerant technique for polaron models and possibly interacting many-body problems,” *Phys. Rev. B* **77**, 125101.
- Punk, M., and S. Sachdev (2013), “Mobile impurity near the superfluid–mott-insulator quantum critical point in two dimensions,” *Phys. Rev. A* **87**, 033618.
- Qi, R., Q. Li, Z. Zhang, S. Chen, J. Xie, Y. Ou, Z. Cui, D. D. Dai, A. Y. Joe, T. Taniguchi, K. Watanabe, S. Tongay, A. Zettl, L. Fu, and F. Wang (2023), “Electrically controlled interlayer trion fluid in electron-hole bilayers,” [arXiv:2312.03251](https://arxiv.org/abs/2312.03251).
- Qi, X.-L., and S.-C. Zhang (2011), “Topological insulators and superconductors,” *Rev. Mod. Phys.* **83**, 1057.
- Qin, F., X. Cui, and W. Yi (2019), “Polaron in a $p + ip$ fermi topological superfluid,” *Phys. Rev. A* **99**, 033613.
- Qu, C., L. P. Pitaevskii, and S. Stringari (2016), “Expansion of harmonically trapped interacting particles and time dependence of the contact,” *Phys. Rev. A* **94**, 063635.
- Radovan, H. A., N. A. Fortune, T. P. Murphy, S. T. Hannahs, E. C. Palm, S. W. Tozer, and D. Hall (2003), “Magnetic enhancement of superconductivity from electron spin domains,” *Nature* **425**, 51.
- Ramšak, A., and P. Horsch (1998), “Spatial structure of spin polarons in the $t - j$ model,” *Phys. Rev. B* **57**, 4308.
- Rana, F., O. Koksai, and C. Manolatou (2020), “Many-body theory of the optical conductivity of excitons and trions in two-dimensional materials,” *Phys. Rev. B* **102**, 085304.
- Randeria, M., J.-M. Duan, and L.-Y. Shieh (1990), “Superconductivity in a two-dimensional fermi gas: Evolution from cooper pairing to bose condensation,” *Phys. Rev. B* **41**, 327.
- Rath, S. P., and R. Schmidt (2013), “Field-theoretical study of the bose polaron,” *Phys. Rev. A* **88**, 053632.
- Reiter, G. F. (1994), “Self-consistent wave function for magnetic polarons in the t - j model,” *Phys. Rev. B* **49**, 1536.
- Rentrop, T., A. Trautmann, F. A. Olivares, F. Jendrzejewski, A. Komnik, and M. K. Oberthaler (2016), “Observation of the phononic lamb shift with a synthetic vacuum,” *Phys. Rev. X* **6**, 041041.
- Ring, P., and P. Schuck (2004), *The Nuclear Many-Body Problem*, Physics and astronomy online library (Springer).
- Rogers, F. J., H. C. Graboske, and D. J. Harwood (1970), “Bound eigenstates of the static screened coulomb potential,” *Phys. Rev. A* **1**, 1577.
- Rose, F., and R. Schmidt (2022), “Disorder in order: Localization without randomness in a cold-atom system,” *Phys. Rev. A* **105**, 013324.
- Ross, J. S., S. Wu, H. Yu, N. J. Ghimire, A. M. Jones, G. Aivazian, J. Yan, D. G. Mandrus, D. Xiao, W. Yao, and X. Xu (2013), “Electrical control of neutral and charged excitons in a monolayer semiconductor,” *Nature Communications* **4** (1), 1474.
- Roy, R., A. Green, R. Bowler, and S. Gupta (2017), “Two-element mixture of bose and fermi superfluids,” *Phys. Rev. Lett.* **118**, 055301.
- Ruderman, M. A., and C. Kittel (1954), “Indirect exchange coupling of nuclear magnetic moments by conduction electrons,” *Phys. Rev.* **96**, 99.
- Sachdev, S. (1989), “Hole motion in a quantum néel state,” *Phys. Rev. B* **39**, 12232.
- Sachdev, S. (2011), *Quantum Phase Transitions*, 2nd ed. (Cambridge University Press, Cambridge, England).
- Salvador, A. G., C. Kuhlenkamp, L. Ciorciaro, M. Knap, and A. Imamoglu (2022), “Optical signatures of periodic magnetization: The moiré zeeman effect,” *Phys. Rev. Lett.*

- 128**, 237401.
- Sánchez-Baena, J., L. A. Peña Ardila, G. E. Astrakharchik, and F. Mazzanti (2024), “Universal properties of dipolar bose polarons in two dimensions,” *Phys. Rev. A* **110**, 023317.
- Santiago-García, M., and A. Camacho-Guardian (2023), “Collective excitations of a bose-einstein condensate of hard-core bosons and their mediated interactions: from two-body bound states to mediated superfluidity,” *New Journal of Physics* **25** (9), 093032.
- Santiago-García, M., S. G. Castillo-López, and A. Camacho-Guardian (2024), “Lattice polaron in a bose-einstein condensate of hard-core bosons,” [arXiv:2403.13635](https://arxiv.org/abs/2403.13635).
- Sarma, G. (1963), “On the influence of a uniform exchange field acting on the spins of the conduction electrons in a superconductor,” *J. Phys. Chem. Solids* **24**, 1029.
- Scalapino, D. (1995), “The case for $d_{x^2-y^2}$ pairing in the cuprate superconductors,” *Physics Reports* **250** (6), 329.
- Scazza, F., G. Valtolina, P. Massignan, A. Recati, A. Amico, A. Burchianti, C. Fort, M. Inguscio, M. Zaccanti, and G. Roati (2017), “Repulsive fermi polarons in a resonant mixture of ultracold ^6Li atoms,” *Phys. Rev. Lett.* **118**, 083602.
- Scazza, F., M. Zaccanti, P. Massignan, M. M. Parish, and J. Levinsen (2022), “Repulsive Fermi and Bose Polarons in Quantum Gases,” *Atoms* **10** (2), 55.
- Scelle, R., T. Rentrop, A. Trautmann, T. Schuster, and M. K. Oberthaler (2013), “Motional Coherence of Fermions Immersed in a Bose Gas,” *Physical Review Letters* **111** (7), 070401.
- Schaibley, J. R., H. Yu, G. Clark, P. Rivera, J. S. Ross, K. L. Seyler, W. Yao, and X. Xu (2016), “Valleytronics in 2d materials,” *Nature Reviews Materials* **1** (11), 16055.
- Schindewolf, A., R. Bause, X.-Y. Chen, M. Duda, T. Karman, I. Bloch, and X.-Y. Luo (2022), “Evaporation of microwave-shielded polar molecules to quantum degeneracy,” *Nature* **607** (7920), 677.
- Schirotzek, A., C. Wu, A. Sommer, and M. W. Zwierlein (2009), “Observation of Fermi polarons in a tunable Fermi liquid of ultracold atoms,” *Phys. Rev. Lett.* **102** (23), 230402.
- Schmidt, R., and T. Enss (2011), “Excitation spectra and rf response near the polaron-to-molecule transition from the functional renormalization group,” *Phys. Rev. A* **83** (6), 063620.
- Schmidt, R., and T. Enss (2022), “Self-stabilized Bose polarons,” *SciPost Phys.* **13**, 054.
- Schmidt, R., T. Enss, V. Pietilä, and E. Demler (2012a), “Fermi polarons in two dimensions,” *Phys. Rev. A* **85**, 021602.
- Schmidt, R., M. Knap, D. A. Ivanov, J.-S. You, M. Cetina, and E. Demler (2018a), “Universal many-body response of heavy impurities coupled to a fermi sea: a review of recent progress,” *Reports on Progress in Physics* **81** (2), 024401.
- Schmidt, R., and M. Lemeshko (2015), “Rotation of quantum impurities in the presence of a many-body environment,” *Phys. Rev. Lett.* **114**, 203001.
- Schmidt, R., and M. Lemeshko (2016), “Deformation of a quantum many-particle system by a rotating impurity,” *Phys. Rev. X* **6**, 011012.
- Schmidt, R., and S. Moroz (2010), “Renormalization-group study of the four-body problem,” *Phys. Rev. A* **81**, 052709.
- Schmidt, R., S. P. Rath, and W. Zwerger (2012b), “Efimov physics beyond universality,” *Eur. Phys. J. B* **85** (11), 1.
- Schmidt, R., H. R. Sadeghpour, and E. Demler (2016), “Mesoscopic rydberg impurity in an atomic quantum gas,” *Phys. Rev. Lett.* **116**, 105302.
- Schmidt, R., J. D. Whalen, R. Ding, F. Camargo, G. Woehl, S. Yoshida, J. Burgdörfer, F. B. Dunning, E. Demler, H. R. Sadeghpour, and T. C. Killian (2018b), “Theory of excitation of rydberg polarons in an atomic quantum gas,” *Phys. Rev. A* **97**, 022707.
- Schmitt-Rink, S., C. M. Varma, and A. E. Ruckenstein (1988), “Spectral function of holes in a quantum antiferromagnet,” *Phys. Rev. Lett.* **60**, 2793.
- Schrieffer, J. (1983), *Theory Of Superconductivity*, Advanced Book Program Series (Avalon Publishing).
- Schrieffer, J. R., and J. S. Brooks (2007), *Handbook of high-temperature superconductivity* (Springer).
- Schurer, J. M., A. Negretti, and P. Schmelcher (2017), “Unraveling the structure of ultracold mesoscopic collinear molecular ions,” *Phys. Rev. Lett.* **119**, 063001.
- Schwartz, I., Y. Shimazaki, C. Kuhlenskamp, K. Watanabe, T. Taniguchi, M. Kroner, and A. Imamoglu (2021), “Electrically tunable feshbach resonances in twisted bilayer semiconductors,” *Science* **374** (6565), 336.
- Seetharam, K., Y. Shchadilova, F. Grusdt, M. B. Zvonarev, and E. Demler (2021), “Dynamical quantum cherenkov transition of fast impurities in quantum liquids,” *Phys. Rev. Lett.* **127**, 185302.
- Shackleton, H., and S. Zhang (2024), “Emergent polaronic correlations in doped spin liquids,” [arXiv:2408.02190](https://arxiv.org/abs/2408.02190).
- Shchadilova, Y. E., R. Schmidt, F. Grusdt, and E. Demler (2016), “Quantum dynamics of ultracold bose polarons,” *Phys. Rev. Lett.* **117**, 113002.
- Shen, K., K. Sun, M. F. Gelin, and Y. Zhao (2024), “Finite-temperature hole-magnon dynamics in an antiferromagnet,” *The Journal of Physical Chemistry Letters* **15** (2), 447.
- Shi, Z.-Y., S. M. Yoshida, M. M. Parish, and J. Levinsen (2018), “Impurity-induced multibody resonances in a bose gas,” *Phys. Rev. Lett.* **121**, 243401.
- Shimazaki, Y., C. Kuhlenskamp, I. Schwartz, T. Smoleński, K. Watanabe, T. Taniguchi, M. Kroner, R. Schmidt, M. Knap, and A. Imamoglu (2021), “Optical signatures of periodic charge distribution in a mott-like correlated insulator state,” *Phys. Rev. X* **11**, 021027.
- Shimazaki, Y., I. Schwartz, K. Watanabe, T. Taniguchi, M. Kroner, and A. Imamoglu (2020), “Strongly correlated electrons and hybrid excitons in a moiréheterostructure,” *Nature* **580** (7804), 472.
- Shin, Y., C. Schunck, A. Schirotzek, and W. Ketterle (2008), “Phase diagram of a two-component Fermi gas with resonant interactions,” *Nature* **451**, 689.
- Shin, Y., M. W. Zwierlein, C. H. Schunck, A. Schirotzek, and W. Ketterle (2006), “Observation of phase separation in a strongly interacting imbalanced Fermi gas,” *Phys. Rev. Lett.* **97**, 030401.
- Shin, Y.-i. (2008), “Determination of the equation of state of a polarized fermi gas at unitarity,” *Phys. Rev. A* **77**, 041603.
- Shraiman, B. I., and E. D. Siggia (1988), “Mobile vacancies in a quantum heisenberg antiferromagnet,” *Phys. Rev. Lett.* **61**, 467.
- Shukla, N., A. G. Volosniev, and J. R. Armstrong (2024), “Anisotropic potential immersed in a dipolar bose-einstein condensate,” *Phys. Rev. A* **110**, 053317.
- Sidler, M., P. Back, O. Cotlet, A. Srivastava, T. Fink, M. Kroner, E. Demler, and A. Imamoglu (2016), “Fermi polaron-

- polaritons in charge-tunable atomically thin semiconductors,” *Nature Physics* **13** (3), 255–261.
- Skou, M. G., K. K. Nielsen, T. G. Skov, A. M. Morgen, N. B. Jørgensen, A. Camacho-Guardian, T. Pohl, G. M. Bruun, and J. J. Arlt (2022), “Life and death of the bose polaron,” *Phys. Rev. Res.* **4**, 043093.
- Skou, M. G., T. G. Skov, N. B. Jørgensen, K. K. Nielsen, A. Camacho-Guardian, T. Pohl, G. M. Bruun, and J. J. Arlt (2021a), “Non-equilibrium quantum dynamics and formation of the bose polaron,” *Nature Physics* **17** (6), 731.
- Skou, M. G., T. G. Skov, N. B. Jørgensen, and J. J. Arlt (2021b), “Initial Dynamics of Quantum Impurities in a Bose–Einstein Condensate,” *Atoms* **9** (2), 22.
- Smoleński, T., P. E. Dolgirev, C. Kuhlenskamp, A. Popert, Y. Shimazaki, P. Back, X. Lu, M. Kroner, K. Watanabe, T. Taniguchi, I. Esterlis, E. Demler, and A. Imamoglu (2021), “Signatures of wigner crystal of electrons in a monolayer semiconductor,” *Nature* **595** (7865), 53.
- Sorout, A. K., S. Sarkar, and S. Gangadharaiah (2020), “Dynamics of impurity in the environment of dirac fermions,” *Journal of Physics: Condensed Matter* **32** (41), 415604.
- Sous, J., H. R. Sadeghpour, T. C. Killian, E. Demler, and R. Schmidt (2020), “Rydberg impurity in a fermi gas: Quantum statistics and rotational blockade,” *Phys. Rev. Research* **2**, 023021.
- Spethmann, N., F. Kindermann, S. John, C. Weber, D. Meschede, and A. Widera (2012a), “Dynamics of single neutral impurity atoms immersed in an ultracold gas,” *Phys. Rev. Lett.* **109**, 235301.
- Spethmann, N., F. Kindermann, S. John, C. Weber, D. Meschede, and A. Widera (2012b), “Inserting single Cs atoms into an ultracold Rb gas,” *Appl. Phys. B* **106** (3), 513.
- von Stecher, J. (2011), “Five- and six-body resonances tied to an efimov trimer,” *Phys. Rev. Lett.* **107**, 200402.
- von Stecher, J., J. P. D’Incao, and C. H. Greene (2009), “Signatures of universal four-body phenomena and their relation to the efimov effect,” *Nature Physics* **5** (6), 417.
- Suchet, D., Z. Wu, F. Chevy, and G. M. Bruun (2017), “Long-range mediated interactions in a mixed-dimensional system,” *Phys. Rev. A* **95**, 043643.
- Suchorowski, M., A. Badamshina, M. Lemesko, M. Tomza, and A. G. Volosniev (2024), “Quantum rotor in a two-dimensional mesoscopic bose gas,” [arXiv:2407.06046](https://arxiv.org/abs/2407.06046).
- Sun, J., O. Rambow, and Q. Si (2004), “Orthogonality Catastrophe in Bose-Einstein Condensates,” [arXiv:0404590](https://arxiv.org/abs/0404590).
- Sun, M., and X. Cui (2017), “Enhancing the efimov correlation in bose polarons with large mass imbalance,” *Phys. Rev. A* **96**, 022707.
- Sun, M., and X. Cui (2019), “Efimov physics in the presence of a fermi sea,” *Phys. Rev. A* **99**, 060701.
- Sun, M., and X. Leyronas (2015), “High-temperature expansion for interacting fermions,” *Phys. Rev. A* **92**, 053611.
- Sun, M., H. Zhai, and X. Cui (2017), “Visualizing the efimov correlation in bose polarons,” *Phys. Rev. Lett.* **119**, 013401.
- Suris, R. A. (2003), “Correlation between trion and hole in fermi distribution in process of trion photo-excitation in doped qws,” in *Optical Properties of 2D Systems with Interacting Electrons*, edited by W. J. Ossau and R. Suris (Springer Netherlands, Dordrecht) pp. 111–124.
- Szwed, E. A., B. Vermilyea, D. J. Choksy, Z. Zhou, M. M. Fogler, L. V. Butov, D. K. Efimkin, K. W. Baldwin, and L. N. Pfeiffer (2024), “Excitonic bose-polarons in electron-hole bilayers,” *Nano Letters* **24** (42), 13219.
- Tajima, H., and S. Uchino (2018), “Many Fermi polarons at nonzero temperature,” *New J. Phys.* **20** (7), 073048.
- Takemura, N., M. D. Anderson, M. Navadeh-Toupchi, D. Y. Oberli, M. T. Portella-Oberli, and B. Deveaud (2017), “Spin anisotropic interactions of lower polaritons in the vicinity of polaritonic feshbach resonance,” *Phys. Rev. B* **95**, 205303.
- Takemura, N., S. Trebaol, M. Wouters, M. T. Portella-Oberli, and B. Deveaud (2014), “Polaritonic feshbach resonance,” *Nature Physics* **10** (7), 500.
- Tan, L. B. (2022), *Interacting Fermi and Bose Exciton-Polaron-Polaritons*, *Doctoral thesis* (ETH Zurich, Zurich).
- Tan, L. B., O. Cotlet, A. Bergschneider, R. Schmidt, P. Back, Y. Shimazaki, M. Kroner, and A. Imamoglu (2020), “Interacting polaron-polaritons,” *Phys. Rev. X* **10**, 021011.
- Tan, L. B., O. K. Diessel, A. Popert, R. Schmidt, A. Imamoglu, and M. Kroner (2023), “Bose polaron interactions in a cavity-coupled monolayer semiconductor,” *Phys. Rev. X* **13**, 031036.
- Tan, S. (2008a), “Energetics of a strongly correlated Fermi gas,” *Ann. Phys. (NY)* **323** (12), 2952.
- Tan, S. (2008b), “Large momentum part of a strongly correlated Fermi gas,” *Ann. Phys. (NY)* **323** (12), 2971.
- Tempere, J., W. Casteels, M. K. Oberthaler, S. Knoop, E. Timmermans, and J. T. Devreese (2009), “Feynman path-integral treatment of the bec-impurity polaron,” *Phys. Rev. B* **80**, 184504.
- Thouless, D. J., M. Kohmoto, M. P. Nightingale, and M. den Nijs (1982), “Quantized hall conductance in a two-dimensional periodic potential,” *Phys. Rev. Lett.* **49**, 405.
- Tiene, A., A. T. Bracho, M. M. Parish, J. Levinsen, and F. M. Marchetti (2024), “Multiple polaron quasiparticles with dipolar fermions in a bilayer geometry,” *Phys. Rev. A* **109**, 033318.
- Tiene, A., J. Levinsen, J. Keeling, M. M. Parish, and F. M. Marchetti (2022), “Effect of fermion indistinguishability on optical absorption of doped two-dimensional semiconductors,” *Phys. Rev. B* **105**, 125404.
- Tiene, A., B. C. Mulkerin, J. Levinsen, M. M. Parish, and F. M. Marchetti (2023), “Crossover from exciton polarons to trions in doped two-dimensional semiconductors at finite temperature,” *Phys. Rev. B* **108**, 125406.
- Tomza, M., K. Jachymski, R. Gerritsma, A. Negretti, T. Calarco, Z. Idziaszek, and P. S. Julienne (2019), “Cold hybrid ion-atom systems,” *Rev. Mod. Phys.* **91**, 035001.
- Trefzger, C., C. Menotti, B. Capogrosso-Sansone, and M. Lewenstein (2011), “Ultracold dipolar gases in optical lattices,” *Journal of Physics B: Atomic, Molecular and Optical Physics* **44** (19), 193001.
- Trumper, A. E., C. J. Gazza, and L. O. Manuel (2004), “Quasiparticle vanishing driven by geometrical frustration,” *Phys. Rev. B* **69**, 184407.
- Upadhyay, P., D. G. Suárez-Forero, T.-S. Huang, M. J. Mehrabad, B. Gao, S. Sarkar, D. Session, K. Watanabe, T. Taniguchi, Y. Zhou, M. Knap, and M. Hafezi (2024), “Giant enhancement of exciton diffusion near an electronic mott insulator,” [arXiv:2409.18357](https://arxiv.org/abs/2409.18357).
- Valtolina, G., K. Matsuda, W. G. Tobias, J.-R. Li, L. De Marco, and J. Ye (2020), “Dipolar evaporation of reactive molecules to below the fermi temperature,” *Nature* **588** (7837), 239.
- Van Houcke, K., F. Werner, and R. Rossi (2020), “High-precision numerical solution of the fermi polaron problem and large-order behavior of its diagrammatic series,” *Phys.*

- Rev. B* **101**, 045134.
- Vashisht, A., I. Amelio, L. Vanderstraeten, G. M. Bruun, O. K. Diessel, and N. Goldman (2024), “Chiral polaron formation on the edge of topological quantum matter,” [arXiv:2407.19093](https://arxiv.org/abs/2407.19093).
- Vashisht, A., M. Richard, and A. Minguzzi (2022), “Bose polaron in a quantum fluid of light,” *SciPost Phys.* **12**, 008.
- Čerenkov, P. A. (1937), “Visible radiation produced by electrons moving in a medium with velocities exceeding that of light,” *Phys. Rev.* **52**, 378.
- Veit, C., N. Zuber, O. A. Herrera-Sancho, V. S. V. Anasuri, T. Schmid, F. Meinert, R. Löw, and T. Pfau (2021), “Pulsed ion microscope to probe quantum gases,” *Phys. Rev. X* **11**, 011036.
- Vivanco, F. J., A. Schuckert, S. Huang, G. L. Schumacher, G. G. T. Assumpção, Y. Ji, J. Chen, M. Knap, and N. Navon (2023), “The strongly driven fermi polaron,” [arXiv:2308.05746](https://arxiv.org/abs/2308.05746).
- Vlietinck, J., J. Ryckebusch, and K. Van Houcke (2013), “Quasiparticle properties of an impurity in a fermi gas,” *Phys. Rev. B* **87**, 115133.
- Vlietinck, J., J. Ryckebusch, and K. Van Houcke (2014), “Diagrammatic monte carlo study of the fermi polaron in two dimensions,” *Phys. Rev. B* **89**, 085119.
- Volosniev, A. G., G. Bighin, L. Santos, and L. A. Peña Ardila (2023), “Non-equilibrium dynamics of dipolar polarons,” *SciPost Phys.* **15**, 232.
- Volosniev, A. G., H.-W. Hammer, and N. T. Zinner (2015), “Real-time dynamics of an impurity in an ideal bose gas in a trap,” *Phys. Rev. A* **92**, 023623.
- Wagner, M., R. Oldziejewski, F. Rose, V. Köder, C. Kuhlenskamp, A. Imamoglu, and R. Schmidt (2023), “Feshbach resonances of composite charge carrier states in atomically thin semiconductor heterostructures,” [arXiv:2310.08729](https://arxiv.org/abs/2310.08729) [[cond-mat.mes-hall](https://arxiv.org/abs/2310.08729)].
- Wang, G., A. Chernikov, M. M. Glazov, T. F. Heinz, X. Marie, T. Amand, and B. Urbaszek (2018a), “Colloquium: Excitons in atomically thin transition metal dichalcogenides,” *Rev. Mod. Phys.* **90**, 021001.
- Wang, G., A. Chernikov, M. M. Glazov, T. F. Heinz, X. Marie, T. Amand, and B. Urbaszek (2018b), “Colloquium: Excitons in atomically thin transition metal dichalcogenides,” *Rev. Mod. Phys.* **90**, 021001.
- Wang, J., J. P. D’Incao, B. D. Esry, and C. H. Greene (2012), “Origin of the three-body parameter universality in efimov physics,” *Phys. Rev. Lett.* **108**, 263001.
- Wang, J., X.-J. Liu, and H. Hu (2019), “Roton-induced bose polaron in the presence of synthetic spin-orbit coupling,” *Phys. Rev. Lett.* **123**, 213401.
- Wang, J., X.-J. Liu, and H. Hu (2022a), “Exact quasiparticle properties of a heavy polaron in bcs fermi superfluids,” *Phys. Rev. Lett.* **128**, 175301.
- Wang, J., X.-J. Liu, and H. Hu (2022b), “Heavy polarons in ultracold atomic fermi superfluids at the bec-bcs crossover: Formalism and applications,” *Phys. Rev. A* **105**, 043320.
- Wasak, T., R. Schmidt, and F. Piazza (2021), “Quantum-zeno fermi polaron in the strong dissipation limit,” *Phys. Rev. Res.* **3**, 013086.
- Wasak, T., M. Sighinolfi, J. Lang, F. Piazza, and A. Recati (2024), “Decoherence and momentum relaxation in fermi-polaron rabi dynamics: A kinetic equation approach,” *Phys. Rev. Lett.* **132**, 183001.
- Weckesser, P., F. Thielemann, D. Wiater, A. Wojciechowska, L. Karpa, K. Jachymski, M. Tomza, T. Walker, and T. Schaetz (2021), “Observation of feshbach resonances between a single ion and ultracold atoms,” *Nature* **600** (7889), 429.
- Weinberg, S. (1995), *The Quantum Theory of Fields*, The Quantum Theory of Fields 3 Volume Hardback Set No. vb. 1 (Cambridge University Press).
- Weldon, H. A. (1989), “Dynamical holes in the quark-gluon plasma,” *Phys. Rev. D* **40**, 2410.
- Wen, H.-H., and S. Li (2011), “Materials and novel superconductivity in iron pnictide superconductors,” *Annual Review of Condensed Matter Physics* **2** (Volume 2, 2011), 121.
- Wenz, A. N., G. Zürn, S. Murmann, I. Brouzos, T. Lompe, and S. Jochim (2013), “From Few to Many: Observing the Formation of a Fermi Sea One Atom at a Time,” *Science* **342** (6157), 457.
- Werner, F., and Y. Castin (2012), “General relations for quantum gases in two and three dimensions. ii. bosons and mixtures,” *Phys. Rev. A* **86**, 053633.
- White, S. R., and I. Affleck (2001), “Density matrix renormalization group analysis of the nagaoka polaron in the two-dimensional $t - j$ model,” *Phys. Rev. B* **64**, 024411.
- Will, M., T. Lausch, and M. Fleischhauer (2019), “Rotational cooling of molecules in a bose-einstein condensate,” *Phys. Rev. A* **99**, 062707.
- Winkler, K., G. Thalhammer, F. Lang, R. Grimm, J. Hecker Denschlag, A. J. Daley, A. Kantian, H. P. Büchler, and P. Zoller (2006), “Repulsively bound atom pairs in an optical lattice,” *Nature* **441** (7095), 853.
- Wosnitzer, J. (2012), “Superconductivity in layered organic metals,” *Crystals* **2** (2), 248.
- Wouters, M. (2007), “Resonant polariton-polariton scattering in semiconductor microcavities,” *Phys. Rev. B* **76**, 045319.
- Wu, C.-H., J. W. Park, P. Ahmadi, S. Will, and M. W. Zwierlein (2012), “Ultracold fermionic feshbach molecules of $^{23}\text{Na}^{40}\text{K}$,” *Phys. Rev. Lett.* **109**, 085301.
- Wu, F., T. Lovorn, E. Tutuc, and A. H. MacDonald (2018), “Hubbard model physics in transition metal dichalcogenide moiré bands,” *Phys. Rev. Lett.* **121**, 026402.
- Wu, T. T. (1959), “Ground state of a bose system of hard spheres,” *Phys. Rev.* **115**, 1390.
- Xiong, R., J. H. Nie, S. L. Brantly, P. Hays, R. Sailus, K. Watanabe, T. Taniguchi, S. Tongay, and C. Jin (2023), “Correlated insulator of excitons in WSe₂-WS₂ moire superlattices,” *Science* **380** (6647), 860.
- Xu, X., W. Yao, D. Xiao, and T. F. Heinz (2014), “Spin and pseudospins in layered transition metal dichalcogenides,” *Nature Physics* **10** (5), 343.
- Xu, Y., S. Liu, D. A. Rhodes, K. Watanabe, T. Taniguchi, J. Hone, V. Elser, K. F. Mak, and J. Shan (2020), “Correlated insulating states at fractional fillings of moiré superlattices,” *Nature* **587** (7833), 214.
- Yan, Z., P. B. Patel, B. Mukherjee, R. J. Fletcher, J. Struck, and M. W. Zwierlein (2019), “Boiling a unitary fermi liquid,” *Phys. Rev. Lett.* **122**, 093401.
- Yan, Z. Z., Y. Ni, C. Robens, and M. W. Zwierlein (2020), “Bose polarons near quantum criticality,” *Science* **368** (6487), 190.
- Yao, X.-C., H.-Z. Chen, Y.-P. Wu, X.-P. Liu, X.-Q. Wang, X. Jiang, Y. Deng, Y.-A. Chen, and J.-W. Pan (2016), “Observation of coupled vortex lattices in a mass-imbalance bose and fermi superfluid mixture,” *Phys. Rev. Lett.* **117**, 145301.
- Yegovtsev, N., G. E. Astrakharchik, P. Massignan, and V. Gurarie (2024), “Exact results for heavy unitary bose po-

- larons,” *Phys. Rev. A* **110**, 023310.
- Yegovtsev, N., and V. Gurarie (2023), “Effective mass and interaction energy of heavy bose polarons at unitarity,” *Phys. Rev. A* **108**, L051301.
- Yegovtsev, N., P. Massignan, and V. Gurarie (2022), “Strongly interacting impurities in a dilute bose condensate,” *Phys. Rev. A* **106**, 033305.
- Yi, W., and X. Cui (2015), “Polarons in ultracold fermi superfluids,” *Phys. Rev. A* **92**, 013620.
- Yin, T., D. Cocks, and W. Hofstetter (2015), “Polaronic effects in one- and two-band quantum systems,” *Phys. Rev. A* **92**, 063635.
- Yoshida, S. M., S. Endo, J. Levinsen, and M. M. Parish (2018a), “Universality of an impurity in a bose-einstein condensate,” *Phys. Rev. X* **8**, 011024.
- Yoshida, S. M., Z.-Y. Shi, J. Levinsen, and M. M. Parish (2018b), “Few-body states of bosons interacting with a heavy quantum impurity,” *Phys. Rev. A* **98**, 062705.
- Yosida, K. (1957), “Magnetic properties of cu-mn alloys,” *Phys. Rev.* **106**, 893.
- You, J.-S., R. Schmidt, D. A. Ivanov, M. Knap, and E. Demler (2019), “Atomtronics with a spin: Statistics of spin transport and nonequilibrium orthogonality catastrophe in cold quantum gases,” *Phys. Rev. B* **99**, 214505.
- Yu, Z., and C. J. Pethick (2012), “Induced interactions in dilute atomic gases and liquid helium mixtures,” *Phys. Rev. A* **85**, 063616.
- Yu, Z., S. Zöllner, and C. J. Pethick (2010), “Comment on “normal phase of an imbalanced fermi gas”,” *Phys. Rev. Lett.* **105**, 188901.
- Zaccanti, M., B. Deissler, C. D’Errico, M. Fattori, M. Jonas-Lasinio, S. Müller, G. Roati, M. Inguscio, and G. Modugno (2009), “Observation of an efimov spectrum in an atomic system,” *Nature Physics* **5** (8), 586.
- Zeng, H., J. Dai, W. Yao, D. Xiao, and X. Cui (2012), “Valley polarization in mos2 monolayers by optical pumping,” *Nature Nanotechnology* **7** (8), 490.
- Zeng, Z., E. Yakaboylu, M. Lemeshko, T. Shi, and R. Schmidt (2023), “Variational theory of angulons and their rotational spectroscopy,” *The Journal of Chemical Physics* **158** (13), 134301.
- Zerba, C., C. Kuhlenskamp, A. İmamoglu, and M. Knap (2024a), “Realizing topological superconductivity in tunable bose-fermi mixtures with transition metal dichalcogenide heterostructures,” *Phys. Rev. Lett.* **133**, 056902.
- Zerba, C., C. Kuhlenskamp, L. Mangeolle, and M. Knap (2024b), “Tuning transport in solid-state bose-fermi mixtures by feshbach resonances,” [arXiv:2409.18176](https://arxiv.org/abs/2409.18176).
- Zhang, C., H. Wang, W. Chan, C. Manolatou, and F. Rana (2014), “Absorption of light by excitons and trions in monolayers of metal dichalcogenide mos2: Experiments and theory,” *Phys. Rev. B* **89**, 205436.
- Zhang, Y., W. Ong, I. Arakelyan, and J. E. Thomas (2012), “Polaron-to-polaron transitions in the radio-frequency spectrum of a quasi-two-dimensional fermi gas,” *Phys. Rev. Lett.* **108**, 235302.
- Zhou, Y., J. Sung, E. Brutschea, I. Esterlis, Y. Wang, G. Scuri, R. J. Gelly, H. Heo, T. Taniguchi, K. Watanabe, G. Zaránd, M. D. Lukin, P. Kim, E. Demler, and H. Park (2021), “Bilayer wigner crystals in a transition metal dichalcogenide heterostructure,” *Nature* **595** (7865), 48.
- Zhu, B., X. Chen, and X. Cui (2015), “Exciton binding energy of monolayer ws2,” *Scientific Reports* **5** (1), 9218.
- Zipkes, C., S. Palzer, C. Sias, and M. Köhl (2010), “A trapped single ion inside a Bose–Einstein condensate,” *Nature* **464** (7287), 388.
- Zöllner, S., G. M. Bruun, and C. J. Pethick (2011), “Polarons and molecules in a two-dimensional fermi gas,” *Phys. Rev. A* **83**, 021603.
- Zwinger, W. (2011), *The BCS-BEC crossover and the unitary Fermi gas*, Vol. 836 (Springer).
- Zwierlein, M. W. (2014), “Superfluidity in ultracold atomic fermi gases,” in *Novel Superfluids, Vol. 2*, edited by K.-H. Bennemann and J. B. Ketterson, Book section 18 (Oxford University Press, Oxford) p. 269–422.
- Zwierlein, M. W. (2016), “Thermodynamics of strongly interacting fermi gases,” in *Quantum Matter at Ultralow Temperatures*, Proceedings of the International School of Physics “Enrico Fermi” (IOS Press) pp. 143–220.
- Zwierlein, M. W., J. R. Abo-Shaeer, A. Schirotzek, C. H. Schunck, and W. Ketterle (2005), “Vortices and superfluidity in a strongly interacting Fermi gas,” *Nature* **435**, 1047.
- Zwierlein, M. W., A. Schirotzek, C. H. Schunck, and W. Ketterle (2006a), “Fermionic superfluidity with imbalanced spin populations,” *Science* **311**, 492.
- Zwierlein, M. W., C. H. Schunck, A. Schirotzek, and W. Ketterle (2006b), “Direct observation of the superfluid phase transition in ultracold Fermi gases,” *Nature* **442**, 54.